Not to be picky: PEPCK-M ensures metabolic flexibility in cancer cells and neuronal progenitors

Petra Hyroššová

Thesis for doctoral degree (Ph.D.)

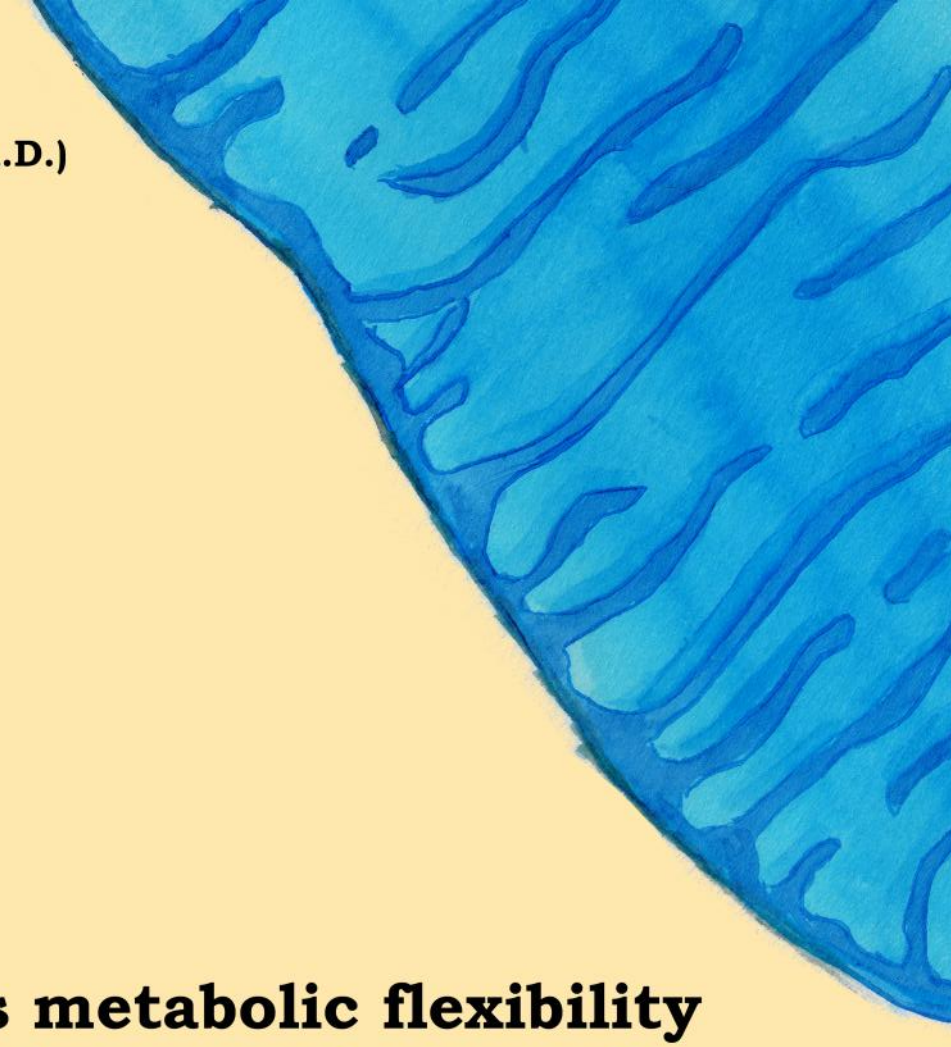

Not to be picky: PEPCK-M ensures metabolic flexibility in cancer cells and neuronal progenitors

UNIVERSITAT DE BARCELONA

Petra Hyroššová, 2017

Thesis for doctoral degree (Ph.D.)

Not to be picky: PEPCK-M ensures metabolic flexibility in cancer cells and neuronal progenitors

by

Petra Hyroššová

under the supervision of

Dr. Jose Carlos Perales Losa

Doctoral Programme in Biomedicine

Department of Physiological Sciences, Faculty of Medicine and Health Sciences

L'Hospitalet de Llobregat, March 2017

UNIVERSITAT DE BARCELONA

Dedicated to all those who will read it.

INDEX

List of figures and tables

INTRODUCTION

RESULTS

Abbreviations

3MPA	3-mercaptopicolinic acid
Ab	antibody
CAN	acetonitrile
AOA	aminooxyacetic acid
Bu.OH	butanol
cAMP	cyclic AMP
CoA	coenzyme A
CV	crystal violet
D_2O	deuterium oxide
DEPC	diethyl pyrocarbonate
dFCS	dialyzed fetal calf serum
ECM	extracellular matrix
EtOH	ethanol
FCS	fetal calf serum
GFP	green fluorescent protein
Gln	glutamine
Glu	glutamate
HG	high glucose
IF	immunofluorescence
IHC	immunohistochemistry
LDH	lactate dehydrogenase
LG	low glucose
LN_2	liquid nitrogen
MeOH	methanol
mQ	ultra pure water purified by Milli-Q® Integral
MTT	thiazolyl blue tetrazolium bromide
NAD+	nicotinamide adenine dinucleotide, oxidized state
NADH	nicotinamide adenine dinucleotide, reduced state
NHS	normal horse serum
NPs	neuronal progenitors
O/N	over nigh
OAA	oxaloacetate
P/S	penicillin G sodium salt 10,000 units/mL, streptomycin sulfate 10 mg/l
PC	pyruvate carboxylase
PDH	pyruvate dehydrogenase
PDK	pyruvate dehydrogenase kinase
PEP	phosphoenolpyruvate

PEPCK-C	cytosolic phosphoenolpyruvate carboxykinase
PEPCK-M	mitochondrial phosphoenolpyruvate carboxykinase
ROS	reactive oxygen species
RT	room temperature
shRNA	short hairpin RNA
siRNA	small interfering RNA
SG	serine and glycine
α-KG	alpha-ketoglutarate

INTRODUCTION

1 Metabolism

Cellular metabolism comprises a set of thousands of different biochemical reactions and transport processes that can break down or synthesize organic compounds and at the same time maximize returns from energy flows through living matter. In a broad sense, metabolism is the engine fueling cell proliferation, tissue development and homeostasis (Caetano-Anollés *et al*, 2009; Markert & Vazquez, 2015). We could contemplate that there would not be life without metabolism. Actually, one of the hypothesis of the origin of life called "Metabolism first" is considering metabolism as the event that enabled the beginning of life. As other hypotheses of life origin, this one also has weakness and there is still not a clear answer to the most fundamental question of evolution biologists: How life begun? However, we can certainly claim that metabolism was a driving force of the evolution forming life.

Billions of years ago, Earth consisted of an environment that favored those organisms which became capable of synthesizing molecules important for life as we know it nowadays (amino acids, nucleotides etc.). The rise of metabolic pathways allowed primitive organisms to become increasingly less-dependent on limiting exogenous sources and therefore could survive exhaustion of the prebiotic compounds (Fani & Fondi, 2009; Cooper, 2000a). It is likely that in the early stages of evolution metabolism would rely only on a limited number of enzymes. These enzymes were probably characterized by low effectiveness and broad specificity. Under natural selection, enzymes became specialized and more effective. Also new enzymes appeared in the metabolic network (by DNA duplication, DNA elongation etc.) and they were subject to increased rates of metabolic evolution (Alves *et al*, 2002; Fani & Fondi, 2009).

Biochemical pathways of modern organisms or their parts were probably present already at the very beginning of evolution in LUCA (Last Universal Common Ancestor), an organism from which descended all living organisms of the three known domains (Archea, Bacteria and Eukarya) (Castresana & Saraste, 1995). To characterize LUCA, common traits of organisms representing all domains have been analyzed. By comparing

metabolism, proteome and genes across all three domains, common characteristics to a broad range of organisms can be found. Those common traits are likely to have been present also in LUCA. Using these methods, several studies tried to define the metabolic capacity of LUCA. Goldman *et al.* outlines that LUCA possibly used amino acids, phospholipids, CoA, and carbohydrate metabolites, however not in the same range as we know it nowadays (Goldman *et al*, 2012). Some studies also claim that partial/reductive TCA cycle and aerobic respiration were present in this organism (Maden, 1995; Huynen *et al*, 1999; Castresana & Saraste, 1995). Therefore, we can assume that central carbon metabolism was present in LUCA in a simpler version and that it was the cornerstone of central carbon metabolism as we know it today. Classic textbooks represent central carbon metabolism as the pathways of glycolysis, pentose phosphate pathway, citric acid cycle and carbon fixation (present in plants and prokaryotic organisms) (Sudarsan *et al*, 2014; Fell, 2010). Nielsen states, that "as a result of evolution, the function of the central carbon metabolism has been fine-tuned to exactly meet the needs for building blocks and Gibbs free energy in conjunction with cell growth" (Nielsen, 2003).

Central carbon metabolism is present in all unicellular and multicellular organisms, however metabolic activity of single pathways is highly affected by the evolutionary pressure and their specific niche. Unicellular organisms are forced by evolution to compete and reproduce quickly in nutrition rich conditions or to adapt their metabolism in unpleasant conditions to survive starvation periods. Cells of multicellular organisms are forced to collaborate and they are exposed to unlimited sources of nutrients. Furthermore, evolution of multicellular organisms required the development of mechanism to control cell division in multicellular organism in order to avoid aberrant proliferation (Vander Heiden *et al*, 2009; Alberts *et al*, 2002).

1.1 Metabolic diversity of proliferating and non-proliferating cells

The difference in the proliferation state of cells affects prioritization of different pathways. The main metabolic task of non-proliferating cells is to provide energy in the form of ATP to maintain basic cellular processes (e.g. ion gradients, transcription, translation and tissue specific biological roles) (Figure I-1) (Mattaini *et al*, 2016; Finley & Thompson, 2014). Catabolic metabolism of non-proliferating cells is associated with preferential use of mitochondrial TCA cycle and oxidative phosphorylation (OXPHOS) (Fritz & Fajas, 2010). On the other hand, proliferating cells face distinct metabolic challenges, where they need to replicate all their biomass to produce daughter cells (Figure I-1). In a simplistic view, it has become commonplace to describe proliferating cells as dependent on fermentation or aerobic glycolysis for energy and building block production (Vander Heiden *et al*, 2009; Lunt & Vander Heiden, 2011).

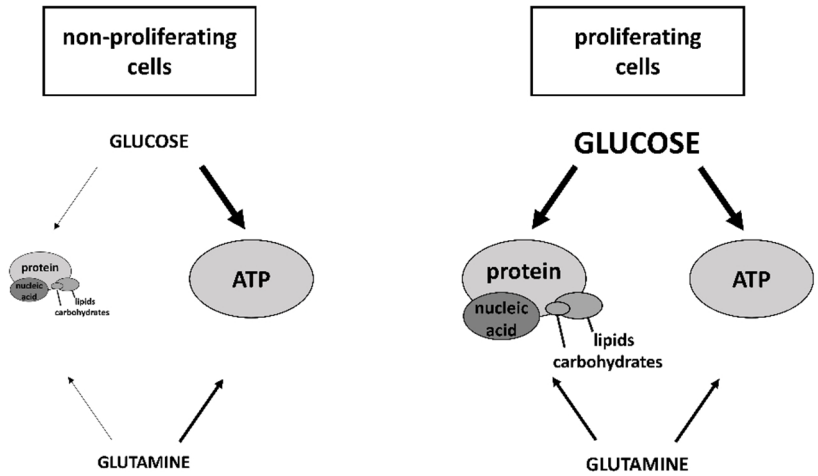

Figure I-1: Simple scheme of metabolic strategies of proliferating and non-proliferating cells (adapted from Vander Heiden *et al.*, 2011).

Even though proliferating and non-proliferating cells use different metabolic strategies to meet their metabolic needs, glycolysis and TCA cycle are at the center of their metabolic networks.

Glycolysis and the Warburg effect

Glucose is a simple carbohydrate and the major source of energy and carbon for new building blocks in most living organisms (Lunt & Vander Heiden, 2011). Glucose can be metabolized to pyruvate by glycolysis, a pathway present in almost all living cells, even though, some prokaryotic organisms utilize other pathways to metabolize glucose, such as the Entner-Duodoroff or hexose monophosphate pathways (Jurtshuk, 1996).

Glycolysis is carried out by a cascade of ten reactions that take place in the cytosol (Figure I-2). The end products of glycolysis are two molecules of pyruvate. The net energy yield being two molecules of ATP and two molecules of NADH. Pyruvate can later enter the TCA cycle and can be oxidized to CO_2 and H_2O while producing a fair amount of ATP through oxidative phosphorylation (Lunt & Vander Heiden, 2011). In this pathway, NADH is recycled by donating electrons to the electron transport chain (ETC). Organisms growing in hypoxic or anoxic conditions or cells lacking mitochondria have to cope with the absence of oxygen and find alternative ways to oxidize pyruvate and recycle NADH. One of these adaptations is fermentation, which is present in prokaryotes, yeasts and some other eukaryotic organisms and cells (e.g. Giardia, Entamoeba, *Carassius carassius*, muscle cells, erythrocytes) (Müller *et al*, 2012). In this scenario, pyruvate is converted to an acid or an alcohol (Jurtshuk, 1996). During fermentation, NADH produced in glycolysis is oxidized by donating electrons to a terminal acceptor that is excreted as the end product (e.g. ethanol, lactate, acetate). Interestingly, some eukaryotic organisms live in fully oxic habitats but do not use oxygen for oxidative phosphorylation (Müller *et al*, 2012). For example, some species of yeasts (e.g. *Saccharomyces*, *Shizosaccharomyces*, *and Torulopsis*) developed schemes that allow fermentation also in the presence of oxygen. Yeast fermentation occurring under aerobic conditions is called the Crabtree effect (Volker, 2001; Dashko *et al*, 2014). The Crabtree effect is advantageous for yeasts within the microbial community by allowing them to consume more sugar, in a faster manner, than other species and use the produced ethanol or acetate as a growth inhibitor for other species. Moreover, some of the Crabtree-positive yeast are able to switch from sugar consumption to ethanol or acetate consumption once the sugars are depleted (Dashko *et al*, 2014; Rozpędowska *et al*, 2011).

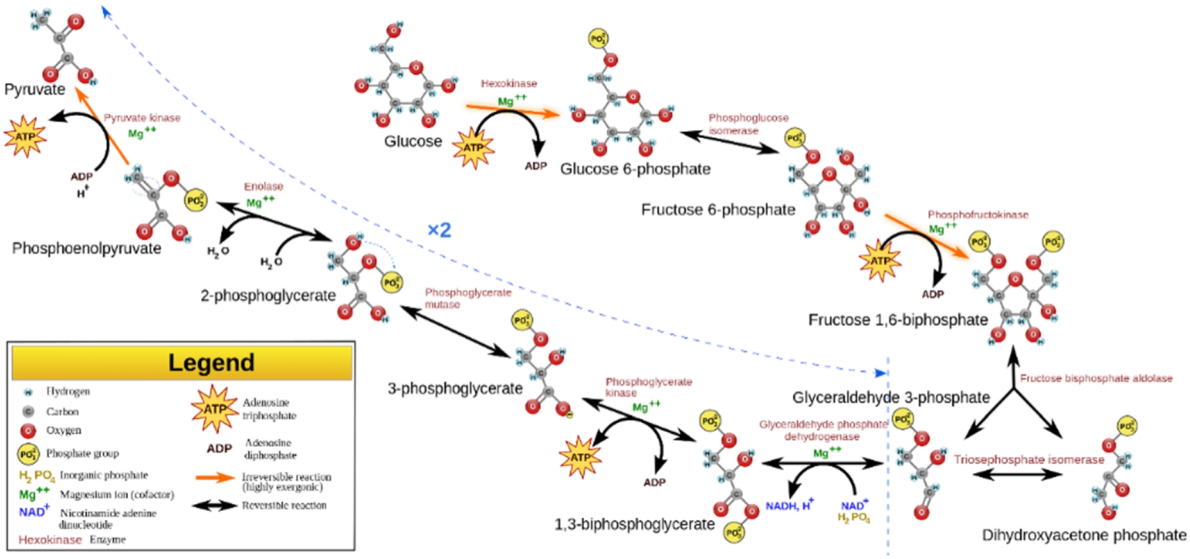

Figure I-2: Glycolysis. During glycolysis, a six carbon molecule of glucose is oxidized to two molecules of pyruvate. Net yield of glycolysis are two molecules of ATP and two molecules of NADH (picture from Marbet, 2009).

The metabolic signature that allows fermentation of glucose into lactate in aerobic conditions have been also described in higher organisms, both in cancer and several normal proliferating cells (Lunt & Vander Heiden, 2011; Shyh-Chang & Daley, 2015). This process is referred to as aerobic glycolysis or Warburg effect (Warburg, 1956). In normal proliferating cells, aerobic glycolysis has been observed in dividing lymphocytes (Hedeskov, 1968), thymocytes (Brand & Hermfisse, 1997) and fast dividing pluripotent stem cells (Folmes *et al*, 2012; Zhang *et al*, 2012). Aerobic glycolysis has been also observed in activated macrophages that are coping with increased biosynthesis upon activation (Kelly & O'Neill, 2015). It is widely accepted that transformed and proliferating cells have high rates of glycolysis (Warburg, 1956; DeBerar*dinis et al*, 2008) and frequently overexpress LDH, responsible for the conversion of pyruvate into lactate, and the recycling of NADH (Locasale & Cantley, 2011).

The presence of the Warburg effect in cancer cells and proliferating cells is suggestive of an advantage for cell growth. As mentioned before, one of the reasons that Crabtree-positive yeasts are over competing other microorganisms is their faster consumption of

carbon sources. Most of the proliferating mammalian cells are exposed to practically unlimited sources of nutrients and therefore should not be in need for competition with other cells (Vander Heiden *et al*, 2009). However, some studies show that increased glycolysis of cancer cells can outcompete tumor-infiltrating lymphocytes which require sufficient glucose for their effector functions (Chang *et al*, 2015; Ho *et al*, 2015). Moreover, cancer cells can be exposed to a niche with limited sources of nutrients, where their ability to compete would give them a higher chance to survive in inhospitable conditions (Kasinskas *et al*, 2014; Le *et al*, 2012b).

Obviously, proliferating cells need to provide sufficient ATP and biosynthetic blocks to build daughter cells. It has been shown that aerobic glycolysis (net production of 2 molecules of ATP) can be more efficient than OXPHOS (net production of up to 36 molecules of ATP) due to the faster rate of energy production (Pfeiffer *et al*, 2001). However, some authors hypothesize that ATP is not a limiting factor for cell growth due to several observations (Lunt & Vander Heiden, 2011; Locasale & Cantley, 2011; Liberti & Locasale, 2016). First, calculations suggest that ATP needs for mammalian division can be far lower than ATP needs for basal maintenance (Kilburn *et al*, 1969; Keibler *et al*, 2016). Second, in some cancer cells OXPHOS still contribute to ATP production (Zu & Guppy, 2004) and moreover metabolites from origins other than glucose have been shown to be oxidized in OXPHOS (DeBerardinis *et al*, 2008; Le *et al*, 2012a; Nieman *et al*, 2011). Another advantage of aerobic glycolysis for proliferating cells can be its capacity to support biosynthesis by providing common intermediates. These intermediates can feed several biosynthetic pathways to synthesize amino acids, nucleotides and lipids (Lunt & Vander Heiden, 2011). Liberti *et al.* proposed that the Warburg effect is an adaptation mechanism to support the biosynthetic requirements of uncontrolled proliferation, although, conversion of glucose into two lactate molecules leaves no room for biomass production (Liberti & Locasale, 2016). However, it has been shown that proliferating cells use less than 10% of glucose carbons to feed biosynthesis (DeBerardinis *et al*, 2007), leaving 90% of glucose to be processed in aerobic glycolysis.

Biosynthesis of new macromolecules is not based only on the availability of carbons and ATP. It is well known that NADPH is essential in anabolic reactions of fatty acids, amino

acids and nucleotide synthesis. An important source of NADPH in cells is the pentose phosphate pathway (PPP), which produces ribose-5-phosphate for the synthesis of nucleotides (Patra & Hay, 2014; Jiang *et al*, 2014). Increased glycolysis rate could therefore feed the needs of proliferating cells for NADPH.

Even though glycolysis is able to supply cells with energy and building blocks, it is not able to work independently of the other central carbon pathways. It is widely accepted that the TCA cycle is an important contributor to biosynthesis and NADPH production in proliferating cells (DeBerardinis *et al*, 2007; Liberti & Locasale, 2016; Gaglio *et al*, 2011). Interestingly, the TCA cycle in proliferating cells has been shown to use alternative substrates to glucose, for example glutamine (DeBerardinis *et al*, 2008; Le *et al*, 2012a; Nieman *et al*, 2011).

TCA cycle and OXPHOS

The tri-carboxylic acid (TCA) cycle, also known as citric acid cycle or Krebs cycle, is a series of eight reactions that oxidize acetyl-CoA derived mainly from fatty acids, carbohydrates and amino acids into two molecules of CO_2 and H_2O (Rustin *et al*, 1997) (Figure I-3). The TCA cycle is a great generator of energy in form of ATP or GTP, and reduced coenzymes (NADH and $FADH_2$) that are fed into oxidative phosphorylation pathway (OXPHOS) to produce ATP (Akram, 2014; White, 2006). Apart from the oxidation of acetyl-CoA, the TCA cycle is linked to other pathways by anaplerotic and cataplerotic reactions (Owen *et al*, 2002). Due to its ability to connect almost all individual metabolic pathways, the TCA cycle is considered to be a metabolic hub for the cell (Akram, 2014). The tri-carboxylic acid cycle has been found to take place in cytosol of prokaryotes and mitochondria of eukaryotes. Despite its generalized presence, not all species are encoding for all enzymes to provide a complete cycle turn (Huynen *et al*, 1999). Variations of the TCA cycle are mainly found in prokaryotes. Some bacteria are missing α-ketoglutarate dehydrogenase, obligate aerobes are oxidizing L-malate directly by molecular O_2 (Jurtshuk, 1996), and a truncated, reverse TCA cycle was found in some autotrophic bacteria and archaea (Huynen *et al*, 1999; Becerra *et al*, 2014). Another variation of the TCA cycle, known as glyoxylate cycle is present not only in bacteria but also in some

eukaryotes including plants, protozoa and fungi (Lorenz & Fink, 2001; White, 2006). The presence of this metabolic pathway in animals is controversial (Dunn *et al*, 2009).

Here we will focus on the TCA cycle occurring in mammals. As mentioned before, TCA cycle oxidatively decarboxylate acetyl-CoA resulting from glycolysis or from fatty acid and amino acid degradation (Rustin *et al*, 1997). The TCA cycle produces in one turn 1 GTP (or ATP), 3 molecules of NADH and 1 molecule of $FADH_2$. NADH and $FADH_2$ can donate their electrons to O_2 and reduce it to H_2O. This process is known as oxidative phosphorylation (OXPHOS) (Figure I-4). Electrons are transferred to oxygen via ETC, allowing free energy to be released in small increments. ETC is located on the inner mitochondrial membrane. During the transfer of electrons, protons are pumped out of the mitochondrial matrix through the membrane and an electrochemical proton gradient is formed. This gradient is then coupled to ATP synthesis by flow of protons moving back to the mitochondrial matrix through the ATP synthase (Lodish *et al*, 2000; Nelson & Cox, 2000).

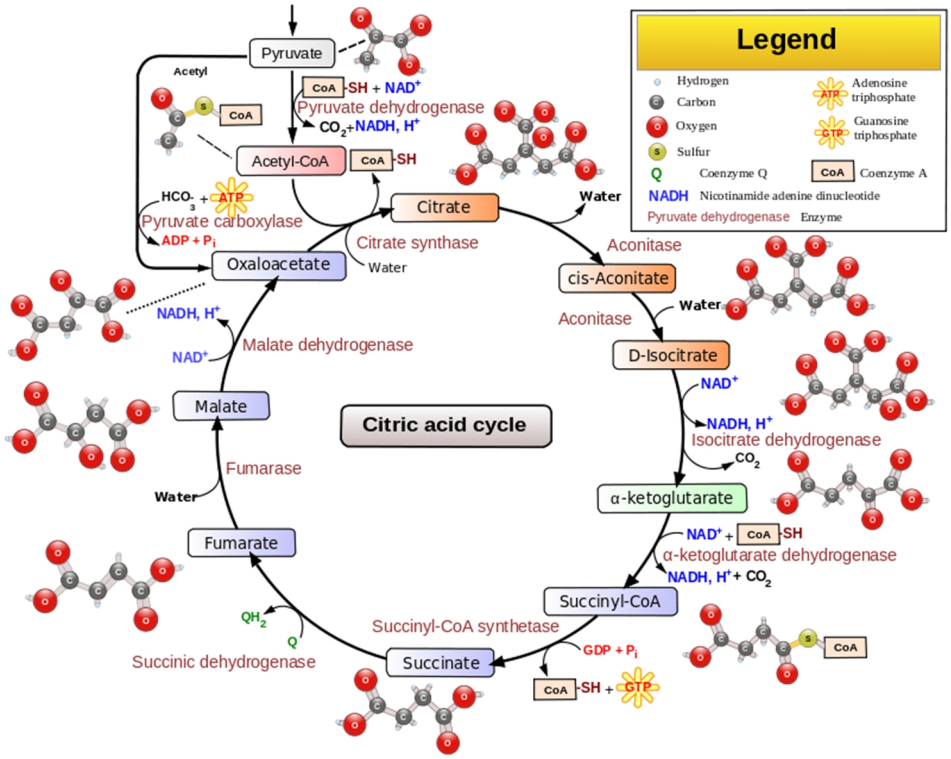

Figure I-3: TCA cycle: Four-carbon oxaloacetate condensate with two-carbon acetyl-CoA and citrate is formed. Citrate is isomerized to isocitrate, which undergo oxidative decarboxylation and alpha-ketoglutarate is formed. At this step, first NADH is formed. Alpha-ketoglutarate is oxidatively decarboxylated to succinyl-CoA and NADH is produced. Succinyl-CoA give rise to succinate and the energy formed by cleavage of the thioester bond is coupled to GTP formation. Succinate is subsequently converted into oxaloacetate in three reactions: oxidation, hydration and oxidation. Fumarate production is coupled with $FADH_2$ production, which donate electrons to ubiquinone (Q) and reduce it to QH2. Another molecule of NADH is formed by oxidation of malate to oxaloacetate. After oxaloacetate formation, the cycle can start again (Nelson & Cox, 2000) (picture from Narayanese *et al.*, 2008).

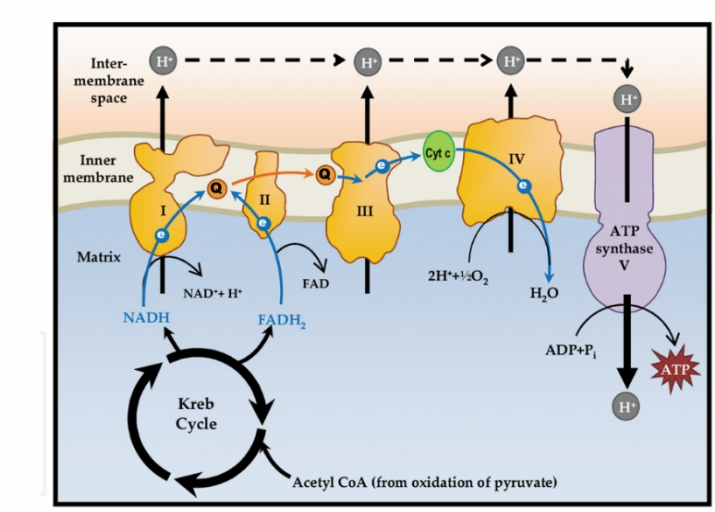

Figure I-4: Oxidative phosphorylation: NADH and $FADH_2$ molecules produced in TCA cycle flow are oxidized and transfer their electrons through series of membrane proteins. Electrons are passed from higher to lower energy level and release energy, which is used to pump H+ ions to intermembrane space and protein gradient is formed. Final acceptor of electrons is oxygen and H_2O is produced. Protein gradient formed across the membrane is flowed through ATP synthase and ATP is produced (Nelson & Cox, 2000) (picture from Yusoff *et al.*, 2015).

Besides its role in oxidative catabolism of carbohydrates, fatty acids and amino acids, the TCA cycle also functions as a provider of precursors for many biosynthetic (anabolic) pathways. Intermediates leave the cycle to be used in biosynthetic processes to produce glucose, fatty acids or non-essential amino acids. The process of removal of intermediates from the TCA cycle is called cataplerosis, however it is not always linked to biosynthetic processes. There are several cataplerotic pathways, mainly driven by PEPCK, aspartate aminotransferase, and glutamate dehydrogenase (Owen *et al*, 2002; Nelson & Cox, 2000). This mechanism serves to avoid the accumulation of anions in the mitochondrial matrix and to maintain its steady state flux. As the intermediates leave the TCA cycle, they have to be replenished by anaplerotic reactions to ensure continued function of the cycle. Pyruvate carboxylation and glutaminolysis are well known anaplerotic reactions (Owen *et al*, 2002; Nelson & Cox, 2000). In mammalian cells, glutamine is an important contributor to the TCA cycle (Deberardinis & Cheng, 2010). The role of glutamine in proliferating cells is mostly in ATP synthesis. In addition, glutamine is an important biosynthetic precursor (DeBerardinis *et al*, 2007; Neermann & Wagner, 1996; Locasale &

Cantley, 2011) and can be metabolized in oxidative or reductive direction.

According to several authors (DeBerardinis *et al*, 2008; Mattaini *et al*, 2016; Fritz & Fajas, 2010), anabolism and catabolism in the TCA cycle are defined by the cell proliferating state. The traditional view of metabolism of non-proliferating cells is to maintain homeostasis that heavily rely on ATP. Therefore the TCA cycle role in non-proliferating cells is to produce the maximum yield of ATP by full oxidation of substrates. Proliferating cells have a necessity to duplicate all macromolecular components when dividing. Therefore, they tend to use the TCA cycle for biosynthesis rather that ATP production (DeBerardinis *et al*, 2008; Mattaini *et al*, 2016; Fritz & Fajas, 2010). Due to the anabolic and catabolic activities, the TCA cycle is characterized also as an amphibolic pathway (Owen *et al*, 2002; Nelson & Cox, 2000).

2 Cancer

Evolution of multicellular organisms required parallel evolution of controlling systems to avoid aberrant proliferation and to maintain their organization and functionality (Alberts *et al*, 2002). Adult multicellular organisms contain proliferating cells (e.g. pluripotent stem cells, skin fibroblasts, epithelial cells), which proliferation is tightly controlled (Cooper, 2000b). However, cancer cells do not respect the regulation by the multicellular organism. We could say that cancer cells evolved from a multicellular organism back to the unicellular state since their only goal is to reproduce quickly. Cancer cells do not respond to control mechanisms of proliferation and their growth rate can only be limited by environmental conditions (availability of nutrients, oxygen, etc.) (Trosko & Kang, 2012; Casás-Selves & Degregori, 2011; Mattaini *et al*, 2016). Most cancers originate from a single cell acquiring mutations that allow it to overcome growth factor dependence and give it a growth advantage. Progressively, cancer cells accumulate more mutations (Alberts *et al*, 2002; Vander Heiden *et al*, 2009). There is growing evidence, that oncogenic mutations are affecting uptake and metabolism of nutrients. Reprogramed metabolism provides malignant properties to cancer cells and promotes cell survival and growth (Vander Heiden *et al*, 2009; DeBerardinis & Chandel, 2016). Interestingly, metabolic changes occurring in cancer lead to a certain dependence on various nutrients such as glucose or glutamine. Both of them can sustain biosynthesis, energy production and antioxidant defense (De Vitto *et al*, 2016).

The study of cancer metabolism is devoted to the identification of metabolic pathways that are critical or selective for tumor growth and survival. Discovery of those pathways has helped to reveal new therapeutic targets (Keibler *et al*, 2016) and to understand the complex interplay of cancer and the organism.

2.1 Cancer metabolism

The Warburg effect

Several hallmarks of cancer metabolism has been identified to date. Probably the best known metabolic hallmark is aerobic glycolysis, also termed the Warburg effect (Warburg, 1956; Pavlova & Thompson, 2016). The Warburg effect is basically a metabolic behavior whereby the rate of glucose uptake is dramatically increased, and glucose tends to be oxidized to lactate even in the presence of oxygen (Warburg, 1956). The advantages of the Warburg effect in proliferating cells have been described in chapter Glycolysis and the Warburg effect. Particularly, increased flux through glycolysis meet higher demands of cancer cells for ATP and biosynthetic precursors. Knowledge that cancer cells consume more glucose than non-proliferating cells was successfully used in diagnostic techniques such as ^{18}F-deoxyglucose positron emission tomography to localize tumor sites in human body (Hsu & Sabatini, 2008; Jones & Thompson, 2009).

Several drivers of the Warburg effect have been identified, being some of them activated by specific conditions of the microenvironment. For example, hypoxia-inducible factor 1α (HIF1a), which induces transcription of glucose transporter, glycolytic enzymes and LDH-A. HIF1a is stabilized under hypoxic conditions (Jaakkola *et al*, 2001). However its stability is a common feature of several cancers even under normoxia, for example due to effect of succinate on HIF1a prolyl hydroxylase inhibition (Selak *et al*, 2005; Lussey-Lepoutre *et al*, 2015). Likewise, oncogene c-MYC can enhance glycolysis by transactivating several glycolytic genes (Osthus *et al*, 2000) and LDH-A (Shim *et al*, 1997). Other regulators of the Warburg effect are the PI3K/AKT/mTOR pathway, RAS and p53. Activated AKT increases glycolysis and lactate production. Moreover, AKT activation in non-transformed cells is sufficient to induce the Warburg effect (Elstrom *et al*, 2004; Rathmell *et al*, 2003) by regulation gene expression of glycolytic enzymes, for example GLUT1 (Barthel *et al*, 1999). Hyperactive RAS has been linked with increased glucose consumption and activation of PFK-1 in transformed cells (Chiaradonna *et al*, 2006; Tong *et al*, 2009). Many cancers contain mutated p53. This mutation leads to the regulation of TIGAR (TP53-induced glycolysis and apoptotic regulator) and subsequent activation of

glycolysis (Jose *et al*, 2011).

Initially, fermentation of glucose to lactate in cancer cells was thought to result from damaged respiration (Warburg, 1956). Further investigation in the past two decades revealed that mitochondria and respiration is intact in most cancers and that most cancer cells use aerobic respiration for ATP production (Zu & Guppy, 2004; Zheng, 2012; Sullivan *et al*, 2015). Besides energy production, mitochondria functions as a factory of anabolic building blocks through the TCA cycle. Constant withdrawal of intermediates from the TCA cycle for biosynthetic purposes require anaplerosis, a process of carbon replenishment.

Metabolism of glutamine

The major anaplerotic sources of carbon are pyruvate (from glycolysis) and glutamine, metabolized by pyruvate carboxylase (PC) and glutaminase (GLS), respectively (Sellers *et al*, 2015). There is growing evidence of the importance of glutamine in cancer, although limited information exists regarding pyruvate carboxylation (Phannasil *et al*, 2015). Recently, non-small lung cancer cells were shown to depend on pyruvate carboxylation for their growth (Sellers *et al*, 2015). Additionally, some cancer cells that can survive in the absence of glutamine were shown to use PC mediated anaplerosis (Cheng *et al*, 2011; Phannasil *et al*, 2015). However, glutamine has been suggested as the most significant anaplerotic precursor in cancer cells. Besides biosynthesis, whether providing nitrogen or anabolic carbons, glutamine contributes to metabolism of cancer cells by supporting cell defenses against ROS and by participating in ATP production (Deberardinis & Cheng, 2010; De Vitto *et al*, 2016).

It is well known that glutamine is the most abundant free amino acid in human blood and also in different culture media (Zong *et al*, 2016; Yang & Xiong, 2012). Several reports show that cancer cell lines display avid glutamine consumption (Le *et al*, 2012a; Cetinbas *et al*, 2016; Bode *et al*, 2002) and that glutamine might turn essential for these cells (Reitzer & Wice, 1979; DeBerardinis *et al*, 2007; Fan *et al*, 2013). Wise *et al*. observed that critical need of glutamine for cancer cells is to support anaplerosis (Wise *et al*, 2008). “Addiction” of cancer cells to glutamine has been linked to c-MYC, which is a commonly

activated oncogene in a variety of tumors. Activation of c-MYC drives glutamine uptake, and c-MYC is implicated in up-regulating GLS expression (Wise *et al*, 2008; Gao *et al*, 2009). Moreover, glutamine starvation leads to apoptosis preferentially in cells with activated c-MYC (Yuneva *et al*, 2007).

The importance of glutamine for cancer cells was supported by experiments targeting glutamine metabolism. Inhibition of GLS caused growth suppression and suppression of transformation (Yang *et al*, 2009c, 2014b; Wang *et al*, 2010; Sellers *et al*, 2015). Additionally, similar effects were observed *in vivo*, where inhibition of GLS decreased tumor growth (Lobo *et al*. 2000; Le *et al*. 2012). Targeting glutamine metabolism as an antitumor strategy moved already to clinic. CB-839, a derivate of the GLS inhibitor BPTES, is currently in phase I clinical trials for solid tumors, lymphoid and myeloid malignancies (Jin *et al*, 2016). All this suggest an important role of glutamine in cancer metabolism.

Glutamine can undergo two fates when entering the TCA cycle. It can be oxidized in a forward direction (glutaminolysis) or it can feed reductive carboxylation (Figure I-5). Glutaminolysis can support an anaplerotic function, ATP fueling and NADPH production through malic enzyme (Vander Heiden *et al*, 2011). Glutamine metabolism via reductive carboxylation pathway forms citrate, which is transported to cytosol and serve as a source of acetyl-CoA and oxaloacetate (Zhang *et al*, 2014; Vander Heiden *et al*, 2011). Acetyl-CoA is an essential unit for lipid synthesis, which is occurring in proliferating cells and is activated by PI3K signaling (DeBerardinis *et al*, 2006). Even though glucose represents a major source of acetyl-CoA in cells (DeBerardinis *et al.*, 2007; C. Yang *et al.*, 2014), it has been observed that glutamine is an important source of lipogenic acetyl-CoA pool in some cancer cells by using reductive carboxylation (Yang *et al*, 2014a; Fendt *et al*, 2013; DeBerardinis *et al*, 2007; Metallo *et al*, 2012). Interestingly, reductive carboxylation of glutamine and acetyl-CoA production in cancer cells was shown to increase under hypoxia (Wise *et al*, 2011; Metallo *et al*, 2012). Besides glutamine and glucose, cytosolic acetyl-CoA was shown to be acquired also by activation of the metabolism of acetate (Schug *et al*, 2015).

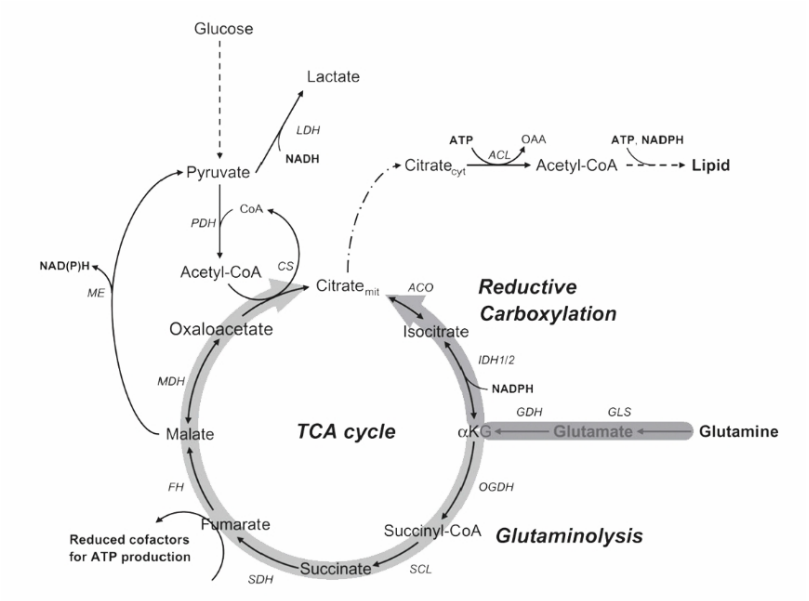

Figure I-5: TCA cycle with indicated two directions of carbon flow from glutamine. Oxidation of glutamine in forward direction is called also glutaminolysis. Reverse direction is referred to as reductive carboxylation (picture from Zhang *et al*, 2014)

Serine synthesis pathway

As mentioned before, the main reason for metabolic changes occurring in cancer cells is the need to support cell growth and proliferation. Recently, attention of several investigators has centered on the anabolic pathway of serine synthesis. Serine synthesis was identified as an important pathway in various cancers (Mattaini *et al*, 2016). Even though serine can be obtained from extracellular sources, amplification of PHGDH, the first enzyme for its *de novo* synthesis, was observed mainly in breast carcinoma and melanoma (Possemato *et al*, 2011; Locasale *et al*, 2011; Mullarky *et al*, 2011). Moreover, inhibition of PHGDH in cancer cells with high PHGDH activity causes cell death even in the presence of extracellular serine (Pacold *et al*, 2016; Possemato *et al*, 2011). Different studies confirmed the importance of PHGDH for cancer cell growth as well as *in vivo* (Possemato *et al*, 2011). Serine fulfil various roles in metabolism. It is an important precursor for other non-essential amino acids like glycine and cysteine, and participate in the production of sphingolipids, phospholipids and phosphatidylserine. Glycine can be

later used for nucleotide synthesis and the synthesis of glutathione (Mattaini *et al*, 2016; Amelio *et al*, 2014). Interestingly, experiments performed with cells requiring extracellular serine have shown that glycine is not able to rescue cells growing in the absence of serine. Furthermore, glycine absence in media had no effect on cell proliferation (Labuschagne *et al*, 2014). The metabolic advantage of serine over glycine is therefore based on its greater anabolic capacity, since conversion of serine to glycine provides carbons that feed one-carbon metabolism pathway. One-carbon metabolism is centered around the transformation of folate and provide components for the synthesis of macromolecules used in cellular growth and proliferation (Amelio *et al*, 2014). The serine synthesis pathway members can be induced by several factors, like c-MYC, NRF2 and ATF4 (Yang & Vousden, 2016).

According to the important role of serine in cancer metabolism, it has been observed that it can serve as an allosteric activator of the M2 isoform of pyruvate kinase (PKM2). This isoform is expressed in proliferating and cancer cells (Yang & Vousden, 2016; Christ*ofk* *et al*, 2008). Chaneton *et al.* observed, that serine can allosterically regulate PKM2, and a drop in serine levels caused decreased PKM2 activity (Chaneton *et al*, 2012). Decreased conversion of PEP to pyruvate favors the accumulation of glycolytic intermediates which can be redirected to anabolic pathways (e.g. serine synthesis and PPP) (Yang & Vousden, 2016), thus providing a feedback loop.

Microenvironment and cancer metabolism

Commonly, solid tumors present significant heterogeneity of nutrients and oxygen availability. Cancer cells are able to cope with unfavorable conditions thanks to the great metabolic plasticity which is characteristic to them (Zheng, 2012; DeBerardinis & Chandel, 2016).

Among the adaptations to hypoxic conditions, the ability of cancer cells to diminish ATP dependent processes to maintain ATP/ADP ratio is of high importance (DeBerardinis & Chandel, 2016). Additionally, some hypoxic cancer cells are able to partially use oxidative phosphorylation to provide ATP from glutamine and maintain the TCA cycle (Le *et al*, 2012a, 2014).

As a result of poor vascularization and high rates of nutrient consumption, cancer cells are often exposed to conditions of nutrient limitation (Pavlova & Thompson, 2016). Under these conditions, cancer cells have access to various catabolic pathways to provide necessary pools of metabolic intermediates (e.g. protein degradation to produce amino acids) (DeBerardinis & Chandel, 2016). Macromolecule recycling autophagy is used by cancer cells in a regulated process in which macromolecules and organelles are degraded in the lysosome. These strategies are not able to provide new biomass but allow cells to survive prolonged periods of nutrient deprivation (DeBerardinis & Chandel, 2016; Pavlova & Thompson, 2016).

The microenvironment of cancer cells can be shaped also by the waste products of cancer metabolism. Glycolysis produces lactate which is extracellularly released. Increasing lactate levels has a positive effect on angiogenesis, for example through the activation of NF-κB and PI3K signaling (Végran *et al*, 2011; Ruan & Kazlauskas, 2013). Lactate transport from cells through MCT transporters is coupled with H+ flux, which is responsible for acidification of the microenvironment. Acidity is suggested to contribute to tumor invasiveness through its negative effect on normal tissue (Estrella *et al*, 2013).

In the context of the novel hypothesis of the reverse Warburg effect pathway in tumors, stromal cells with increased glycolysis would release lactate to the extracellular microenvironment, where cancer cells may consume it as a bioenergetic substrate to support cell growth and proliferation (Pavlides *et al*, 2009; Witkiewicz *et al*, 2012).

Study of cancer metabolism revealed several metabolic specificities that can be used in developing new targeting strategies in cancer therapy. However, difficulty lies in the great flexibility of the metabolic network and the ability of cancer cells to adapt to challenging conditions. Therefore, complete understanding of cancer metabolism is necessary to develop the chemotherapeutical strategies that are broad enough to cover multiple approaches. There are still many pathways and metabolites that should be investigated in the context of cancer. One of the pathways that is waiting for its rediscovery is the reverse glycolytic pathway that is initiated by the conversion of oxaloacetate to PEP by PEPCK enzyme. This reaction is the first step of gluconeogenic pathway in the liver and kidney and bypasses the thermodynamically irreversible conversion of pyruvate to PEP.

3 Metabolism of undifferentiated cells; the case of neuronal progenitors

Every cell in the mammalian body originate its existence from embryonal stem cells (ESCs). ESCs have self-renewal capacity and form mature cells through the process known as differentiation (Reya *et al*, 2001). In this process, ESCs give rise to other populations of organ specific stem cells and progenitors. It is interesting to mention that stem cells share several characteristics with cancer cells. They both have self-renewal capacity and common pathways might be implicated in the regulation of this process (Reya *et al*, 2001). Additionally, stem cells and cancer cells, both proliferating cells, might use similar metabolic strategies to fulfill energetic and anabolic requirements of proliferation (Shyh-Chang *et al*, 2013; Varum *et al*, 2011). Moreover, both cancer and stem cells are metabolically plastic (flexible) (Folmes *et al*, 2012; Ramanujan, 2015). Metabolic plasticity seems to be important for stem and progenitor cells when coping with changing energetic and biosynthetic demands during differentiation (Folmes *et al*, 2012; Agathocleous *et al*, 2012), and when adapting to specific niches with varied availability of nutrients (Simsek *et al*, 2010).

It is well known that mammals can produce lactate in placenta and transfer it to the fetus (Jones, 1976; Villee, 1953; Battaglia & Meschia, 1978). Moreover, lactate is considered to be an important substrate for oxidative fetal and neonatal metabolism (Beard & Nathanielsz, 1984; Platt & Deshpande, 2005; Bartelds *et al*, 1999; Char & Creasy, 1976) and has been studied as a potential energy and carbon substrate for the developing brain for decades. In this context, neurons and neuronal stem cells are able to survive in glucose-free medium containing lactate as their only energy source (Wohnsland *et al*, 2010). In addition, various studies bring evidence of its presence in normally developing brain (Bolaños & Medina, 1993; Medina *et al*, 1996; Lust *et al*, 2003).

3.1 Brain metabolism during development

The concentration of lactate in rat brain is changing with developmental stage. Lactate concentration in fetal brain is higher when compared to postnatal day 7 and adult brain (Lust *et al*, 2003). Similarly, decreasing brain lactate concentration with increasing age was observed in human neonates, together with higher lactate concentration in the neonatal periods comparing to 1-2 months of age (Tomiyasu *et al*, 2016). Consistently, an increased rate of lactate transport through the blood brain barrier was found in fetal rats and guinea-pigs. This transport declined with advancing age (Bissonnete *et al*, 1991; Cremer *et al*, 1976). The importance of lactate as an energy substrate was demonstrated in late gestation in rats by Bolaños and Medina. Moreover, they observed the utilization of lactate as a substrate for lipogenesis (Bolaños & Medina, 1993). Interestingly, lipogenesis seems to be important for neurogenesis of stem and progenitor cells also in the adult brain (Knobloch *et al*, 2013).

The metabolic profile of neural progenitors has been described to involve aerobic glycolysis, whereas neurons relay on oxidative phosphorylation (Zheng *et al*, 2016; Agathocleous *et al*, 2012; Candelario *et al*, 2013). Similarly, low oxidative phosphorylation was identified also in progenitors of other origins, like hematopoietic progenitors (Simsek *et al*, 2010). Dependency for glycolysis in neural stem cells seems to be more relevant in the context of metabolic intermediate production (e.g. PPP) rather than ATP production, as cell viability is affected only partially by change of glucose to galactose that yields no ATP during its metabolism (Candelario *et al*, 2013). It is important to mention, that studies claiming high aerobic glycolysis in neural progenitors and stem cells do ignore the fact that lactate or ketone bodies are present as metabolic substrates in developing brain and use glucose and glutamine as the only energy and carbon sources.

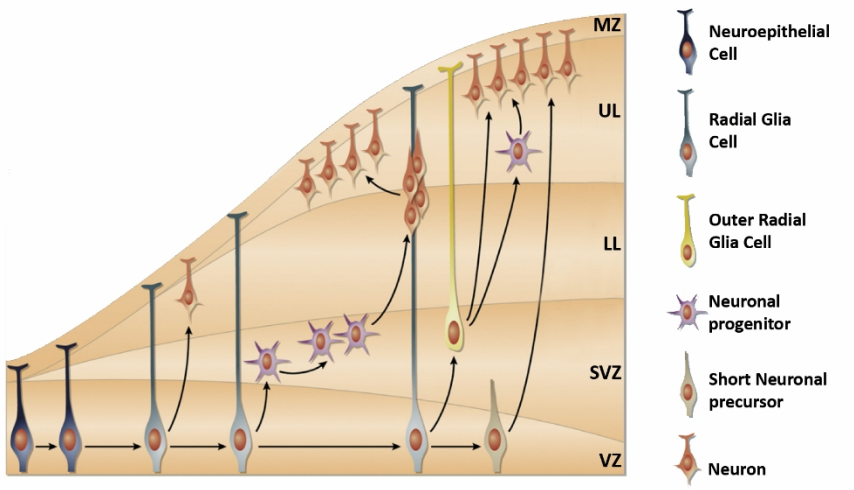

Figure I-6: Developing of neurons in neocortex. All cells of the nervous system are originating from neuroepithelial cells (NECs) which during embryogenesis act as a neural stem cells (Götz & Barde 2005; Yamashita 2013). NECs start neocortex formation and they divide symmetrically to expand pool and later transform to radial glia cells (RGs). RGs is providing several precursors for neuron formation and helps newborn neurons to migrate toward marginal zone (MZ). The best known function of RGs is its ability to guide radial migration of newborn neurons thanks to the radial extension of their cell body through subventricular zone and cortex layers to the marginal zone (Campbell & Götz 2002). RGs divide symmetrically (to expand pool) or asymmetrically, where neuronal progenitor (NP)/ neuron and RGs are produced (Noctor *et al.* 2004; Homem *et al.* 2015). RGs can give rise also to short neuronal precursor and outer radial glia. Neuronal progenitors in subventricular zone (SVZ) undergo one or two symmetrical divisions where at the end 2 or 4 neurons are produced, respectively (Kowalczyk *et al.* 2009; Pontious *et al.* 2007; Wu *et al.* 2005; Franco & Müller 2013). NPs can be distinguished from RGs by its reduced expression of Pax6 and increased expression of the progenitor marker TBR2.Ventricular zone (VZ), Subventricular zone (SVZ), Lower layers (LL) V-VI, Upper layers (UL) II-IV, Marginal zone (MZ) –layer I (adapted from Franco and Müller, 2013).

Shortly after birth, neonates undergo important extrauterine metabolic adaptations. Blood glucose concentration drops after birth and get stabilized approximately after three hours (Platt & Deshpande, 2005), when hepatic gluconeogenesis is already sufficiently effective (Kalhan *et al*, 1980). An increased lactate consumption was observed during the first two hours after birth, which suggest the importance of lactate in this challenging period (Cuezva *et al*, 1980). Interestingly, it has been suggested that fasted neonates can supply only 80% of the brain energy needs through glucose oxidation, emphasizing the need for alternative substrates (e.g. lactate and ketone bodies) (Denne & Kalhan, 1986).

All this suggest that lactate or ketone bodies might play a relevant role as a metabolic fuel of immature developing brain in fetal, early newborn and suckling mammals. However it is important to mention that ketone bodies are more relevant to lipogenesis (Paton *et al*, 1989) or amino acid synthesis (DeVivo *et al*, 1975) rather than its oxidation during the development in mammals.

3.2 Brain metabolism in the adulthood

Neurogenesis does not take place solely during embryogenesis and during early development, but a population of neural stem cells is maintained also in adult brain in the subventricular zone of the lateral ventricle and subgranular zone of the hippocampal dentate gyrus (Seaberg & Van Der Kooy, 2003; Tonchev *et al*, 2003). It has been suggested that the population of stem cells in adult brain proceed from a type of progenitor cell called radial glia (Candelario *et al*, 2013; Malatesta *et al*, 2008).

The presence and functionality of lactate in adult brain has been subject of discussion for a long time. Traditionally, the adult brain is considered a high energy demanding organ with glucose as a major substrate (Agostini *et al*, 2016) that provides necessary ATP for the maintenance of physiological brain functions, cell maintenance and neurotransmitter synthesis (Mergenthaler *et al*, 2013). However, several *in vitro* studies have shown that cultured brain cells or brain slices are able to metabolize other substrates, for example lactate (Bouzier-Sore *et al*, 2003; Wohnsland *et al*, 2010; Qu *et al*, 2000; Gallagher *et al*, 2009a). In 1994, Pellerin & Magistretti developed the hypothesis of "astrocyte to neuron lactate shuttle" (ANLS). They observed that glutamate released from synapses stimulates glucose uptake and lactate production in astrocytes (Pellerin & Magistretti, 1994). Similarly, other studies observed lactate production by glial cells *in vitro* (Dringen *et al*, 1993; Poitry-Yamate *et al*, 1995). ANLS hypothesis suggest that lactate produced by astrocytes is used as a primary energy substrate by neurons (Pellerin & Magistretti, 1994; Pellerin *et al*, 1998). It is worth to mention that lactate can inhibit glucose consumption in neurons. This effect was observed in primary cultures of neurons, in the presence of elevated concentration of lactate (Tabernero *et al*, 1996; Bliss

& Sapolsky, 2001). However, several studies argue that neurons are able of efficient glucose consumption that can also support oxidative phosphorylation (Dienel, 2012; Simpson *et al*, 2007). The debate on lactate function in adult brain reached a consensus as stated lately by Tang *et al.*: "astrocytes can release L-lactate upon various stimuli and that L-lactate may affect neuronal function, but the mechanism of L-lactate action remains unclear" (Tang *et al*, 2014).

Another context where lactate is important for brain metabolism seems to be certain pathological conditions. Lactate has been shown as a preferred substrate in the brain after traumatic brain injury (Glenn *et al*, 2015) or after exposure to hypoxia (Bliss & Sapolsky, 2001). Interestingly, several materials proposed for regenerative medicine for damaged brain contain lactic acid as a component (Alvarez *et al*, 2013; Lampe *et al*, 2009; Orive *et al*, 2009). This type of biomaterials containing lactic acid polymers are able to support neural stem cell niche and sustain neurogenesis (Alvarez *et al*, 2013). This points to the importance of lactate not only in the developing brain but also the adult brain undergoing reparation.

3.3 Lactate metabolism

Lactate is a hydroxycarboxylic acid that is chiral and in mammals we can find both stereoisomers L-(+)-lactate and D-(-)-lactate (Ewaschuk *et al*, 2005; Adeva-Andany *et al*, 2014). Lactate is formed from pyruvate and for a long time was considered as a waste product that is mainly generated by glycolysis under various physiological or pathological conditions (Gladden, 2004). However, lactate can serve also as an energy substrate and can be metabolized to pyruvate. Reversible conversion of pyruvate to L-lactate is catalyzed by lactate dehydrogenase (LDH) and requires NAD+ which is reduced to NADH. In the case of D-lactate metabolism, D-lactate dehydrogenase (D-LDH) is used (Ling *et al*, 2012). L-lactate forms the majority of lactate in mammalians, whereas D-lactate is present at very low concentrations (Ewaschuk *et al*, 2005; Maessen *et al*, 2014).

Lactate is transported through the cytoplasmic membrane by proton-linked monocarboxylate transporters MCT1, MCT2, MCT3 and MCT4. Besides lactate, these

MCT transporters are able to transfer other substrates, such as pyruvate and ketone bodies (Pérez-Escuredo *et al*, 2016; Halestrap & Wilson, 2012). Amongst all MCTs, MCT4 shows the lowest affinity for lactate. MCT1 and MCT3 shows intermediate affinity, and MCT2 the highest. In the brain, MCT1, MCT2 and MCT4 expression has been detected. MCT1 and MCT2 were found to be expressed both in neurons and astrocytes, with prominent expression of MCT2 in neurons. The expression of MCT4 seems to be restricted to astrocytes (Debernardi *et al*, 2003; Pierre & Pellerin, 2005).

MCT1 and MCT2 transporters were also found in mitochondria of neurons, located on the inner membrane (Hashimoto *et al*, 2008). Similarly, the mitochondrial localization of MCT1 was found in cardiac and skeletal muscle (Brooks *et al*, 1999a). Lactate transported to the mitochondria can be converted to pyruvate by mitochondrial LDH that was found in neurons, cardiac muscle and some cancer cells (Hashimoto *et al*, 2008; Chen *et al*, 2016; Brooks *et al*, 1999b). Lactate, independently of its localization (cytosolic or mitochondrial) can be further metabolized through pyruvate in the TCA cycle or in the gluconeogenic pathway, as it is observed in the liver (Nelson & Cox, 2000).

In addition to its metabolic role, lactate can affect cAMP levels through the G-protein coupled receptor GPR81 (HCAR1) receptor (Ahmed *et al*, 2010). Lactate binding to GPR81 decreases cAMP production and therefore can regulate the activity of several pathways. It has been found, that GPR81 is widely distributed in the brain tissue, mainly in neurons (Bergersen & Gjedde, 2012).

4 PEPCK and gluconeogenesis

Gluconeogenesis is a metabolic pathway that produces glucose from non-carbohydrate precursors. The physiological role of gluconeogenesis is to maintain blood glucose levels during fasting (Chandramouli *et al*, 1997) and exercise (Petersen *et al*, 2004). The primary gluconeogenic organ is the liver (Rui, 2014). This pathway has several steps in common with glycolysis, but three irreversible reactions catalyzed by hexokinase, phosphofructokinase and pyruvate kinase are bypassed by new reactions catalyzed by glucose 6-phosphatase, fructose 1,6-bisphosphatase and phosphoenolpyruvate carboxykinase (PEPCK), respectively (Figure I-7). This pathway can feed several metabolic pathways besides glucose production. One of them is implicated in the synthesis of glycerol, backbone of triacylglycerol in a pathway known as glyceroneogenesis (Hanson *et al*, 2006). Glyceroneogenesis is an abbreviated version of gluconeogenesis, in which dihydroxyacetone phosphate is reduced by glycerol-3-phosphate dehydrogenase into glycerol. This pathway has been shown to function in adipose tissue and liver upon fasting and plays a role in triglyceride turnover (Kalhan *et al*, 2001; Ballard *et al*, 1967; Nye *et al*, 2008). Free fatty acids released during lipolysis upon fasting are re-esterified to triglycerides in the liver and adipose tissue and deposited back in the adipose tissue (Hanson *et al*, 2006).

PEPCK catalyzes the first step in the gluconeogenic pathway (Nelson & Cox, 2000). This enzyme allows the synthesis of intermediates that can be fed through the glycolytic pool into glycerol, and possibly to serine and one-carbon metabolites, among others, as well.

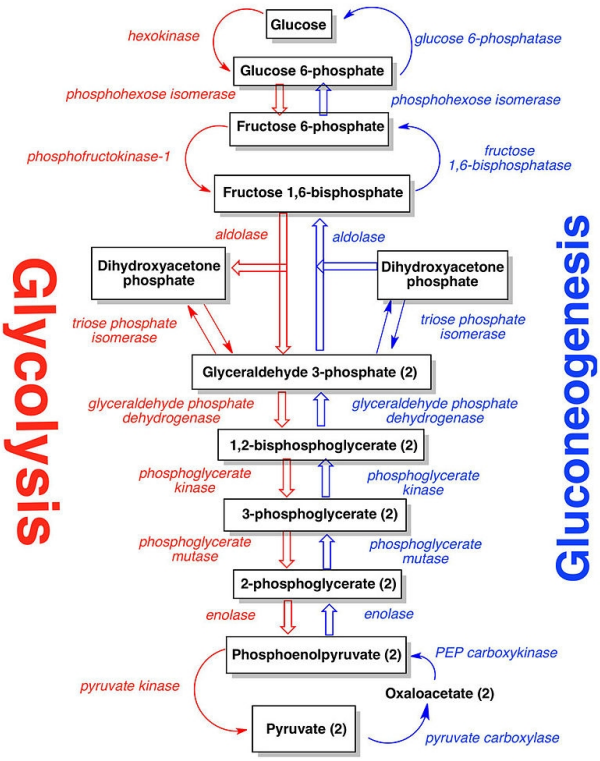

Figure I-7: Comparison of gluconeogenic and glycolytic pathways. These two pathways differ in three steps that are catabolized by hexokinase, phosphofructokinase-1 and pyruvate kinase. These three reaction are energetically unfavorable in the reverse direction and cannot occur. Therefore, gluconeogenesis overcome these reactions by using glucose 6-phosphatase, fructose 1,6-bisphosphatase and phosphoenolpyruvate carboxykinase (PEPCK). Oxaloacetate, the substrate of PEPCK is synthesized by pyruvate carboxylase from pyruvate (picture from Dwong527, 2013).

4.1 PEPCK

Phosphoenolpyruvate carboxykinase (PEPCK) is an enzyme that catalyzes the nucleotide dependent reversible decarboxylation of oxaloacetate (OAA) to phosphoenolpyruvate (PEP) with the concomitant transfer of a phosphate group from nucleoside triphosphate, mainly GTP (Figure I-8). The reaction also requires bivalent metal ions as magnesium and manganese (Lee *et al*, 1981). By using PEPCK, the cell can bypass the thermodynamically unfavorable conversion of pyruvate to phosphoenolpyruvate (PEP). It is important to note that the PEPCK reaction is the only pathway that is able to communicate TCA cycle

intermediates with the glycolytic intermediary pool above pyruvate.

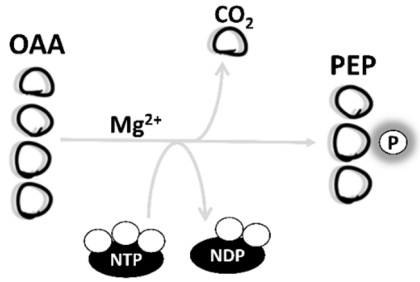

Figure I-8: Conversion of oxaloacetate to phosphoenolpyruvate catalyzed by PEPCK. PEPCK catalyze metal-nucleotide coupled decarboxylation of OAA to PEP.

PEPCK is present in all known groups of living organisms. Higher eukaryotes, most of archaea and some bacteria contains GTP (ITP) dependent PEPCK. Whereas ATP dependent PEPCK is present in fungi, plants and most bacteria (Aich & Delbaere, 2007; Valle *et al*, 2017; Fukuda *et al*, 2004). Amino acid sequences of PEPCKs show considerable homology (Hanson & Reshef, 1997; Delbaere *et al*, 2004; Fukuda *et al*, 2004). Aich *et al*. performed extensive amino acid sequence alignment which shows that the active, metal binding and catalytic domains are almost, but not completely, conserved in PEPCK of different origins. Nucleotide binding sites are also almost conserved within each category (GTP and ATP dependent PEPCKs) (Aich & Delbaere, 2007).

The reaction catalyzed by PEPCK is reversible, however *in vivo* in mammals this conversion is unfavorable due to higher Km for PEP and GDP when compared to its physiological concentrations, whereas Km for oxaloacetate and GTP is within their physiological concentration range (Nowotny & Yang, 2009; Hanson & Garber, 1972; Ballard, 1970). This suggests that the direction of PEPCK reaction in mammals is towards PEP production. This is not the rule in other species, where the reverse reaction has been observed, such as in bacteria (Riedel *et al*, 2001), helminth parasites and nematodes (Kumar Verma *et al*, 2013). In these species PEPCK shows anaplerotic activity by synthesizing oxaloacetate. Interestingly, Latorre *et al*. recently found a mutant of PEPCK-C in pigs with amino acid Met139Leu substitution occurring far away from the active center. PEPCK-C 139Leu showed increased activity in the anaplerotic direction compered

to 139Met PEPCK-C (Latorre *et al*, 2016).

It is well known that PEPCK activity in the majority of eukaryotes is distributed between two different proteins; a cytosolic (PEPCK-C) and a mitochondrial (PEPCK-M) isoform. Both are coded for by distinct nuclear genes; PCK1 and PCK2, respectively. Molecular masses of both isoforms are virtually identical (about 74,000 kDa) (Croniger *et al*, 2002a; Ballard & Hanson, 1969) and both enzymes have similar kinetic properties (Hanson & Patel, 1994). Yang *et al*. suggest that genes for PEPCK-C and PEPCK-M diverge from a common bacterial enzyme by duplication and gene rearrangement (Yang *et al*, 2009b).

Despite PEPCK-C and PEPCK-M are catalyzing chemically identical reactions with very similar kinetics, the regulation of both enzymes is completely different (Ballard & Hanson, 1969; Hanson & Garber, 1972; Méndez-Lucas *et al*, 2014). The expression of PEPCK-C is regulated by diet and hormones. Fasting has been shown to increase cytosolic enzyme activity at least 3 fold in different tissues (Reshef *et al*, 1969), via transactivation of the PEPCK-C promoter in response to cAMP, glucocorticoids and thyroid hormone, whereas insulin inhibits the synthesis of PEPCK-C mRNA (Hanson & Reshef, 1997). In contrast, PEPCK-M is constitutive in nature and is not controlled by fed/fasting cycles (Croniger *et al*, 2002b; Modaressi *et al*, 1998). However, transcriptional regulation by ATF4 under endoplasmic reticulum (ER) stress has been described recently in our laboratory (Méndez-Lucas *et al*, 2014) for this gene. Until now, no allosteric modifications of PEPCK enzymes have been described (Balan *et al*, 2015; Yang *et al*, 2009b). Therefore, the activity of PEPCKs in cells is determined by the balance between its synthesis and degradation. Half-life of PEPCK-C protein in the fed liver is about 6-8h (Hopgood & Ballard, 1973) and its mRNA half-life is 30-60 min (Tilghman *et al*, 1974), allowing immediate control of PEPCK-C gene expression levels by transcription factors . On the other hand, PEPCK-M protein shows longer half-life (>50h) (Hanson & Patel, 1994).

Quantitative distribution of both PEPCK isoforms varies in different species. Most species studied to date (humans, dogs, cats, cows, sheep) show about equal activity of both isoforms in the liver. PEPCK activity in the liver of rat, hamster and mouse is mostly accounted for by the cytosolic isoform (90 - 99% of total activity), whereas in rabbit liver PEPCK-C accounts only for 10% of total activity. Some species of birds (e.g. pigeon and

chicken) express solely PEPCK-M in their livers after hatching (Croniger *et al*, 2002b; Söling *et al*, 1973; Nordlie & Lardy, 1963).

As mentioned above, PEPCK is catalyzing the formation of PEP from OAA. This is the first committed step of gluconeogenesis and glyceroneogenesis. PEPCK-C in mammals fulfil a gluconeogenic function in the liver and kidney (Croniger *et al*, 2002b; Hanson & Reshef, 1997), and a glyceroneogenic one in the liver and adipose tissue (Kalhan *et al*, 2001; Reshef *et al*, 2003). Interestingly, glyceroneogenesis in adipose tissue has been shown to be of relevance for the formation of glyceride-glycerol even in the presence of glucose (Nye *et al*, 2008). Besides PEPCK-C presence in gluconeogenic/glyceroneogenic tissues, its expression was observed also in other tissues such as small intestine, mammary gland during lactation, brain, lung and muscle (Hanson & Reshef, 1997; Zimmer & Magnuson, 1990). Even though the role of the enzyme in these tissues has not been clearly established, some studies shed light on this problematic and identified the possible role of PEPCK-C in some of the tissues. PEPCK-C expression in small intestine is significantly higher in suckling, starved and diabetic rats when compared to the fed adults (Watford & Alicia, 1989; Mithieux *et al*, 2004). Several studies claim the presence of active gluconeogenesis in the small intestine (Mithieux *et al*, 2005; Troy *et al*, 2008). However, a critical review by Previs *et al*. points to various problems in the estimation of gluconeogenesis in the small intestine, concluding that there is no credible evidence of glucose synthesis in the small intestine (Previs *et al*, 2009). The suggested role of PEPCK-C in the adipocytes of mammary glands during lactation is the contribution to triglyceride synthesis through glyceroneogenesis (Hsieh *et al*, 2009; Jiménez *et al*, 1987), as the lipids are the main component of the milk (Bobrovnikova-Marjon *et al*, 2008). The implication of PEPCK-C in glyceroneogenesis was also reported in skeletal muscle by Nye *et al*, where glyceroneogenesis was the main contributor to triglycerides production in fed or fasted state (Nye *et al*, 2008). Interestingly, overexpression of PEPCK-C in skeletal muscle of mice has a great impact on their physical activity. These mice are 7-10 times more active than control mice and are able to run for long distances at high speed without stopping. Muscles of these mice showed five-times higher storage of triglycerides that may reflect elevated TCA cycle dynamics (Hanson & Hakimi, 2008).

The role of PEPCK-C in cataplerosis (removing carbons from TCA cycle) to support the TCA cycle has been recently shown (Hakimi *et al*, 2005; Burgess *et al*, 2004). Suggestions that PEPCK-C may interact with energy generation in the TCA cycle was based on observed impairment of hepatic energy metabolism in liver specific (Burgess *et al*, 2004) and whole-body PEPCK-C knock-out models (Hakimi *et al*, 2005; Semakova *et al*, 2017). It has been shown that TCA cycle flux and the flux through PEPCK-C are linearly proportional (Burgess *et al*, 2007). Lack of PEPCK-C expression in the liver lead to the accumulation of TCA cycle intermediates and a blockage of gluconeogenesis. Additionally, the inhibition of the TCA cycle in the liver also affect fatty acid oxidation, one of the anaplerotic pathways, and lead to the accumulation of lipids in the liver (Burgess *et al*, 2004). Similar consequences were observed as well in the whole-body knock-out model (Semakova *et al*, 2017; Hakimi *et al*, 2005). Interestingly, the inhibition of PEPCK-C in the liver was shown to diminish ROS production, which is formed in the liver under some pathological or dietary conditions as a consequence of increased TCA cycle flux and oxidative metabolism of fatty acids (Satapati *et al*, 2015).

4.2 The metabolic role of PEPCK-M

The study of the metabolic role of PEPCK-M was in the shade of its cytosolic counterpart for a long time. As Hakimi accurately said, “this neglect is ironic, since Utter and Kurahashi discovered PEPCK-M in the livers of chickens and used it to delineate the pathway of gluconeogenesis” (Hakimi *et al*, 2005). PEPCK-M is strongly expressed in liver, kidney, small intestine, fibroblasts and pancreas (beta cells) and weakly expressed in brain, heart and placenta in humans (Modaressi *et al*, 1998; Stark *et al*, 2009). Interestingly, PEPCK-M shows high expression in cancer cell lines of different origins (Méndez-Lucas *et al*, 2014) and neural progenitors (Álvarez *et al*, 2014). Interestingly, mice express almost exclusively the cytosolic isoform in the liver, however during fetal development the mitochondrial isoform is preferentially expressed (Hanson & Reshef, 1997).

It can be speculated that human PEPCK-M provides gluconeogenesis from lactate as it

has been observed in birds (Hanson & Reshef, 1997). However at this time, there is no direct proof of the role of PEPCK-M in gluconeogenesis in mammals, and this enzyme continues to be poorly understood. Interestingly, Stark *et al.* speculate that the PEPCK-M pathway is theoretically the most direct pathway for PEP production from lactate since it offers metabolic advantages over PEPCK-C pathway (Stark *et al*, 2014), and therefore could be more important in gluconeogenesis than was originally thought. Preferential use of lactate as a gluconeogenic substrate for PEPCK-M might be explained by the fact that lactate conversion to pyruvate does provide reducing equivalents and there is no need to shift them from mitochondria to cytosol. On the other hand, cytosolic PEPCK require shuffling of NADH and oxaloacetate from mitochondria to cytosol in the form of malate (Modaressi *et al*, 1998). In our laboratory, Méndez *et al.* studied the ability of PEPCK-M to rescue the liver specific PCK1 KO mice. We demonstrated that PEPCK-M can contribute to hepatic glucose production from PEP, however is not able to fully recover the ability of the cytosolic isoform to restore cataplerosis and fully support gluconeogenesis. Interestingly, simultaneous expression of PEPCK-M and PEPCK-C in mouse hepatocytes amplify total gluconeogenic capacity. PEPCK-M in the presence of cytosolic isoform facilitate flux with lactate as a substrate, although in the absence of PEPCK-C there was no substrate preference (Méndez-Lucas *et al*, 2013).

Apart from gluconeogenesis/glyceroneogenesis, other possible implications of PEPCK (mitochondrial or cytosolic) in metabolism has been suggested; amino acid synthesis, cataplerosis/anaplerosis and PEP/pyruvate cycling (Hanson & Patel, 1994). PEP cycling involving PEPCK-M was suggested in two independent models. Firstly, in brown adipose tissue of hamster and rat, where PEP cycling would allow to export energy produced in mitochondria (Drahota *et al*, 1983), since GTP or GDP transport from mitochondria to cytosol has not been identified in higher eukaryotes (Stark & Kibbey, 2014), except hearth tissue where slow transport of GTP/GDP was observed (McKee *et al*, 2000). PEPCK-M, pyruvate kinase (PK) and pyruvate carboxylase (PC) have been proposed to contribute to this cycle. Secondly, a similar activity was suggested by Stark *et al.* to be implicated in the regulation of insulin secretion in beta cells of pancreas (Stark *et al*, 2009). The same group identified that mitochondrial GTP produced by succinyl-CoA synthetase in the TCA

cycle is an indicator of TCA flux that is important for glucose stimulated insulin secretion (GSIS) (Kibbey *et al*, 2007). PEPCK-M would be, in this context, an important recycler of GTP in mitochondria. Moreover PEP cycle links PC flux and TCA cycle flux to stimulate insulin release and may act to prevent inappropriate insulin secretion (Stark *et al*, 2009).

4.3 Regulation of PEPCK-M

Acetylation of cytosolic PEPCK as a mechanism of regulation was observed recently (Zhao *et al*, 2010; Lin *et al*, 2009). Acetylation of PEPCK-C was connected with observed decrease in protein level (Zhao *et al*, 2010), which was assigned to degradation by increased ubiquitination upon acetylation (Jiang *et al*, 2011). Interestingly, acetylation was also observed in the case of mitochondrial isoform of PEPCK in human liver (Zhao *et al*, 2010). Obviously, there is still need of further investigation to examine whether PEPCK-M responds to acetylation in the same manner.

Regarding regulation by hormones, it has been described that PEPCK-M does not respond to changes in levels of hormones known to regulate cytosolic isoform (Modaressi *et al*, 1998; Croniger *et al*, 2002a). PEPCK-M is considered to be expressed constitutively (Modaressi *et al*, 1998; Croniger *et al*, 2002b).

However, in our laboratory we have observed that cancer cells respond to ER stress and amino acid deprivation by increasing PEPCK-M expression. We described that the proximal promoter of PCK2 contains two amino acid response element (AARE) consensus sites also known as C/EBP-ATF composite site. AARE is a binding site for ATF4, ATF3 and C/EBP. PEPCK-M was shown to be regulated only by ATF4 through the AARE1 site. This regulation was shown to be occurring under ER stress and also amino acid deprivation and suggests an important role of PEPCK-M in the response to these types of stress (Méndez-Lucas *et al*, 2014).

Aims

Aims

The main aim of this thesis is to study the implication of PEPCK-M in metabolic adaptations of undifferentiated cells, specifically neuronal progenitors and cancer cells.

Specific aims

- To analyze the effect of glucose and lactate on the differentiation phenotype of embryonic neuronal cultures.
- To evaluate the role of PEPCK-M in neuronal progenitors maintenance.
- To test the viability, growth and metabolic adaptations dependent on PEPCK-M in cancer cell lines using knocked-down, basal and overexpressed PEPCK-M models.
- To evaluate the effects of changes in PEPCK-M activity on TCA cycle and PEPCK-M dependent pathways using metabolomics.
- To evaluate the growth rates and angiogenic capacity of HCT116 and MCF7 xenografts with wild-type and knocked-down PEPCK-M levels in mice.

RESULTS

1 Neuronal progenitor maintenance requires lactate metabolism and PEPCK-M directed cataplerosis

Glucose is still considered the major fuel for adult brain, even though lactate signaling or utilization by neurons has been commonly observed both *in vitro* and *in vivo* (Gallagher *et al*, 2009a; Bouzier-Sore *et al*, 2003; Wohnsland *et al*, 2010). This is especially the case in the developing brain, where lactate is an important substrate for oxidative metabolism in addition to being utilized as an anabolic source for cell proliferation and differentiation (Bolaños & Medina, 1993; Nehlig & Pereira de Vasconcelos, 1993; Medina *et al*, 1996; Vicario & Medina, 1992).

The effect of two different carbon substrates (glucose and L-lactate) on glial and neuronal cell phenotype, was studied in collaboration with the laboratory of Dr. Alcántara (Alvarez *et al*, 2013).

We initially observed, that embryonic neuronal and glial cell culture development *in vitro* is affected by the availability of glucose and lactate. Glial cells were not able to survive in the presence of lactate as main source of carbons and results strongly suggested that glial cells use glucose as the primary energy substrate. On the other hand, neuronal cultures were able to survive in medium containing lactate as well as in medium containing glucose. Moreover, lactate medium seemed to affect differentiation state of neurons (Alvarez *et al*, 2013).

1.1 Effect of lactate on neuronal progenitor survival and differentiation

Our initial data led us to study in more detail the role of lactate in differentiation of neuronal cultures. The results presented in this part of the thesis were obtained in equal contribution with Dr. Zaida Álvarez Pinto from the laboratory of Dr. Alcántara, University of Barcelona.

All experiments were performed with primary neuronal cultures that were extracted from the cortex of mice at embryonic day E16. Primary neuronal cultures were grown for desired length of time in three different serum free Neurobasal® media containing combination of glucose and lactate (Table R-1).

Denomination of media	Glucose and lactate concentration
glucose	25 mM glucose, 0 mM L-lactic acid
glucose + lactate	25 mM glucose, 4 mM L-lactic acid
lactate	0 mM glucose, 4 mM L-lactic acid

Table R-1: Types of media used in experiments with indicated concentration of glucose and lactate.

The state of differentiation of primary neuronal cultures was analyzed by western blot analysis using differentiation markers (Figure R-1). Neuronal cultures can contain a proportion of glial cells that survive purification of neuronal cultures. Therefore, the expression of glial markers was also analyzed. Neuronal cultures grown in glucose and glucose + lactate media equally expressed radial glia marker nestin (intermediate filament protein) and mature astroglial marker GFAP (glial fibrillary acidic protein) indicating the presence of glial cells. In lactate condition, expression of these markers has dramatically dropped indicating a reduction of the glial cell population in this condition. These results were consistent with the observation that glial cells are not able to survive in lactate media (Alvarez *et al*, 2013). Differentiation state of neuron population was detected by mature neurons markers (PSD95 and TUJ-1) and neuronal restricted progenitor marker TBR2 (T-box brain protein 2). Glucose media favored the presence of neurons expressing

PSD95 (postsynaptic density protein 95) and TUJ-1 (class III beta tubulin), while progenitor marker TBR2 was expressed weakly. This expression pattern indicates that the culture is formed mainly by mature neurons. In lactate condition, a drop of PSD95 and TUJ-1 expression, and increased TBR2 expression were observed, suggesting that the population of cells is less differentiated and enriched of neuronal restricted progenitors. Treatment with medium containing both glucose and lactate also showed increased TBR2 and slightly decreased TUJ-1 expression, when compared to glucose condition. PSD95 expression was maintained at the same level. This indicates the presence of a mixed population formed by neuronal restricted progenitors together with more differentiated neurons.

Bipotential radial glia-like cell marker PAX6 (paired-box protein) and neural stem cell marker SOX2 (SRY-box 2 protein) were not expressed in any condition (data not shown). Absence of expression of these two markers in lactate conditions indicate that present progenitors are mostly TBR2 positive neuronal restricted progenitors.

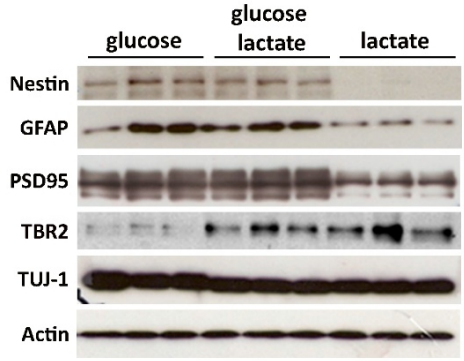

Figure R-1: Expression of the differentiation markers in neuronal cell culture. Western blot of nestin (radial glial marker), GFAP (mature astroglial marker), PSD95 (post-synaptic density neuronal marker), TBR2 (intermediate progenitor marker) and TUJ-1 (post-mitotic neuronal marker) in neuronal cultures grown in glucose, glucose + lactate and lactate media for 5 days. Actin was used as loading control. Expression of SOX2 and PAX6 were not detected. Actin was used as a loading control.

To evaluate the differentiation progress and self-renewal in neuronal progenitors, neuronal cultures were grown for 1 and 5 days in glucose, glucose + lactate and lactate medium (Figure R-2). Under these conditions, the number of cells and progenitors was evaluated. Total number of cells was obtained by counting TO-PRO-3 positive cells and number of cycling neuronal progenitors was assessed by counting Ki67 positive cells. The absence of SOX2 positive progenitors and astrocytes in lactate culture (Figure R-1) indicates that the Ki67 positive progenitors were mostly TBR2 positive neuronal progenitors.

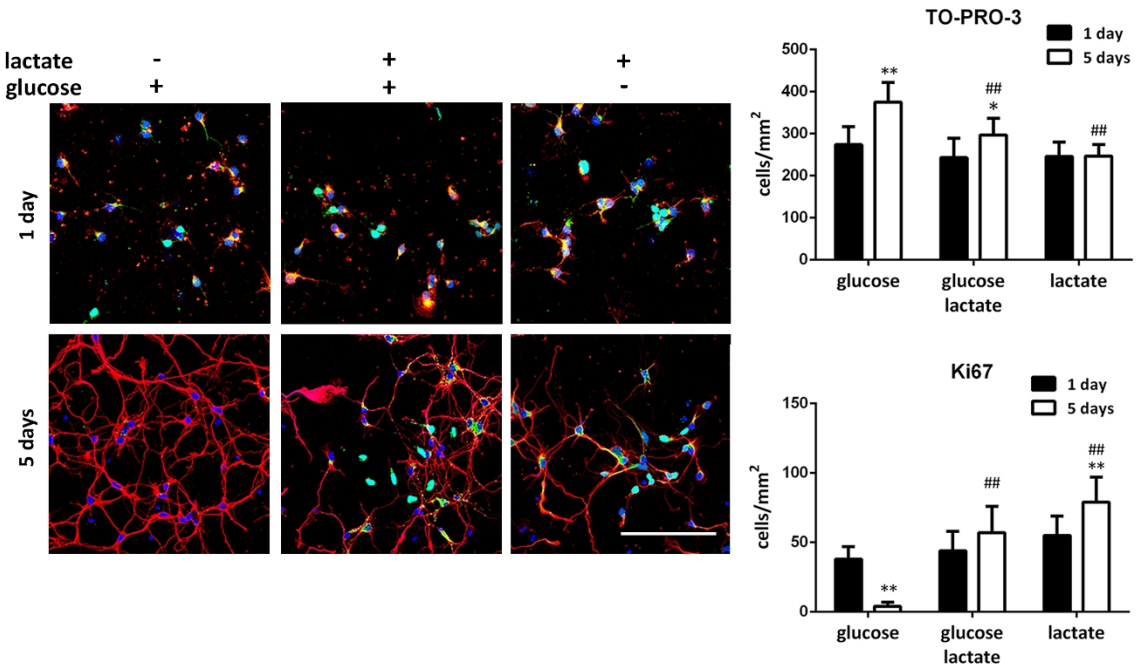

Figure R-2: Effect of lactate on primary neuronal cultures. Confocal images of embryonic neuronal cell cultures grown in glucose, glucose + lactate and lactate medium for 1 and 5 days. Neurons were stained with TUJ-1 (red), nuclei with TO-PRO-3 (blue) and nuclei of cycling progenitors with Ki67 (green). Scale bar = 50 µm. Graphics represent quantification of the total number of cells (TO-PRO-3 positive) and cycling progenitors (Ki67 positive) after 1 and 5 days of incubation in glucose, glucose + lactate, or lactate medium. Data are plotted as mean ± SD, *P<0.05 and **P<0.01, day 1 versus day 5 within the same condition. #P<0.05, ##P<0.01 versus cells grown in glucose.

At the first time point (1 day), neuronal cultures consisted of a similar number of cells and cycling progenitors. At day 5, neuronal cultures showed signs of differentiation. Neurons identified by staining with the neuronal marker TUJ-1 exhibited well-developed neurites, particularly in glucose medium. Also the total number of cells growing in glucose and glucose + lactate medium was significantly higher when compared to day 1 time point. In contrast, cells growing in lactate medium maintained the same total number of cells from day 1 to day 5 (Figure R-2).

All neuronal cultures at day 1 showed a similar number of Ki67 positive progenitors. At the end of the experiment, the amount of cycling progenitors dramatically dropped in glucose condition. However, no change was observed in glucose + lactate condition, and a significant increase in the proportion of Ki67 positive cycling progenitors was observed

in neuronal cultures growing for 5 days in lactate media (Figure R-2).

The data above suggest that the presence of glucose promotes the differentiation of neuronal progenitors while lactate is required for maintenance and division of neuronal progenitors.

The following experiment was designed to confirm these effects of glucose and lactate on neuronal cultures. Cells grown for 5 days in lactate medium were changed to either glucose medium or lactate medium and grown for 2 more days. At the end of the experiment the total number of cells (TO-PRO-3 positive) and the number of Ki67 positive progenitors was determined (Figure R-3). Neuronal cells growing in lactate for 5 days contained a population of Ki67 positive progenitors (Figure R-2) that were lost when lactate was switched to glucose for 2 more days. When the cells were maintained for the whole experiment in lactate, the population of Ki67 positive cells remained (Figure R-3 A). At the end of the experiment, the total number of cells was higher in the condition with additional 2 days treatment in glucose medium (Figure R-3 B). These results suggested that glucose medium induced one terminal division of Ki67 positive progenitors that led to differentiation. When the opposite experiment was performed, and neuronal cultures were grown in glucose medium for 5 days and then for 2 more days either in the same medium or in lactate medium, no differences in cell numbers were observed (Figure R-3 C,D). Therefore, we conclude that lactate is not able to reprogram terminal differentiation of neuronal cells in our model.

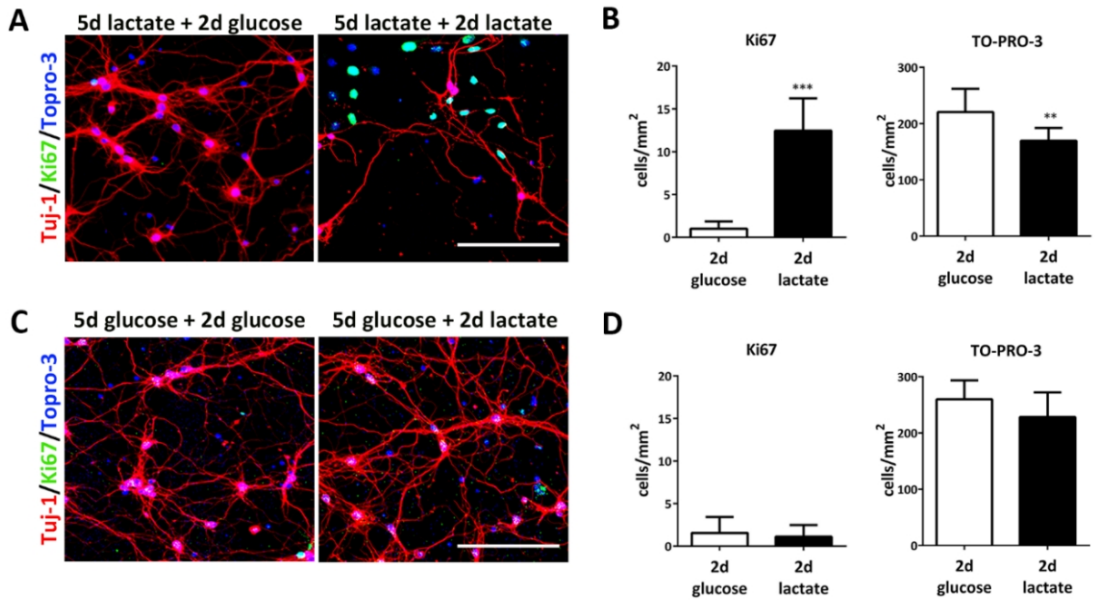

Figure R-3: Study of differential and self-renewal capacity of neuronal primary cultures grown in the presence of glucose and lactate. (A) Confocal images showing neurons (TUJ-1, red), nuclei (TO-PRO-3, blue), and cycling progenitor cells (Ki67, green) in neuronal cultures grown in lactate medium for 5 days followed by 2 more days either in glucose medium or in lactate medium. Scale bar = 50 µm **(B)** Quantification of Ki67positive (proliferative cells) and TO-PRO-3 positive (total number of cells) under the same conditions as in A. **(C)** Confocal images showing neurons (TUJ-1, red), nuclei (TO-PRO-3, blue), and cycling progenitor cells (Ki67, green) in neuronal cultures grown in glucose medium for 5 days followed by 2 more days either in lactate medium or in glucose medium. Scale bar = 50 µm **(D)** Quantification of Ki67positive (proliferative cells) and TO-PRO-3 positive (total number of cells) under the same conditions as in C. (B,D) Data are plotted as mean ± SD, **P<0.01, ***P<0.001 indicate significant treatment effect of lactate.

As we had hypothesized, the difference in total number of cells growing in glucose versus lactate media (Figure R-2, Figure R-3 B) can be brought about by terminal division of Ki67 positive progenitors (in glucose medium) and asymmetric/symmetric division of progenitors (in medium containing lactate). However, differences in cell numbers could also be caused by cell death. Therefore we examined the presence of apoptosis and oxidative stress in neuronal primary cultures (Figure R-4). Cells were grown in lactate medium for 5 days and later changed to either glucose or lactate medium for 1h or 48h. Staining of caspase-3 was analyzed in order to detect the presence of apoptotic cells in neuronal cultures. The percentage of caspase-3 positive cells was very low in both conditions. However, after 1h, there was a slightly higher number of caspase-3 positive

cells in lactate media (1.74 ± 2.56 in glucose condition and 5.45 ± 3.36 in lactate condition, Figure R-4 B). This difference disappeared, when cells were analyzed after 2 days. Even though there is significant difference in the percentage of apoptotic cells at 1h time point, it does not explain the differences in total number of cells grown in glucose versus lactate condition. Therefore, we can conclude that differences in cell number are not caused by cell death and a more probable cause is cell division (terminal, asymmetric/symmetric) of Ki67 positive progenitors.

To detect oxidative stress, cells were incubated with CellROX, which when oxidized by ROS yields a stable fluorochrome. CellROX fluorescence was slightly higher in neuronal cultures treated for one hour with glucose media when compared to lactate media. This increase in ROS concentration might be explained as an immediate reaction to the main carbon source change as after 2 days no difference was observed between glucose and lactate treated cells (Figure R-4 A).

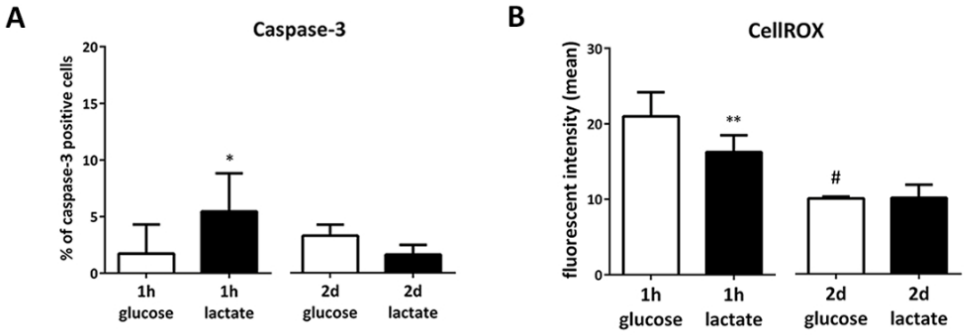

Figure R-4: Apoptosis and oxidative stress induction in primary neuronal cultures. (A) Percentage of caspase-3 positive cells and **(B)** quantification of CellROX fluorescent intensity in cultures that were grown in lactate medium for 5 days followed by incubation either 1 h or 2 days in glucose medium or in lactate medium. Data are plotted as mean **±** SD. *P<0.05, **P<0.01 indicate significant treatment effect of lactate, and #P<0.05 indicate significant differences between 1h and 2d within the same treatment.

All in all, these data confirmed that lactate is able to redirect the fate of neuronal culture and support less differentiated state of neuronal cultures by preserving a significant pool of neuronal restricted progenitors.

1.2 Metabolic profile of neuronal progenitors

As mentioned earlier, maintenance of neuronal restricted progenitors is dependent on the presence of lactate in medium. More detailed information about lactate fate in neuronal cultures was obtained by measuring levels of lactate in neuronal culture media (Figure R-5 A). Cells were treated with glucose, glucose + lactate and lactate media for 5 days and the final concentration of lactate in media was analyzed. Cells growing in lactate media expectedly consumed lactate as it was their main source of carbons. On the other hand, cells growing in glucose and glucose + lactate medium were producing lactate likely as the result of glycolysis. However, we were not able to analyze turnover of lactate in glucose + lactate medium because of the mixed population of more differentiated neurons and progenitors, where one population might produce lactate and the other consume it.

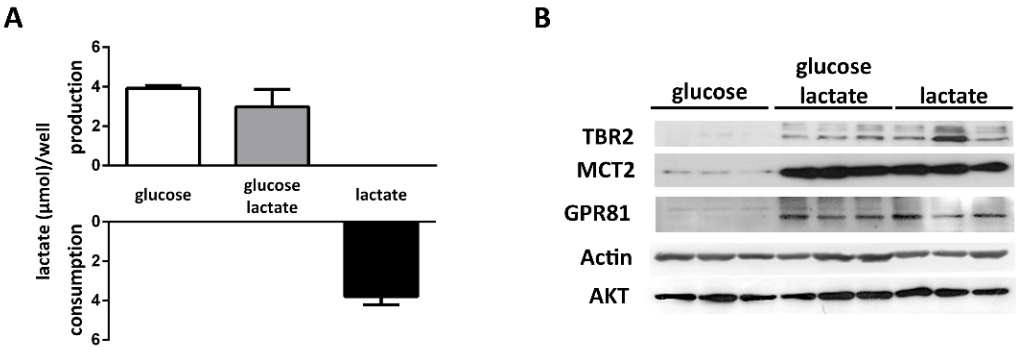

Figure R-5: Lactate consumption/production and expression of the lactate metabolic machinery in neuronal cultures. (A) Amount of consumed/produced lactate in neuronal cultures grown for 5 days in glucose, glucose + lactate and lactate media. Lactate concentration in glucose + lactate and lactate condition was normalized by ratio of number of cells in these conditions to number of cells in glucose condition. Data are plotted as mean ± SD. Statistical analysis was not conducted. **(B)** Western blot analysis shows changes in the expression of the neuronal restricted progenitor marker TBR2, and the lactate metabolic machinery proteins MCT2, and GPR81 in neuronal cultures cultured as in A. Actin and AKT were used as loading controls.

The presence of lactate in the media can influence cells in two different ways; (i) as a metabolite, which is transported to neurons through MCT2 transporter, or (ii) by activation of G-protein-coupled lactate receptor (GPR81), which regulates cAMP levels in cells.

MCT2 and GPR81 analysis showed higher expression levels in the neuronal primary cultures grown in lactate media (Figure R-5 B). Therefore, to distinguish mechanism responsible for maintenance of neuronal restricted progenitors, we treated cells with an agonist of GPR81 (3,5-dihydroxybenzoic acid (3,5-DHBA), 1 mM) or an inhibitor of MCT1/2 (AR-C155858, 100 nM) (Figure R-6). The agonist of GPR81 (3,5-DHBA) was added to glucose medium or to glucose and lactate free medium at day 1, and cells were grown for 5 more days. 3,5-DHBA as an agonist of GPR81 was intended to mimic lactate in media through the activation of GPR81 receptor. However, 3,5-DHBA was not able to support the neuronal restricted progenitors in glucose medium. Moreover, it was not able to promote cell survival of cells in glucose and lactate free medium. Cell death in this condition was most likely caused by insufficient availability of carbon source, as the media contained only 0.5 mM glutamine. However, the total number of cells in glucose medium was not altered in cells treated with agonist (glucose: 255 ± 46, glucose + 3,5-DHBA: 216 ± 79).

On the other hand, the presence of MCT1/2 inhibitor (AR-C155858) in glucose + lactate medium condition for 5 days caused a depletion of Ki67 positive progenitors from primary neuronal cultures (Figure R-6). The presence of AR-C155858 did not affect the total number of cells in glucose + lactate medium (without inhibitor 211 ± 51 and with inhibitor 240 ± 24). In lactate media, the presence of MCT1/2 inhibitor caused massive cell death probably caused by limiting the main source of carbons in this condition.

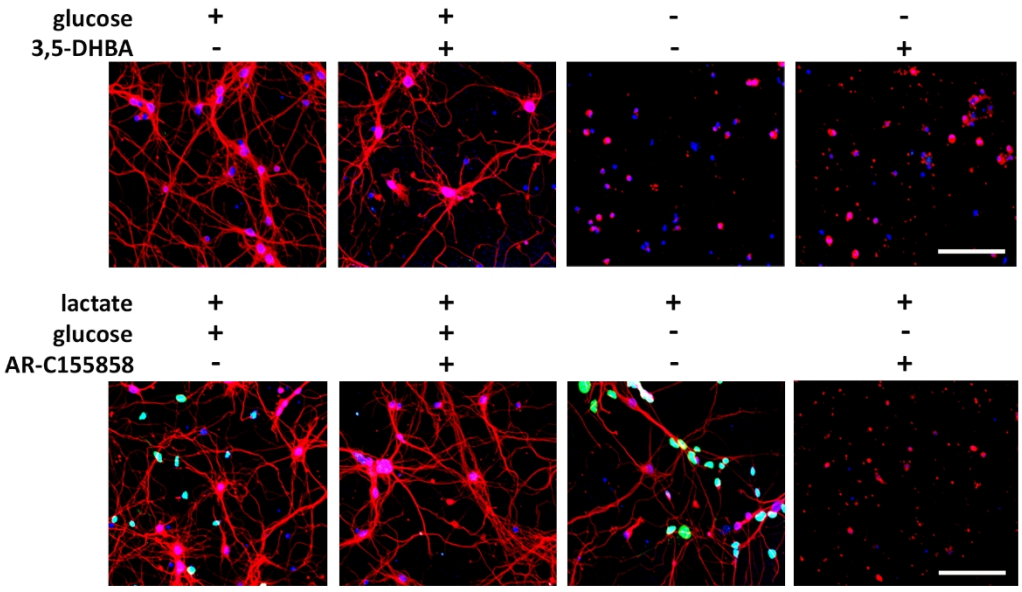

Figure R-6: Consequences of inhibition of lactate machinery on cycling progenitor cells. Cells were grown for 5 days in glucose or in glucose/lactate free medium in the presence or absence of 3,5-DHBA (1 mM) or in glucose + lactate medium or in lactate medium in the presence or absence of lactate transporters MCT1/2 inhibitor AR-C155858 (100 nM). In confocal images cells were stained with TUJ-1 (red), nuclei with TO-PRO-3 (blue) and cycling progenitors with Ki67 (green).

These data indicate that the effect of lactate on maintenance of neuronal progenitors require transport of lactate into the cell through MCT2 transporter and its subsequent metabolism.

Next, the metabolic profile of neuronal cultures was performed in order to evaluate the resulting metabolic changes. Several metabolic markers were analyzed to assign specific metabolic profiles to each condition. Mitochondria were visualized by epifluorescence using MitoTracker, a cell-permeable active mitochondrial fluorochrome (Figure R-7 A). Neuronal cultures grown for 5 days in glucose, glucose + lactate or lactate medium displayed more intense mitochondrial labeling in immature neurons and progenitors (TUJ-1 negative) than mature neurons (TUJ-1 positive). Consistent with progenitor enrichment, mitochondrial staining was highest in lactate medium and indicate higher mitochondrial membrane potential of these cells that might be fed by lactate oxidation

through the TCA cycle. No differences in cellular ATP levels were observed in either condition (Figure R-7 B).

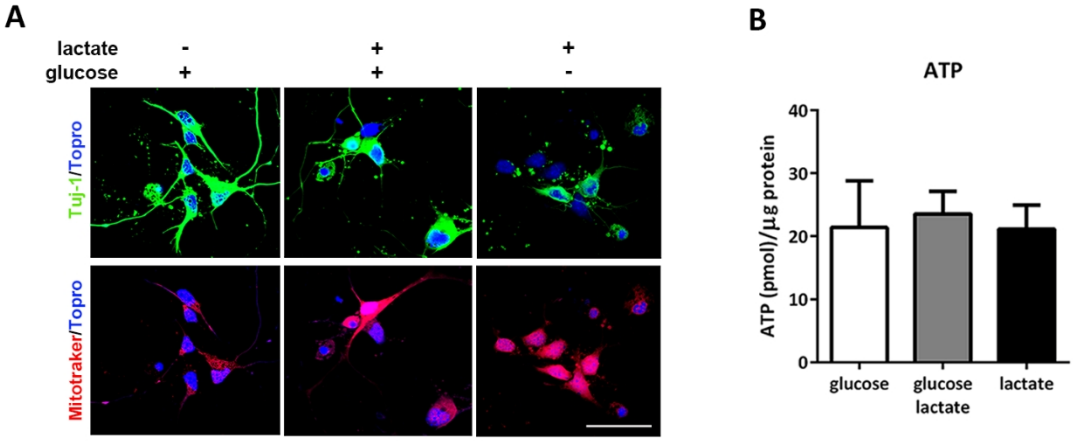

Figure R-7: Metabolic profile of neuronal cultures. (A) Confocal images of neuronal cell cultures grown in glucose, glucose + lactate and lactate medium for 5 days. Cells were stained with TUJ-1 (neurons, green), MitoTracker (mitochondria, red) and TO-PRO-3 (nuclei, blue). **(B)** Quantification of ATP in cells cultured as in (A). Data are plotted as mean ± SD. ATP amount in cell extracts was normalized by the total protein concentration.

To better evaluate the metabolic profile of neuronal progenitors the level of expression of different metabolic markers was analyzed in neuronal primary cultures grown for 5 days in the presence of either substrate (Figure R-8). NAD-dependent deacetylase sirtuin-1 (SIRT), a protein that is activated by NAD+ was decreased when lactate was present as only carbon source. Consistently with increased mitochondrial activity in lactate containing cultures, the degree of phosphorylation of AMPK (a sensor of the cell energy state) was very low as compared to glucose and glucose + lactate media. Finally we were interested in evaluating the regulator of pyruvate flux into mitochondria by examining the phosphorylation state of PDH, which is inactivated by PDKs via its phosphorylation at E1-alpha subunit. Again, the data showed that PDH phosphorylation was low suggesting higher pyruvate oxidation in the mitochondria under conditions where lactate is the only carbon source. Interestingly, no differences were observed between glucose and glucose + lactate treatments relative to these sensors of energy change, pyruvate metabolism and redox potential. These data are consistent with a dramatic shift to

oxidative metabolism of lactate which becomes the main source of energy and carbons in the cell growing in lactate condition.

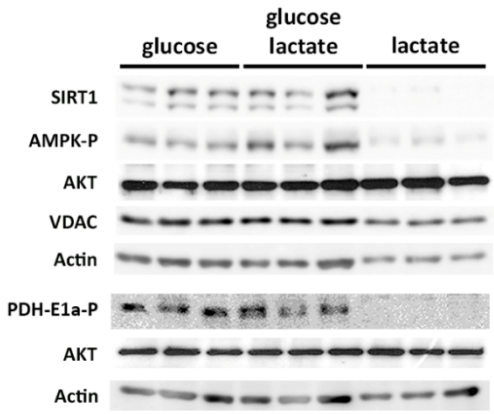

Figure R-8: Level of activity of metabolic sensors in neuronal cultures. Western blot of SIRT1 (NAD-dependent deacetylase sirtuin-1), AMPK-P (adenosine monophosphate-activated protein kinase), and phosphorylated PDH-E1a (pyruvate dehydrogenase E1 alpha) in neuronal cultures grown for 5 days in glucose, glucose + lactate and lactate media. AKT and actin were used as loading controls.

1.3 PEPCK-M activity is essential for maintenance of neuronal progenitors

Cells growing in lactate media find themselves in a situation where they must cope with the absence of intermediates coming from the upper part of glycolysis that are essential for cell growth and survival. Therefore, we hypothesize that under these metabolic conditions cells might utilize alternative pathways to provide essential intermediates. The enzyme PEPCK has the capability to provide these intermediates, by catalyzing the first step of gluconeogenesis by converting oxaloacetate to phosphoenolpyruvate. It is the only enzyme to enable glycolytic intermediates synthesis from lactate and TCA cycle intermediates. Therefore we were interested if PEPCK is expressed in these neuronal cultures, and whether expression was linked to the metabolic shift observed in cultures growing on lactate. Expression of PEPCK was examined in neuronal cultures grown for 5 days in various media. Primary cultures expressed mitochondrial isoform of PEPCK (PEPCK-M) in all conditions (Figure R-9 A, C, D). The cytosolic isoform was not expressed in either one of the conditions (Figure R-9 B). Cells growing in glucose + lactate media shown 1.3- fold increase in PEPCK-M expression, though cells growing in lactate medium 5-fold higher expression of PEPCK-M when compared to control (Figure R-9).

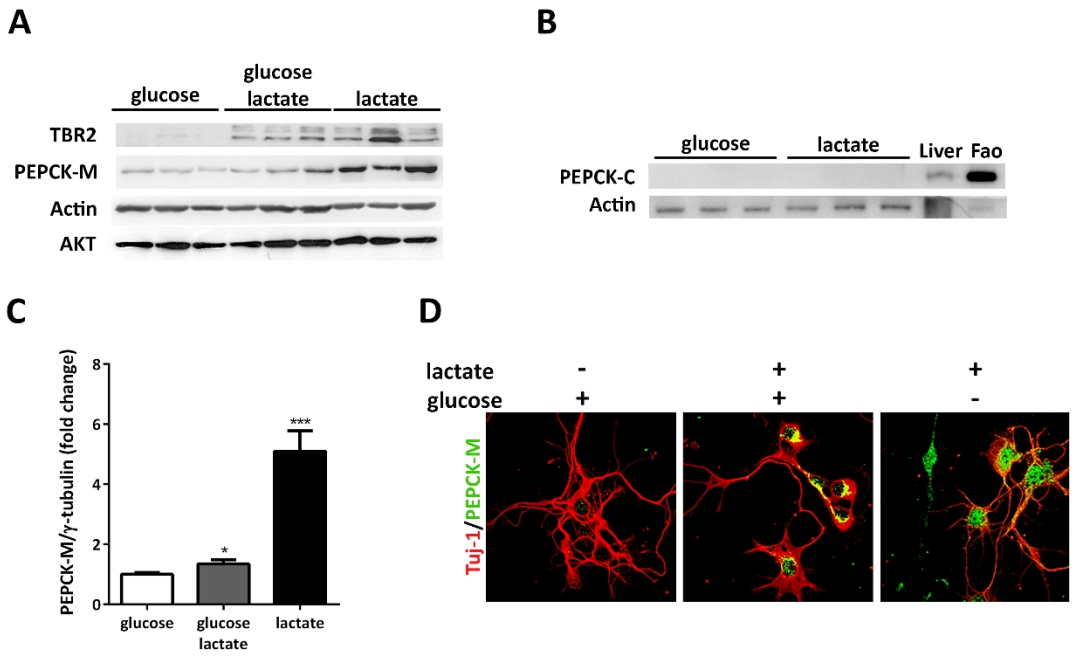

Figure R-9: PEPCK-M and PEPCK-C expression in neuronal cultures. (A) Western blot of TBR2 (marker of neuronal restricted progenitor) and PEPCK-M in neuronal cultures grown for 5 days in glucose, glucose + lactate and lactate condition. AKT and actin were used as loading controls. **(B)** Western blot of PEPCK-C in neuronal cultures grown for 5 days in glucose and lactate media. As a positive control of PEPCK-C expression was used extract of fasted mouse liver and Fao cells (rat hepatoma). **(C)** Quantification of PEPCK-M expression detected by western blot from three different experiments. *P<0.05, ***P<0.001 versus glucose. **(C)** Confocal images of cultures grown for 5 days in glucose, glucose + lactate and lactate medium that were stained for PEPCK-M (green) and TUJ-1 (red).

To examine the importance of carbons shuttling from lactate into various metabolic pools via PEPCK-M on neuronal culture differentiation state, cells were treated with 3-mercaptopicolinic acid (3MPA). 3MPA is a well-known inhibitor of PEPCK activity (Balan *et al*, 2015). In this experiment, cells were grown in glucose, glucose + lactate and lactate medium in the presence of 100 µM 3MPA or DMSO (control). After 5 days, nuclei were stained with TO-PRO-3 and cycling progenitors were labeled using Ki67 antibody. Total number of cells (TO-PRO-3 positive) and the number of Ki67 positive progenitors was then determined (Figure R-10). We observed that inhibition of PEPCK-M had no effect on the number of cells or progenitors in glucose media. However, the inhibition of PEPCK-M activity in glucose + lactate or lactate media caused a complete depletion of Ki67 positive

cells, indicating that PEPCK-M activity is important for maintenance of cycling neuronal progenitors (Figure R-10 A,C). Besides, the total number of cells was significantly reduced in these media when PEPCK-M was inhibited (Figure R-10 B).

When lactate concentration in lactate medium was analyzed in the presence of 3MPA, higher levels of lactate were detected after 5 days (Figure R-10 D), suggesting that when PEPCK-M was inhibited neurons consumed less lactate. However, a decrease in lactate consumption could also be caused by decreased cell number in this condition (Figure R-10 B).

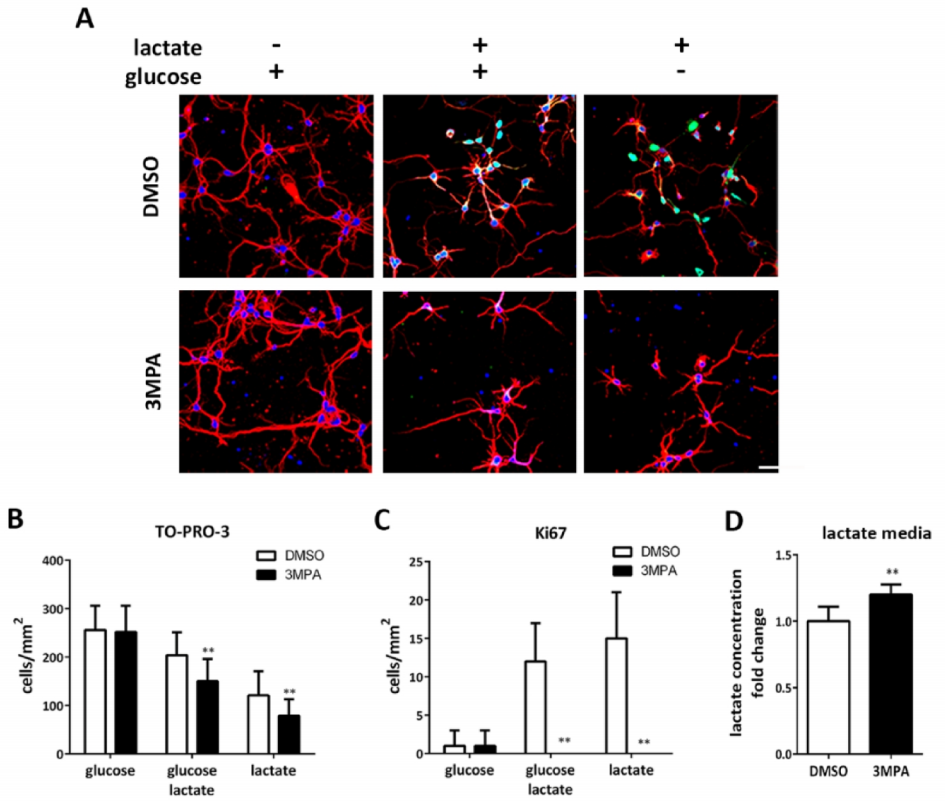

Figure R-10: Effect of PEPCK-M inhibition on neuronal progenitors. Neuronal primary cultures grown in glucose, glucose + lactate and lactate medium were treated with PEPCK-M inhibitor 3MPA (100 µM) or DMSO (control) for 5 days. **(A)** Neurons were stained with TUJ-1 (red) and proliferative progenitors with Ki67 (green). Nuclei were stained with TO-PRO-3 (blue). Scale bar = 75 µm. **(B)** Graphic displays quantification of the total number of cells (TO-PRO-3 positive) and **(C)** quantification of Ki67 positive proliferative progenitors. **(D)** Fold change of lactate concentration in lactate media obtained from cells cultured for 5 days in lactate media in the presence or absence of 3MPA (100 µM). Data are plotted as mean ± SD. *P<0.05, **P<0.01 indicate significant treatment effect.

One of the possible contributions of PEPCK-M on the metabolism of neuronal cultures growing in lactate could be favoring biosynthesis and glycosylation of extracellular matrix proteins (ECM). Laminin, a key component of ECM proteins (Lathia *et al*, 2007), is glycoprotein and its expression is associated mainly with progenitor cells (Kazanis *et al*, 2010). Consistently, laminin expression was higher in the cells grown in lactate containing media by western blot (Figure R-11).

We hypothesized that neuronal progenitors growing in lactate media would require PEPCK-M expression to maintain laminin biosynthesis and glycosylation. In this context, PEPCK-M is the only pathway that can export carbons from lactate and other TCA cycle intermediates (i.e., glutamine) into the triose and hexose pools, through PEP synthesis (Méndez-Lucas *et al*, 2013). Therefore we evaluated implication of PEPCK-M activity on laminin levels (Figure R-11). Cells were grown for 5 days in lactate medium and last 24h were treated with 3MPA or DMSO. Inhibition of PEPCK-M resulted in a substantial decrease in laminin content in cell culture. When expression of TBR2 (neuronal restricted progenitor marker) was evaluated, a decrease of its expression was also present in cultures treated with 3MPA (Figure R-11). This is in line with the observed depletion of Ki67 positive progenitors (Figure R-10).

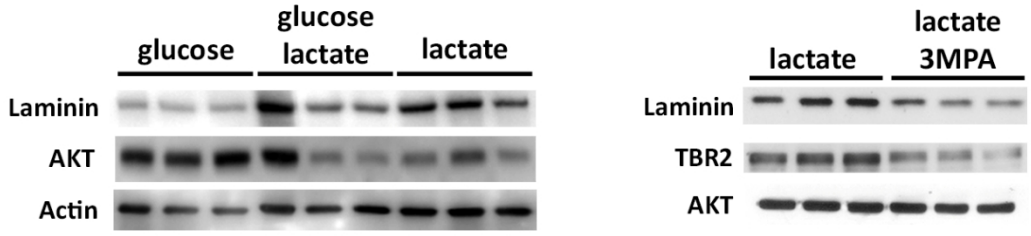

Figure R-11: Laminin expression in neuronal cultures. Western blot of laminin (basal lamina marker) in neuronal cultures grown for 5 days in glucose, glucose + lactate and lactate condition. AKT and actin were used as controls. Western blot of laminin and the neuronal restricted progenitor marker TBR2 in neuronal cultures grown for 4 days in lactate medium and treated for 1 more day with 3MPA (100 μM) or DMSO in the same medium. AKT was used as the loading control.

These results are consistent with our hypothesis that PEPCK-M pathway is relevant as a link of the mitochondrial and glycolytic pools of building blocks necessary to sustain biosynthetic processes in these cellular models and provides a novel and unique

explanation to the reprogramming of metabolism identified in neuronal progenitors by means of alternative carbon sources.

To confirm that progenitor maintenance in the cerebral cortex was effectively mediated by lactate and PEPCK-M catalytic activity, we performed *in vivo* experiments. Newborn mice (postnatal day 0, P0) were treated with lactate (5 mM), an inhibitor of PEPCK-M (3MPA, 100 μM) or vehicle. Two microliters of the solution were injected into the lateral ventricle of brain. The effect of lactate and the inhibition of PEPCK-M on progenitors were evaluated by immunofluorescent staining.

We observed that injection of lactate highly increased the expression of PEPCK-M in the germinal VZ/SVZ. 3MPA blocks the activity of PEPK-M, but does not affect its expression. As expected, expression levels of PEPCK-M in control and 3MPA treated mice was similar. The number of Ki67 positive cycling cells and TBR2 positive neuronal progenitors was determined in the ventricular/subventricular and intermediate zones (VZ/SVZ, IZ). Lactate treatment had positive effects on numbers of TBR2 and Ki67 positive cells that were significantly higher than in control. On the contrary, inhibition of PEPCK-M activity caused a decrease in the number of those cells, when compared to controls.

As mentioned before, *in vitro* experiments have shown laminin expression to be affected by availability of lactate and catalytic capacity of PEPCK-M (Figure R-11). Similar results were obtained *in vivo*, where laminin expression in the germinal VZ/SVZ dramatically increased in lactate-injected animals but decreased in 3MPA injected animals. Taken together these data provide *in vivo* corroboration of the crucial role of PEPCK-M and lactate metabolism in neuronal progenitors.

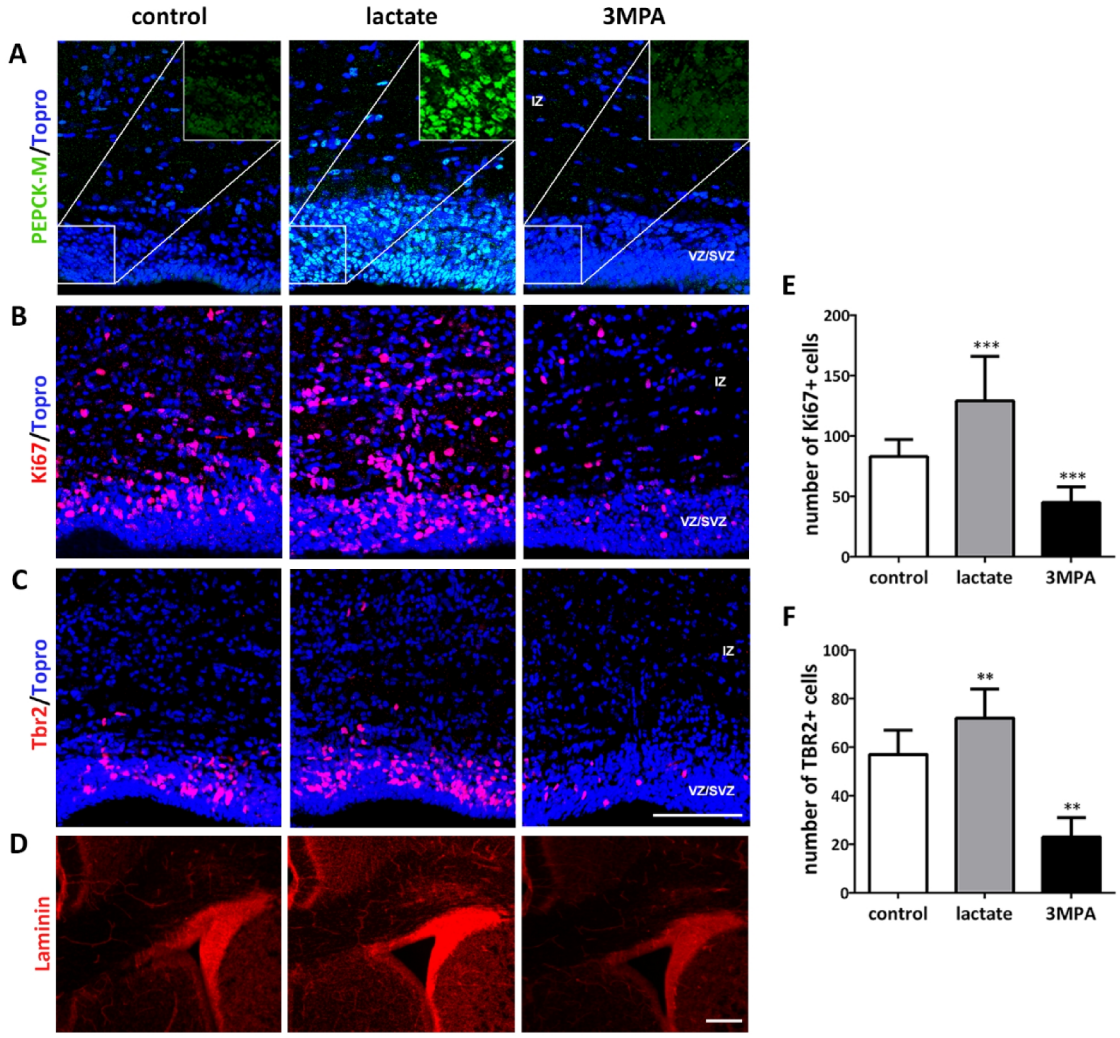

Figure R-12: Effect of lactate and PEPCK-M inhibitor 3MPA on neuronal progenitors *in vivo*. Coronal sections of postnatal day 3 (P3) mouse cerebral cortex injected at P0 with vehicle (control), lactate (5 mM) and PEPCK-M inhibitor 3MPA (100 µM). Nuclei were visualized with TO-PRO-3 (blue) and following staining of coronal sections was proceeded: **(A)** PEPCK-M (green), **(B)** Ki67 (cycling progenitors, red), **(C)** TBR2 (neuronal restricted progenitors, red), and **(D)** laminin (basal lamina, red). **(A)** 1.7 x zoom of selected section, where only PEPCK-M (green) is pictured. (A,B,C,) Scale bar = 100 µm for section. **(D)** Scale bar = 500 µm. **(E,F)** Graphics displays quantification of the number of cells expressing Ki67 and TBR2 in the ventricular/subventricular and intermediate zones (VZ/SVZ and IZ) of coronal sections. Values are the average of 8–10 animals. Data are plotted as mean ± SD. **P<0.01, ***P<0.001 versus control.

2 PEPCK-M role in cancer metabolism

Expression of PEPCK-M in healthy human organism is mainly located in gluconeogenic organs, like kidney and liver, but also in other tissues, like small intestine and beta cells of pancreas (Modaressi *et al*, 1998). However, we observed that its expression pattern changes in cells undergoing tumorigenic activation, presenting high levels of expression in cancer cell lines and also tumors of different origins (Table R-2, Table R-4, Figure R 14). High expression of *PCK2* was observed in various cancer cell lines with raw CTs around 26.9 (24.1-34.3), whereas CT values detected for *PCK1* in these cell lines were mostly over the 35 that indicates minimal amount of mRNA (Table R-2). This points to a preferential expression of the mitochondrial isoform in cancer cell lines.

Interestingly, analysis of several datasets from Oncomine (Rhodes *et al*, 2004), also shows a tendency to increase *PCK2* expression upon malignant transformation of tissues with originally low PEPCK-M expression. Furthermore, tumors originating from tissues that highly express PEPCK-M (e.g. kidney, liver and colon) showed decreased *PCK2* expression (Figure R-13, Table R-3). This tendency was also observed by immunohistochemical analysis of tissue microarray consistent of multiple normal and cancer tissues. Tumors originating from tissues such as liver, pancreas, kidney and gastrointestinal tract showed lower expression of PEPCK-M in cancer cells as compared to their non-malignant healthy counterparts. On the contrary, most other tissues showed increased expression of PEPCK-M when underwent malignant transformation (Figure R 14, Table R-4, Figure R-15 A). Increased PEPCK-M expression was observed for example in cancer of prostate, lung, uterus, testis (Figure R 14, Table R-4) and breast (Figure R-15 A, Table R-4). Some structures of healthy tissue of these organs (glands of prostate and uterus, and cells of seminiferous tubules) were also positively stained with PEPCK-M antibody and these structures are known for their high anabolic capacity.

Interestingly, values of *PCK1* expression in the same Oncomine datasets used to mine *PCK2* data in Figure R-13 indicate decreased *PCK1* expression in all types of tumors regardless the levels of its original expression in healthy tissue. This points to a preferential role of the mitochondrial isoform of PEPCK in cancer cells.

PEPCK-M expression in breast cancer is increased as indicated by Oncomine datasets analysis and also by immunohistochemical analysis. To evaluate its relevance in the clinical outcome of patients we performed analysis of all publicly available gene expression datasets of breast cancer patients using a Kaplan-Meier Plotter tool (Győrffy *et al*, 2010; Szász *et al*, 2016). This analysis showed that increased expression of *PCK2* is related to worsen relapse free survival in these patients Figure R-15 B).

All this led us to hypothesize that PEPCK-M could play an important role in cancer metabolism. Therefore we decided to conduct experiments that would help us identify the mechanism for its implication in cancer biology.

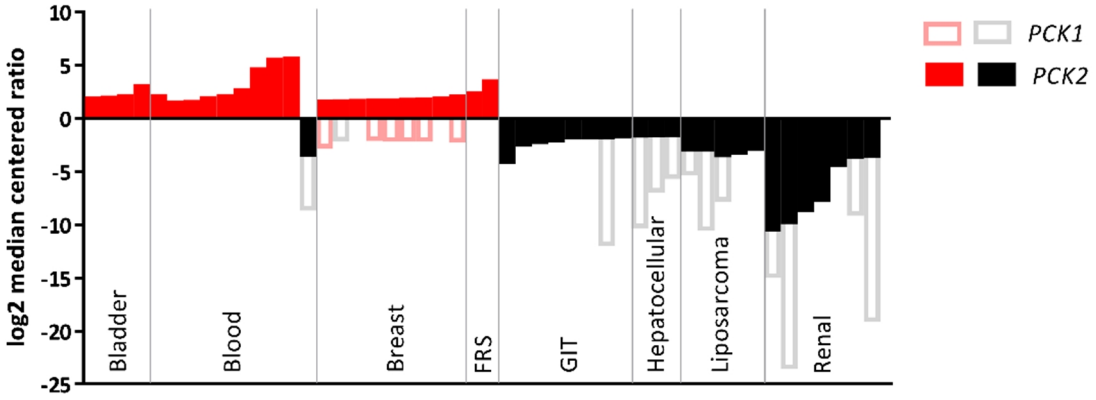

Figure R-13: *PCK1* and *PCK2* expression in cancer cell lines and tumors. Graphical representation of log2 median centered ratio of *PCK2* and *PCK1* mRNA expression acquired from Oncomine database (https://www.oncomine.org; Rhodes *et al.*, 2004). References and values are listed in the Table R-3. Missing values for *PCK1* expression were not significant or were not analyzed in mentioned dataset.

Cell line	Origin	Raw CT *PCK2*	SD	Raw CT *PCK1*	SD	Raw CT *Ctrl*	SD
HeLa	epithelioid cervix carcinoma (Hs)	**28.41**	0.55	**36.04**	0.54	**25.23**	0.09
Jurkat	T lymphocyte cells (Hs)	**28.93**	0.35	**38.99**	1.75	**25.71**	0.1
MCF7	breast adenocarcinoma (Hs)	**27.38**	0.34	**36.55**	2.99	**26.7**	0.22
SaOs-2	osteogenic sarcoma (Hs)	**25.62**	0.28	**34.56**	0.38	**26.7**	0.11
T98	glioblastoma (Hs)	**26.53**	0.40	**36.80**	0.07	**25.55**	0.25
U-2 OS	osteosarcoma (Hs)	**25.44**	0.06	**35.35**	1.50	**24.81**	0.05
U87	glioblastoma (Hs)	**26.51**	0.45	**35.68**	1.34	**25.28**	0.09
SW480	colon adenocarcinoma (Hs)	**25.60**	0.09	**32.75**	0.32	**24.67**	0.19
MDA-MB-231	breast adenocarcinoma (Hs)	**24.49**	0.45	**33.80**	0.18	**23.63**	0.2
SH-SYSY	bone marrow neuroblast (Hs)	**34.28**	0.38	not detected		**33**	0.07
3T3 L1	embryonic fibroblast (Mm)	**24.09**	0.19	**32.39**	0.19	**19.68**	0.06
C2C12	immortalized myoblast (Mm)	**29.13**	0.22	**32.68**	0.25	**23.96**	0.02
MC3T3	preosteoblast (Mm)	**24.75**	0.31	**33.89**	0.70	**19.8**	0.03
3T3-KRas	embryonic fibroblast (Mm)	**25.42**	0.17	**34.53**	3.68	**2.96**	0.02
MEF	embryonic fibroblast (Mm)	**24.19**	0.24	**36.33**	1.09	**19.29**	0.02

Table R-2: Expression levels of *PCK1* and *PCK2* in selected cell lines. Raw CT values of *PCK1* and *PCK2* mRNA expression in various human (Hs) and murine (Mm) cancer cell lines and immortalized cell lines were identified by quantitative real time PCR. As endogenous control (Ctrl) TBP was used for human cell lines and β-actin for mouse cell lines, except 3T3-KRas where 18S was used.

Tissue of origin	Log2 median centered ratio		Oncomine dataset (reference)
	PCK2	*PCK1*	
Bladder	1.864	-	Sanchez-Carbayo Bladder 2 (Sanchez-Carbayo *et al*, 2006)
Bladder	1.927	-	Dyrskjot Bladder 3 (Dyrskjøt *et al*, 2004)
Bladder	2.101	-	Dyrskjot Bladder 3 (Dyrskjøt *et al*, 2004)
Bladder	3.063	-	Sanchez-Carbayo Bladder 2 (Sanchez-Carbayo *et al*, 2006)
Blood	2.098	-	Pyeon Multi-cancer (Pyeon *et al*, 2007)
Blood	1.501	-	Zhan Myeloma 3 (Zhan *et al*, 2008)
Blood	1.542	-	Zhan Myeloma 3 (Zhan *et al*, 2008)
Blood	1.914	-	Brune Lymphoma (Brune *et al*, 2008)
Blood	2.097	-	Brune Lymphoma (Brune *et al*, 2008)
Blood	2.641	-	Piccaluga Lymphoma (Piccaluga *et al*, 2007)
Blood	4.610	-	Andersson Leukemia (Andersson *et al*, 2007)
Blood	5.489	-	Andersson Leukemia (Andersson *et al*, 2007)
Blood	5.602	-	Piccaluga Lymphoma (Piccaluga *et al*, 2007)
Blood	-3.378	-8.432	Finak Breast (Finak *et al*, 2008)
Breast	1.572	-2.608	Curtis Breast (Curtis *et al*, 2012)
Breast	1.618	-1.949	Curtis Breast (Curtis *et al*, 2012)
Breast	1.636	-	Curtis Breast (Curtis *et al*, 2012)
Breast	1.685	-1.893	Curtis Breast (Curtis *et al*, 2012)
Breast	1.704	-1.98	Curtis Breast (Curtis *et al*, 2012)
Breast	1.747	-1.971	Curtis Breast (Curtis *et al*, 2012)
Breast	1.809	-1.982	Curtis Breast (Curtis *et al*, 2012)
Breast	1.884	-	Ma Breast 4 (Ma *et al*, 2009)
Breast	2.077	-2.043	Curtis Breast (Curtis *et al*, 2012)
Breast	1.572	-	Pyeon Multi-cancer (Pyeon *et al*, 2007)
FRS	2.333	-	Biewenga Cervix (Biewenga *et al*, 2008)
FRS	3.470	-	Yoshihara Ovarian (Yoshihara *et al*, 2009)

Table R-3: Oncomine datasets reference list. Continuing on the next page

Gastrointestinal	-4.035	-	Cho Gastric (Cho *et al*, 2011)
Gastrointestinal	-2.409	-	Chen Gastric (Chen *et al*, 2003)
Gastrointestinal	-2.162	-	Skrzypczak Colorectal 2 (Skrzypczak *et al*, 2010)
Gastrointestinal	-2.020	-	Kaiser Colon (Kaiser *et al*, 2007)
Gastrointestinal	-1.741	-	Kaiser Colon (Kaiser *et al*, 2007)
Gastrointestinal	-1.736	-	Kaiser Colon (Kaiser *et al*, 2007)
Gastrointestinal	-1.730	-11.78	Gaedcke Colorectal (Gaedcke *et al*, 2010)
Gastrointestinal	-1.647	-	Kaiser Colon (Kaiser *et al*, 2007)
Gastrointestinal	-1.576	-10.11	Skrzypczak Colorectal 2 (Skrzypczak *et al*, 2010)
Gastrointestinal	-1.546	-6.755	Skrzypczak Colorectal 2 (Skrzypczak *et al*, 2010)
Gastrointestinal	-1.501	-5.458	Kaiser Colon (Kaiser *et al*, 2007)
Heptocellular	-2.862	-5.15	Chen Liver (Zhou *et al*, 2002)
Heptocellular	-2.862	-10.35	Roessler Liver (Roessler *et al*, 2010)
Hepatocellular	-3.400	-7.603	Roessler Liver (Roessler *et al*, 2010)
Liposarcoma	-3.191	-	Barretina Sarcoma (Barretina *et al*, 2010)
Liposarcoma	-2.817	-	Barretina Sarcoma (Barretina *et al*, 2010)
Renal	-10.41	-14.78	Beroukhim Renal (Beroukhim *et al*, 2009)
Renal	-9.677	-23.35	Beroukhim Renal (Beroukhim *et al*, 2009)
Renal	-8.552	-	Lenburg Renal (Lenburg *et al*, 2003)
Renal	-7.623	-	Gumz Renal (Gumz *et al*, 2007)
Renal	-4.330	-	Jones Renal (Jones *et al*, 2005)
Renal	-3.547	-8.938	Jones Renal (Jones *et al*, 2005)
Renal	-3.474	-18.9	Jones Renal (Jones *et al*, 2005)

Table R-3: Oncomine datasets reference list. Log2 median centered ratio of *PCK1* and *PCK2* in different cancers analyzed with Oncomine (https://www.oncomine.org; Rhodes *et al.*, 2004). Analysis type: Cancer versus Normal, threshold at p=1E-5 and top gene rank 10%. Graphical representation of the data is in Figure R-13. Missing values for PCK1 expression were not significant or were not analyzed in given dataset. Reference to original study is listed.

ID	Organ	Histological diagnosis	Differen-tiation	+ scale	Intensity (mean)
A1-3	**Esophagus**	Squamous cell carcinoma	Poorly	+++, +, ++	68.4, 14.8, 33.9
B1-3		Esophagus tissue (normal)		+/-, +/-, +/-	10.6, 23.4, 15.3
A4	**Stomach**	Adenocarcinoma	Moderately	+	28.10
A5		Fibrous tissue, smooth muscle		+	35.10
A6		Mucinous adenocarcinoma	Poorly	+/-	11.90
B4-6		Gastric body tissue (normal)		+++, +, +++	70.3, 38.1, 63.8
A7	**Colon**	Mucinous adenocarcinoma	Poorly	+/-	15.00
A8		Mucinous adenocarcinoma	Moderately	+++	84.00
A9		Fibrous tissue		++	66.5
B7-9		Colon tissue (normal)		++, +++, +/-	27.4, 55.7, 25
A10-12	**Prostate**	Adenocarcinoma		+++, +++, ++	89.4, 87.8, 66.7
B10-12		Prostate tissue (normal)		+, ++, +	19.1, 43.5, 30.4
C1, 2	**Liver**	Hepatocellular carcinoma	Moderately	++, ++	53.6, 87,5
C3		Hepatocellular carcinoma	Poorly	+	30.4
D1-3		Nodular cirrhosis (normal)		+++, +++, +++	143.5, 120.4, 104.8
C4, 5	**Lung**	Adenocarcinoma	Moderately	+, +/-	13.8, 9
C6		Squamous cell carcinoma	Moderately	+	24.1
D4-6		Lung tissue (normal)		+/-, +/-, +/-	4.6, 7.4, 10
C7, 8	**Kidney**	Clear cell carcinoma		+/-, +	27.4, 42.2
C9		Nephroblastoma		+/-	15.2
D7-9		Kidney tissue (normal)		+, ++, ++	26.2, 70.5, 56.8
C10, 11	**Breast**	Infiltrating ductal carcinoma	Moderately	++, ++	23.2, 38.7
C12		Infiltrating ductal carcinoma	Well	+	23.4
D10-12		Breast tissue (normal)		+/-, +/-, +/-	2.4, 8, 5
E1	**Uterine cervix**	Squamous cell carcinoma	Poorly	+	10.8
E2, 3		Squamous cell carcinoma	Moderately	++, +	38.6, 10.2
F1		Cervical canal tissue (normal)		+/-	6.2
F2		Fibrous tissue (normal)		+/-	7.1
F3		Cervix tissue (normal)		+/-	3.9

Table R-4: Evaluation of PEPCK-M expression in 48 cores of tumors and 48 cores of normal tissue from microarray BCN962 (US Biomax). Continuing on the next page.

E4-6	**Ovary**	Serous adenocarcinoma	Poorly	++, +/-, +/-	20.3, 11.6, 8.1
F4-6		Ovary tissue (normal)		+, +, +/-	16.9, 12.3, 12.2
E7, 9	**Bladder**	Urothelial carcinoma	Moderately	+/-, ++	4.5, 56.4
E8			Poorly	+++	19.8
F7-9		Bladder tissue (normal)		+, ++, +	23.5, 33.3, 29.7
E10-12	**Lymph node**	Large B-cell lymphoma		+, +, +/-	14.1, 17, 6.6
F10-12	**Stomach**	Lymph node tissue (normal)		+, +, +	24, 17.3, 22.3
G1-2	**Skin**	Squamous cell carcinoma	Well	++, +++	41.4, 59.7
G3			Poorly	++	45.2
H1-3		Skin tissue (normal)		+, ++, +	24.9, 24, 17.1
G4, 6	**Pancreas**	Adenocarcinoma	Poorly	+/-, ++	7.5, 32
G5		Pancreas tissue		+++	61.2
H4-6		Pancreas tissue (normal)		++, +++, +++	30.1, 66.7, 67.4
G7, 8	**Testis**	Seminoma		++, ++	45.9, 49.7
G9		Testis tissue		+	11.7
G10		Fibrofatty tissue		+	18.4
G11		Embryonic rhabdomyosarcoma		+/-	4.3
H7-10		Testis tissue (normal)		+, ++, ++, ++	38.5, 40.4, 49.6, 41.2
G12	**Tongue**	Alveoloar rhabdomyosarcoma		+/-	13.1
H11-12	**Placenta**	Placenta tissue (normal)		++, +	30.5, 33.7

Table R-4: Evaluation of PEPCK-M expression in 48 cores of tumors and 48 cores of normal tissue from microarray BCN962 (US Biomax). The organ type, histological diagnosis, differentiation, PEPCK-M expression status (+/- no or very weak, + weak, ++ moderate and +++ strong) and mean intensity of PEPCK-M staining are shown for each sample. Mean intensity was evaluated with ImageJ using plugin IHC Toolbox (Shu *et al*, 2013).

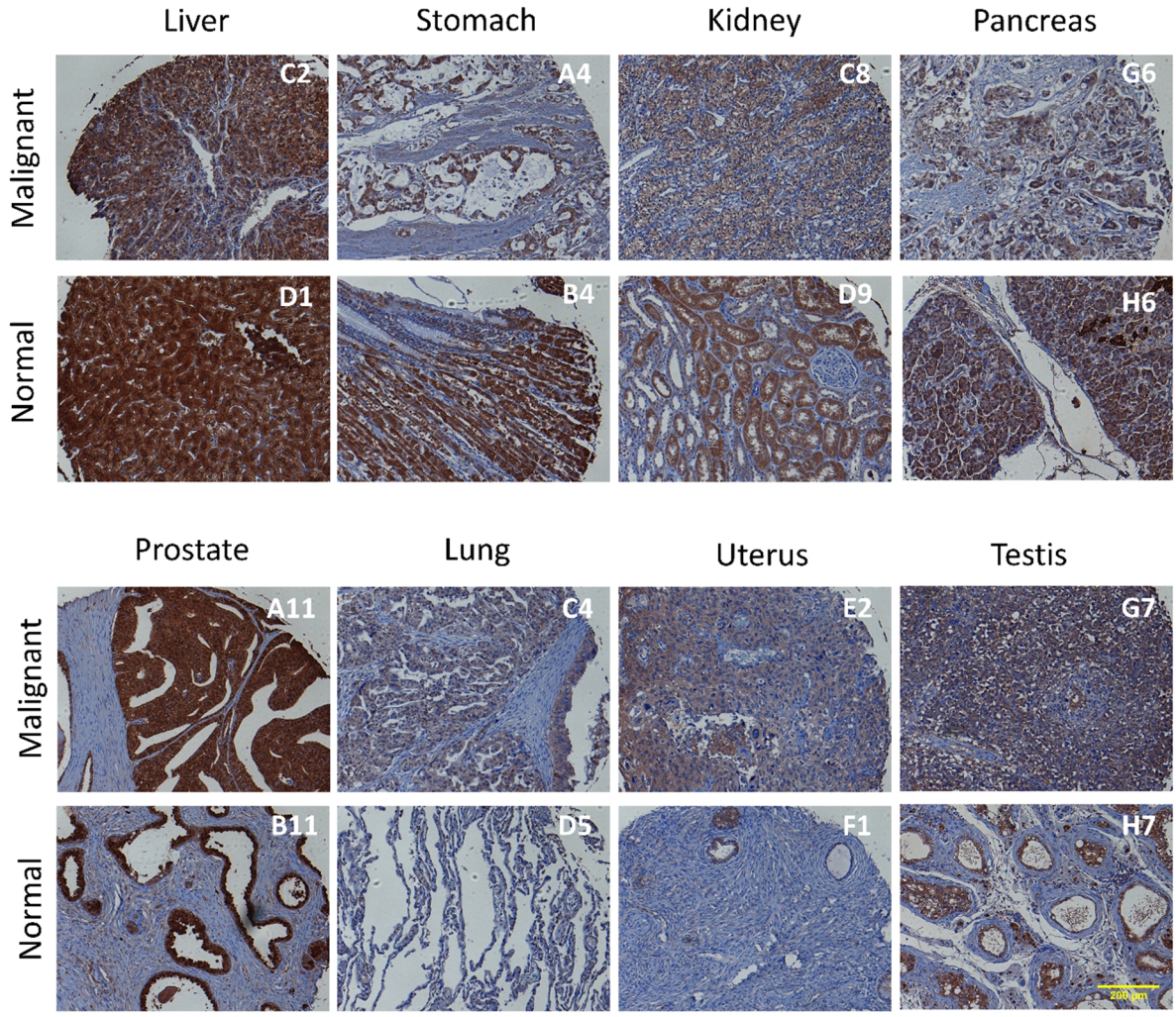

Figure R 14: PEPCK-M expression in different malignant and normal tissues. Immunohistochemical analysis of PEPCK-M expression in selected types of tumors and their matched non-neoplastic tissue microarray BCN962 (US Biomax). Samples were stained with hematoxylin and PEPCK-M antibody. Scale bar = 200 μm.

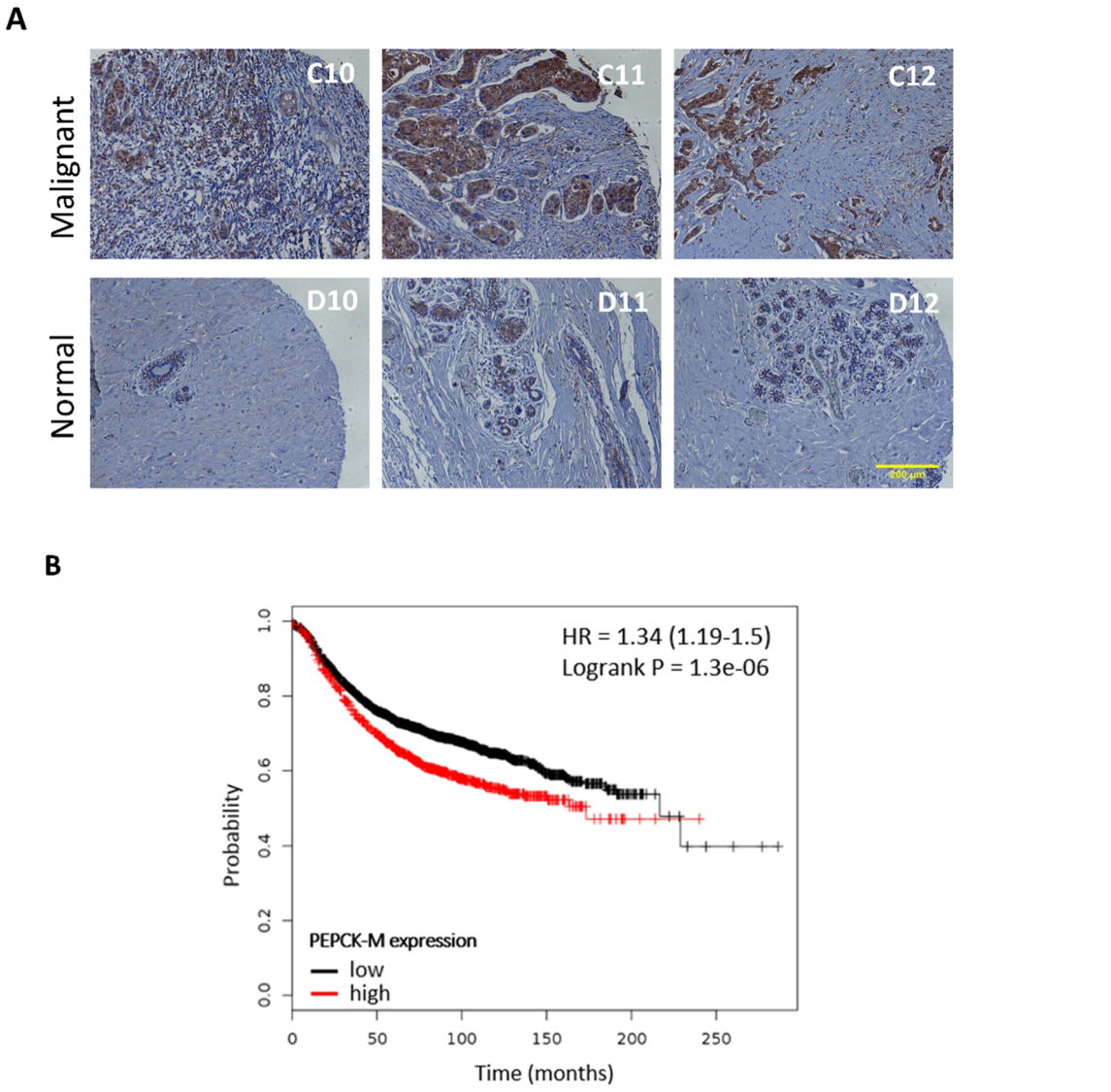

Figure R-15: PEPCK-M expression in breast cancer and its impact on survival. (A) Imunohistochemistry of PEPCK-M expression in three independent human breast cancer samples and their non-neoplastic counterparts from tissue microarray panel BCN962 (US Biomax). Scale bar = 200 µm. **(B)** Relapse free survival of breast cancer patients with high and low expression levels of PEPCK-M. Data from publically available dataset (GEO (Affymetrix microarrays only), EGA and TCGA) were compiled and analyzed using a Kaplan-Meier plotter tool for breast cancer (http://kmplot.com/analysis/index.php?p=service; Győrffy *et al.*, 2010; Szász *et al.*, 2016). Number of analyzed cases is 3955 and no restriction for breast cancer subtypes was applied.

2.1 Model for the study of PEPCK-M role in cancer cell metabolism

For the most part, experiments have been performed on human breast cancer cells, MCF7. Another two cell lines, NIH-3T3-KRas (transformed mouse embryonic fibroblasts carrying a mutation at codon 12 $KRas^{G12V}$, denominated 3T3-KRas) and HCT116 (human colon cancer cell line), were used to complement the results. All cell lines used were subjected to manipulation of PEPCK-M expression to obtain stable lines with reduced or increased PEPCK-M levels. 3T3-KRas showed resistance to silencing with either siRNA or shRNA lentiviral vectors. Therefore, the experiments with 3T3-KRas cells were performed by chemical inhibition of PEPCK activity with 3MPA.

Silencing of PEPCK-M was obtained by infecting cells with lentiviral vector containing shRNA against the mitochondrial isoform of PEPCK or scrambled shRNA. We derived two MCF7 lines with effective knock down of PEPCK-M denominated sh1-PCK2 and sh2-PCK2. These cells expressed roughly 35% (sh1-PCK2) and 44% (sh2-PCK2) of PEPCK-M protein when compared to wild-type MCF7 (Figure R-16 A,B). MCF7 cells expressing scrambled shRNA, denominated shCtrl, were used as a control and showed similar expression of PEPCK-M as the wild type cells (Figure R-16 A,B). Analysis of *PCK2* mRNA expression showed a 74% reduction in sh1-PCK2 MCF7 cells (Figure R-16 C). Lastly, we examined the impact of silencing on enzymatic activity. PEPCK-M activity was reduced to 50% (sh2-PCK2) and 53% (sh1-PCK2) when compared to shCtrl MCF7 cells (Figure R-16 D).

Overexpression of PEPCK-M in MCF7 cells was acquired by infecting cells with lentiviral vector expressing human *PCK2* cDNA under the CMV promoter and cells were denominated L-PCK2. A 2.5-fold increase in PEPCK-M protein expression was obtained as compared to MCF7 WT (Figure R-16 A,B). Analysis of *PCK2* mRNA expression showed a 29-fold induction in L-PCK2 MCF7 cells (Figure R-16 C) and enzymatic activity of PEPCK-M was 3.3-fold higher in these cells when compared to shCtrl MCF7 (Figure R-16 D).

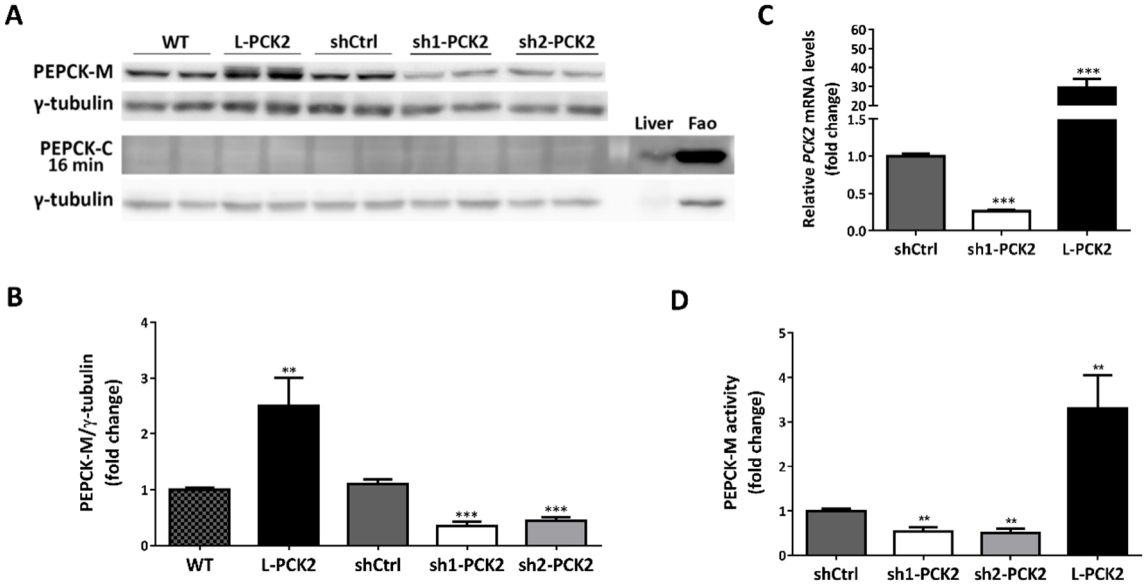

Figure R-16: MCF7 model for the study of PEPCK-M role in cancer. Stable silencing and overexpression of PEPCK-M in MCF7 cell line were obtained using lentiviral vectors containing inserts of shRNA against *PCK2* or inserts of *PCK2* cDNA, respectively. **(A)** Western blot analysis of mitochondrial and cytosolic PEPCK expression levels in MCF7 with altered PEPCK-M expression levels: overexpressed (L-PCK2), basal (shCtrl and WT) and knocked down PEPCK-M (sh1-PCK2 and sh2-PCK2). As a positive control of PEPCK-C expression, extracts from mouse liver and Fao hepatoma cells were used. **(B)** Western blot quantification of PEPCK-M protein abundance in MCF7 modified lines. **(C)** Quantitative real-time PCR was performed to determine *PCK2* mRNA levels in MCF7 shCtrl, sh1-PCK2 and L-PCK2 cells. The quantification of *PCK2* expression was normalized to *GAPDH* and *TBP*. **(D)** PEPCK-M enzyme activity in MCF7 cell lines shCtrl, sh1-PCK2, sh2-PCK2 and L-PCK2. (B) **P<0.01, ***P<0.001 versus WT (C,D) **P<0.01, ***P<0.001 versus shCtrl.

Western blot analysis of PEPCK-M in MCF7 L-PCK2 showed two different bands with a small difference in molecular weight (Figure R-17 A). The lower band was identified as intrinsic PEPCK-M as it has the same size as the wild type protein. Increased molecular weight in the upper band is probably caused by the fact that the *PCK2* cDNA is inserted before a V5 tag in lentiviral vector. Overlap of two western blot images demonstrated that the upper band of PEPCK-M is identical to the band detected by a V5 specific antibody (Figure R-17 A). Therefore, the upper band belongs to PEPCK-M protein produced from the lentiviral vector and its size is increased by the V5 tag. As the size of PEPCK-M protein in L-PCK2 is bigger, immunohistochemistry was performed to confirm that the presence

of the V5 tag does not prevent the protein from its mitochondrial import. PEPCK-M originating from L-PCK2 MCF7 was visualized by staining with anti-V5 antibodies. V5 staining merged with MitoTracker colabeled mitochondria, demonstrating appropriate localization and no negative effects of the V5 tag on protein maturation and transport in L-PCK2 cells (Figure R-17 B).

All the results of expression and enzymatic activity confirm that we obtained a successful model to the study of PEPCK-M relevance in cancer metabolism in the MCF7 background.

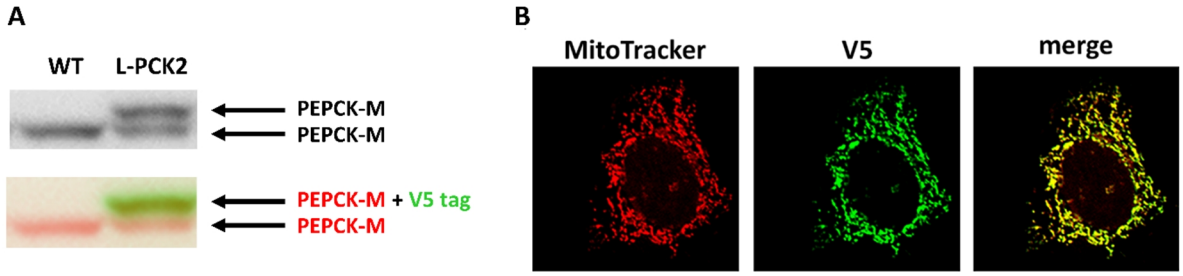

Figure R-17: L-PCK2 MCF7 cell line. (A) Comparison of PEPCK-M band distribution in WT and L-PCK2 MCF7 cells. An overlap of western blot images shows band of PEPCK-M (red) and V5 (green) in MCF7 WT and L-PCK2. **(B)** Immunofluorescence staining of MCF7 L-PCK2 cells. Cells were stained for V5 tag (green) and mitochondria were visualized by MitoTracker (red). Merge of V5 and MitoTracker is showed in yellow.

Most cell lines, and among them also MCF7 breast cancer cell line, do preferentially express mitochondrial isoform of PEPCK rather than the cytosolic one (Table R-2). We confirmed this by western blot analysis where we observed that parental MCF7 cell line (WT) does not express cytosolic isoform of PEPCK and that changes in PEPCK-M expression do not have any effect on the expression of PEPCK-C, which stays undetected in sh1-PCK2, sh2-PCK2, shCtrl and L-PCK2 (Figure R-16 A).

HCT116 cell line with knocked down PEPCK-M (shPCK2) was obtained by infecting cells with a mix of 3 different lentiviral vectors containing shRNAs against PEPCK-M. We obtained a stable line with 27% of the PEPCK-M protein expression levels found in shCtrl cells (Figure R-18). Similarly to MCF7 cell lines, we did not detect PEPCK-C expression in shCtrl, neither in shPCK2 cells (Figure R-18).

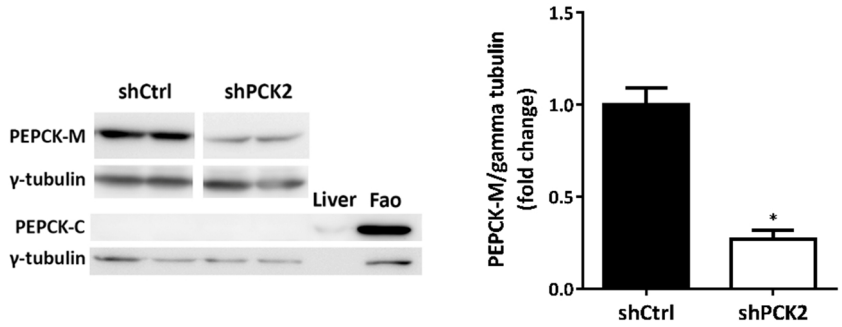

Figure R-18: HCT116 model with silenced PEPCK-M expression. Western blot analysis of PEPCK-M in stably silenced and control HCT116 cell lines. Silencing was obtained by infecting cells with a mixture of lentiviral vectors containing shRNA against PEPCK-M. As a control, HCT116 cell line expressing scrambled shRNA was used. Western blot quantification of PEPCK-M abundance is displayed in the graphic on the right, * $P<0.05$.

2.2 Consequences of PEPCK-M silencing on growth and metabolism

Preferential expression of PEPCK-M detected in different tumors and cancer cell lines encouraged our hypothesis of an important role of PEPCK-M in tumor metabolism. As a first indicator of changes in metabolism, we decided to analyze growth induced by changes in PEPCK-M activity in our model lines. MCF7 cells were grown in DMEM media with 25 mM glucose and the number of cells was indirectly assessed using either MTT or crystal violet (CV) assays (Figure R-19). MCF7 cells with knocked down PEPCK-M (sh1-PCK2 and sh2-PCK2) showed significant decrease in cell count when compared to control. This effect was detected using either assay: MTT (11% reduction) and CV (18% reduction) for sh1-PCK2 and 21% (MTT) and 20% (CV) for sh2-PCK2 (Figure R-19 A,B). Overexpression of PEPCK-M did not favor growth rates when compared to shCtrl at least for the range of examined time, as no significant effects were detected (Figure R-19 A,B). Similarly, a negative impact of PEPCK-M silencing on growth was observed in HCT116 cells. ShPCK2 HCT116 cells showed decreased cell number after 24h of growth in DMEM media containing 25 mM glucose. When compared to shCtrl, cell number for shPCK2 cells was decreased by 17% when analyzed by MTT assay and by 10% when analyzed by CV assay.

To analyze the effect of the inhibition of PEPCK-M on cell growth in 3T3-KRas cells, we

cultured them in DMEM medium with 25 mM glucose in the presence of DMSO (control) or 100 μM 3MPA (inhibitor of PEPCK enzymatic activity). Crystal violet assay showed that inhibition of PEPCK-M decreased cell count by 21.5% in this cell line (Figure R-19 C). Taken together, PEPCK-M inhibition demonstrated an impact on cell growth in MCF7, HCT116 and 3T3-KRas cell lines. These differences in growth can be caused by slower growth, or by induced cell death. Therefore the presence of apoptosis and necrosis was evaluated.

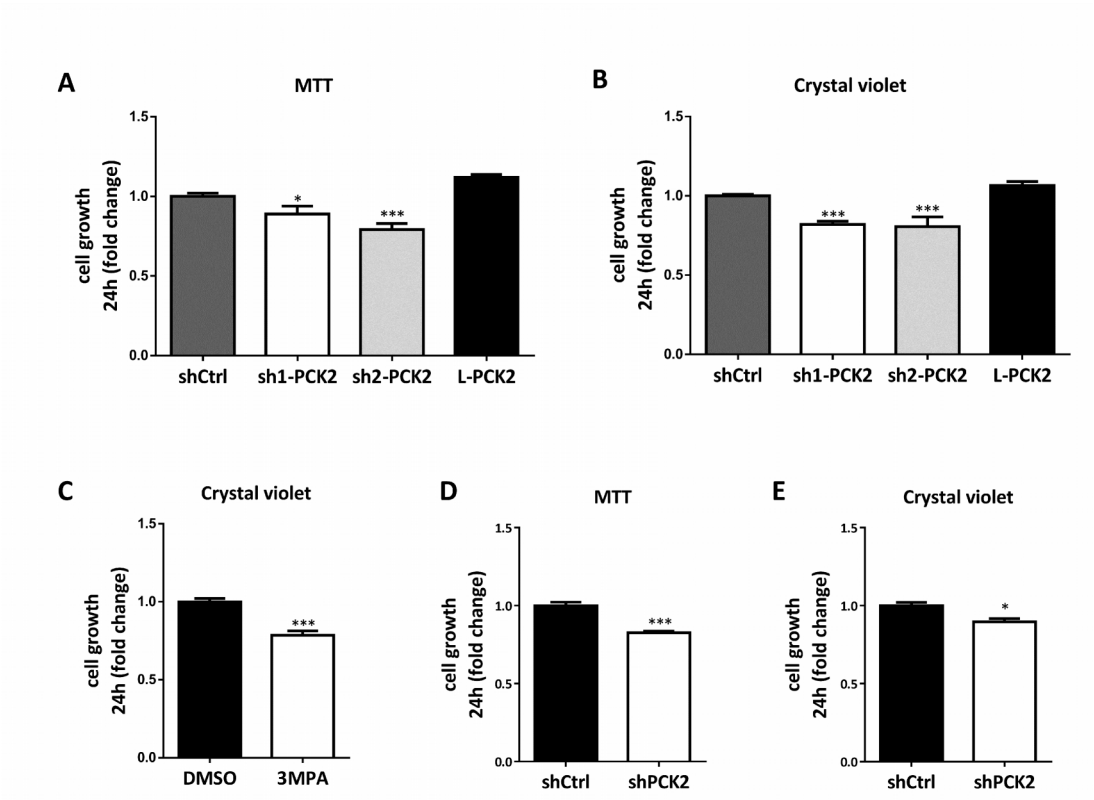

Figure R-19: Cell growth rates of MCF7, 3T3-KRas and HCT116 cells with altered PEPCK-M activity. (A,B) MCF7 cells with basal (shCtrl), reduced (sh1-PCK2, sh2-PCK2) and increased (L-PCK2) levels of PEPCK-M were grown in DMEM media with 25 mM glucose. Cell number was analyzed at 24h by MTT assay (A) and crystal violet assay (B). **(C)** 3T3-KRas cells treated with DMSO and 3MPA (100 μM) were grown in DMEM media with 25 mM glucose and growth was evaluated using crystal violet assay at 24h. **(D,E)** ShCtrl and shPCK2 HCT116 cells were grown in DMEM media with 25 mM glucose and cell number was analyzed at 24h with MTT (n=1) (D) and CV (n=1) (E) assay. (A,B,C,D,E) Ratio to shCtrl was plotted. *P<0.05, ***P<0.001 versus shCtrl (A,B) or DMSO (C).

We did not observe any morphological changes that would indicate the presence of cell death in MCF7 and 3T3-KRas cells with decreased PEPCK-M activity grown in DMEM with 25 mM glucose. Nevertheless, apoptosis and necrosis were analyzed by Annexin V staining by flow cytometry. Annexin V binds preferentially to phosphatidylserine, which is exposed in outer plasma membrane, when cell undergo apoptosis. Therefore, cells stained with Annexin V are identified as apoptotic. Cells stained with Annexin V and 7AAD (cell impermeable DNA stain) at the same time are identified as necrotic or as cells in late apoptosis. Annexin V staining was assessed in MCF7 shCtrl and sh1-PCK2 cells, and 3T3-KRas cells treated with DMSO or 3MPA (100 μM). Results showed a very low percentage of dying cells in either condition. No significant changes were found when comparing MCF7 shCtrl and MCF7 sh1-PCK2 cells (2.6 ± 0.36% and 3.21 ± 0.62%, respectively) (Figure R-20 A), or when comparing 3T3-KRas cells with basal (DMSO – 9.33 ± 0.68%) and inhibited (3MPA – 8.07 ± 1.04%) PEPCK activity (Figure R-20 B).

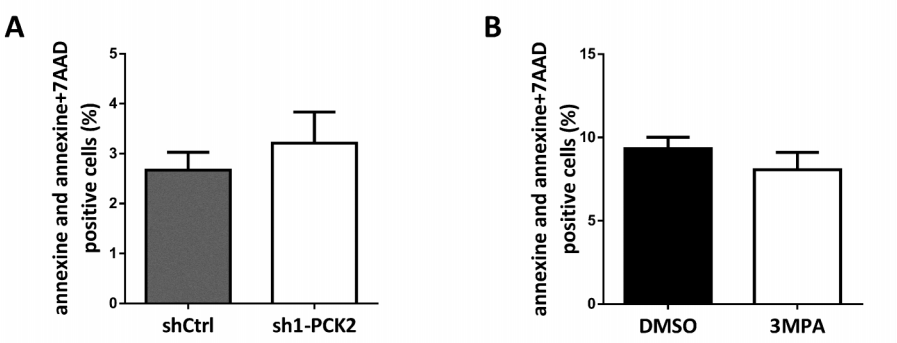

Figure R-20: Cell death quantification in MCF7 and 3T3-KRas cells. Analysis of apoptotic (annexin positive) and late apoptotic/necrotic (annexin+7AAD positive) cells by flow cytometry. **(A)** Percentage of apoptotic MCF7 cells grown in DMEM media with 25 mM glucose for 24h. **(B)** Percentage of apoptotic 3T3-KRas cells growing in DMEM media with 25 mM glucose for 48h in the presence of DMSO or 3MPA (100 μM).

Taken together, these data suggest that decrease in cell number in MCF7 and 3T3-KRas cells with reduced/inhibited PEPCK-M activity is not caused by apoptosis or necrosis. Therefore we conclude that the difference in the observed number of cells (Figure R-19) is caused by the growth rate impairment in cells lacking a full complement of PEPCK-M activity. At this point we examined cell cycle that could give us more detailed picture of

changes occurring upon PEPCK-M silencing in cell growth. However, analysis of cell cycle in shCtrl and sh1-PCK2 cells did not show any differences that would explain decreased growth of silenced MCF7 cells (Figure R-21).

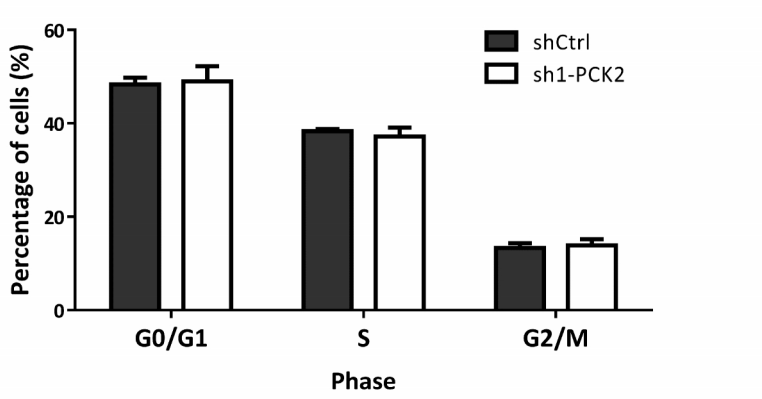

Figure R-21: Cell cycle analysis of MCF7 cells. MCF7 cells were grown in 25 mM glucose media for 24h. Cells were not synchronized and were analyzed in exponential phase of growth. Analysis of cell cycle was done using 7AAD staining. Fluorescence was measured by flow cytometry and data were analyzed using ModFit LT V3.3.11.

Findings that lower PEPCK-M activity has an effect on growth of cells in media with a rich source of metabolites pointed to the importance of metabolic changes occurring under PEPCK-M silencing. Therefore we decided to submit MCF7 cells to analysis of its metabolic profile.

First, glycolytic metabolism was evaluated by analyzing glucose consumption and lactate production in cells in exponential phase growing in the presence of 25 mM (high glucose/HG) and 1 mM (low glucose/LG) glucose. Incubation in low glucose conditions was decreased to 8h to avoid glucose exhaustion.

Silencing of PEPCK-M caused a 12% decrease in glucose consumption in HG and a 5% decrease in LG conditions, when compared to control cell line, however analysis of lactate production showed no differences.

Results of glucose and lactate metabolism were also used to calculate lactate/glucose ratio, which indicate how many incoming molecules of glucose are converted to lactate. One molecule of glucose can give rise to two molecules of lactate. Therefore, values can

range from 0 (0% conversion) to 2 (100% conversion) without taking into account possible flux of glutamine carbons into lactate as we did not confirmed this flux in MCF7 cells (Figure R-32). We saw, that MCF7 sh1-PCK2 cells show higher lactate/glucose ratio (1.79 in HG; 1.83 in LG) as compared to shCtrl (1.64 in HG; 1.76 in LG) and L-PCK2 (1.64 in HG; 1.71 in LG) (Figure R-22 C). Therefore, sh1-PCK2 cells convert 89.5% (in HG) or 91.5% (in LG) of consumed glucose molecules to lactate, whereas shCtrl converts 82% (in HG) and 88% (in LG), and L-PCK2 82% (in HG) and 85.5% (in LG) (Figure R-22 D).

Observed differences in glucose/lactate ratio indicate possible alterations on the destination of glucose derived pyruvate in cells. Therefore, we were interested if silencing of PEPCK-M has any effect on mitochondrial respiratory activity by measuring oxygen consumption rates. Analysis of oxygen consumption in shCtrl and sh1-PCK2 cells did not reveal any changes in oxygen consumption rates (Figure R 22). Additionally, these results were supported by western blot analysis, where we observed similar levels of pyruvate dehydrogenase (PDH) phosphorylation (Figure R 23). PDH is the enzyme that participates at the conversion of pyruvate into acetyl-CoA that is oxidized in the TCA cycle. Phosphorylation is inhibiting the activity of this enzyme and can indicate regulation of the flux of pyruvate into mitochondria. Therefore, similar levels of PDH phosphorylation would indicate similar activity of this enzyme. No changes in respiration are also consistent with results obtained by metabolomics studies, where glutamine consumption was unchanged upon silencing PEPCK-M (Figure R 27).

Decreased glucose consumption observed in sh1-PCK2 cells (Figure R-22) and previously described reduction of glycolytic rate in MCF7 cells upon PEPCK-M silencing in our laboratory (Méndez-Lucas *et al.*, 2014) led us to evaluate PI3K pathway implicated in the regulation of glycolysis by analyzing AKT phosphorylation (pAKT). However, no changes in AKT phosphorylation that would correlate with observed changes in glucose metabolism were observed (Figure R 23). Interestingly, the phosphorylation pattern of S6 ribosomal protein (pS6) the mTOR pathway downstream of PI3K signaling was highly affected by PEPCK-M silencing (Figure R 23). This would suggest the implication of other pathways that activate S6, a protein connected to enhanced translation, in sh1-PCK2 cells. Overexpression of PEPCK-M had no effect on glucose consumption. However,

decreased lactate production was observed in L-PCK2 MCF7 cells when grown in LG conditions. L-PCK2 had lower pAKT expression but no changes were observed in S6 or PDH phosphorylation.

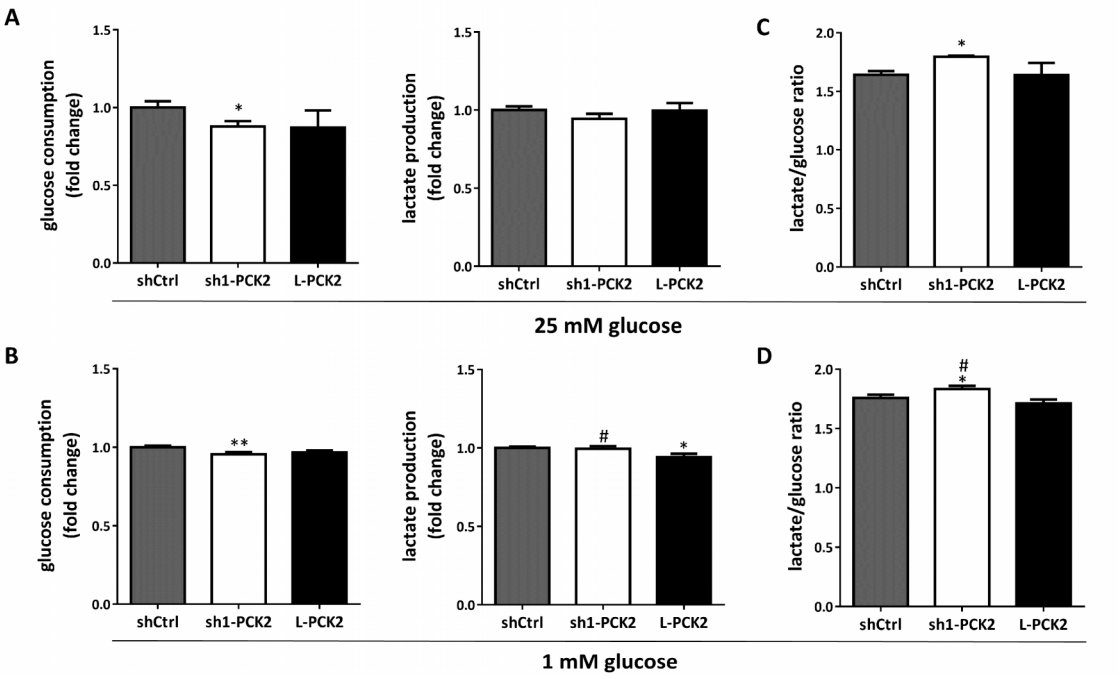

Figure R-22: Glucose and lactate metabolism in MCF7 cells. (A) Fold change of glucose consumption and lactate production (µg/mg of protein*h) in MCF7 cells grown in 25 mM glucose medium for 24h. **(B)** Fold change of glucose consumption and lactate production (µg/mg of protein*h) in MCF7 cells grown in 1 mM glucose medium for 8h. **(C)** Glucose to lactate ratio in cells grown in 25 mM glucose medium for 24h. **(D)** Glucose to lactate ratio in cells grown in 25 mM glucose medium for 8h. *P<0.05, **P<0.01 versus shCtrl, #P<0.05 sh1-PCK2 versus L-PCK2.

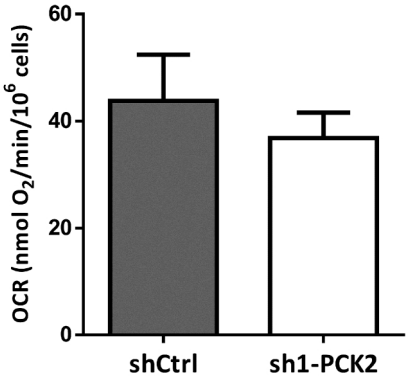

Figure R-23: Oxygen consumption rates in MCF7 cells. Oxygen consumption rates (OCR) were taken from routine respiration using a high resolution apparatus (Oxygraph-2K). During the assay, MCF7 shCtrl and sh1-PCK2 cells were incubated in respiration media and data was taken after stabilization for at least 10 min.

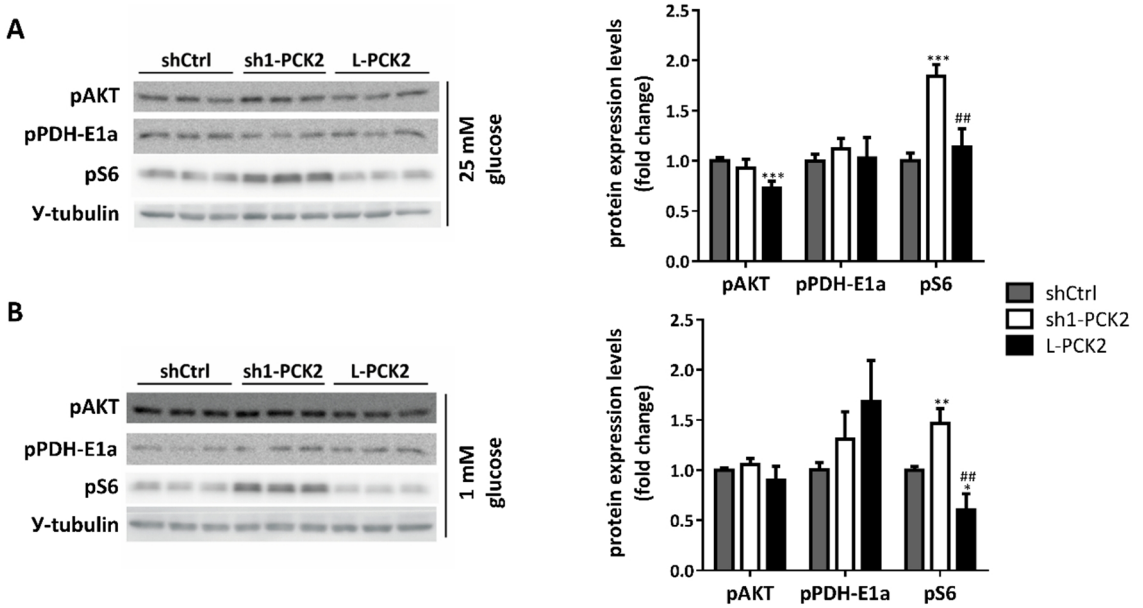

Figure R-24: Western blot analysis and relative quantification of selected proteins. Expression of pAKT, pPDH-E1a and pS6 was detected in MCF7 cells growing for 24h in DMEM media containing **(A)** 25 mM glucose (HG) and **(B)** 1 mM glucose (LG). Quantification of western blots was performed: pAKT (HG n=4, LG n=1), pPDH-E1a (HG n=6, LG=1), pS6 (HG n=6, LG n=3). **P<0.01, ***P<0.001 versus shCtrl. ##P<0.01 versus sh1-PCK2.

2.3 Effect of PEPCK-M expression levels on TCA cycle metabolism

The impact of PEPCK-M expression on glucose metabolism and the associated changes in lactate/glucose ratio point to possible PEPCK-M dependent metabolic alterations in the TCA cycle and its cataplerotic and anaplerotic capacities. Therefore we decided to subject our MCF7 models to metabolomics analysis, which was performed in collaboration with the laboratory of Dr. Shawn Burgess at UT Southwestern, Dallas, USA. Concentration and stable isotope labeling of several amino acids and organic acids were quantified.

To analyze TCA cycle metabolism, cells were fed with uniformly labeled glutamine containing carbon isotope ^{13}C ([U-^{13}C] glutamine). As ^{13}C from glutamine is distributed among various metabolites, their mass increase proportionally to the number of incorporated carbons. This increase in mass was detected by mass spectrometry. Isotope distribution in metabolites is marked as m+x, where the m stands for natural mass of the metabolite and the x indicate number of incorporated ^{13}C carbons.

[U-^{13}C] glutamine can be metabolized in the TCA cycle in forward (oxidative metabolism) and reverse direction (reductive carboxylation) (Zhang *et al*, 2014), depending on the metabolic adaptations of the tumor. ^{13}C isotope distribution from [U-^{13}C] glutamine into TCA cycle and other intermediates give us important information about anaplerosis, cataplerosis and the TCA cycle activity.

The possible carbon flow from [U-^{13}C] glutamine into TCA cycle intermediates and other metabolites is explained in the schemes in Figure R-25.

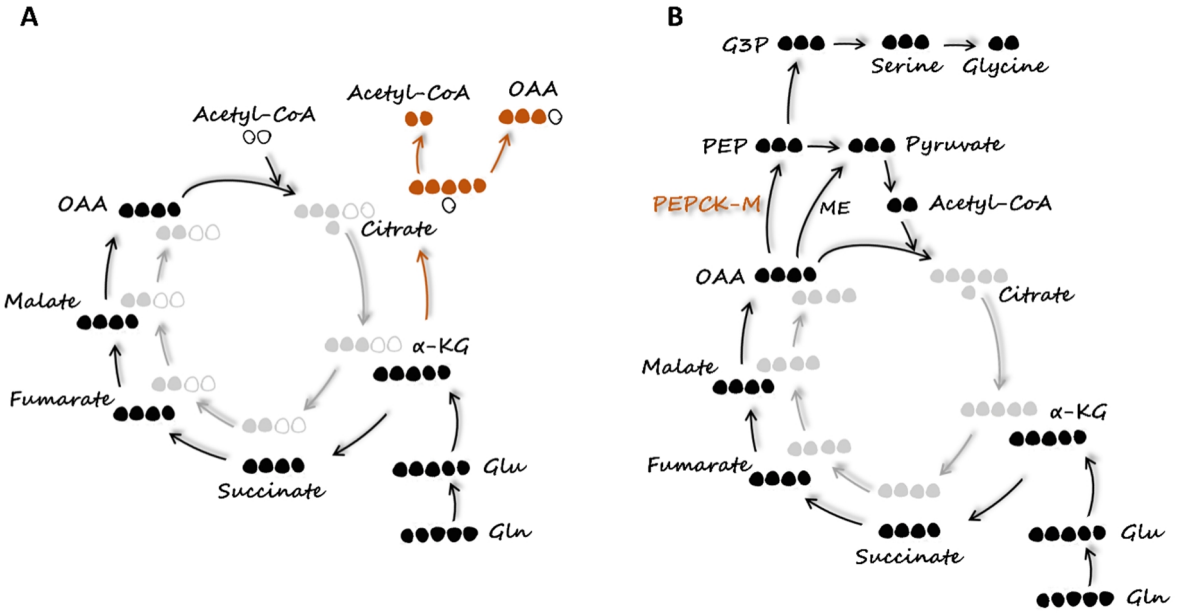

Figure R-25: Schematic diagram of isotope distribution from [U-^{13}C] glutamine. (A) Oxidative metabolism of glutamine: [U-^{13}C] glutamine transfer four ^{13}C carbons to TCA cycle intermediates, generating m+4 succinate, fumarate, malate and oxaloacetate (OAA). In the second cycle, m+2 succinate, fumarate, malate and oxaloacetate are formed**.** Reductive metabolism of glutamine: [U-^{13}C] glutamine transfer five ^{13}C isotopes to alpha-ketoglutarate (α-KG), which is converted to m+5 citrate. M+5 citrate give rise to acetyl-CoA (fully labeled – m+2) and m+3 OAA, malate and fumarate in the reverse reactions. **(B)** During oxidative metabolism of glutamine, PEPCK-M can convert fully labeled OAA (m+4) to fully labeled PEP (m+3) and subsequently to fully labeled pyruvate (m+3). M+3 pyruvate can be also formed through malic enzyme (ME) from m+4 malate. M+3 pyruvate can be later converted to m+3 lactate or m+2 acetyl-CoA. M+2 acetyl-CoA than form m+6 citrate, when condensates with m+4 OAA. M+6 citrate generate fully labeled intermediates of the TCA cycle. Although, if labeled acetyl-CoA is formed, it might not rich 100% and therefore, in second cycle m+4 or m+2 four carbon intermediates can be formed. If fully labeled PEP is formed, it can be converted to glycerol-3 phosphate, which is precursor for formation of different glycolytic intermediates and amino acids. In the protocol we used, we detected isotopomer distribution into serine and glycine. (A,B) ^{13}C are represented in first cycle by black circles and in second by grey circles. Empty circles represents ^{12}C. Reductive carboxylation pathway is represented by orange circles (^{13}C).

To analyze the behavior of the TCA cycle in the presence of glucose, MCF7 cells with basal (shCtrl), reduced (sh1-PCK2) and increased (L-PCK2) expression of PEPCK-M were grown in DMEM medium containing 25 mM glucose. When cells reached 70-80% confluency, medium was changed to the same type of medium containing 2mM [U-^{13}C] glutamine tracer. Cells were incubated for 4h and quenched. Enrichment of TCA cycle intermediates, selected amino acids, pyruvate and lactate were detected.

The distribution of ^{13}C from glutamine into TCA cycle intermediates showed several differences among MCF7 cells with modified PEPCK-M expression levels (Figure R-26). Generally, MCF7 sh1-PCK2 showed significantly lower percentage of non-labeled (m+0) pool in α-KG, succinate, malate and oxaloacetate, when compared to shCtrl and L-PCK2 MCF7 cells. On the contrary, a greater distribution of labeled metabolites mainly in m+4 species of succinate, malate and oxaloacetate was observed in sh1-PCK2 cells (Figure R-27). Labeling of m+4 species originates from oxidative metabolism of glutamine (Figure R-25). One of the potential explanations for increased labeling in sh1-PCK2 could be the presence of higher anaplerotic flux of glutamine through the TCA cycle. Examination of isotopomer distribution shows that 95% of glutamine in all cell lines is fully labeled (m+5). Our isotopomer distribution data reveals small changes in m+5 glutamate and α-ketoglutarate. However, these changes cannot explain the observed accumulation of m+4 species in sh1-PCK2 cells. Thereby, we can exclude that transport or altered anaplerotic entry of glutamine through α-ketoglutarate into the TCA cycle are responsible for changes in m+4 pools. Moreover, this finding is supported by the fact that glutamine consumption in these cells showed very similar rates after 24h of incubation in DMEM media containing 25 mM glucose (Figure R-28). Expression analysis of genes implicated in glutamine metabolism showed expression of *GLS1* isoform of glutaminase, whereas *GLS2* isoform was not detectable. Expression of *GLUL*, glutamine synthetase was also detected. *GLS1*/*GLUL* expression ratio is 0.77 in all; shCtrl, sh1-PCK2 and L-PCK2 cells; indicating glutamine catabolic activities. Cells overexpressing PEPCK-M showed significant increase of *GLS1* expression.

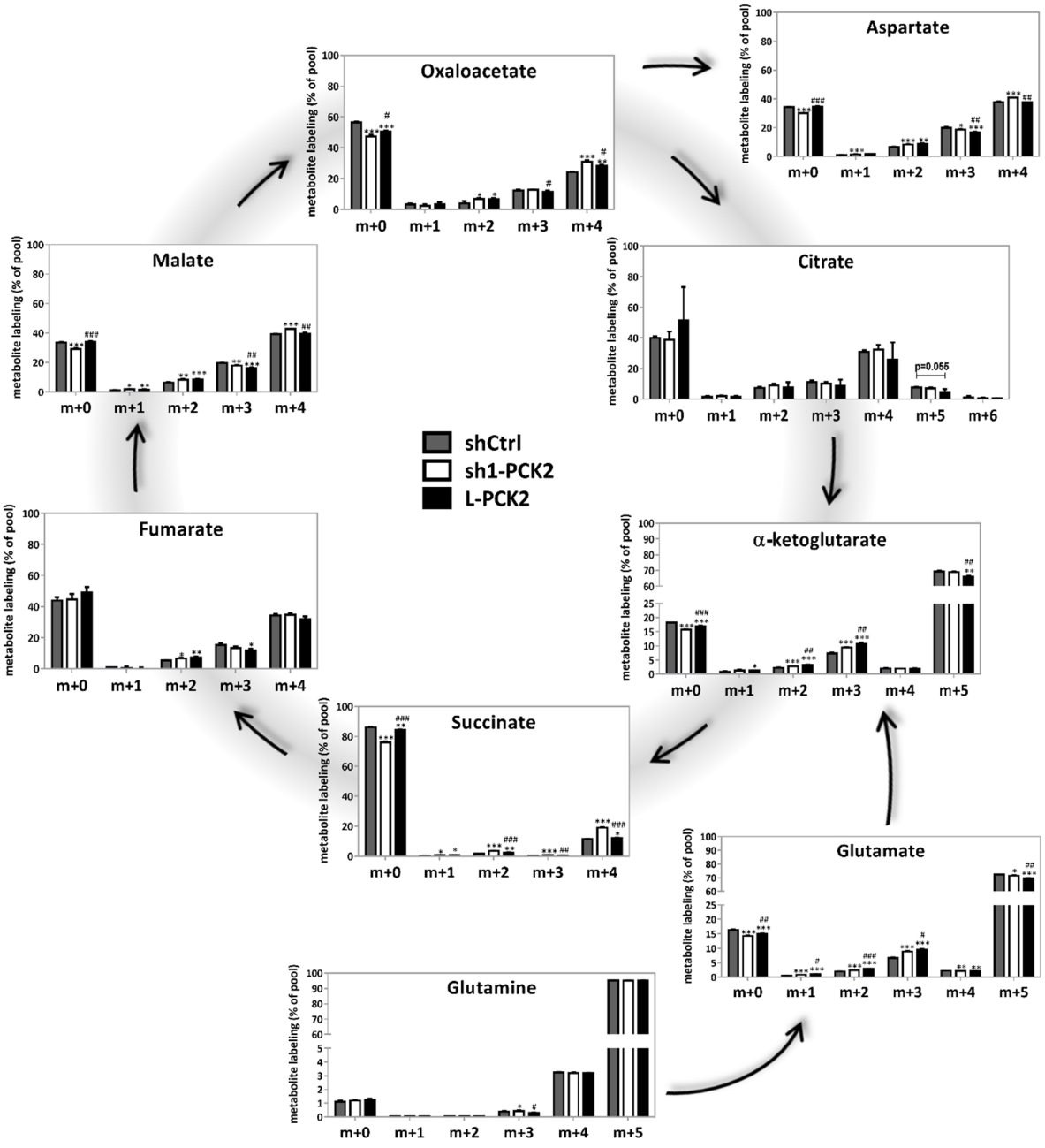

Figure R-26: ^{13}C isotopomer distribution from fully labeled glutamine into TCA cycle intermediates. MCF7 cells with different expression levels of PEPCK-M were exposed to 2mM [U-^{13}C] Gln in DMEM media containing 25 mM glucose and 10% dFCS. Isotopomer distribution was detected by GC-MS. Data are plotted as mean ± SD. *P<0.05, **P<0.01, ***P<0.001 versus shCtrl. #P<0.05, ##P<0.01, ###P<0.001 versus sh1-PCK2.

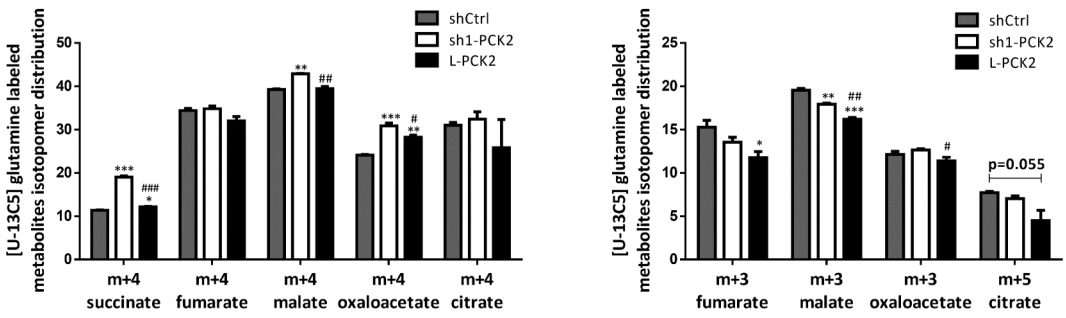

Figure R-27: Metabolism of glutamine. Abundance of m+4, m+3 and m+5 species of selected TCA cycle intermediates from Figure R-26. *P<0.05, **P<0.01, ***P<0.001 versus shCtrl. #P<0.05, ##P<0.01 versus sh1-PCK2.

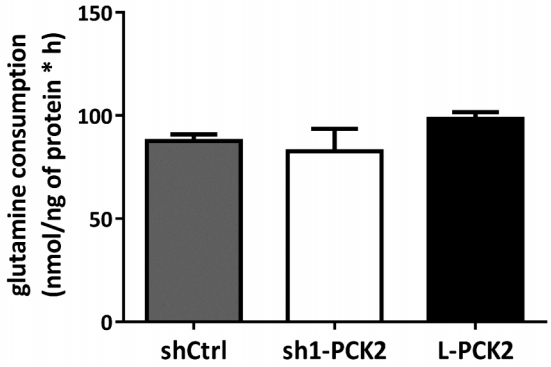

Figure R-28: Glutamine utilization by MCF7 cells. Consumption rate of glutamine in MCF7 cells grown 24h in DMEM media with 25 mM glucose, 10% dFCS and 2mM Gln. Concentration of glutamine in medium was analyzed by LC-MS.

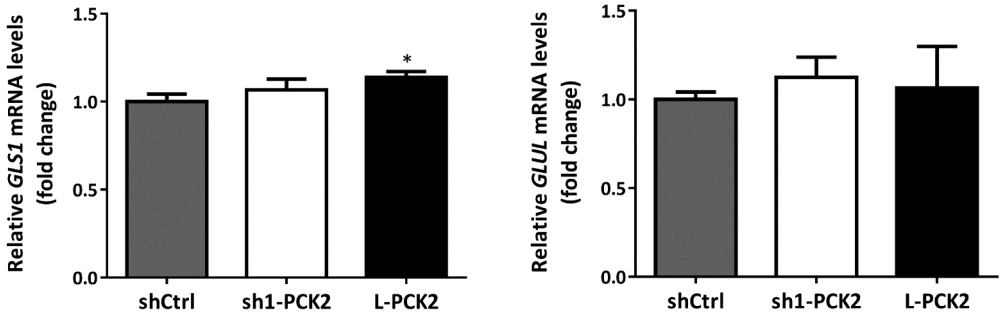

Figure R-29: Expression pattern of enzymes involved in glutamine metabolism. Quantitative real time analysis was used to analyze expression of *GLS1* and *GLUL* (n=2) in cells grown 24h at presence of 25 mM glucose. The quantification of mRNA was normalized to *TBP* and *GUSB*. *P<0.05 versus shCtrl.

It is noteworthy that succinate, from all the TCA cycle intermediates, shows the most significant changes in the pool of m+4 species (Figure R-27). Sh1-PCK2 showed a 1.7-fold increase in m+4 labeling of succinate when compared to control and a 1.6-fold increase when compared to L-PCK2. As we mentioned, glutamine flux into the TCA cycle does not seem to play a role in changes of m+4 species, therefore we assume that differences observed in succinate labeling in sh1-PCK2 MCF7 versus shCtrl and L-PCK2 might be caused by changes in the metabolism of α-KG into succinate or by alternative pathways that could metabolize glutamine into succinate (for example the GABA shunt).

Interestingly, m+4 species of succinate form 11.4 – 19% of its pool whereas m+5 species of α-KG (the precursor of m+4 succinate) accounted for 66-69%. This inequality can be explained by the presence of a larger pool of unlabeled succinate in the cells which might proceeds from other sources than the oxidative TCA cycle. Therefore we evaluated the consumption of branched-chain amino acids that are catabolized into succinate. Valine, leucine and isoleucine consumption stand together for 27.11% of detected consumed amino acids in MCF7 shCtrl cells (Figure R-30). However, comparison of concentrations of consumed valine, leucine and isoleucine did not show any significant differences among infected MCF7 cells. In the case of isoleucine, L-PCK2 showed slightly higher consumption of this amino acid ($p = 0.066$) when compared with shCtrl.

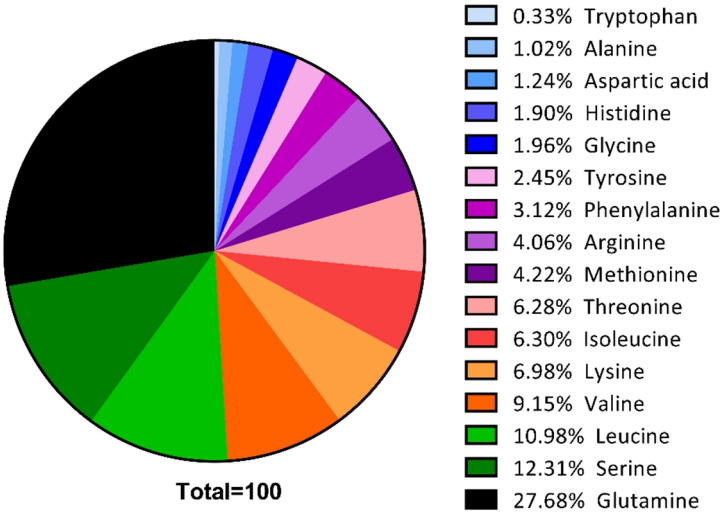

Figure R-30: Percentage of amino acid consumption by MCF7 shCtrl cells. MCF7 shCtrl cells were grown in high glucose media for 24h. Amino acid consumption was calculated by subtraction of concentration in the media incubated without cells from concentration measured in the media incubated with cells. Consumption was normalized by total protein concentration. Amino acid concentration was detected by LC-MS. Percentage of amino acid consumption were calculated. Amino acid cysteine is not included in calculation because was not detected.

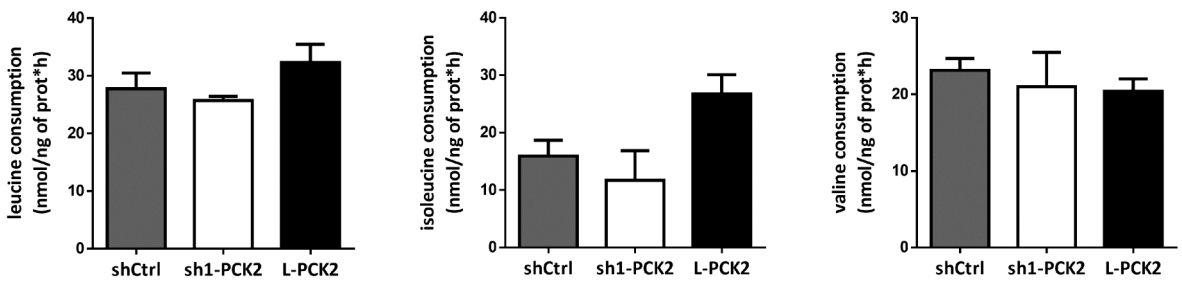

Figure R-31: Consumption of leucine, isoleucine and valine. Amino acid consumption of cells incubated 24h in DMEM high glucose medium. Amino acid consumption was calculated by subtraction of concentration in the media incubated without cells from concentration measured in the media incubated with cells. Consumption was normalized by total protein concentration. Amino acid concentration as analyzed by LC-MS.

Evaluation of the TCA cycle reductive carboxylation is routinely done by measurement of m+5 citrate and m+3 oxaloacetate, malate and fumarate. It is important to mention that m+3 oxaloacetate and subsequent species can be formed also from fully labeled pyruvate

in a reaction catalyzed by pyruvate carboxylase (PC). However, negligible levels of fully labeled pyruvate (m+3 = 0.51-0.65%) and lactate (m+3 = 0.15-0.17%) were observed (Figure R-32). Therefore we consider reductive carboxylation of glutamine as the only source of m+3 oxaloacetate, malate and fumarate labelling pattern. Based on the fact that sh1-PCK2 cells showed lower abundance of these isotopomers, we suggest they exhibit decreased reductive carboxylation. L-PCK2 cells similarly showed lower incorporation of labeled carbons into the products of reductive TCA cycle when compared to shCtrl.

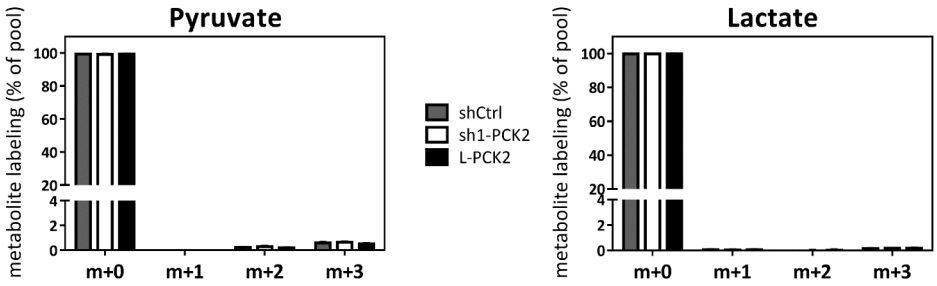

Figure R-32: ^{13}C isotopomer distribution from glutamine to pyruvate and lactate. MCF7 cells with different levels of PEPCK-M expression were exposed to 2 mM [U-^{13}C] Gln for 4h in DMEM media containing 25 mM glucose and 10% dFCS. Isotopomer distribution was analyzed by GC-MS.

Estimation of oxidative or reductive metabolism can be done as well by calculating relative proportion between certain fractions of TCA cycle intermediates. The ratio between fully labeled glutamate (m+5) and m+5 citrate indicates reductive metabolism, and the ratio between fully labeled glutamate (m+5) and m+4 citrate indicates oxidative glutamine metabolism (Meiser *et al*, 2016a; Battello *et al*, 2016; Meiser *et al*, 2016b). No significant changes were observed in oxidative metabolism of MCF7 cells with different levels of PEPCK-M expression. However, calculation of the rate of reductive metabolism confirmed that reductive glutamine metabolism in L-PCK2 was lower (Figure R-33), consistent with the labeling patterns shown in Figure R-27.

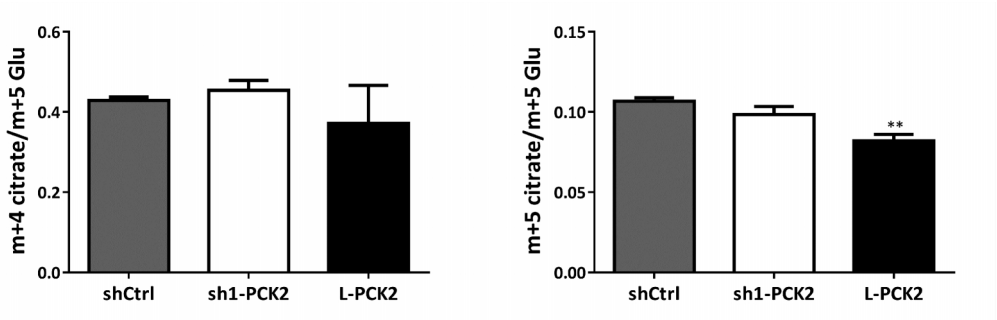

Figure R-33: Estimation of glutamine metabolism. Estimation of oxidative (m+4 citrate/m+5 Glu) and reductive (m+5 citrate/m+5 Glu) glutamine metabolism of MCF7 cells incubated 4h in DMEM medium containing 25 mM glucose, 10% FCS and 2 mM [U-^{13}C] glutamine. **P<0.01 compared with shCtrl.

Metabolomics analysis of well fed (HG) MCF7 cells with different PEPCK-M expression levels showed that cells with decreased expression of PEPCK-M undergo several metabolic changes. To allow additional requirements for PEPCK-M role to surface in our model, we exposed cells to nutritional stress generated by glucose deprivation. Glucose deprivation has been shown to activate a stress response related to endoplasmic reticulum (ER) stress (Ding *et al*, 2016). ER stress leads to the activation of several transcription factors, among them ATF4. We have previously shown that ATF4 activates PEPCK-M expression by binding to its proximal promoter (Méndez-Lucas *et al*, 2014). In accordance, we observed increased expression of *ATF4* (3-fold at 12h) and *PCK2* (4.5-fold at 12h and 7.6-fold at 24h) in shCtrl MCF7 cells exposed to DMEM media lacking glucose (Figure R-34 A,B). Although *PCK2* expression was increased 7.6 times at 24h, sh1-PCK2 maintained its silencing capacity, and showed only 17% of *PCK2* mRNA expression levels when compared to shCtrl (Figure R-34 C).

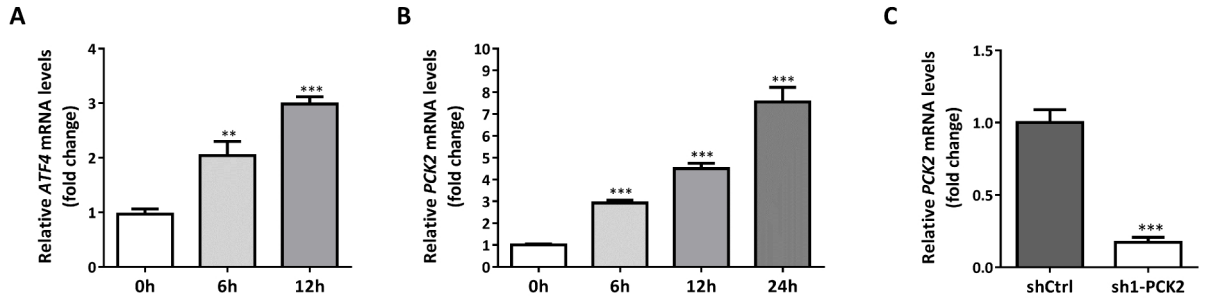

Figure R-34: Effect of glucose deprivation on *ATF4* and *PCK2* expression. Quantitative real time PCR was used to determine **(A)** *ATF4* and **(B)** *PCK2* expression in MCF7 shCtrl cells grown in DMEM medium without glucose up to 24h. (A,B) mRNA quantification was normalized to *TBP* and *GUSB* and fold induction was related to 0h time point. **P<0.01, ***P<0.001 significant difference versus time point 0h. **(C)** Comparison of *PCK2* expression levels in shCtrl and sh1-PCK2 cells after 24h of glucose deprivation. mRNA quantification was normalized to *TBP* and *GUSB*, ***P<0.001.

Induction of PEPCK-M expression under glucose deprivation suggest its importance for coping with metabolic changes occurring under these conditions. Therefore we expected that the effects of altered PEPCK-M expression will be more significant after glucose withdrawal.

For this condition MCF7 cells were first seeded in high glucose DMEM medium and medium was changed to DMEM without glucose supplemented with 2mM glutamine and 10% dFCS after reaching 60-70% confluency. Three hours later, medium was replenished with the same medium containing 2mM [U-^{13}C] glutamine tracer. Cells were incubated for four more hours and quenched. Enrichment of selected amino acids, TCA cycle intermediates, pyruvate and lactate were detected and quantified.

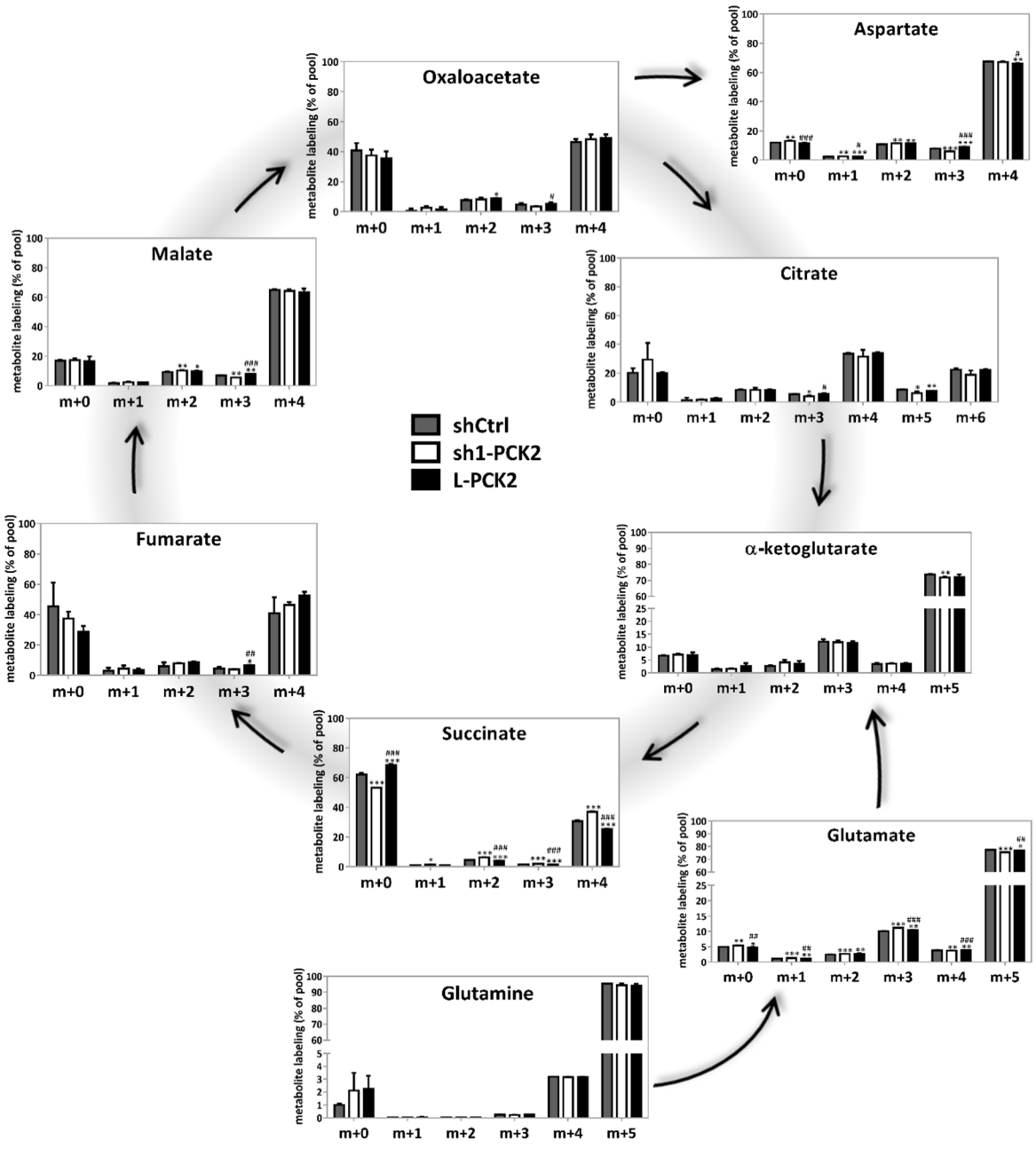

Figure R-35: ^{13}C isotopomer distribution from fully labeled glutamine into TCA cycle intermediates. MCF7 cells with different expression levels of PEPCK-M were exposed to 2mM [U-^{13}C] Gln for 4h in DMEM medium containing 0 mM glucose and 10% dFCS. Cells were pretreated for 3h with DMEM medium lacking glucose, 10% dFCS and 2mM Gln. Isotopomer distribution was analyzed by GC-MS. Data are plotted as mean ± SD. *P<0.05, **P<0.01, ***P<0.001 versus shCtrl. #P<0.05, ##P<0.01, ###P<0.001 versus sh1-PCK2.

A general overview of TCA cycle labeling patterns showed an overall increase in labeling of fully labeled species when compared to high glucose conditions (Figure R-36), indicating increased glutamine oxidation in TCA cycle under glucose deprivation conditions. Expression levels of *GLS1* were not significantly increased after exposure to 0 mM glucose, when compared to control (0h).

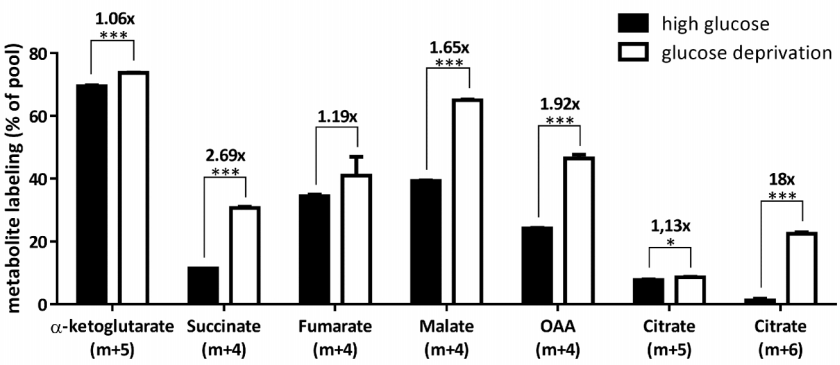

Figure R-36: Labeling pattern of selected TCA cycle intermediates in high glucose and glucose deprivation conditions. MCF7 shCtrl cells were exposed to 2mM [U-^{13}C] Gln for 4h in DMEM medium containing 25 mM glucose (high glucose) or 0 mM glucose (glucose deprivation) and 10% dFCS. Isotopomer distribution was analyzed by GC-MS. *P<0.05, ***P<0.001. Numbers indicate fold increase.

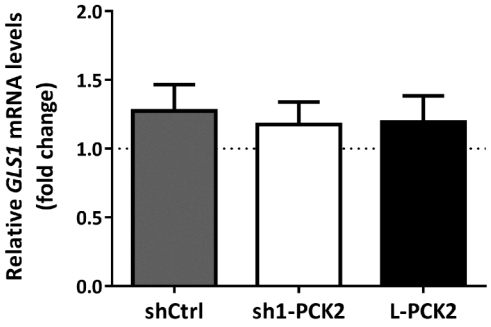

Figure R-37: Expression pattern of glutaminase (*GLS1*) under glucose deprivation. Quantitative real time PCR was used to determine *GLS1* expression in MCF7 cells grown in DMEM media with 1 mM glucose (glucose exhaustion conditions) for 24h. Fold change to 0h time point (dotted line) was calculated for each group. mRNA expression levels were normalized to *TBP* and *GUSB*.

As mentioned before, oxidation of glutamine in high glucose conditions results in formation of m+5 citrate mainly because of the absence of fully labeled acetyl-CoA.

However, glucose deprivation increased the pool of m+6 citrate species, which is formed by condensation of fully labeled oxaloacetate (m+4) and fully labeled acetyl-CoA (m+2) that can be generated by PDH from pyruvate m+3 (Figure R-25) that was formed in these conditions (Figure R-38).

In contrast with high glucose conditions (Figure R-32), MCF7 cells grown under glucose deprivation displayed significant production of fully labeled pyruvate (Figure R-38). We suggested that m+3 pyruvate was produced from malate by malic enzyme as no PEPCK-M dependent changes in labeling were observed. The process of recycling carbons to maintain TCA cycle flux is called pyruvate cycling. Labeling pattern of pyruvate was not in equilibrium with lactate labeling (Figure R-38), as much lower percentage of fully labeled lactate and increased m+3 lactate in sh1-PCK2 cells were observed. Increase in m+3 lactate formation in sh1-PCK2 cells can be caused by a slightly lower incorporation of m+3 pyruvate into the TCA cycle (m+6 citrate) (Figure R-35), however this reduction is not significant. The inhibition of the cataplerotic pathways catalyzed by PEPCK-M might also take a part in mentioned labeling outcome.

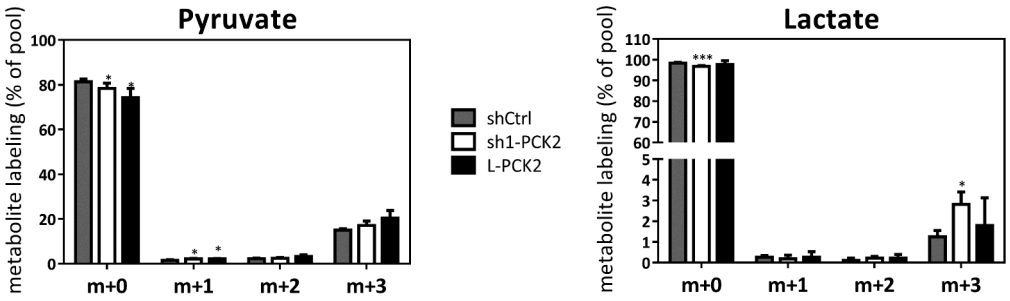

Figure R-38: ^{13}C isotopomer distribution from glutamine to pyruvate and lactate. MCF7 cells with different levels of PEPCK-M expression were exposed to 2mM [U-^{13}C] Gln for 4h in the DMEM media containing 0 mM glucose and 10% dFCS. Isotopomer distribution was analyzed by GC-MS. *P<0.05 versus shCtrl.

Comparison of concentration of lactate, pyruvate and TCA cycle intermediates in MCF7 cells shows decreased concentration of fumarate, citrate, malate, lactate and pyruvate under glucose exhaustion. Concentration of oxaloacetate was very low overall, and was not changed. The only metabolite that increased its concentration under glucose

exhaustion was succinate and we observed its significant increase in all MCF7 lines independently on PEPCK-M expression.

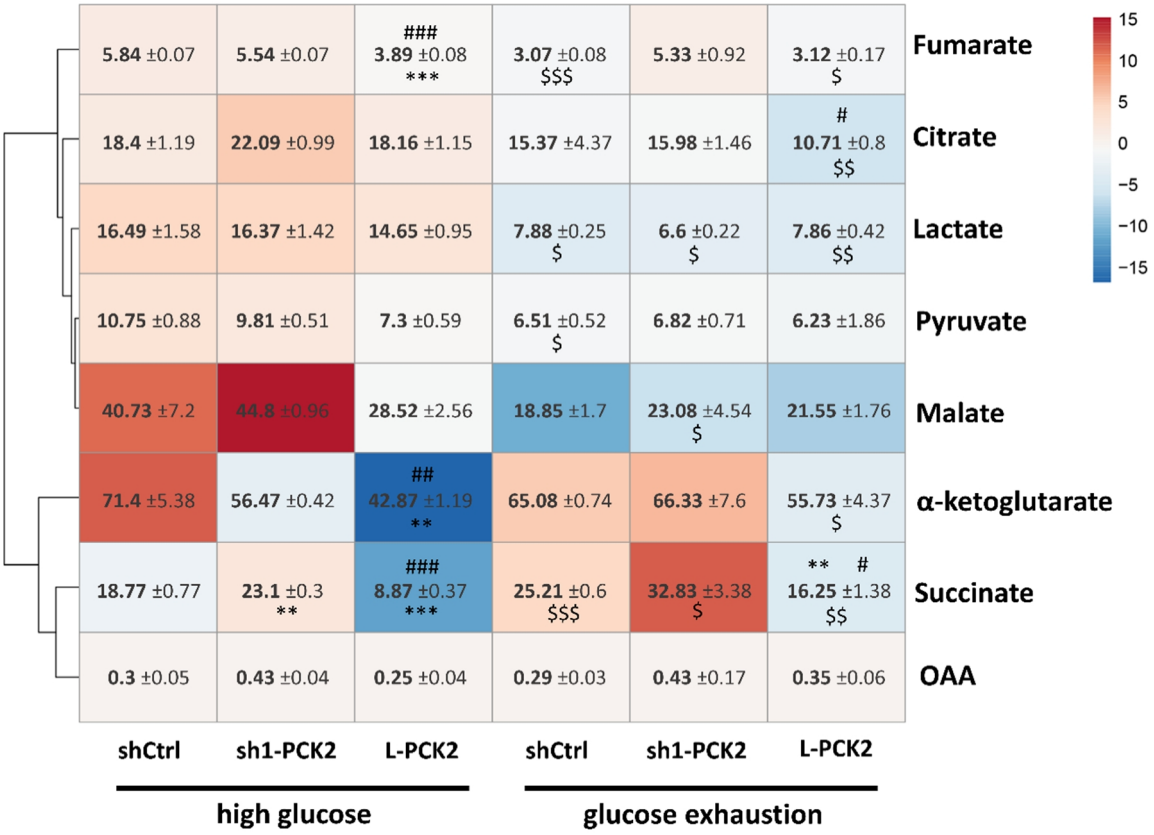

Figure R-39: Heatmap representing concentration changes in organic acids in high glucose and glucose exhaustion conditions. Concentration of organic acids in cell extracts of MCF7 cells grown 24h in high glucose conditions (25 mM glucose) and glucose exhaustion conditions (1 mM glucose). Values of selected metabolites are displayed as concentration (ng/µg of protein). Values were processed and visualized by using ClustVis tool with Pareto scaling (Metsalu & Vilo, 2015). Samples are compared within the rows and median clustering method for rows was used. Values are expressed as mean ±SEM. **P<0.01, ***P<0.001 versus shCtrl within the same conditions; #P<0.05, ##P<0.01, ###P<0.001 compared sh1-PCK2 versus L-PCK2 in the same conditions; $P<0.05, $$P<0.01, $$$P<0.001 compared high glucose versus glucose exhaustion conditions.

Analysis of isotopomer distribution from [U-^{13}C] glutamine in sh1-PCK2, shCtrl and L-PCK2 cells grown in the absence of glucose showed similar labeling in various TCA cycle intermediates indicating no changes in oxidative metabolism of glutamine (Figure R-40). Variances were observed only in succinate enrichment. Comparably to the labeling

pattern in high glucose conditions (Figure R-27), knock-down of PEPCK-M showed increased m+4 pool of succinate (1.2-fold) under glucose deprivation (Figure R-40). Interestingly, overexpression of PEPCK-M brought down the pool of m+4 succinate by 36.4% when compared to control (Figure R-40). Similar pattern was also observed in m+2 succinate, which is representing the second turn of the cycle if m+4 labeled oxaloacetate condensate with unlabeled acetyl-CoA (Figure R-25).

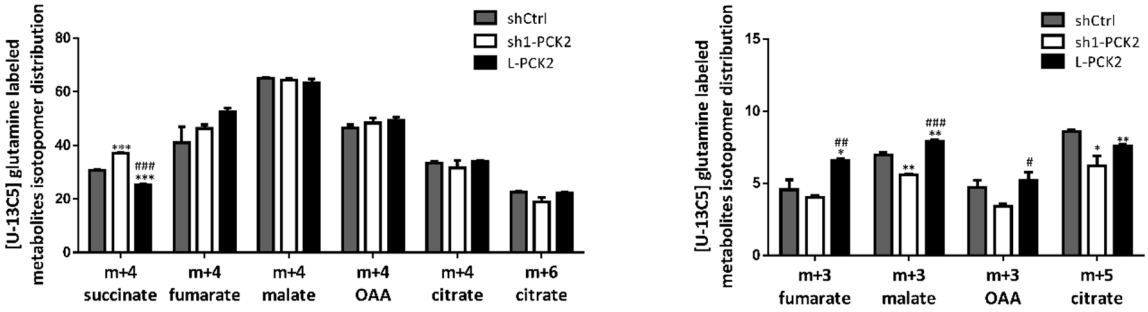

Figure R-40: Metabolism of glutamine. Abundance of m+4, m+3, m+5 and m+6 species in selected TCA cycle intermediates from Figure R-35. *P<0.05, **P<0.01, ***P<0.001 versus shCtrl. #P<0.05, ##P<0.01, ###P<0.001 versus sh1-PCK2.

We would hypothesize that even though m+3 labeled pyruvate is present, it is improbable that it would be used to produce m+3 oxaloacetate through the PC complex. This carboxylation reaction would waste 1 molecule of ATP and would cause accumulation of oxaloacetate that would decrease flux of TCA cycle in conditions of glucose deprivation. Therefore, we identified m+5 species of citrate and m+3 species of oxaloacetate, malate and fumarate as products of reductive carboxylation. Analysis of those species showed significantly decreased enrichment of reductive TCA cycle species in sh1-PCK2 when compared to control (m+5 citrate and m+3 malate) or to L-PCK2 (m+5 citrate and m+3 OAA, malate and fumarate) (Figure R-40).

Changes in oxidative and reductive metabolism of glutamine were analyzed also by ratio calculation (Figure R-41). Oxidative metabolism was calculated by the ratio m+5 glutamate and m+4 citrate. As we also obtained a relevant proportion of m+6 citrate from condensation of m+4 oxaloacetate and m+2 acetyl-CoA, we calculated the ratio of m+5

glutamate and m+6 citrate. Reductive metabolism was indicated by the ratio of m+5 citrate to m+5 glutamate. No significant changes in oxidative metabolism were detected. Decreased reductive metabolism was quantified in sh1-PCK2 and L-PCK2, consistent with labeling patterns shown in Figure R-35. However, L-PCK2 effects on reductive metabolism of glutamine shown in citrate were not maintained in the rest of metabolites.

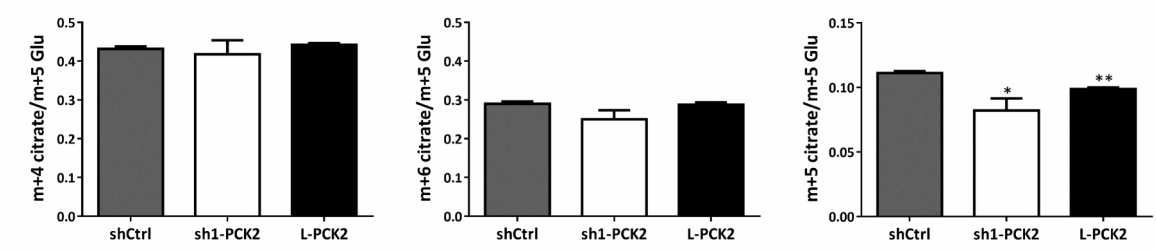

Figure R-41: Estimation of glutamine metabolism. Estimation of oxidative (m+4 citrate/m+5 Glutamate (Glu); m+6 citrate/m+5 Glu) and reductive (m+5 citrate/m+5 Glu) glutamine metabolism of MCF7 cells with different expression levels of PEPCK-M in high glucose conditions. *P<0.05, **P<0.01 versus shCtrl.

2.4 Succinate and oxidative stress

As mentioned before, the most significant changes of isotopomer distribution of ^{13}C from fully labeled glutamine were observed in succinate. Label distribution in succinate was indicating PEPCK-M dependence, and a similar outcome was present in both conditions, high glucose (Figure R-26) and glucose deprivation (Figure R-35). To further investigate changes of succinate metabolism, we measured the total levels of this metabolite in cell extracts (Figure R-42). Concentration was evaluated after 24h of growth in high glucose and glucose exhaustion conditions. Glucose exhaustion was performed by growing cells for a longer period of time (24h) in DMEM medium supplemented with 1 mM glucose. Glucose became consumed during the first 15-18 hours and cells were exposed to no glucose for the rest of the incubation. Succinate levels had a tendency to be slightly increased in sh1-PCK2 cells, however this increase was not significant (p=0.45 in high glucose; p=0.09 under glucose exhaustion) (Figure R-42). Increased levels of PEPCK-M had the opposite effect on succinate levels; succinate concentration was reduced by

44.4% in high glucose conditions and by 35.5% in glucose exhaustion conditions. Sh1-PCK2 cells showed twice as much succinate levels as L-PCK2 cells in either case.

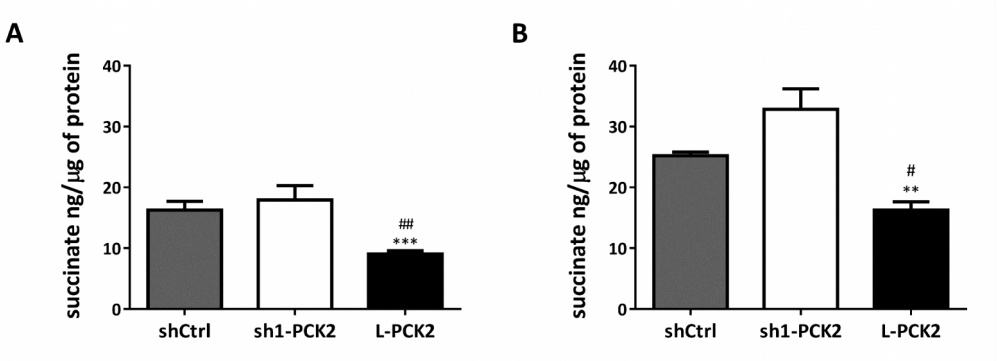

Figure R-42: Succinate concentration. Concentration of succinate in cell extracts of MCF7 cells grown 24h in **(A)** high glucose conditions (25 mM glucose) and **(B)** glucose exhaustion conditions (1 mM glucose). Concentration was evaluated using GC-MS. **P<0.01, ***P<0.001 versus shCtrl. #P<0.05, ##P<0.01 versus sh1-PCK2.

Changes in succinate levels are often linked to changes in oxidative respiration and ROS production. Analysis of mitochondrial superoxide was performed in cells grown in high glucose and low glucose DMEM media. Analysis of mitochondrial superoxide revealed increased levels in cells with silenced PEPCK-M (1.2-fold in both conditions) when compared with control (Figure R-43). On the contrary, L-PCK2 cells showed lower levels of superoxide (approximately 20% decrease in both conditions) than shCtrl.

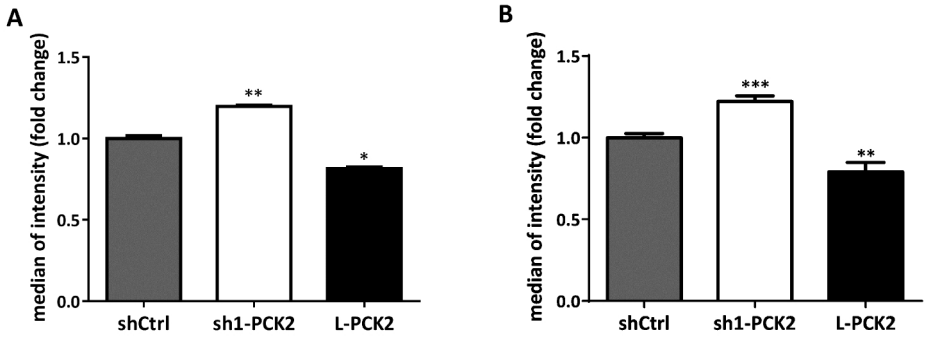

Figure R-43: Production of mitochondrial superoxide. MCF7 cells were treated for 3h in **(A)** 25 mM glucose conditions and in **(B)** 1 mM glucose conditions. Superoxide was quantified using MitoSOX fluorescent marker and intensity was measured by flow cytometry. *P<0.05, **P<0.01, ***P<0.001 versus shCtrl.

The presence of oxidative stress in cells can affect the expression of several genes, like p53 and SOD2. P53, a sensor of oxidative stress, regulates cell cycle through p21 inhibition of cyclins, and it can be activated in the presence of oxidative stress in the cell. However, we detected that sh1-PCK2 cells that display increased ROS production does not show any changes in p53 levels. Interestingly, levels of p21 were higher in these cells in high glucose (1.3-fold increase) and glucose exhaustion (1.5-fold increase) conditions. MCF7 cells overexpressing PEPCK-M did show decreased levels of p53 in high glucose conditions that were not maintained in conditions of glucose exhaustion.

SOD2, a mitochondrial superoxide dismutase, plays an important role in ROS homeostasis. Consistently with increased ROS concentration, significant increase in SOD2 expression was observed in sh1-PCK2 cells growing in both conditions (1.83 times higher in high glucose conditions and 1.66 times higher in glucose exhaustion).

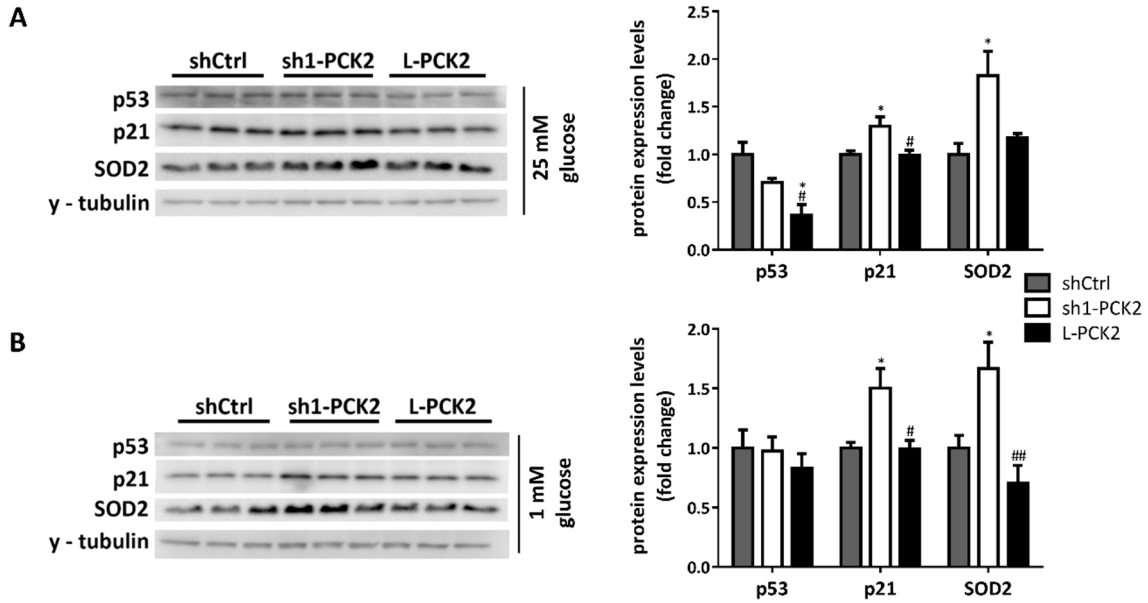

Figure R-44: Western blot analysis and relative quantification of oxidative stress related proteins. Expression of p53, p21 and SOD2 was detected in MCF7 cells grown in **(A)** 25 mM glucose conditions (HG for 24h) and **(B)** conditions of glucose exhaustion (LG for 24h). Relative quantification of western blots was performed: p53 (HG n=1, LG n=1), p21 (HG n=3, LG=2), SOD2 (HG n=3, LG n=2. *P<0.05, ***P<0.001 versus shCtrl. #P<0.05, ##P<0.01 versus sh1-PCK2.

Production of ROS can be linked to metabolism of different metabolites. As we mentioned, one of them might be succinate. Another metabolite which metabolism might contribute to ROS production is proline (Figure R-45). Therefore we analyzed whether there are changes related to PEPCK-M expression in its metabolism.

Proline concentration was detected in MCF7 cells grown in high glucose conditions and conditions of glucose exhaustion (1 mM glucose for 24h). It is important to mention that cells were grown in both conditions in the absence of proline, as it is not supplemented in DMEM media. MCF7 cells with different PEPCK-M expression levels showed similar proline concentration under high glucose conditions. Slightly lower levels were observed in sh1-PCK2 cells (48.4±1.02 nmol/μg of protein) when compared to shCtrl (57.78±5.02 nmol/μg of protein) and L-PCK2 (58.46±1.69 nmol/μg of protein) (Figure R-46). Differences in proline levels in cells were more marked under glucose exhaustion. Cells overexpressing PEPCK-M showed significantly higher levels of proline (70.25±4.33 nmol/μg of protein) when compared to shCtrl (21.13±0.93 nmol/μg of protein). Levels of proline in silenced MCF7 cell line (5.79±0.56 nmol/μg of protein were significantly lower when compared to shCtrl (Figure R-46). These observations show that proline concentration in MCF7 cells grown under glucose exhaustion correlate with PEPCK-M expression levels.

We can assume that the concentration levels of proline detected in high glucose conditions are representing basal levels of this amino acid in our model as they are routinely grown in media with the same composition. Therefore, observed changes in proline content upon glucose exhaustion in shCtrl and sh1-PCK2 cells suggest that these cells under glucose exhaustion conditions do decrease proline content by enhancing its degradation. In these condition proline can be metabolized to glutamate and feed the TCA cycle or it can be used in biosynthesis. It is interesting to mention that mRNA expression levels of *PYCR1* and *POX*, two enzymes involved in the metabolism of proline, were significantly increased in sh1-PCK2 cells grown under glucose exhaustion when compared to high glucose conditions (Figure R-48). This might indicate increased proline metabolism in these cells.

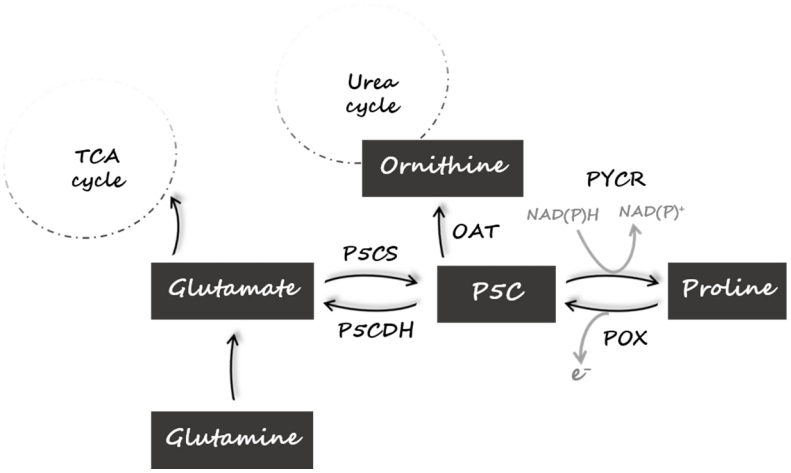

Figure R-45: Schematic of proline metabolism. Synthesis of proline is connected with glutamine metabolism, TCA cycle and urea cycle. Enzymes involved in proline synthesis are pyrroline-5-carboxylate synthase (P5CS) and pyrroline-5-carboxylate reductase (PYCR), which catalyzes the NAD(P)H dependent conversion of pyrroline-5-carboxylate to proline. Oxidation of proline to pyrroline-5-carboxylate by POX (PRODH) enzyme is associated with the release of electrons, which can be transferred to either electron transfer systems or to molecular oxygen and form ROS.

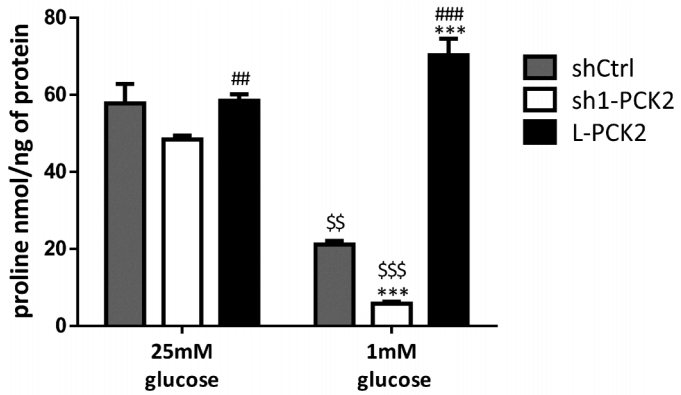

Figure R-46: Concentration of proline in cell extracts. Concentration of proline was measured in MCF7 cells grown for 24h in DMEM media containing 25 mM and 1 mM glucose. Amount of proline was normalized per ng of protein. Concentration was analyzed by LC-MS. ***P <0.001 versus shCtrl within the same treatment, ###P<0.001 compare sh1-PCK2 versus L-PCK2 within the same treatment, $$P<0.01, $$$P<0.001 indicate significance of treatment effect.

During proline degradation by proline dehydrogenase (PRODH/POX), an electron is passed into the electron transport chain (ETC) to generate ROS (Figure R-45). Analysis of mRNA expression showed increased expression of *POX* in sh1-PCK2 cells in high glucose and glucose exhaustion conditions (Figure R-47) when compared to shCtrl or L-PCK2,

indicating higher degradation of proline and therefore possible impact on ROS production.

It is worth mentioning that average raw CT value for *POX* expression in MCF7 cells was 31.7 and 23.62 for *PYCR1* meaning that MCF7 cells show higher expression levels of enzymes involved in the synthesis of proline.

Expression levels of *PYCR1* did not show significant differences among MCF7 cells with different expression levels of PEPCK-M except when L-PCK2 cells were grown in high glucose conditions. In this case, its expression was 1.89 times higher when compared with control cells and 1.57 times higher when compared with sh1-PCK2 cells. This is consistent with observed proline secretion in these conditions. L-PCK2 cells showed significantly higher levels of proline in media after 24h incubation in the presence of high glucose. As mentioned before, media does not contain proline and therefore it can be synthetized only by the cells.

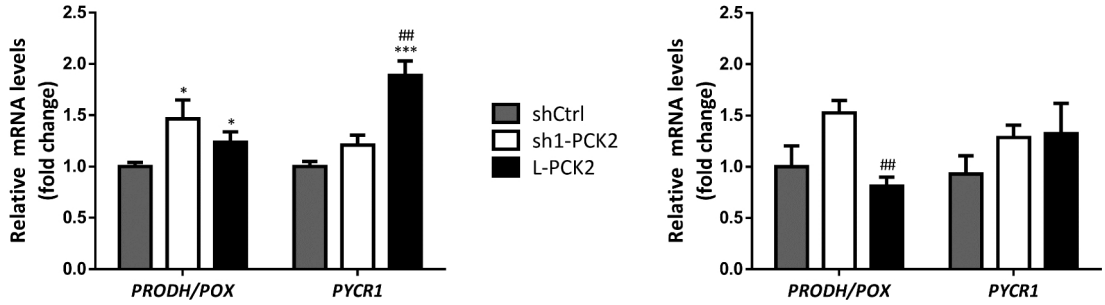

Figure R-47: Expression pattern of proline dehydrogenase (*POX*) and pyrroline-5-carboxylate reductase (*PYCR*). Quantitative real time PCR was used to determine *POX* and *PYCR1* expression in MCF7 shCtrl, sh1-PCK2 and L-PCK2 cells grown in DMEM media with 25 mM glucose (left, n=3) and 1 mM glucose (glucose exhaustion conditions, right, n=1) for 24h. mRNA expression levels were normalized to *TBP*. * P < 0.05, *** P < 0.001 versus shCtrl. ## P <0.01 versus sh1-PCK2.

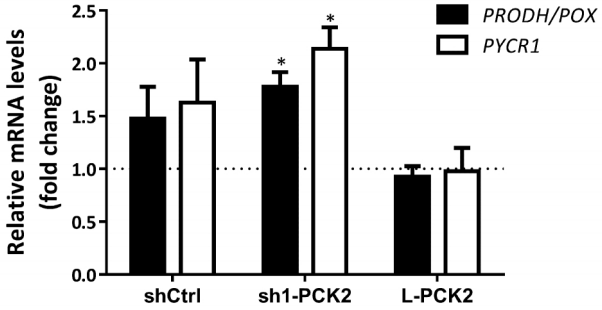

Figure R-48: Changes in expression of proline dehydrogenase (*POX*) and pyrroline-5-carboxylate reductase (*PYCR*) when undergoing glucose exhaustion. Quantitative real time PCR was used to determine *POX* and *PYCR1* expression in MCF7 cells grown in DMEM media with 1 mM glucose for 24h. Fold change of mRNA expression in 1 mM glucose condition related to 25 mM glucose condition is plotted. mRNA expression was normalized to *TBP*. N=1, *P<0.05 indicate significant treatment effect of glucose exhaustion.

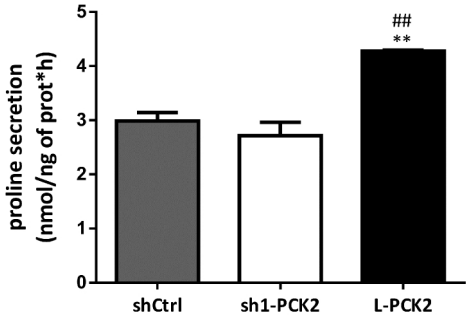

Figure R-49: Secretion rate of proline. Concentration of proline in DMEM media containing 25 mM was measured after 24h of incubation. Secretion of proline was measured as subtraction of proline concentration in media incubated without cells from concentration of proline in media incubated in the presence of cells. Concentration was analyzed by LC-MS. **P<0.01 versus shCtrl, ##P<0.01 compared sh1-PCK2 versus L-PCK2.

2.5 Study of pathways involved in succinate synthesis

Different succinate labeling from glutamine correlating with PEPCK-M expression levels was one of the highest impact changes occurring in MCF7 cells (Figure R-27 and Figure R-40). Variations in expression of succinate dehydrogenase (SDH) complex were suspected as one of the possible causes. This was not confirmed, as western blot analysis did not reveal any significant variations in SDH complex expression (Figure R-50). Therefore, we suggest that decreased oxidation of succinate to fumarate is not responsible for the observed changes in succinate labeling from [U-^{13}C] glutamine.

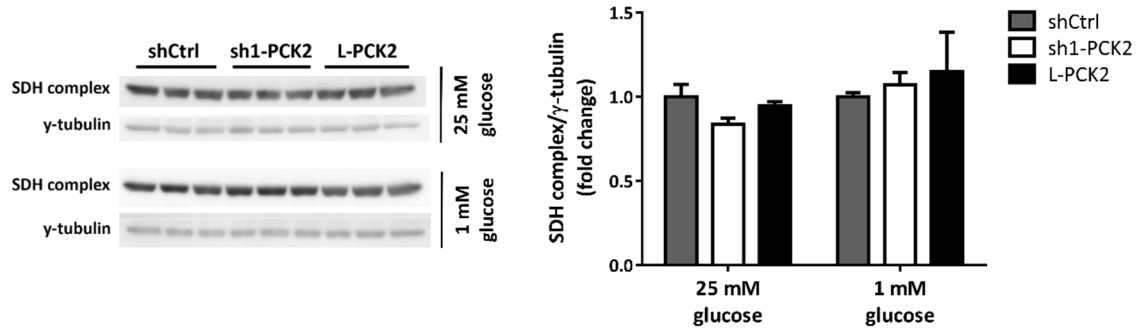

Figure R-50: Western blot analysis and relative quantification of SDH complex expression. Expression of SDH complex in MCF7 cells was evaluated. Cells were grown in basal conditions (25 mM glucose for 24h) or conditions of nutritional stress (glucose deprivation for 3h at 0 mM glucose/exhaustion for 24h at 1 mM glucose 24h**.** In basal conditions, the difference between SDH complex expression in sh1-PCK2 and L-PCK2 was close to significance with P=0.053.

Another pathway that can contribute to the synthesis of labeled succinate from [U-^{13}C] glutamine is the gamma-aminobutyric acid (GABA) pathway (Figure R-51).

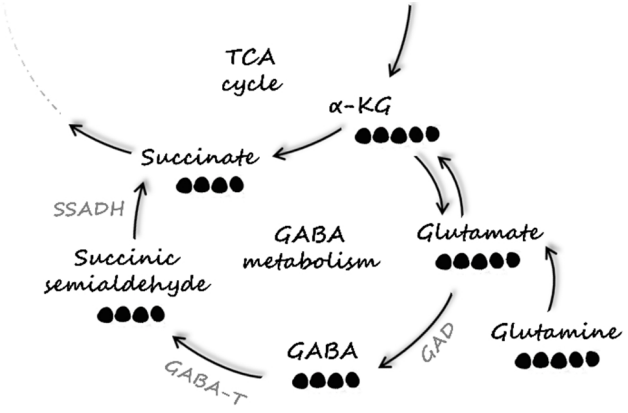

Figure R-51: Gamma-aminobutyric acid pathway: GABA is synthesized from glutamate by glutamic acid decarboxylase (GAD). Source of glutamate is glutamine/α-KG. GABA is later transaminated by gamma aminobutyrate transaminase (GABA-T) to succinic semialdehyde. Finally succinate is formed by conversion of succinic semialdehyde by succinic semialdehyde dehydrogenase (SSADH).

To evaluate the importance of the GABA pathway in our model, we analyzed the expression of two key enzymes of GABA metabolism: GABA-T and SSADH (Figure R-52). Both enzymes exhibit the same level of mRNA expression in shCtrl and sh1-PCK2. Although, MCF7 cells overexpressing PEPCK-M showed a 45% reduction of mRNA

expression of *GABA-T* and a 1.6 times increased expression of *SSADH*. The average raw CT values of shCtrl cells was 33.3 for *GABA-T* and 29 for *SSADH*.

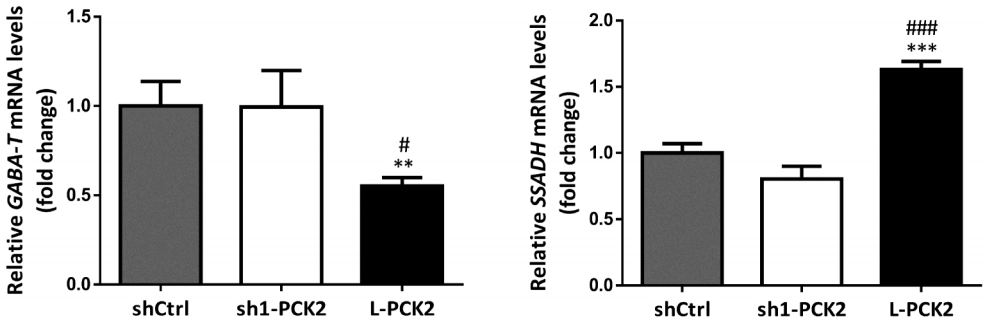

Figure R-52: Expression pattern of enzymes involved in GABA metabolism. Quantitative real time analysis was used to analyze expression of *GABA-T* and *SSADH* in cells grown 24h at presence of 25 mM glucose. The quantification of mRNA was normalized to *TBP* and *GUSB*. **P<0.01, ***P<0.001 versus shCtrl. #P<0.05, ###P<0.001 compared sh1-PCK2 versus L-PCK2.

Nevertheless, expression analysis of enzymes involved in GABA synthesis did not show any changes associated to PEPCK-M silencing. Therefore, we used another approach to analyze the importance of this pathway in these cells by inhibiting GABA-T enzyme with aminooxyacetic acid (AOA), an aminotransferase inhibitor. We observed that administration of AOA had a negative impact on growth of MCF7 cells. AOA administration to shCtrl cells showed a 48% inhibition on growth at 24h when compared to cells without treatment (Figure R-53 A). The impact on growth was even more significant in the cells with silenced PEPCK-M. Increased sensitivity of sh1-PCK2 cells to AOA inhibitor was observed both in high glucose conditions and conditions of glucose exhaustion. Sh1-PCK2 showed a reduction of cell growth by 46.6% (at 24h) and by 40.8% (at 48h) in high glucose conditions, and reduction of growth by 36.6% (at 24h) and by 41.8% (at 48h) in conditions of glucose exhaustion when compared to shCtrl (Figure R-53 B,C). Considering that AOA is also affecting the activity of other types of aminotransferases and the absence of more robust data, these results have to be taken as preliminary and more experiments are needed to shed light on the possible importance of the GABA pathway in succinate production.

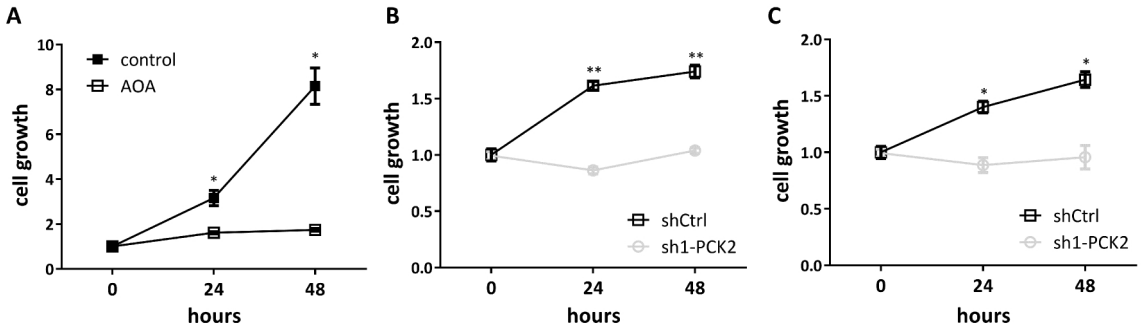

Figure R-53: Impact of AOA inhibitor on cell growth of MCF7 cells. (A) MCF7 shCtrl cell were grown 48h in 25 mM glucose medium with addition or absence of 0.2 mM AOA. **(B,C)** MCF7 shCtrl and sh1-PCK2 cells were treated for 48h in conditions of high glucose (25 mM glucose; B) and glucose exhaustion (1 mM glucose; C). Cell growth was analyzed by crystal violet assay and normalized by 0h time point (n=1). (A) *P<0.05 indicate significant treatment effect. (B,C) *P<0.05, **P<0.01 versus sh1-PCK2 at the same time point.

2.6 Effect of different PEPCK-M expression levels on metabolism of fatty acids

Biosynthesis of new molecules is an important feature of dividing cells. As we detected decreased growth in sh1-PCK2 MCF7 cells, we analyzed the impact of PEPCK-M silencing and overexpression on metabolism of cells. Besides amino acid and TCA cycle intermediates analysis, we looked for a possible impact on fatty acid synthesis.

Analysis of fatty acid synthase (FAS) expression, an enzyme implicated in synthesis of fatty acids pointed to increased expression in MCF7 cells with overexpressed PEPCK-M (Figure R-54). Analysis of acetyl-CoA (ACC) carboxylase by western blot showed very low levels of its inactive form (phosphorylated AAC, pACC) in MCF7 cells grown in the presence of high glucose (Figure R-55). This indicates that beta oxidation in this condition is blocked and cells are synthesizing fatty acids. Upon glucose exhaustion, MCF7 cells showed higher expression levels of pACC with no observed changes among the cells with altered PEPCK-M levels.

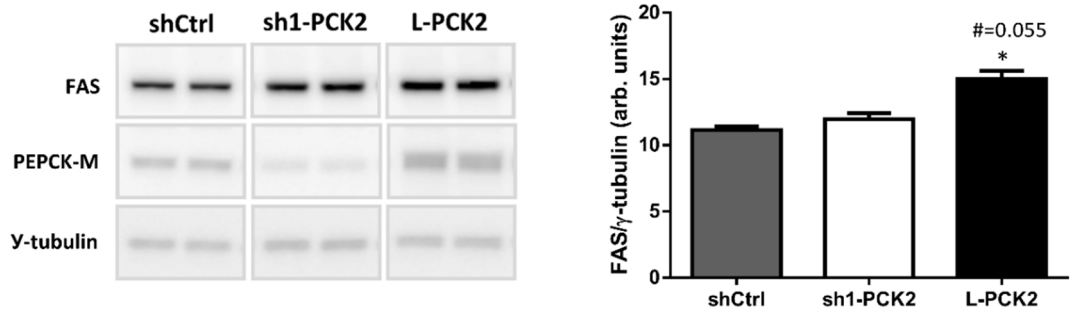

Figure R-54: FAS expression in MCF7 cells. Western blot analysis of FASN and PEPCK-M expression in MCF7 cells grown for 24h in high glucose DMEM medium. Cells were subjected to FCS starvation O/N prior to treatment. Pictured bands from western blot are from the same blot. Relative quantification of FSN expression was performed and Y-tubulin was used as normalizer. N=1, *P<0.05 versus shCtrl. #compared sh1-PCK2 versus L-PCK2.

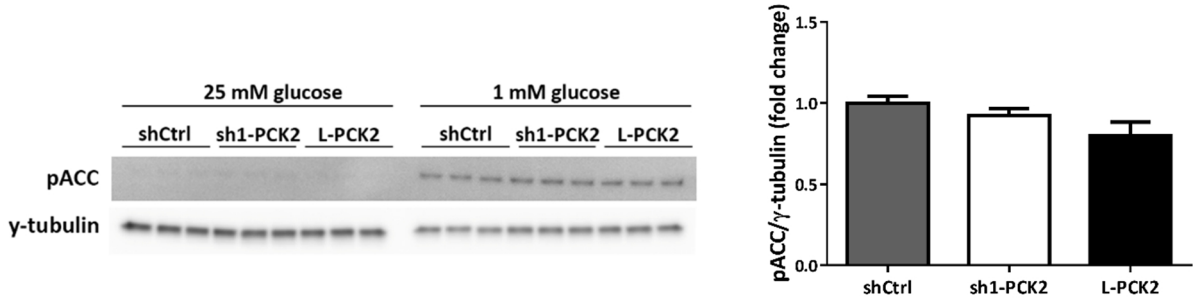

Figure R-55: Western blot analysis of pACC in MCF7 cells. Phosphorylation of ACC was evaluated in MCF7 cells grown for 24h in DMEM media containing 25 mM and 1 mM glucose. Relative quantification of pACC expression in 1 mM condition (n=2) was performed and expression was normalized to Y-tubulin.

To evaluate *de novo* synthesis of fatty acids, cells were treated with D_2O in the presence of 25 mM glucose. Specific signal of incorporated deuterium into newly made fatty acids was determined by NMR spectrometry. Obtained data allowed us to calculate the *de novo* synthesis of fatty acids. In accordance with increased expression of FAS enzyme in L-PCK2 cells, a significantly higher *de novo* synthesis of fatty acids was observed in these cells (Figure R-56).

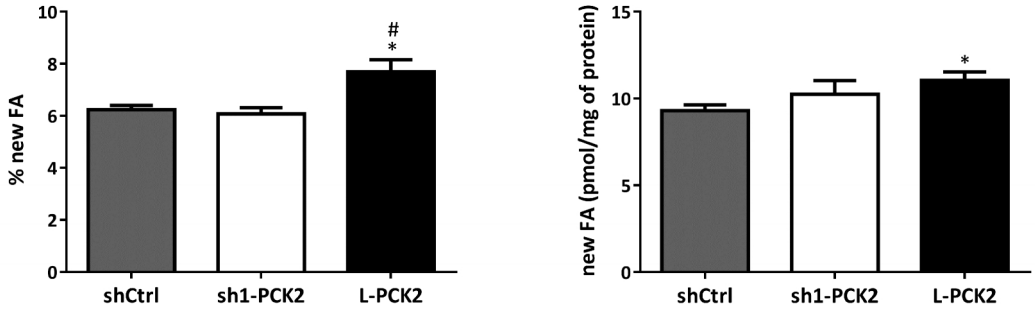

Figure R-56: Quantification of *de novo* synthesis of fatty acids. *De novo* synthesis of fatty acids was evaluated by NMR spectrometry by using D_2O label. MCF7 cells were grown 16h in high glucose DMEM media in presence of 30% D_2O. Cholesterol concentration was used as an internal standard to calculate the mass of fatty acids. *P<0.05 versus shCtrl. #P<0.05 compared sh1-PCK2 versus L-PCK2.

2.7 Silencing of PEPCK-M blunts cell growth under physiological conditions

The ability of cells to grow in an anchorage independent manner is an indicator of tumorigenic and metastatic potential (Ke *et al*, 2004; Mori *et al*, 2009). In these conditions, cells tend to grow in the form of spheres. Typically, the farther a cell is situated from the surface the less oxygen and nutrients are available. Growth in spheres is therefore mimicking the tumor, which is also characterized by diminished nutrient availability and increased microenvironment stress.

To evaluate the effect of PEPCK-M silencing on the ability of MCF7 cells to grow in anchorage independent manner, we subjected cells to growth in semisolid media. MCF7 cells independently on PEPCK-M expression were able to form colonies visible to the naked eye (Figure R-57), yet cells with silenced PEPCK-M (sh1-PCK2 and sh2-PCK2) showed reduced capacity of anchorage independent growth. Sphere formation in sh1-PCK2 cells was diminished by 70% (sh2-PCK2 by 43%), when compared to shCtrl (Figure R-58 A). Similarly, when we treated MCF7 WT cells with PEPCK-M inhibitor (inh#2), a C-8 modification of 3-alkyl-1,8-dibenzylxanthin synthetized in the laboratory of Dr. Carmen Escolano (University of Barcelona), an inhibition of spheres formation by 83% was observed (Figure R-58 B). These results were later confirmed in 3T3-KRas cell line, upon inhibition of PEPCK-M by 3MPA (reduced sphere formation by 48%) (Figure R-58 C).

Overexpression of PEPCK-M in MCF7 cells (L-PCK2) slightly increased the number of spheres, however this increase was not significant.

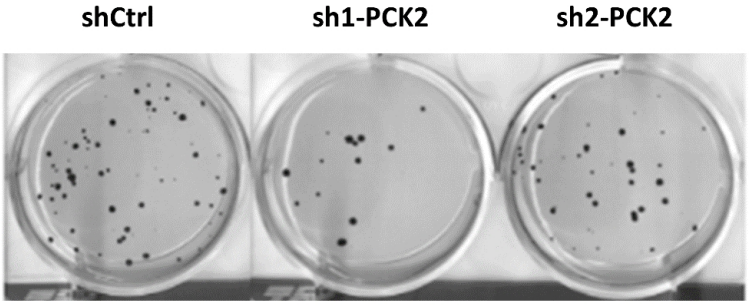

Figure R-57: Image of MCF7 spheres grown in soft agar. MCF7 cells were seeded in semisolid agar prepared with DMEM high glucose media 1:1 in a 6 well plate. Cells were grown for four weeks. Medium was replenished every 3 or 4 days. Spheres were visualized by MTT staining at the end of the incubation.

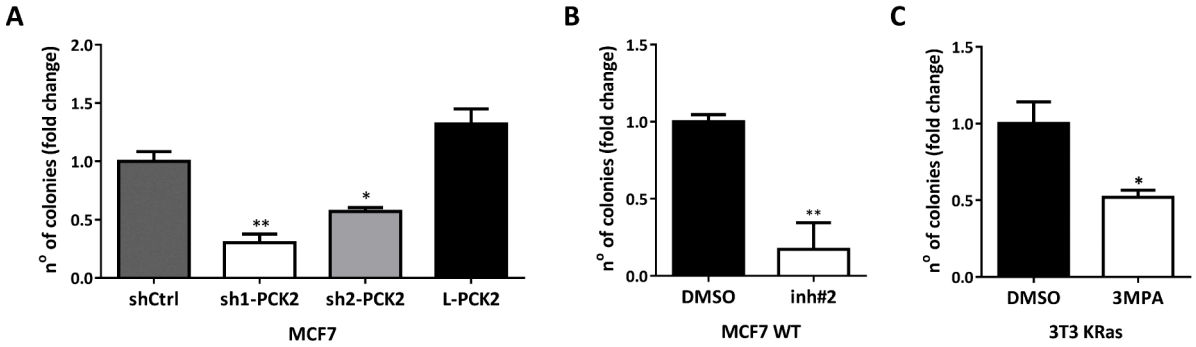

Figure R-58: Quantification of anchorage independent growth of MCF7 and 3T3-KRas cells: (A,B,C) MCF7 cells and 3T3-KRas cells were seeded in semisolid agar prepared with DMEM high glucose media 1:1. Cells were grown for four weeks. Medium was replenished every 3-4 days. At the end of incubation, cells were stained with MTT and number of spheres was counted. *P<0.05, **P<0.01 versus shCtrl. **(B)** MCF7 WT cells were additionally treated with DMSO and PEPCK-M inhibitor inh#2 (8.68 μM). Treatment was refreshed every 3-4 days. **(C)** 3T3-KRas cells were additionally treated with DMSO and 3MPA (100 μM). Treatment was refreshed every 3-4 days. *P<0.05, **P<0.01 versus DMSO.

After reaching a specific size, spheres have to cope with decreased diffusion of nutrients and oxygen. We observed that nutrient depletion has a negative impact on survival of cells with knocked-down PEPCK-M (Figure R-66 B; Méndez-Lucas *et al.*, 2014). Similarly, cells with knocked-down PEPCK-M showed impairment of growth when exposed to hypoxic conditions. At 24h, silencing of PEPCK-M caused inhibition of growth by 20% in sh2-PCK2 and by 32.5% in sh1-PCK2 cells, respectively (Figure R-59 A). Additionally, an evaluation of cell death using Annexin V and 7ADD showed a higher number of dead cells

in sh1-PCK2 cells (14.4%) when compared to shCtrl (10.5%) (Figure R-59 B). This increase in cell death does not explain the significant differences observed by MTT assay (Figure R-59 A). Moreover, increased number of apoptotic/necrotic cells was not confirmed in a second PEPCK-M silenced cell line, sh2-PCK2 (Figure R-59 B).

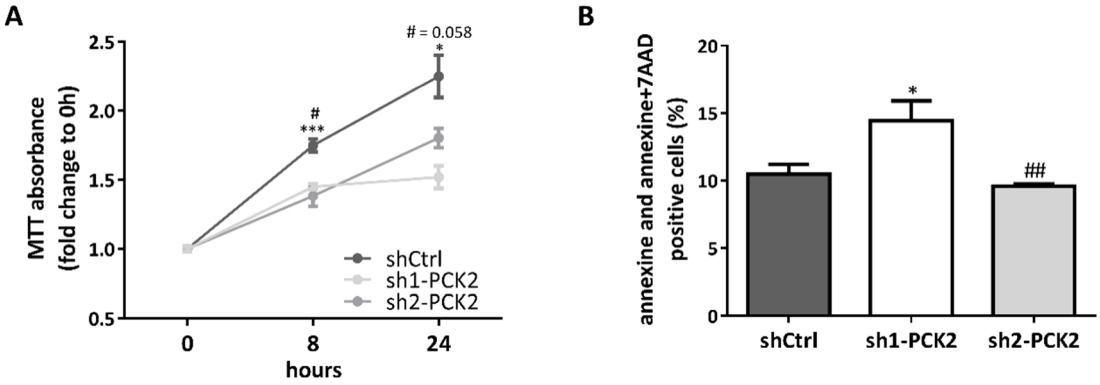

Figure R-59: Evaluation of MCF7 cell growth and survival under hypoxia. (A) MCF7 cells were grown for 24h in high glucose DMEM media at the presence of 2% oxygen. Cell growth was evaluated at 8 and 24 hours by MTT assay and absorbance values were normalized to 0h time point. N=2, *P<0.05, ***P<0.001 versus sh1-PCK2. #P<0.05 versus sh2-PCK2. **(B)** MCF7 cells were grown for 8h in high glucose DMEM media at the presence of 2% oxygen. Presence of apoptotic (annexin positive) and late apoptotic/necrotic (annexin+7AAD positive) cells was analyzed by flow cytometer FACSCanto™. N=1, *P<0.05 versus shCtrl, ##P<0.01 sh1-PCK2 versus sh2-PCK2.

2.8 MCF7 cells produce serine and glycine from glutamine in a PEPCK-M dependent manner

As previously mentioned, glucose deprivation activates expression of transcription factor *ATF4* and its target gene *PCK2* (Figure R-34). Other targets of ATF4 were upregulated in MCF7 cells grown in the absence of glucose, such as *PHGDH* and *PSAT1*. These two enzymes are involved in the synthesis of serine and glycine (Figure R-61). *PHGDH* mRNA expression was increased 1.7 times after 24h exposure to DMEM medium lacking glucose. Likewise, expression of *PSAT1* was increased 1.6 times in these conditions (Figure R-60). This suggests an important role of cataplerosis in serine and glycine synthesis under glucose deprivation in MCF7 cells.

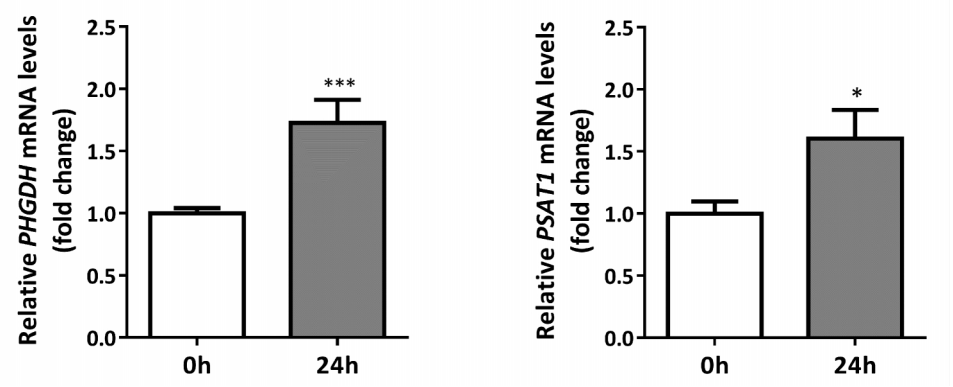

Figure R-60: Effect of glucose deprivation on expression of enzymes of serine and glycine synthesis pathway. MCF7 shCtrl cells were grown in DMEM medium without glucose for 24h. Expression levels pf *PHGDH* and *PSAT1* were identified by quantitative real time PCR. Quantification of mRNA expression was normalized to *TBP* and *GUSB*. *P<0.05, ***P<0.001.

Serine, the precursor of glycine, is synthetized from 3-phosphoglycerate (3-PG) which is an intermediate in the glycolytic pathway. Under glucose deprivation, glycolytic intermediates could be synthesized by cataplerosis from OAA in a pathway where PEPCK-M plays an irreplaceable role. PEPCK-M catalyzes decarboxylation of oxaloacetate to PEP. PEP can be converted to 3-PG, which can give rise to serine, and later glycine (Figure R-61).

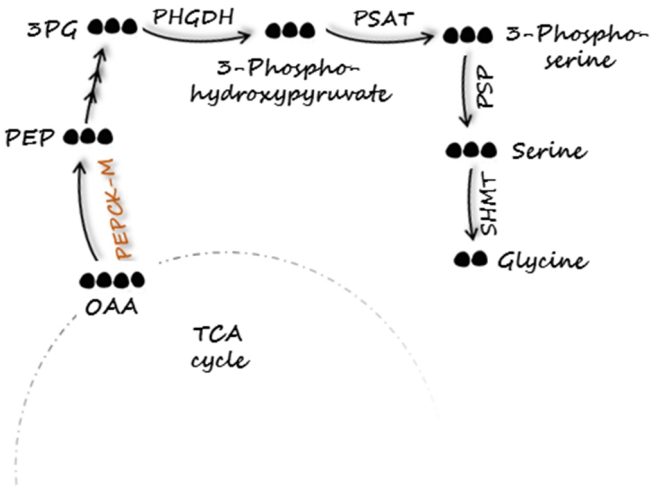

Figure R-61: Serine and glycine synthesis pathway. Phosphoglycerate dehydrogenase catalyzes conversion of 3-phosphoglycerate (3PG) to 3-phosphohydroxypyruvate. Phosphoserine aminotransferase (PSAT) catalyzes reversible conversion of 3-phosphohydroxypyruvate to 3-phosphoserine. Serine is later formed by phosphoserine phosphatase (PSP). Serine is precursor of glycine, which is formed in reaction catalyzed by serine hydroxymethyl transferase (SHMT).

To evaluate PEPCK-M functional activity in serine/glycine synthesis we quantified the incorporation of labeled carbons from [U-^{13}C] glutamine into serine and glycine metabolites. Analysis was performed in MCF7 cells expressing different levels of PEPCK-M (sh1-PCK2, shCtrl and L-PCK2) and grown in two different conditions (high glucose and glucose deprivation). It is important to mention that DMEM media routinely contain serine and glycine.

Isotopomer analysis of serine and glycine in high glucose conditions showed solely the presence of unlabeled species (Figure R-62), meaning that no labeled carbons from oxaloacetate (proceeding from [U-^{13}C] glutamine) were contributing to serine and glycine synthesis. However, null detection of incorporation of ^{13}C into serine and glycine can be also caused by a high dilution of labeled serine and glycine by their unlabeled counterparts synthesized from glucose or absorbed from medium.

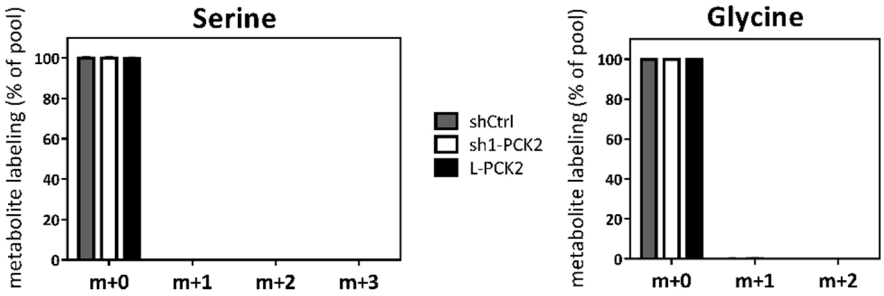

Figure R-62: ^{13}C isotopomer distribution from glutamine into serine and glycine. MCF7 cells with different levels of PEPCK-M expression were exposed to 2mM [U-^{13}C] Gln for 4h in the DMEM media containing 25 mM glucose and 10% dFCS. Incorporation of ^{13}C was analyzed using GC-MS.

Under conditions of glucose deprivation, incorporation of labeled carbons into serine and glycine from [U-^{13}C] glutamine was observed. Four hours of labeling were sufficient to produce 2.2 % of fully labeled serine (m+3) and 0.5% of each m+2 and m+1 serine in MCF7 shCtrl cells (Figure R-63). Moreover, serine labeling was dependent on PEPCK-M expression levels. Silencing of PEPCK-M in sh1-PCK2 cells diminished the pool of fully labeled serine by 83%. Lower enrichment was observed also in other species of serine m+1 (decreased by 82.7%) and m+2 (decreased by 63.9%). On the other hand, overexpression of PEPCK-M significantly increased the pool of labeled species of serine. Labeled species m+3 and m+1 were increased 1.6 times and m+2 was increased 1.5 times (Figure R-63). Pathways participating in production of m+2 and m+1 species of serine are probably the backward reaction from fully labeled glycine to serine (m+2) and serine synthesis from unlabeled glycine and one labeled carbon lost in conversion of serine to glycine (m+1).

Similar PEPCK-M dependent distribution of label was present as well in glycine, which is synthetized from serine in a reaction catalyzed by serine hydroxymethyl transferase (SHMT) (Figure R-61). Occurrence of fully labeled glycine in control conditions was 0.9% and silencing of PEPCK-M decreased labeling of glycine by 73.7%. On the other hand, overexpression of PEPCK-M increased m+2 glycine 1.5 times (Figure R-63).

The overall low percentage of ^{13}C incorporation into serine and glycine can be caused by the presence of extracellular sources of serine and glycine in the media.

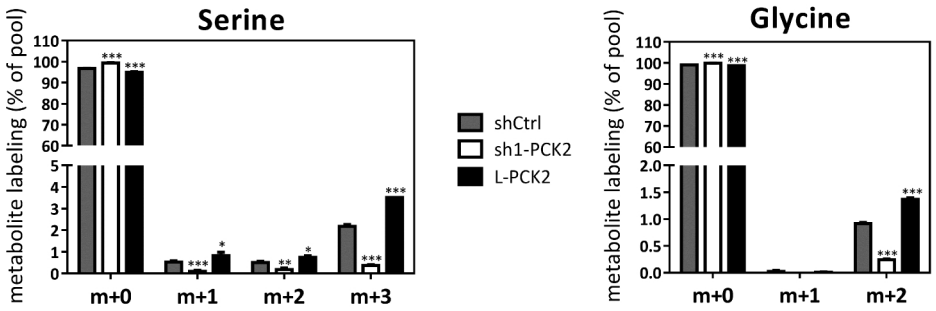

Figure R-63: ^{13}C isotopomer distribution from glutamine into serine and glycine. Sh1-PCK2, shCtrl and L-PCK2 cells were exposed to 2mM [U-^{13}C] Gln for 4h in the DMEM media containing 10% dFCS and 0 mM glucose. *P<0.05, ***P<0.001 versus shCtrl. Incorporation of ^{13}C was analyzed using GC-MS.

Besides isotopomer distribution, the concentration of amino acids in cellular extracts was evaluated and it was represented as molar fraction of amino acids. Molar fraction determines the relative concentration of amino acids in the solution and it is calculated as nmol of amino acid divided by nmol of all amino acids. Interestingly, we have seen a PEPCK-M related tendency to change the ratio of amino acids connected to the glycolytic pathway. Molar fraction of amino acids was evaluated in conditions of high glucose and glucose exhaustion (Figure R-64). Serine, glycine and tyrosine had increased molar fraction with increasing PEPCK-M expression in either conditions. In contrast, alanine shows an opposite behavior. Serine, glycine and tyrosine are present in DMEM medium in both conditions at concentration of 0.4 mM. Therefore, not only the synthesis but also its consumption can produce a higher molar fraction of these amino acids. However, when we analyzed amino acid consumption in high glucose medium, we did not detect any difference in glycine and tyrosine consumption (Figure R-65). Moreover, overall consumption of glycine and tyrosine is low. At 24h, cells consumed 2-6% of glycine and 7-8% of tyrosine. As tyrosine can be in cells synthetized from phenylalanine (0.4 mM in medium), we also evaluated the consumption of this amino acid, but no changes were measured (Figure R-65). Regarding serine, cells consumed 30-45% of serine at 24h. Moreover, serine consumption rate was significantly different between shCtrl and L-PCK2, being 1.15 times higher in L-PCK2 (Figure R-65). Interestingly, we did not detect a significant change between sh1-PCK2 and L-PCK2. It is worth to mention that synthesis

of amino acids with increased molar fraction in L-PCK2 (serine, glycine and tyrosine) under glucose exhaustion conditions is dependent on PEPCK-M in contrast to alanine. This could be one of the explanations for increased molar fraction of these amino acids in L-PCK2 cells. Additionally, we have shown that serine and glycine synthesis is PEPCK-M dependent under glucose deprivation (Figure R-63).

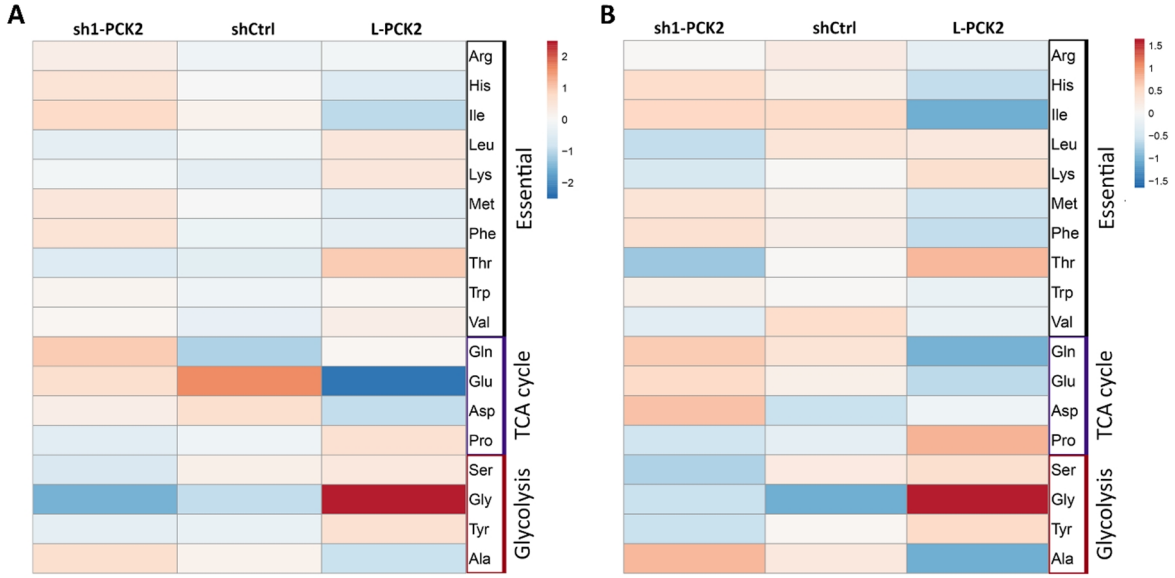

Figure R-64: Heatmap of amino acid distribution. Relative AA concentration was determined in the cell extracts of MCF7 cells grown for 24h in DMEM media containing 25 mM glucose (A) and in media containing 1 mM glucose (B, glucose exhaustion conditions). Values of molar fraction of selected amino acids were processed and visualized by using ClustVis tool with Pareto scaling (Metsalu & Vilo, 2015). Comparison of samples is realized within the rows.

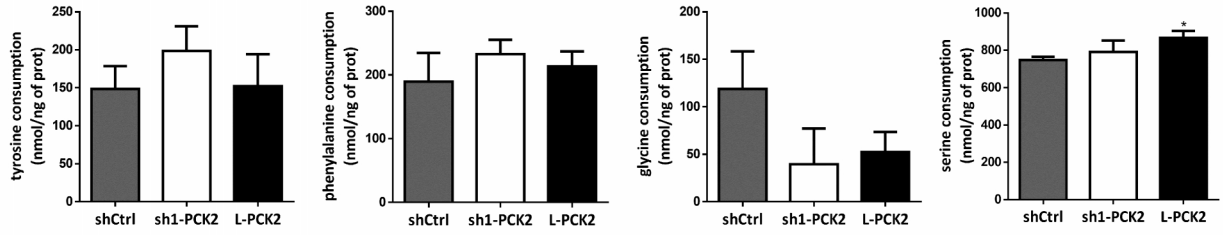

Figure R-65: Consumption of tyrosine, phenylalanine, glycine and serine. AA consumption in MCF7 cells incubated 24h in DMEM high glucose medium. AA consumption was calculated by subtraction of concentration in the media incubated with cells from concentration in the media incubated without cells. Consumption was normalized by total protein concentration. Concentration of AA was analyzed using LC-MS. *P<0.05 compared with shCtrl.

Above results of isotopomer distribution into serine and glycine demonstrated the importance of PEPCK-M in the synthesis of these amino acids under glucose deprivation, even in the presence of extracellular sources of these amino acids. This led us to evaluate the importance of this pathway under stress, using media MEM lacking glucose, serine and glycine. Absence of serine and glycine increased PEPCK-M expression in shCtrl cells (Figure R-66 A). Exposure of MCF7 cells with modified PEPCK-M expression to MEM media lacking glucose, serine and glycine resulted in decreased cell number over time. As expected, MCF7 cells with impaired PEPCK-M were more susceptible to stress induced by nutrient deprivation. At the time 72h, MCF7 sh1-PCK2 showed a decreased number of cells by 43.5% versus control and by 51.2% versus L-PCK2. Supplementation of MEM medium with serine and glycine eliminated any significant differences in cell number between sh1-PCK2 and shCtrl. L-PCK2 cells grown in MEM medium with serine and glycine still showed a significantly higher number of cells at 72h, although the difference between L-PCK2 and sh1-PCK2 cells was decreased by 45.4% when compared to MEM medium without serine and glycine (Figure R-66 B).

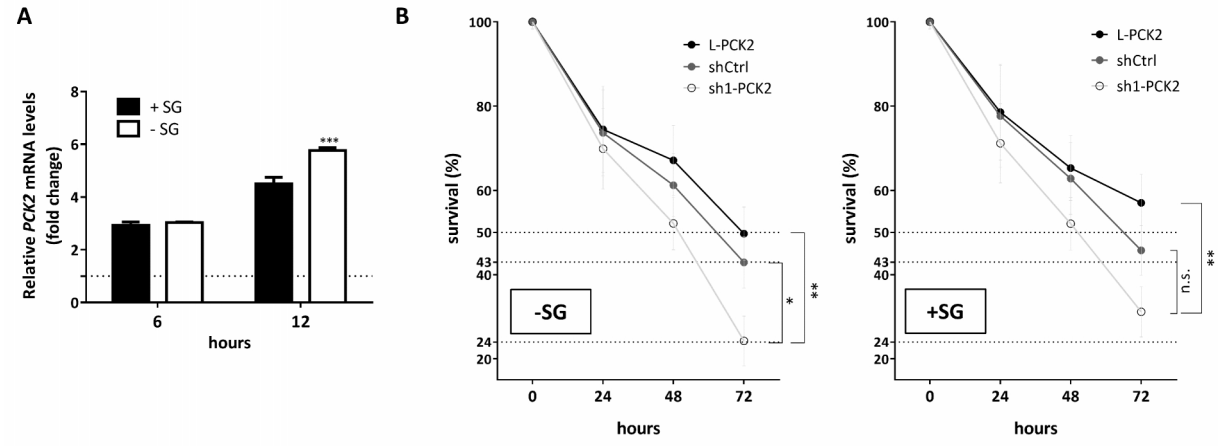

Figure R-66: Survival under nutrient deprivation. (A) Quantitative real time PCR was used to detect *PCK2* expression levels of shCtrl MCF7 grown in 0 mM glucose MEM media with or without serine and glycine (SG). Values were normalized to time 0h. 0h=1 and is marked with dotted line. *PCK2* expression levels were normalized to *TBP*. N=1, ***P<0.001 –SG versus +SG at the same time point. **(B)** MCF7 cells were treated for 72h in the glucose deprived MEM medium with (right) or without (left) serine and glycine (SG). Survival of cells was detected with MTT and CV assay. *P<0.05, **P<0.01.

As shown before (Figure R-22 on page 99), sh1-PCK2 cells consumed less glucose and produced less lactate in conditions of 1 mM or 25 mM glucose when compared to control. Deprivation of serine and glycine in MEM media containing 1 mM glucose caused a significant decrease in glucose consumption and lactate production in shCtrl and L-PCK2 cells. Interestingly, this effect of serine and glycine deprivation was not observed in MCF7 cells with knocked-down PEPCK-M (Figure R-67).

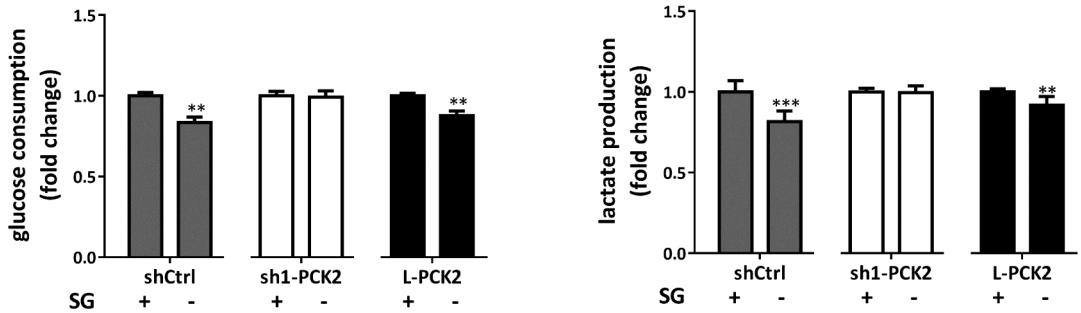

Figure R-67: Glucose and lactate metabolism of MCF7 cells under serine and glycine deprivation. MCF7 cells were grown in 1 mM MEM containing or lacking serine and glycine (SG) for 8h. Measured metabolites were normalized by protein. Graphics represent relative glucose consumption (left) and lactate production (right) and values were calculated as a fold change of -SG to +SG conditions separately for each type of infected MCF7 cells. **P<0.01, ***P<0.001 indicate significant difference between +SG and –SG treatment.

2.9 Effect of PEPCK-M inhibition in tumor xenografts

All previous results reinforced our hypothesis that PEPCK-M is an important enzyme for tumor growth *in vivo*. We decided to perform *in vivo* xenograft experiments, where HCT116 and MCF7 cell lines with reduced and endogenous expression of PEPCK-M were used. These cells were transplanted into immunocompromised mice and tumor growth was evaluated.

HCT116 xenograft model

HCT116 cells were used due to its advantage of their growth in the absence of hormonal treatment. HCT116 cells with silenced (shPCK2) and endogenous expression (shCtrl) of PEPCK-M were injected subcutaneously into flanks. 10 injections were performed with each shCtrl and shPCK2. Two weeks after we started to measure the volume of tumors for up to eight days when tumors were dissected. From ten tumor inoculations we observed growth of seven tumors in the case of sh1-PCK2 and five in the case of shCtrl. Growth of shPCK2 and shCtrl tumors did not show any differences (Figure R-68). Interestingly, analysis of PEPCK-M expression in tumors revealed loss of PEPCK-M silencing in tumors originating from shPCK2 cells (Figure R-69). HCT116 shPCK2 cells before injection showed an 83% decrease in PEPCK-M expression (Figure R-18, page 94). Western blot analysis of shCtrl and shPCK2 tumors revealed that the efficiency of silencing dropped from 83% to 23% at the end of the experiment, suggesting that HCT116 tend to lose PEPCK-M silencing when injected into mice and therefore the growth of shPCK2 tumors is unaffected. Next, we decided to perform another *in vivo* tumor growth study using the MCF7 cell model with different expression levels of PEPCK-M.

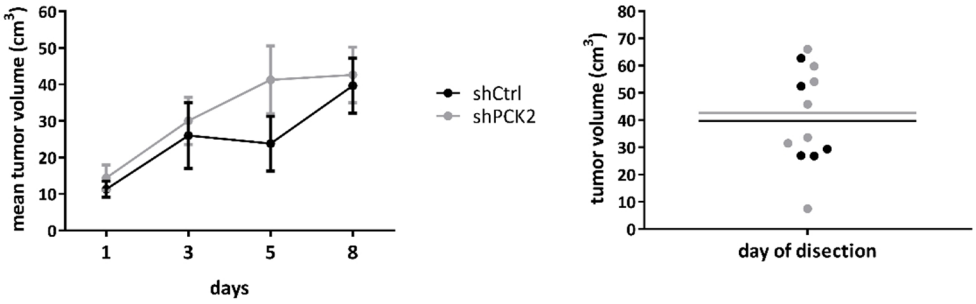

Figure R-68: Effect of PEPCK-M on tumor growth. HCT116 shCtrl and shPCK2 cells were injected into flanks (2.10^6 cells per flank). Two weeks later, size of tumors was measured every 2-3 days. Tumor volume was calculated as (length+width^2)/2 (left) Mean of measured volumes is plotted (left). Distribution of tumor volumes at eighth day of dissection is showed (right).

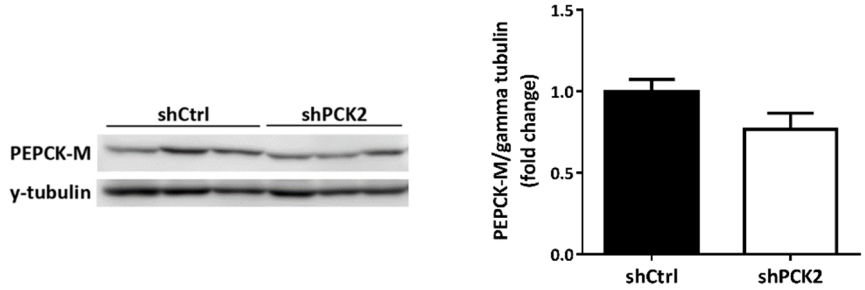

Figure R-69: PEPCK-M expression in tumor xenografts of HCT116 cells. Expression of PEPCK-M was analyzed by western blot. Western blot image on the left shows PEPCK-M levels in three shCtrl and three shPCK2 tumors. On the right is showed graphic with quantification of western blot.

MCF7 xenograft model

MCF7 cells require hormonal treatment of host. Therefore prior to injection we implanted to mice estradiol pellets that were placed under the skin, where they consistently released estradiol. Mice were injected orthotopically with MCF7 cells with three different expression levels of PEPCK-M: shCtrl with endogenous expression of PEPCK-M (18 injections), and sh1-PCK2 and sh2-PCK2 with reduced PEPCK-M expression (16 injections each). After two weeks, we started to measure tumor size for 11 days. We have evaluated the growth of 15 tumors in the case of sh1-Ctrl and 14 tumors in the case of sh2-PCK2 and shCtrl. Analysis of tumor volume did not show any differences in tumor growth between control cell line and PEPCK-M silenced cell lines. Moreover, the weight of the tumors after dissection was similar in all cases (Figure R-70).

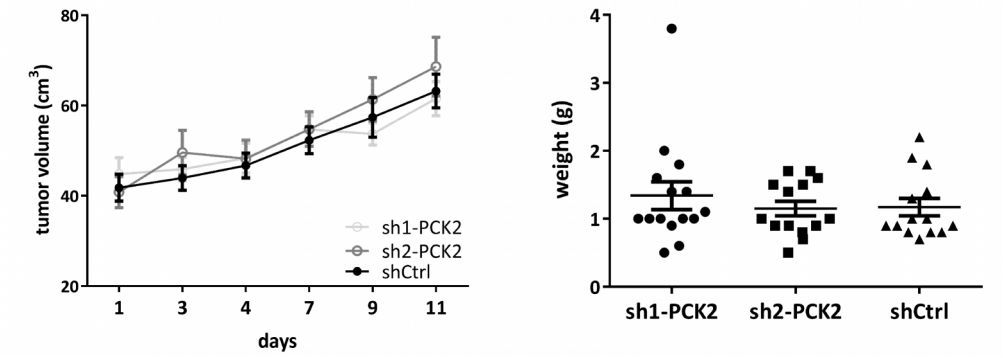

Figure R-70: Effect of PEPCK-M on tumor growth. MCF7 shCtrl, sh1-PCK2 and sh2-PCK2 were injected orthotopically into mammary fat pad in nude mice. Tumor growth was analyzed by measuring its size every two or three days. Tumor volume was calculated as (length+width^2)/2 (left). Mice were sacrificed after 11 days and tumor weight was measured (right).

Similarly to HCT116 cells, we investigated whether the levels of PEPCK-M in sh1-PCK2 and sh2-PCK2 cells were maintained during the experiment. Western blot analysis revealed loss of silencing in the case of both sh1-PCK2 and sh2-PCK2 (.
Figure R-71).

Even we did not detect any inhibition of tumor growth in either of used xenograft model, we are not able to form any conclusion, because of the loss of silencing in both cell lines *in vivo.*

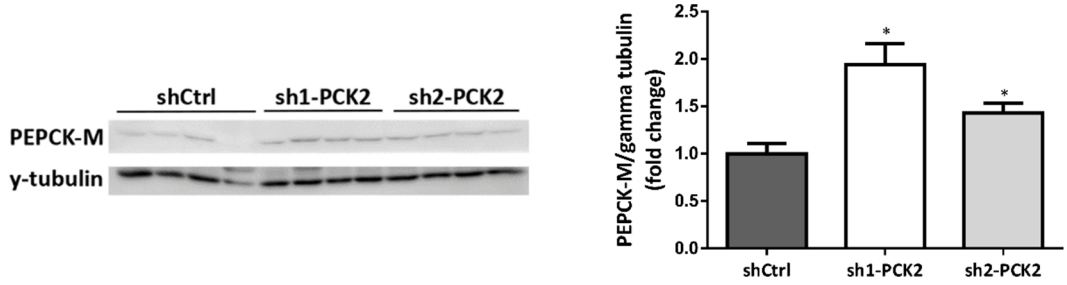

Figure R-71: PEPCK-M expression in tumor xenografts of MCF7 cells. Western blot analysis was used to measure PEPCK-M expression in tumors originating from injection of shCtrl, sh1-PCK2 and sh2-PCK2. On the right is graphic of western blot quantification. *P<0.05 versus shCtrl.

Discussion

In 1954 Utter and Kurahashi isolated and identified an oxalacetic carboxylase enzyme from avian liver (Utter & Kurahashi, 1954a, 1954b). Nowadays we know that the oxalacetic carboxylase enzyme was actually the PEPCK enzyme. More precisely, the mitochondrial isoform of PEPCK that is the only isoform present in the liver of pigeon and chicken after hatching (Söling *et al*, 1973; Croniger *et al*, 2002b). More than 60 years have passed from this finding that opened the door to other great discoveries on the implication of PEPCK in metabolism. The laboratory of Richard Hanson and collaborators brought an important insight in this field by shedding light on the role of PEPCK in gluconeogenesis and glyceroneogenesis (Hanson *et al*, 2006), and its regulation by dietary and hormonal signals (Hanson & Reshef, 1997). However, during these years, more emphasis was given to the cytosolic isoform rather than the mitochondrial one. This was mostly due to a couple of facts. Firstly, commonly used animal models (mice and rats) express very low levels of PEPCK-M in their livers, where it accounts only for about 5-10% of total PEPCK activity (Croniger *et al*, 2002b; Söling *et al*, 1973). Secondly, PEPCK-M was often underestimated because of its expression not being regulated by gluconeogenic cues as it is the case of PEPCK-C (Croniger *et al*, 2002a). In spite of that, recent discoveries brought PEPCK-M back in to the game.

It is widely accepted that the mitochondrial isoform accounts for about 50% of total PEPCK activity in the liver of most mammals including humans (Croniger *et al*, 2002b). The gluconeogenic capacity of PEPCK-M has been demonstrated only recently (Méndez-Lucas *et al*, 2013). Additionally, the role of PEPCK-M in glucose homeostasis through PEP cycling and GTP recycling has been linked to GSIS in pancreatic beta cells (Stark *et al*, 2009; Kibbey *et al*, 2007). Mitochondrial localization of PEPCK-M suggested its weaker rapid transcriptional regulation (Stark & Kibbey, 2014). However, our laboratory observed induction of PEPCK-M expression under several stress conditions. We demonstrated that amino acid limitation and ER stress increase expression of ATF4 which mediates transcriptional up-regulation of *PCK2* (Méndez-Lucas *et al*, 2014).

One of the characteristic features of PEPCK-M is its expression in non-gluconeogenic tissues and cells in undifferentiated state, like cancer cell lines (Méndez-Lucas *et al*, 2014), induced pluripotent cells (Varum *et al*, 2011) and others. In the present work we

also show PEPCK-M expression in developing brain and neuronal restricted progenitor cultures in addition to a number of cancer cell lines and tumors.

The case of neuronal progenitors

Our findings show that cycling neuronal progenitors are metabolically dependent on lactate, which is favoring maintenance of their undifferentiated state. Lactate can feed anabolic pathways and sustain ATP production by its oxidation in the TCA cycle. However, essential pathways like PPP, glycerol synthesis or one carbon metabolism pathways would require carbons to feed the glycolytic intermediate pool. Therefore, the discovery of PEPCK-M expression in neuronal progenitors points to a relevant role of this pathway in the fulfillment of metabolic requirements of neuronal progenitors.

In the past, lactate was referred to as metabolic waste product. The knowledge about lactate has changed and now is considered to be an important intermediate in numerous metabolic processes (Gladden, 2004). Lactate, under physiological conditions or during exercise, can be metabolized in various organs like the heart (Gertz *et al*, 1988; Neglia *et al*, 2007), skeletal muscle (Brooks *et al*, 1999b), brain (Qu *et al*, 2000) and the liver (Exton & Park, 1967). The importance of lactate is also exemplified by its role in cell to cell shuttle. In brain, the ANLS hypothesis that claim that astrocytes produce lactate which is taken up and oxidized by neurons was proposed (Pellerin & Magistretti, 1994). A similar principle was suggested for the "reverse Warburg effect" where lactate production from glycolytic stromal cells would feed oxidative metabolism of cancer cells (Pavlides *et al*, 2009).

The ANLS hypothesis was supported by several studies that observed oxidative metabolism of lactate by neurons even in the presence of glucose (Bouzier-Sore *et al*, 2003; Tabernero *et al*, 1996; Gallagher *et al*, 2009b; Itoh *et al*, 2003). Criticism was raised against of some of these studies that prove oxidative metabolism of lactate using isotope labels. It has been pointed that these studies lack consideration for the reversible equilibrium of LDH reaction which exist regardless of its net direction and this might affect labeling patterns (Chih & Roberts Jr, 2003; Roberts Jr, 2009). However, these criticisms ignore the fact that neurons express preferably the LDH1 isoform that has been

argued to favor the reaction in the direction from lactate to pyruvate (Pellerin *et al*, 1998; Bittar *et al*, 1996), and MCT2 transporter (Pierre & Pellerin, 2005; Debernardi *et al*, 2003) which shows high affinity to lactate (Pérez-Escuredo *et al*, 2016).

Lactate supports the presence of undifferentiated state of primary neuronal culture

Regardless of the criticisms to the ANLS hypothesis, the utilization of lactate by neurons in adult brain is an accepted concept, although lactate is not considered as their main substrate (Roberts Jr, 2009). In developing brain however, several studies brought evidence of a critical role of lactate in its metabolism (Bolaños & Medina, 1993; Rinholm *et al*, 2011). Additionally, lactate importance is supported by the fact that there are significantly higher concentrations of lactate in the developing brain than in adult brain (Lust *et al*, 2003; Tomiyasu *et al*, 2016). In accordance with these observations we tested and fully demonstrated that lactate supports and maintain undifferentiated neuronal restricted progenitors.

Undifferentiated state of neuronal culture growing in lactate media was demonstrated by decreased elongation of neurites and by the expression pattern of specific markers. High expression of TBR2, a marker of neuronal restricted progenitors (intermediate progenitors) and low expression of markers of more immature progenitors (like SOX2 and PAX6) is restricted to cultures formed mostly by neuronal restricted progenitors (Englund *et al*, 2005; Sessa *et al*, 2008). However, expression of TBR2 might be maintained also in early post-mitotic neurons (Englund *et al*, 2005). Therefore as a marker of neuronal progenitors we also used Ki67, a well known marker of cycling cells. In our neuronal culture, Ki67 would stain only progenitors as the post-mitotic neurons do not undergo proliferation. However, it is important to mention that not all progenitor cells are actively proliferating and therefore, Ki67 staining might underestimate the overall population of neuronal progenitors in our model.

Lactate was also efficient in maintaining neuronal progenitors in the media containing glucose. In these conditions, a mixed population of more and less differentiated neurons was present as these cells expressed markers of neuronal restricted progenitors and also

post-mitotic neurons.

Importantly, neuronal cultures grown exclusively in glucose medium showed signs of more differentiated cells. Neurons grown in glucose had elongated neurites and expressed markers of post-mitotic neurons and spared TBR2 expression. Glucose supported a more differentiated state of neurons in consistence with the observations made by Agostini *et al.* that have shown the importance of the glycolytic pathway for differentiation of neurons (Agostini *et al*, 2016).

Neuronal restricted progenitors have limited proliferative potential and can undergo 1-3 divisions. Division of neuronal progenitors can be symmetric or asymmetric giving rise to 2 more progenitors or 2 neurons, or 1 progenitor and one neuron, respectively (Noctor *et al*, 2004; Wu *et al*, 2005; Huttner & Kosodo, 2005). Analysis of cell number during the growth of neuronal culture in glucose media showed increase in total number of cells that can be explained by the division of preexisting Ki67 positive progenitors at day 1. Therefore, the increase in cell number and the depletion of progenitors after 5 days in glucose medium is compatible with 2 rounds of progenitor division; first an asymmetric division giving rise to a progenitor and a differentiated cell, and then a symmetric division of the progenitor giving 2 differentiated cells. The observation in glucose + lactate medium of an increased number of cells together with progenitor maintenance is compatible with one round of asymmetric progenitor division giving rise to a self-renewing progenitor and a differentiated cell; and finally, the increase in progenitors but not in the total cell number in lactate medium suggests self-renewing symmetric divisions and an enrichment in progenitor cells compared with the initial pool of terminally differentiated cells.

Active transport of lactate into cell is required for neuronal progenitor maintenance

In accordance with our results, a positive effect of lactate on the maintenance of less differentiated cells in neuronal cultures was observed also by Lampe *et al.* (Lampe *et al*, 2009). They proposed that this shift might be caused by the action of lactate as a scavenger of ROS, although no direct evidence was presented (Lampe *et al*, 2009). ROS

was shown to be present in lower concentration in neuronal progenitors than in neurons (Tsatmali *et al*, 2006). However, in our study, neuronal cultures with different state of differentiation do not display any alterations in ROS quantity and therefore we suggest that lactate does not act in our cultures differentiation process through the regulation of ROS levels.

It is common knowledge that lactate is capable of entering cells through the MCT transporters or act as a signaling molecule through the activation of the GPR81 receptor (Cai *et al*, 2008; Bergersen & Gjedde, 2012). In the context of brain, expression of GPR81 was detected in different cerebral structures, mostly in neurons (Lauritzen *et al*, 2014), and its expression *in vivo* was shown to be induced by administration of lactate (Castillo *et al*, 2015). GPR81 activation, as was shown in adipose tissue, can inhibit lipolysis through the inhibition of cAMP signaling (Liu *et al*, 2009). Interestingly, it has been shown that increased cAMP levels induce neuronal differentiation (Lepski *et al*, 2013). Lepski *et al*. showed that higher cAMP levels increase Ca^{2+} influx and they suggest that these two factors might induce differentiation through the activation of CREB, an important transcription factor in neuronal development (Lepski *et al*, 2013; Merz *et al*, 2011). Therefore we investigated the possibility that activation of GPR81 and subsequent inhibition of cAMP might play a role in the maintenance of neuronal progenitors in neuronal cultures exposed to lactate. Our findings demonstrate that activation of GPR81 by an agonist is not sufficient to reprogram the differentiation process of neuronal culture in the manner by which population of neuronal progenitors would be maintained.

The same conclusion was obtained by another approach: Neuronal culture was exposed to lactate in the presence of a MCT1/2 inhibitor to impede lactate metabolism. In this condition, lactate interaction with GPR81 remains unaltered. Consistently with previous results, GPR81 was not able to reprogram the differentiation process, in the absence of lactate transport. Importantly, this experiment provided a first demonstration that transport of lactate into the cell is required for maintenance of neuronal progenitors. Lactate entry to cells was corroborated by measuring its consumption from the media. Lactate consumption was demonstrated in neuronal cultures enriched in neuronal progenitors grown in lactate media. However, we did not observe the same effect in the

cells growing in glucose + lactate media. Since neuronal culture in glucose + lactate media is a mixed population of neurons in different states of development, we assume that this heterogeneity mask the metabolic activity of neuronal progenitors. More differentiated neurons in this culture are presumably producing lactate from glucose as it was observed in glucose only conditions. The importance of lactate metabolism for the maintenance of neuronal progenitors in glucose + lactate conditions is supported by the fact that the MCT2 inhibition led to their disappearance.

Various studies claim a prevalence of glycolytic metabolism in neural stem cells (NSCs) that shifts toward increased use of oxidative phosphorylation during differentiation of neurons (Zheng *et al*, 2016; Agathocleous *et al*, 2012), however the exact nature of their metabolic state was not defined for specific stages of differentiation. It is important to mention that none of these studies took into account the complex metabolic niche of the developing brain, where both lactate and glucose are present at the same time. Interestingly, Jady *et al*. have shown the ability of NSCs to oxidatively metabolize lactate (Jády *et al*, 2016). This is indicative of metabolic plasticity as described in stem cells, and its importance to match demands during lineage specification and cell fate determination (Folmes *et al*, 2012).

It is well known that lactate, upon entry to the cell, is converted to pyruvate which is directed to mitochondria where it feeds the TCA cycle and OXPHOS as it is observed in different tissues (for example heart and liver) (Gertz *et al*, 1988; Neglia *et al*, 2007; Exton & Park, 1967). Consistently, we found markers of oxidative metabolism in progenitors including increased mitochondrial membrane potential and higher PDH activity, as shown by the absence of inactive phosphorylated PDH form in neuronal cultures grown in lactate media. Analysis of other metabolic markers did reveal low levels of phospho-AMPK in progenitors grown in lactate conditions. AMPK responds very quickly to changes of energy charge in cells and is activated (phosphorylated) when there is an increased AMP/ATP ratio. Its activation occurs typically upon glucose deprivation and leads to stimulation of alternative pathways to compensate imbalances in energy charge (Shirwany & Zou, 2014). Low levels of phospho-AMPK suggest adequate compensation of lactate for ATP production in neuronal progenitors. Similarly, decreased SIRT1 expression

indicate high bioenergetic capacity of neuronal progenitors. SIRT1, an NAD+ dependent deacetylase, is activated by high NAD+/NADH ratio. Moreover, it has been suggested that NADH can regulate SIRT1 expression through HIC1:CtBP complex, however this paper was retracted recently (Zhang *et al*, 2007). Interestingly, SIRT1 expression was found to be increased during NSCs differentiation (Prozorovski *et al*, 2008; Ma *et al*, 2014), and SIRT1 knock-outs showed increased self-renewal capacity and proliferation of NSCs and neural progenitors (Ma *et al*, 2014). All this indicates that neuronal progenitors grown in lactate media use lactate as oxidative substrate to support their bioenergetic needs.

As previously mentioned we identified neuronal progenitors in our model by detection of Ki67 expression, a marker that is strictly associated with proliferation (Scholzen & Gerdes, 2000). Analysis of cells number in neuronal cultures grown in lactate media suggest that Ki67+ progenitors undergo 1 symmetric division during 4 days. Lower proliferation rates seems to be typical for some progenitors grown *in vitro*. For example, long doubling time was observed in neuronal stem cells (2.6 days or more) (Hermann *et al*, 2004). Additionally, differentiation is associated with lengthening of G1 phase of cell cycle (Salomoni & Calegari, 2010; Arai *et al*, 2011). Despite low proliferation rates, neuronal progenitors need to produce sufficient amount of ATP, nucleotides, amino acids, lipoproteins, etc., to build daughter cells. Obviously, lactate cannot fill up glycolytic metabolism to support proliferation in the absence of a pathway that moves pyruvate into intermediary PEP, pointing that PEPCK activity is required for full functionality of anabolic processes in these conditions. Lactate can feed the PEPCK pathway as already observed in the liver (Méndez-Lucas *et al*, 2013; Exton & Park, 1967). However, the functionality of the gluconeogenic pathway in proliferating cells was only proposed lately in some lung cancer cell lines that were shown to consume lactate and express PEPCK-M under glucose depletion (Leithner *et al*, 2015). Here we show high expression of PEPCK-M in neuronal progenitors that are dependent on lactate metabolism. Interestingly, PEPCK-M inhibition by 3MPA in neuronal cultures grown in the presence of lactate (glucose + lactate and lactate only media), and enriched by proliferating neuronal progenitors, led to depletion of these progenitors. The observation that PEPCK-M inhibition correspond with a significant reduction in the total number of cells as well as

the complete depletion of Ki67 positive progenitors indicates that in the presence of lactate, PEPCK-M inhibition leads to progenitor cell death. Administration of 3MPA to neuronal culture grown in lactate media did not only show depletion of Ki67 positive progenitors, but also decreased expression of TBR2, a marker of NRPs.

The negative impact of PEPCK-M inhibition on maintenance of neuronal progenitors points to its importance in providing glycolytic intermediates to ensure synthesis of metabolites relevant to proliferating cells. However, anabolic requirements of neuronal progenitors are not associated only with proliferation. It is well known that NSCs and progenitors are embedded in a niche which is rich in extracellular matrix (ECM) (Ma *et al*, 2008). ECM is important for proliferation and differentiation of NSCs and abundant amounts of ECM are present during differentiation (Lathia *et al*, 2007; Ma *et al*, 2008). One of the key components of ECM is laminin, a glycoprotein that enhance neural progenitor expansion and differentiation (Lathia *et al*, 2007; Ma *et al*, 2008). This may explain the high expression of laminin that we observed in neuronal cultures with less differentiated phenotype. Synthesis of a molecule like laminin requires fully active machinery of amino acids synthesis and glucosamine 6-phosphate production to secure its glycosylation. Both of these processes in lactate dependent progenitors should require PEPCK-M activity. PEPCK is the only enzyme that can move intermediates from TCA cycle into the glycolytic pool of intermediates. This is important to maintain glycosylation, and the synthesis of some amino acids that originates from glycolytic intermediates (e.g. serine, glycine, cysteine and tyrosine). Moreover, Satapati *et al.* observed that PEPCK-C inhibition decrease flux of the TCA cycle (Satapati *et al*, 2015) which might suggest also impact on anaplerosis and amino acid synthesis.

Accordingly, inhibition of PEPCK-M had a high impact on laminin synthesis. A loss in the capacity to synthetize sufficient amounts of laminin can be one of the causes of progenitor depletion. However, lower laminin production might be also caused by loss of neuronal progenitors as they are suggested to be the main site for synthesis of laminin.

Additionally, experiments performed *in vivo* support these conclusions. We observed that inhibition of PEPCK-M in newborn brain using 3MPA has a strong impact on the presence of neuronal restricted progenitors and proliferating cells, as well as laminin

Taken together, our results provide evidence of the strict dependence of neuronal progenitors on lactate metabolism that fulfil all biosynthetic needs of neuronal progenitors. Moreover, our results demonstrate metabolic dependence of neuronal progenitors on PEPCK-M activity (summarized in Figure D-1). However, more experiments are required to uncover key pathways required by neuronal progenitors to fulfill their functionality. Additionally, lactate might be relevant in some stages of neuronal development as the metabolism was shown to shift from glycolysis in neural stem cells, toward oxidative metabolism in mature neurons (Agathocleous *et al*, 2012; Zheng *et al*, 2016).

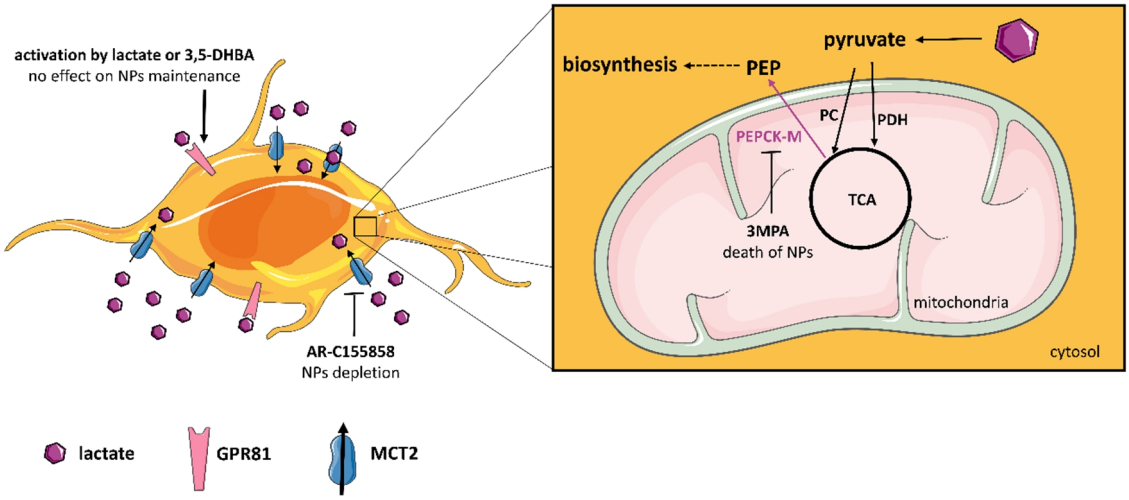

Figure D-1: Schematic representation of the proposed effect of lactate on neuronal progenitor cells (NPs). Graphic was made using Servier Medical Art image bank (Servier Medical Art, 2016).

Our results partially disclose importance of lactate presence in the niche of the developing brain. Knowledge of lactate restricted metabolic requirements of neuronal progenitors can be of use in regenerative medicine where several biomaterials contain L-lactic acid that form the supporting niche for neuronal progenitors (Alvarez *et al*, 2013). Interestingly, lactate has been shown as a preferred substrate in the brain after traumatic injury (Glenn *et al*, 2015) or after exposure to hypoxia (Bliss & Sapolsky, 2001).

Future challenges for the definition of the precise role of PEPCK-M in lactate metabolism

in neuronal progenitors will require deeper characterization of its metabolic profile by using approaches like metabolomics analysis. This will allow us to focus on more specific pathways in further studies. Identification of key metabolic pathways will help us to better understand the metabolic requirements of undifferentiated cells. This information might be applied also in other cell models, like cancer cells.

The case of cancer

Cancer cells are often compared with stem or progenitor cells as they share some common characteristics. It is important to mention that cancer cells are very heterogeneous and this characterization is not always universal. However, it seems that more invasive or resistant tumors are matching characteristics common to stem cells, for example self-renewal capacity (Yamada *et al*, 2014; Pardal *et al*, 2005), undifferentiated phenotype (Holmberg *et al*, 2011; Zhao *et al*, 2016) and metabolic plasticity (Ramanujan, 2015; Simoes *et al*, 2015; Agathocleous *et al*, 2012). Metabolic flexibility allows stem or progenitor cells to cope with different metabolic requirements during the differentiation (Agathocleous *et al*, 2012; Folmes *et al*, 2011). In cancer cells, metabolic flexibility allows cells to support their growth and adapt to conditions with reduced nutrient or oxygen availability that are present in the tumor microenvironment (Simoes *et al*, 2015; Reid *et al*, 2013). Cancer cells are often described as metabolically addicted to glucose. Metabolism of glucose by cancer cells was mainly assigned to aerobic glycolysis (Warburg effect), which is marked by increased glucose uptake and lactate production (Warburg, 1956; Pavlova & Thompson, 2016). However, often forgotten OXPHOS was show to be an active pathway in different cancer cells (Zu & Guppy, 2004; Sanchez-Alvarez *et al*, 2013). OXPHOS can be maintained by oxidation of either glucose derived pyruvate or glutamine. Avid glutamine oxidation was observed in cancer cell lines (Bode *et al*, 2002; Cetinbas *et al*, 2016; Le *et al*, 2012a) where glutamine was shown as an important source of energy and an anaplerotic substrate (DeBerardinis *et al*, 2007; Fan *et al*, 2013; Reitzer & Wice, 1979). Several studies described the ability of cells to switch from one type of metabolism to other based on nutrient availability. For example, cells can turn on glutamine utilization when glucose is absent and vice versa (Lim *et al*, 2014; Le *et al*, 2012a;

Cetinbas *et al*, 2016). The ability of cancer cells to activate their metabolism based on microenvironmental conditions and bioenergetic and biosynthetic demands is providing an effective strategy for their survival and progress. Metabolic plasticity of cancer cells depends on their ability to change expression of key metabolic enzymes to support their needs. For example they can regulate the rate of pyruvate oxidation through changes in PDH activity via its phosphorylation. Decrease in PDH activity of human lung carcinoma cells can promote reductive carboxylation (Fendt *et al*, 2013). Often, cancer cells also show high expression levels of glutaminase 1 (GLS1) that is regulated by c-MYC (Gao *et al*, 2009; Cheng *et al*, 2011). Enhanced glutamine metabolism is very important when cells find themselves in conditions of impaired transport of pyruvate into the TCA cycle (Yang *et al*, 2014a).

In accordance with changes in their metabolic profile, we found that expression of mitochondrial phosphoenolpyruvate carboxykinase (PEPCK-M) is significantly increased in many tumors and cancer cell lines.

PEPCK is a well-known gluconeogenic enzyme that under physiological conditions contributes to glucose homeostasis by producing glucose in the liver and kidney. In the context of cancer metabolism, PEPCK might be advantageous to cancer cells via several mechanisms. First, it is important to note that the PEPCK reaction is the only pathway that is able to communicate mitochondrial intermediates with the glycolytic intermediary pool above PEP. This ability would add great advantages to cells growing in conditions with limited sources of glucose that is considered the main substrate for PPP, SSP, one carbon metabolism, glycerol synthesis, etc. Moreover, PEPCK-M was shown to play a role in a pro-survival pathway in cancer cells undergoing ER stress and amino acid limitation, although the exact mechanism was not described (Méndez-Lucas *et al*, 2014). Second, PEPCK was shown as an important regulator of TCA cycle flux. Disruption of cataplerosis through PEPCK-C inhibition led to the accumulation of TCA cycle intermediates in the liver, and to a decrease of TCA cycle flux (Burgess *et al*, 2004). Additionally, it has been shown that inhibition of PEPCK-C activity can decrease ROS production caused by elevated anaplerosis/cataplerosis (Satapati *et al*, 2015). ROS is usually elevated in cancer cells and it is acting as a positive factor for cancer cell development, however high levels

of ROS can be also damaging to cancer cells (Nogueira *et al.*, 2008). All this suggest that PEPCK-M might be an important enzyme in cancer cells with the ability to regulate the TCA cycle and support metabolic requirements in normal or stressed conditions.

Mitochondrial versus cytosolic PEPCK in cancer

There are two known isoforms of PEPCK, the mitochondrial and the cytosolic isozyme that are catalyzing chemically identical reactions. Interestingly, the mitochondrial isoform is preferentially expressed in undifferentiated cells or stem cells as observed by us (Álvarez *et al*, 2014), and as shown GEO database by others (Barberi *et al.* 2005 GDS1288; Edgar *et al.* 2002; Poon *et al.* 2013 GDS5603, Cherqui *et al.*, 2006 GDS1701; Eckfeldt *et al.*, 2005 GDS1230).

Preferential expression of PEPCK-M was also observed in mice liver during fetal development, whereas after birth mostly the cytosolic isoform is expressed (Hanson & Reshef, 1997; Croniger *et al*, 2002b). Interestingly, re-expression of fetal isoforms of some enzymes is typical of undifferentiated cells and often observed in cancer cells. For instance, cancer cells often express the embryonic isoform of pyruvate kinase, PKM2, which is subject to allosteric regulation (Christofk *et al*, 2008). Similarly, brain-type glycogen phosphorylase (BGP) is suggested to be the major isoform in tumor and fetal tissues (Sato *et al*, 1972). Next, adult liver is known to express liver–type glutaminase 2 (GLS2). However, when undergoing malignancy, cells switch from GLS2 to glutaminase 1 (GLS1) expression, which is also present in embryonic hepatocytes (Yuneva *et al*, 2012; Hu *et al*, 2011).

In line with these observations, in this work we show that several cancer cell lines highly express mitochondrial PEPCK, while they show very low or no expression of PEPCK-C. As mentioned before, mitochondrial isoform is preferentially expressed in undifferentiated cells. Consistent with our data, several studies also observed high expression of mitochondrial PEPCK in cancer cells (Vincent *et al*, 2015; Leithner *et al*, 2015). Moreover we did detect higher PEPCK-M expression in several human tumors (e.g. breast cancer, leukemia, lung cancer, prostate cancer, etc.) when compared to their non-neoplastic counterparts. Interestingly, the tumors originating from tissues that originally express

cytosolic and mitochondrial isoform, such as kidney and liver, maintain expression of both of them upon malignancy. However, PEPCK-C expression heavily drop in these tumors. In agreement with our observations, several studies report significant decrease of PEPCK-C expression in hepatocellular carcinoma and colon cancer compared with normal tissue (Khan *et al*, 2015; Ma *et al*, 2013b). PEPCK-M expression also tend to decrease in these types of tumors, however the drop in expression is substantially lower. Similarly to the striking drop of PEPCK-C expression, lower levels of glucose-6 phosphatase and fructose bisphospatase-1 are observed upon malignancy of gluconeogenic tissues (Ma *et al*, 2013b; Wang *et al*, 2012). This indicates a deleterious impact of cancer progression on pathways characteristic of differentiated tissues, such as gluconeogenesis in hepatocellular carcinoma. Mechanism of downregulation of gluconeogenic enzymes is not elucidated yet, however several studies show that downregulation of PGC1-α transcription factor through miR-23a (Wang *et al*, 2012) and inactivation of endogenous glucocorticoid signaling (Ma *et al*, 2013b) could play a role. Also, FOXO1, a positive regulator of *PCK1*, is downregulated in hepatocellular carcinoma and colon cancer (Khan *et al*, 2015). It should be noted that activation of PEPCK-C mediated gluconeogenic pathway through activation of FOXO1 in hepatocellular carcinoma cells was shown to negatively affect their survival (Khan *et al*, 2015). Similarly, Ma *et al.* observed that activation of gluconeogenesis in tumors by synthetic glucocorticoids can suppress the growth of ectopic hepatocarcinoma (Ma *et al*, 2013b). The negative effect of gluconeogenesis activation could be explained by the fact that cancer cells are forced to futile synthesis of glucose by external factors and this would lead to waste of energy and carbon sources in the cancer cell setting. Therefore, it seems logic that cancer cells would prefer the mitochondrial isoform which expression could be more manageable by the needs of the cell (for example induction by ER stress or amino acid depletion) and not PEPCK-C that is regulated by hormones and diet (Reshef *et al*, 1969; Hanson & Reshef, 1997).

PEPCK-M expression in cancer cells is suggesting of its importance for the metabolic state of cancer cells that are coping with high bioenergetics and biosynthetic demands, and nutritional stress, together with a possible contribution to metabolic plasticity. Therefore

it is relevant to study the role of PEPCK-M in cancer metabolism to better understand cancer biology and to discover new pathways that might be used in the development of new strategies for cancer therapy.

PEPCK-M relevance for cancer cell growth

Metabolism and growth are tightly connected, therefore most of the metabolic studies use cell growth analysis as a first indicator of the relevance of an enzyme or pathway for cancer cells. We observed that silencing or inhibition of PEPCK-M cause a decrease of growth of cancer cells in conditions of abundant glucose. A more significant impact on the growth was observed using soft-agar assay. Soft-agar assay is used to predict carcinogenic capacity (Borowicz *et al*, 2014). Cells with reduced PEPCK-M activity show decreased ability to form colonies when grown in anchorage independent conditions. Similar effects of PEPCK-M inhibition on cell growth were reported also by Park *et al*. and Leithner *et al*. In agreement with our results, PEPCK-M impairment in these studies reduced the proliferation rate and spheroid growth, respectively (Park *et al*, 2014; Leithner *et al*, 2015). A negative impact of PEPCK inhibition on proliferation was demonstrated also in the case of cytosolic isoform in colon cancer (Montal *et al*, 2015) and melanoma (Li *et al*, 2015). However, it is necessary to stress that these studies underestimated the possible role of the mitochondrial isoform in this context and they did not show expression levels of PEPCK-M, neither silencing specificity to the cytosolic isoform.

In this work we show that PEPCK-M overexpression has no impact on proliferation of MCF7 cancer cells in abundant glucose conditions. We could hypothesize that overexpression of PEPCK-M in these conditions is not facilitating cell growth due to reached metabolic capacity of endogenous PEPCK-M. However, to increase it by activation of its metabolism.

However, we will consider in future investigations to overexpress this enzyme in non-tumorigenic cell line (e.g. MCF710a), which proliferation is considerably lower and have the ability to enhance it by activation of its metabolism.

The observed negative impact of PEPCK-M silencing on cancer cell growth indicated

relevance of the enzyme in tumor growth. Unfortunately, loss of silencing in two different xenograft models prevented us from evaluating the importance of PEPCK-M for tumor growth *in vivo*. Although, the importance of PEPCK-M for tumor growth was supported by a recent study by Vincent *et al.* (Vincent *et al*, 2015) showing impaired growth of PEPCK-M knocked-down lung cancer cell line xenografts. To confirm the role of PEPCK-M for tumor growth in our models, we plan to implement a new approach by using CRISPR gene editing. Generation of *PCK2* knock-out using CRISPR/Cas9 system will avoid the problem of reactivation of its expression.

The impact of PEPCK-M inhibition on growth was an indicator of an important metabolic role of this enzyme in cancer cells to support their growth.

TCA cycle changes upon different PEPCK-M expression levels

As mentioned above, PEPCK-C is able to influence the TCA cycle flux and its inhibition leads to accumulation of TCA cycle intermediates in the liver (Burgess *et al*, 2004). Mitochondrial and cytosolic PEPCK catalyze the same reaction and therefore we could expect similar effects on the behavior of the TCA cycle after PEPCK-M inhibition.

PEPCK-M reaction is GTP dependent what makes PEPCK-M a candidate for recycling of GTP produced in the TCA cycle reaction catalyzed by succinyl-CoA synthetase. Recycling of GTP is important since no general transporter of GTP/GDP has been identified in higher eukaryotes (Stark & Kibbey, 2014). Even though, tissue specific guanine nucleotides transport into mitochondria was detected in heart, but at very slow rates that might only fulfill non-proliferating cell requirements (McKee *et al*, 2000). Importance of PEPCK-M in GTP recycling is supported by the study that describe a functional coordination between GTP synthesis and recycling by PEPCK-M in pancreatic beta cells (Stark *et al*, 2009). Both these examples of PEPCK-M interaction with the TCA cycle suggested that PEPCK-M silencing might affect TCA cycle metabolism in our cells.

We demonstrated the functionality of PEPCK-M driven cataplerosis in MCF7 cells grown under the glucose deprivation by showing synthesis of serine and glycine from glutamine. However, in the presence of glucose, glutamine participation in serine or glycine synthesis was not detected. These data does not exclude the possibility that the PEPCK-M reaction

is active, as serine synthesis in these conditions might be fully covered by glucose metabolism. Moreover, Vincent *et al.* in their study showed PEP synthesis from glutamine in cancer cells grown in the presence of 25 mM glucose, even though at very low levels (Vincent *et al*, 2015). The functionality of the PEPCK-M pathway in our model might be evaluated by its effects on isotopomer distribution of TCA cycle intermediates. Our data show several metabolic changes occurring at the level of the TCA cycle upon modification of PEPCK-M expression in MCF7 cells grown in abundant glucose media. Glutamine metabolism was evaluated by measurement of isotopomer distribution from fully labeled glutamine into various metabolites.

Silencing of PEPCK-M lead to an increase of fully labeled four carbon metabolites of the TCA cycle, namely succinate, malate and oxaloacetate. However, no changes in anaplerosis from glutamine were observed as suggested by similar contribution of label from glutamine to α-ketoglutarate. This was supported by similar levels of glutamine consumption in these cells. Consistent with previous findings, we did not observe any changes in GLS1 mRNA expression that is a significant player in the anaplerosis of the TCA cycle in various cancer cells (Sellers *et al*, 2015; Yang *et al*, 2014b) and changes in its activity serve as an indicator of changes in anaplerosis of glutamine (Le *et al*, 2012a; Yuneva *et al*, 2012). In addition, we observed equilibration of glutamate and aspartate with their keto acids.

Based on previous observations we assume that the increased pool of labeled intermediates in PEPCK-M deficient cells might result from impaired cataplerosis through this enzyme. Therefore oxaloacetate would not be taken out from the TCA cycle at the same rate as in control cells and this would lead to a larger pool of labeled oxaloacetate in the first and also second turn. The labeling pattern of oxaloacetate is mirrored into prior intermediates, malate and succinate. Similarly, increased levels of m+4 malate and fumarate originating from fully labeled glutamine were observed in colon carcinoma cell line upon inhibition of PEPCK-C (Montal *et al*, 2015).

Citrate does not copy the label distribution of oxaloacetate. This might be explained by the same rate of pyruvate oxidation as the m+4 citrate is equal in silenced and control cells. This is supported by the similar levels of phosphorylated pyruvate dehydrogenase

(PDH). PDH phosphorylation, caused by pyruvate dehydrogenase kinases (PDK1-4), inactivates the enzyme. Based on similar levels of PDH phosphorylation, we speculate that pyruvate oxidation in the TCA cycle is not changed upon PEPCK-M inhibition. In addition, routine oxygen consumption rates of MCF7 cells with basal and decreased PEPCK-M expression was unchanged, supporting the fact that pyruvate oxidation is not affected.

Even though oxidation of pyruvate seems unchanged, PEPCK-M impairment decreased glucose consumption. At the same time, lactate production was not significantly changed. Similar effect of PEPCK silencing on glucose consumption was also observed in melanoma (Li *et al*, 2015) and HeLa cells (Méndez-Lucas *et al*, 2014). Based on the calculations of lactate to glucose ratio we might assume that PEPCK-M inhibition appears to increase conversion of glucose to lactate, having in mind that glutamine does not participate in lactate production as negligible label distribution from [U-^{13}C] glutamine into lactate was observed in our model.

Overexpression of PEPCK-M showed slightly decreased anaplerosis of glutamine into the TCA cycle in glucose abundant conditions as suggested by lower incorporation of glutamine into m+5 α-ketoglutarate. However, this was not confirmed by analysis of glutamine consumption or GLS1 expression.

Moreover, the labeling pattern of α-ketoglutarate was not mirrored in other TCA cycle intermediates. Therefore we assume that differences in glutamine to α-ketoglutarate conversion are negligible.

Interestingly, PEPCK-M overexpression led to an increase in fully labeled four carbon TCA cycle intermediates made from uniformly labeled glutamine, but at the same time the amount of isotopologues produced by reductive carboxylation of glutamine (m+5 citrate and m+3 oxaloacetate, malate and fumarate) was decreased. This might indicate that more carbons from glutamine are moved into the oxidative pathway, rather than through reductive carboxylation. Concurrently, no changes were observed in the glycolytic pathway as overexpression of PEPCK-M did not affect glucose consumption or lactate production.

Cancer cells as proliferating cells need to support several biosynthetic pathways. It is

know, that fatty acid synthesis is active pathway in cancer cells (Medes *et al*, 1953; Kuhajda *et al*, 1994) and inhibition of this pathway was shown to impair growth of cancer cells (Nishi *et al*, 2016; Wilmanski *et al*, 2016). Cancer cells also show increased expression levels of fatty acid synthase (FAS), and high levels of FAS synthesis are often linked with worsen prognosis (Visca *et al*, 2004; Sebastiani *et al*, 2004; Gansler *et al*, 1997). Our data show, that PEPCK-M overexpression is able to metabolically support fatty acid synthesis since cells with overexpressed PEPCK-M displayed increased their *de novo* synthesis. This observation is paralleled by increased expression of fatty acid synthase (FAS). Previously, PEPCK-C overexpression in colon cancer cells showed a similar effect on fatty acid synthesis (Montal *et al*, 2015). Fatty acid synthesis is relevant for cells to support biosynthesis of membranes and signaling molecules (Currie *et al*, 2013). Therefore, increased capacity of cells to synthetize fatty acids might support growth of cells. However, PEPCK-M overexpression did not show any positive impact on MCF7 cell line growth that would suggest this type of advantage in our model.

Metabolic changes in MCF7 cells under glucose deprivation

Tumor cells find themselves surrounded by a microenvironment, which is mostly defined by nutrient and oxygen concentration gradient. Microenvironment is heterogeneous and change within the tumor. Vascularization might not be always sufficient to supply metabolites and oxygen to all parts of the tumor and the cells located farther from the surface are exposed to lower concentration of oxygen and nutrients (Serganova *et al*, 2011). This is mostly caused by decreased diffusion towards the tumor center and by the fact that cells at the surface might consume a major part of available nutrients (Lavrentovich *et al*, 2013; Greenspan, 1972; Gatenby & Gillies, 2008). Tumor cells use various metabolic adaptations to cope with this precarious microenvironment (Baldini *et al*, 2016; Simoes *et al*, 2015). For example, many cancer cells exposed to glucose deprivation are able to switch in glutamine utilization to ensure survival and growth (Yang *et al*, 2009a; Le *et al*, 2012a).

Functioning of the TCA cycle under glucose deprivation was identified by the production of labeled TCA cycle intermediates from [U-^{13}C] glutamine. Moreover, withdrawal of

glucose from media was followed by an increased proportion of glutamine derived TCA cycle intermediates when compared to high glucose media. These observations point to increased flux of glutamine into the TCA cycle under glucose deprivation in MCF7 cells. This behavior was observed also in other cancer cells grown in the absence of glucose like lymphoma, where higher anaplerosis of glutamine into TCA cycle was correlated with expression of c-MYC (Le *et al*, 2012a), an oncogene that is highly expressed in MCF7 cell line (Liu *et al*, 2012a).

Maintenance of the TCA cycle flux under glucose deprivation is conditioned by supply of acetyl-CoA. We found that glucose deprivation induces acetyl-CoA formation from glutamine as we observed incorporation of m+2 acetyl-CoA in the formation of fully labeled citrate. We assume that the main source of labeled acetyl-CoA in MCF7 cells is pyruvate which was synthetized under glucose deprivation from glutamine. M+6 citrate was barely detectable under high glucose conditions, indicating activation of this pathway upon glucose withdrawal. Synthesis of acetyl-CoA from glutamine through reductive carboxylation and its usage in the synthesis of citrate was discarded. Acetyl-CoA formed in this reaction would bare one labeled carbon and therefore would form m+5 or m+1 citrate. As there were no changes in m+5 or m+1 citrate levels upon glucose withdrawal and moreover isotopologues indicating reductive carboxylation were decreased, we assume that reductive carboxylation does not play important role in maintenance of functional TCA cycle.

Participation of glutamine carbons in pyruvate formation can be mediated through malic enzyme, which decarboxylates malate to pyruvate, or mitochondrial phosphoenolpyruvate carboxykinase, which converts oxaloacetate to PEP. Labeling patterns of pyruvate suggest that PEPCK-M does not participate in its production, since isotopomer distribution does not show PEPCK-M dependent contribution from carbons from [U-^{13}C] glutamine, in contrast to what we observed in serine and glycine. Therefore, we suggest that fully labeled pyruvate is produced by malic enzyme from m+4 malate. Moreover, participation of mitochondrial isoforms of malic enzyme on pyruvate production under glucose deprivation was observed in other models (Yang *et al*, 2014a). Labeling pattern of lactate suggests that pyruvate formed from glutamine derived TCA

cycle intermediates is driven mostly to citrate. However, some pyruvate was moved into lactate and m+3 lactate was formed. Interestingly, MCF7 cells with silenced PEPCK-M showed higher levels of m+3 lactate, suggesting its increased formation. Even though these changes are not reflected in pyruvate, this might be caused by reduced PEPCK-M driven cataplerosis as seen by lower serine and glycine enrichment in PEPCK-M depleted cells.

Regarding anaplerosis, α-ketoglutarate labeling and GLS1 expression levels suggest that this pathway is not significantly affected by silencing nor by overexpression of PEPCK-M. As will be discussed later, we observed PEPCK-M dependent cataplerosis in MCF7 cells deprived of glucose. Interestingly, changes in cataplerosis through PEPCK-M were not mirrored in the labeling of TCA cycle intermediates. M+4 oxaloacetate and malate levels proceeding from glutamine showed equal labeling, independent on PEPCK-M expression levels. The only intermediate that copied label distribution similar to high glucose condition was succinate. On the other hand, species indicating reductive carboxylation were formed to a lesser extent in cells with silenced PEPCK-M and this might indicate decreased reductive carboxylation in these cells under glucose deprivation.

PEPCK-M role in serine and glycine synthesis

As mentioned before, tumors might be exposed to microenvironment with limiting nutrients or oxygen (Serganova *et al*, 2011), and they might escape the negative impact of these conditions by various metabolic adaptations (Baldini *et al*, 2016; Simoes *et al*, 2015).

Some cancer cell lines, for example non-small cell lung cancer (NSCLC) cells, are able to resist glucose deprivation and even proliferate in the presence of other carbon source, glutamine (Vincent *et al*, 2015). MCF7 cells are not able to withstand the severe stress induced by total glucose depletion as they stop to grow and decrease total cell number over time. However, MCF7 cells with overexpressed PEPCK-M are more resistant to these stress conditions than silenced ones. It has been shown that glucose deprivation activate a stress response related to ER stress and activate transcription factor ATF4 (Ye *et al*, 2010; Ding *et al*, 2016), which is known to positively regulate *PCK2* expression as was

described in our laboratory (Méndez-Lucas *et al*, 2014). Decreased resistance to ER stress initiated by glucose deprivation in MCF7 cells with silenced PEPCK-M is in agreement with the participation of PEPCK-M in the survival program initiated upon ER stress and amino acid depletion (Méndez-Lucas *et al*, 2014). PEPCK-M dependent survival under ER stress might include various pathways, yet unidentified. One of the metabolic implications of PEPCK-M is to feed glucose side-branch metabolism as it is the only enzyme that can connect TCA cycle intermediates with glycolytic pool above PEP. Presumably, this role becomes more relevant under glucose deprivation. Some enzymes of glucose side-branch pathways, like the ones for serine synthesis were shown to be overexpressed in different cancer cells growing under glucose deprivation even in the presence of exogenous serine and glycine (Ma *et al*, 2013a; Sun *et al*, 2015), and were shown to be regulated by ATF4 transcription factor similarly to *PCK2* (Ye *et al*, 2012; DeNicola *et al*, 2015). In accordance with this, we observed that MCF7 cells treated with media lacking glucose do express higher levels of PHGDH and PSAT1, enzymes implicated in SSP. The importance of functional serine synthesis pathway (SSP) for growth of cancer cells *in vitro* and *in vivo* has been confirmed by several studies (Mattaini *et al*, 2015; Pacold *et al*, 2016; Possemato *et al*, 2011). Interestingly, the inability of exogenous serine to rescue cancer cells with impaired SSP suggests that flux through the SSP might be important for cell metabolism beyond providing serine (Possemato *et al*, 2011; Mattaini *et al*, 2015). Serine and glycine synthesis is relevant for production of glutathione, nucleotides, methylation of homocysteine (Nelson & Cox, 2000) or the support of anaplerosis of glutamate into α-ketoglutarate (Possemato *et al*, 2011). Blunt of this pathway can therefore affect synthesis of molecules relevant for growth and survival.

It was observed that inhibition of serine synthesis pathway under glucose deprivation in the presence of serine and glycine accelerated cell death (Sun *et al*, 2015; Ma *et al*, 2013a). Based on the fact that both, PEPCK-M and SSP enzymes, are responding to the same transcriptional factor and the fact that PECPK-M is the only known enzyme that can support SSP under glucose deprivation led us to speculate that PEPCK-M is relevant for the maintenance of functional SSP under initiated ER stress induced by glucose deprivation. This was confirmed and we observed increased cell death in cells with

decreased PEPCK-M expression. Moreover withdrawal of serine and glycine in the absence of glucose had an even more significant impact on the survival of cells with reduced levels of PEPCK-M. On the other hand, cells overexpressing PEPCK-M showed increased resistance to stress caused by nutrient withdrawal.

To confirm the functional relevance of PEPCK-M for SSP, a metabolomics study was designed, whereby MCF7 cells treated with uniformly labeled glutamine under glucose deprivation. Cataplerosis through the PEPCK-M enzyme towards SSP was hence demonstrated for the first time, as we have shown that flux of carbons from glutamine into serine and glycine is directly dependent on PEPCK-M activity under these conditions. Later, Vincent *et al.* also observed that PEPCK-M drive carbons from TCA cycle to serine under glucose deprivation (Vincent *et al*, 2015). Additionally, cells with overexpressed PEPCK-M contain higher molar fraction of amino acids which synthesis is starting from PEP (tyrosine) or 3PG (serine and glycine) supporting the relevance of PEPCK-M expression in the metabolism of these amino acids. Even though AA levels in cell extract might be influenced by their uptake from medium, no changes in consumption of those AA in glucose abundant medium were detected, except for serine, where PEPCK-M overexpressing cells showed higher serine consumption than control cells. Consistent with serine being metabolically more potent amino acid (Mattaini *et al*, 2016), MCF7 cells consumed preferentially serine over glycine.

Recently, Ma *et al.* described the induction of glutamine utilization for serine and glycine synthesis under nutrient deprivation in protein kinase C (PKC) zeta deficient SW480 cells. In this model, metabolic reprogramming under PKC zeta deficiency supports cell growth in the absence of glucose (Ma *et al*, 2013a). Based on our results, we believe that in this model, PEPCK-M is an important player that is necessary to support successful metabolic reprogramming by fluxing carbons from glutamine into SSP and to enhance the ability of cells to adapt and better respond to nutritional stress. Relevance of PKC zeta suppression in tumor growth is supported by several studies that detect a negative impact of PKC zeta overexpression on tumor growth (Mustafi *et al*, 2006; Nazarenko *et al*, 2010).

The abundance of labeled serine and glycine in our study is low, however this is consistent with the study of Vincent *et al.* (Vincent *et al*, 2015) which analyzed serine

synthesis in very similar conditions. A low percentage of labeled serine and glycine might be caused by the short time of labeling that we performed in order to avoid changes due to more profound stress conditions during glucose deprivation that could affect metabolomics studies. It is important to mention that labeling studies were performed in the presence of exogenous serine and glycine. This may lead to an underestimation of isotope labeling experiments due to equilibration between labeled intracellular and unlabeled exogenous sources as pointed out by DeNicola *et al.* (DeNicola *et al*, 2015).

Flux of carbons from glutamine into serine and glycine was abolished when glucose was present in culture media. This might be caused by the predominant participation of unlabeled glucose in SSP. However, to definitely discard the possible implication of PEPCK-M in SSP in the presence of glucose, an additional experimental condition with increased labeling time needs to be performed. Seemingly improbable bidirectional functioning of glycolysis and gluconeogenesis is supported by the phenomenon occurring in adipocytes, where glyceroneogenesis is the main source of triglycerides even in the presence of glucose (Nye *et al*, 2008). It is important to mention that glucose is generally considered the main substrate for serine and glycine *de novo* synthesis (Maddocks *et al*, 2013; Locasale *et al*, 2011). However, it is interesting that Maddocks *et al.* detected formation of unlabeled serine in HCT116 cells grown in the presence of fully labeled glucose and in the absence of exogenous serine and glycine (Maddocks *et al*, 2013). This points to implication of other pathway in serine synthesis, which might be PEPCK-M dependent.

All in all, PEPCK-M under glucose deprivation drive carbons from glutamine into glycolytic intermediates above PEP and support synthesis of intracellular serine to the levels that might be necessary to support growth and survival.

PEPCK-M dependent succinate labeling pattern

Analysis of isotopomer distribution from fully labeled glutamine into TCA cycle intermediates revealed that succinate labeling pattern was inversely correlated with PEPCK-M expression. This was observed in both, glucose abundant and glucose deprived conditions, with more profound effects under glucose deprivation. Moreover, the

concentration of succinate is copying the same behavior and we found increased concentration of succinate in MCF7 cells with knocked-down PEPCK-M. Production of succinate is commonly the result of oxidative metabolism of glutamine (Fan *et al*, 2013; Meiser *et al*, 2016a) or conversion of fumarate to succinate by reverse reaction of SDH (Chouchani *et al*, 2014) or by reduction of fumarate through NADH-fumarate reductase (Tomitsuka *et al*, 2009). Barely detectable m+3 succinate which only source is m+3 fumarate suggest absence of reverse carbon flow from fumarate to succinate. Therefore, labeled succinate originates only from oxidative metabolism of glutamine. Accumulation of m+4 succinate is often ascribed to impaired SDH enzyme (Lussey-Lepoutre *et al*, 2015). In our cells this reaction seems to be unaffected as fumarate labeling was not impaired. Moreover, SDH expression upon PEPCK-M silencing or overexpression was unchanged. This supports the fact that succinate labeling is not affected by changes in SDH reaction. Labeling pattern of succinate highly differ from other related intermediates. This led us to speculate that other pathways originating from glutamine might participate in succinate formation, for example the GABA shunt pathway. GABA is well known as the inhibitory neurotransmitter in mammalian brain, yet its presence was found also in various types of cancers (Azuma *et al*, 2003; Mazurkiewicz *et al*, 1999).

GABA conversion to succinate is processed through two reactions catalyzed by GABA-T and SSADH enzyme. However, mRNA expression of these enzymes was not increased in PEPCK-M silenced MCF7 cells.

GABA pathway can be inhibited by aminooxyacetic acid that is used to inhibit GABA-T enzyme (Löscher & Hörstermann, 1994). However, this inhibitor is not specific and is often used also to inhibit various aminotransferases, like GOT and AST (Montal *et al*, 2015; LaMonte *et al*, 2013). Therefore, significant impact of aminooxyacetic acid on growth of PEPCK-M deficient cells might be caused by unselected targets. Moreover, a recent study showed that inhibition of aminotransferases by aminooxyacetic acid leads to depletion of various amino acids, and can induce ER stress (Korangath *et al*, 2015; Qing *et al*, 2012), causing inhibition of breast cancer cells growth (Korangath *et al*, 2015). This would be a straightforward explanation for the observed PEPCK-M dependent growth response to aminooxyacetic acid as we know that PEPCK-M is important for the activation

of a survival pathway under ER stress (Méndez-Lucas *et al*, 2014).

Besides significant changes in carbon distribution from glutamine to succinate, we observed that the proportion of unlabeled succinate is higher when compared with other TCA cycle intermediates. Unlabeled succinate can be supplemented by catabolism of branched chained amino acids (BCAAs) (Meiser *et al*, 2016b). Interestingly, BCAAs belong to the group of most consumed amino acids in high glucose media. Therefore we would hypothesize that they participate in the production of the high unlabeled pool of succinate. Concentration of succinate was higher in PEPCK-M knocked-down cells and lower in cells overexpressing PEPCK-M. However, consumption of BCAAs was not significantly different upon silencing or overexpression and therefore we assume that consumption of BCAAs is not responsible for the differences in succinate concentrations. Pattern of different succinate concentrations were maintained also under glucose exhaustion. Moreover, glucose exhaustion caused overall increase in succinate concentration.

The connection between the succinate pathway and PEPCK-M is also supported by the observation that loss of SDH enzyme activity causes accumulation of succinate and leads to *PCK2* overexpression (Lussey-Lepoutre *et al*, 2015). More experiments are necessary to understand the exact mechanism of how PEPCK-M affect succinate concentration and synthesis from glutamine.

Proline metabolism is stimulated by PEPCK-M

Our data suggest that PEPCK-M in neuronal progenitors affects the capacity of these cells to form laminin, part of the extracellular matrix microenvironment. Extracellular matrix (ECM) is similarly forming the microenvironment of tumors. Extracellular matrix is composed of different molecules, including proteins, glycoproteins, polysaccharides and proteo-glycans, and form a niche with specific biochemical and physical properties (Lu *et al*, 2012). Additionally, signaling molecules and growth factor are also present in ECM that support tumor growth. All this point to essential role of ECM microenvironment for cancer evolution and spread (Balkwill *et al*, 2012). Production of ECM is mostly assigned to cancer associated fibroblasts (Sounni & Noel, 2013), however it has been shown that

breast cancer cells can also take part in its production (Xiong *et al*, 2014; Lü *et al*, 2014). Synthesis of ECM require active machinery of protein synthesis, polysaccharide synthesis and glycosylation. Based on the results obtained in neuronal progenitors, we believe that PEPCK-M might be necessary to support the synthesis of ECM molecules. Obviously, this role might be more needful in cells grown under glucose deprivation, where PEPCK-M is the only connection between the TCA cycle and glycolytic intermediates. This connection is essential for the synthesis of some amino acids (e.g. serine and glycine) and glycosylation. However, PEPCK-M could also affect the synthesis of other amino acids through its effect on the TCA cycle.

One of the amino acids that is richly present in ECM, more specifically in collagen, is proline (Phang *et al*, 2015). Proline is a non-essential amino acid that is not routinely supplied in DMEM medium. Therefore cells needs to synthetize it.

Several studies provide evidence of the importance of proline biosynthesis for cancer growth (Liu *et al*, 2015; Kardos *et al*, 2015). Moreover, increased synthesis of proline was activated by c-MYC (Liu *et al*, 2012b).

MCF7 cells grown in high glucose media showed active synthesis of proline as we detected its secretion into media. Interestingly, proline secretion was significantly increased in MCF7 cell with overexpressed PEPCK-M. Increased secretion of proline correlates with higher expression of PYCR enzyme that converts pyrroline-5-carboxylate to proline. This indicates that PEPCK-M is supporting biosynthesis of proline. It is interesting to mention, that increased proline secretion was associated with higher invasiveness of ovarian cancer cells (Yang *et al*, 2014b). Besides participation of proline in protein synthesis, recently Liu at al. suggested that proline cycling, instead of synthesis, supports cell growth. This cycling between proline and pyrroline-5-carboxylate support recycling of NAD(P)H to $NAD(P)^+$. Moreover, the conversion of glutamate to pyrroline-5-carboxylate also oxidizes NADPH to $NADP^+$ (Liu *et al*, 2015).

The capacity of MCF7 cells with increased PEPCK-M expression to synthetize more proline was confirmed also by analysis of intracellular levels of proline. More significant differences were observed under glucose exhaustion. In these conditions we also observed significantly lower proline concentration upon PEPCK-M silencing.

Proline levels in cells treated in high glucose media and in glucose exhaustion media show significant differences. As the cells are routinely grown in high glucose media we can assume that the concentration observed in high glucose conditions is the starting concentration of proline in cells treated in glucose exhaustion media. Therefore we assume that a drop of proline concentration in control and silenced cells is mostly caused by proline consumption. On the other hand, MCF7 cells with overexpressed PEPCK-M show no differences in proline concentration in high glucose and glucose exhaustion media.

Proline consumption upon glucose withdrawal in PEPCK-M silenced and control cells under glucose deprivation might feed the TCA cycle or the ornithine cycle (Phang *et al*, 2012) to support their functionality.

Analysis of enzymes implicated in synthesis and degradation of proline showed higher expression of POX, an enzyme involved in catabolism of proline, in MCF7 silenced cells that showed lower proline concentration. This behavior was observed both in high glucose and glucose deprivation conditions. This might point to increased proline turnover or consumption in these cells.

It is well-known that during the conversion of proline into pyrroline-5-carboxylate by POX, ROS is produced by donating electrons to FAD. Increased POX expression might be related to the observed mitochondrial ROS increase in MCF7 cells with silenced PEPCK-M. Besides proline, other metabolites are often related to ROS production, for example changes in succinate levels. Macrophages that accumulate succinate to a greater extent are shown to produce more ROS (Mills *et al*, 2016). Similarly, Chouchani *et al*. also shows that high succinate levels are linked to ROS production (Chouchani *et al*, 2014). However, studies connecting ROS and succinate levels are showing much higher changes of succinate levels (Chouchani *et al*, 2014) than those observed in our studies.

The presence of increased ROS correlates with overexpression of ROS scavenging enzyme SOD2 and induction of p21 expression. The activation of p21 expression under oxidative stress has been observed (El Alami *et al*, 2014; Qiu *et al*, 1996) in accordance with our observations. Activation of p21 is also related to growth arrest (Abbas & Dutta, 2009) which correlates with shown growth in PEPCK-M silenced MCF7 cells, although an effect

on cell cycle could not be demonstrated.

We have shown the importance of PEPCK-M in ensuring metabolic flexibility in biosynthetic processes relevant to cancer and neuronal progenitor cells. PEPCK-M role in these pathways is also supported by coexpression enrichment analysis (Figure D-2). Analysis of breast cancer cells and stem cells showed that *PCK2* enzyme coexpressor genes are involved in amino acid synthesis pathways (e.g. proline, serine and glycine), glycosylation, once carbon metabolism, etc.
Additionally, the top KEGG pathway enrichment of genes that most significantly coexpress with *PCK2* linked them to five pathways that were present in both, cancer and stem cells, suggesting that *PCK2* might participate in processes that metabolically support both these two systems (Figure D-2).

All in all, our work described mechanisms for metabolic flexibility in undifferentiated and cancer cells that are dependent on PEPCK-M activity and shall grant further investigation of its role in cancer biology, and support development of new therapeutic strategies that further validates this enzyme as a target in this pathology. This information will serve as set point for continuing our studies on PEPCK and related pathways in our laboratory.

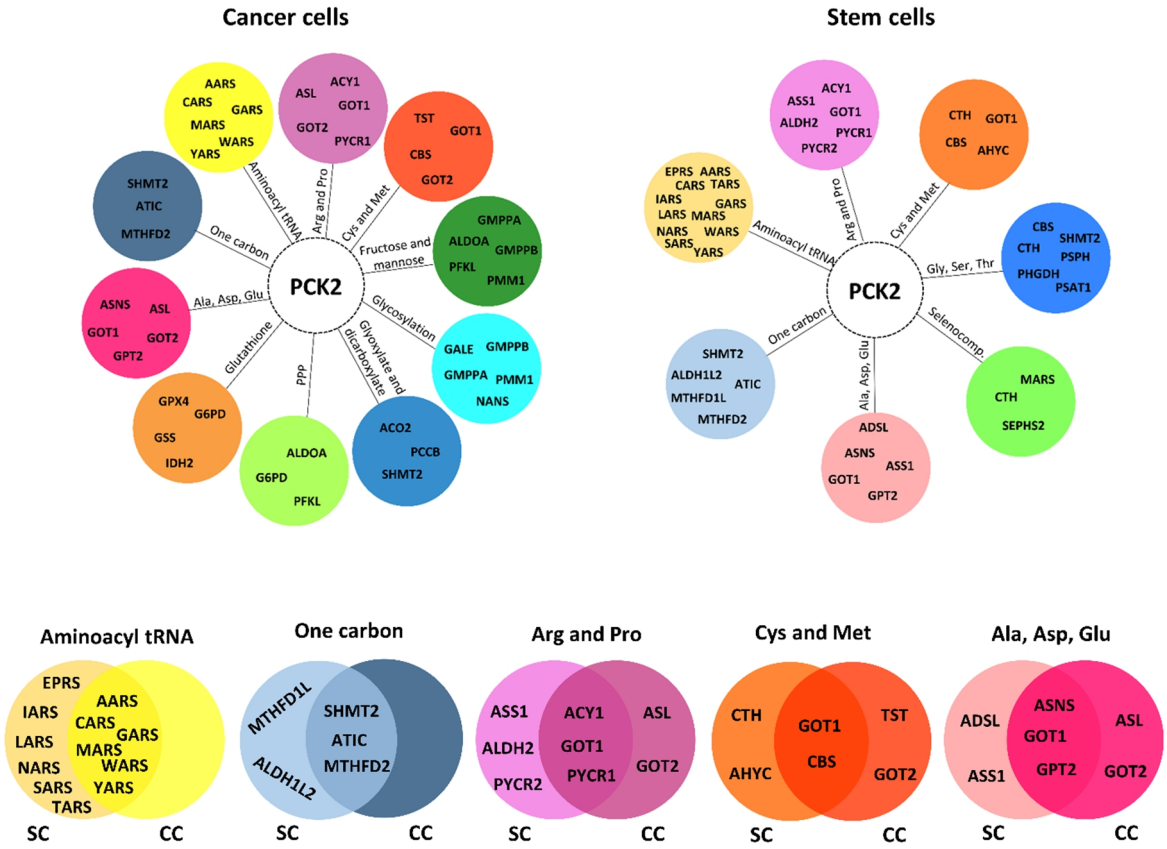

Figure D-2: Coexpression enrichment analysis. *PCK2* coexpression in human breast cancer and stem cells datasets was analyzed using SEEK, a query-based search engine developed by the Department of Computer Science of Princeton University (http://seek.princeton.edu; Zhu *et al*, 2015)**.** We analyzed top 200 genes and coexpressed genes were organized by KEGG pathway functional database. Significant results with minimal p value 1.11E-02 were included. Following metabolic pathways were included: Aminoacyl tRNA biosynthesis, Alanine aspartate and glutamate metabolism (Ala, Asp, Glu), Fructose and mannose metabolism, Amino sugar and nucleotide sugar metabolism (Glycosylation), Arginine and proline metabolism (Arg and Pro), Cysteine and methionine metabolism (Cys and Met), One carbon pool by folate (One carbon), Glyoxylate and dicarboxylate metabolism, Glutathione metabolism, Pentose phosphate pathway (PPP), Glycine serine and threonine metabolism (Gly, Ser, Thr) and Selenocompound metabolism (selenocomp.). Five pathways common to SC (stem cells) and CC (cancer cells) are visualized by Venn diagram and common coexpressed genes with *PCK2* are placed within the intersection.

CONCLUSIONS

- TBR2 positive neuronal progenitor maintenance and growth is promoted by L-lactate in primary neuronal cultures and developing brain.
- Differentiation state of neuronal progenitors is dependent on lactate metabolism; signaling of lactate through the GPR81 receptor is not sufficient to reprogram cell fate of primary neuronal cultures.
- Mitochondrial PEPCK activity is essential for preservation of neuronal progenitors and their anabolic requirements in L-lactate fed primary neuronal cultures and developing brain.
- Mitochondrial PEPCK is preferentially expressed in less differentiated cells and cancer cells.
- Higher levels of PEPCK-M expression are associated with worsen prognosis (relapse free survival) in breast cancer patients.
- PEPCK-M silencing impacts cell growth, but not apoptosis, in well-fed cancer cells cultured in 2D, and reduces colony formation in anchorage-independent conditions.
- Under glucose abundance, no apparent changes in anaplerosis from glutamine are found in PEPCK-M silenced MCF7 cells.
- Increase in fully labeled TCA cycle intermediate pools from uniformly labeled glutamine in well-fed MCF7 cells with silenced PEPCK-M suggests reduced label dilution.
- PEPCK-M overexpression metabolically supports *de novo* synthesis of fatty acids in well-fed MCF7 cells.
- Cellular content of proline correlates with PEPCK-M expression levels suggesting the implication of PEPCK-M in proline metabolism under glucose abundant and glucose exhaustion conditions, where the effect was more pronounced.
- Total and fully labeled succinate pools are inversely proportional to PEPCK-M expression levels in a manner that does not mimic other TCA cycle intermediates, suggesting PEPCK-M effects on alternative pathways contributing to, or originating from, succinate.
- Higher proportion of fully labeled TCA cycle intermediates from [U-^{13}C] glutamine points to elevated glutamine influx into the TCA cycle in MCF7 cells under glucose

deprivation.

- MCF7 cells produce pyruvate from glutamine derived intermediates to support TCA cycling under glucose deprivation. Similar enrichment of pyruvate amongst MCF7 lines suggests implication of malic enzyme rather than PEPCK-M in this pathway.
- Carbon labeling at serine and glycine originating from [U-^{13}C] glutamine is directly dependent on PEPCK-M activity; therefore PEPCK-M cataplerosis supports glycolysis branched pathway of serine and glycine synthesis under glucose deprivation.

Materials and methods

1 Cell culture

1.1 MCF7, HCT116, NIH 3T3-KRas G12V

Cell lines used throughout were of different origin. MCF7 is a human breast adenocarcinoma cell line expressing estrogen receptor. MCF7 cells possess luminal epithelial phenotype and are characterized as a low invasive cancer cell line. HCT116 have origin in human colon carcinoma and has epithelial morphology. NIH-3T3-KRas G12V (3T3-KRas) is a mouse embryonic fibroblast cell line carrying a knock-in mutation at codon 12 of KRAS gene, which causes expression of a mutant oncogene KRAS.

Cells were maintained at 37°C in humidified atmosphere with 5% CO_2 in complete DMEM medium (Biological Industries, # 01-055-1A) with following composition: 25 mM glucose, 2mM Gln, 10ml/l Pen-strep solution (penicillin G sodium salt 10,000 units/mL, streptomycin sulfate 10 mg/l) (P/S) and 10% fetal calf serum (FCS) (all purchased from Biological Industries). Cells were passed every 2-3 days.

Cell lines were purchased from ATCC, except for 3T3-KRas cells that were a kind gift from Dr. Francesc Viñals, IDIBELL.

During experiments, cells were treated with DMEM (Biological Industries, #01-055-1A, #01-057-1A) with and MEM (Biological Industries, #01-025-1A) media with different concentration of glucose (0 mM, 1 mM and 25 mM). MEM medium with 0 mM glucose is not commercially available and therefore was prepared in the laboratory using the same composition, except glucose, as commercially obtained MEM medium (Biological Industries, #01-025-1A).

1.2 Stable MCF7 and HCT116 cell lines

Principle: Lentiviral vectors are able to infect non-dividing cell and have a tendency to integrate into high transcription level sites. Lentivirus is an RNA virus. After infection of the cell, RNA is transcribed into DNA and inserted into the genome. In this stage, the

virus is called provirus. Provirus is stable and is passed to progeny. For safety reasons, lentiviral vectors are not able to replicate and produce new viral particles.

Silencing

Silencing of PCK2 in MCF7 and HCT116 cell lines was completed with GIPZ™ Leniviral shRNA (Thermo Scientific, # V3LMM_427490 and V3LHS_328126, denominated sh1-PCK2 and sh2-PCK2, respectively). In the case of HCT116 a mixture of both lentiviral particles was used and silenced cell line was denominated sh-PCK2.

As a negative control, a GIPZ™ non-silencing lentiviral shRNA (Thermo Scientific, #RHS-4348) was used. Negative control was denominated shCtrl. ⓘ *Product GIPZ™ Lentiviral shRNA is now commercialized by GE Healthcare under the same catalog numbers.*

Transduction was preformed following the protocol supplied by the manufacturer. GIPZ™ Lentiviral shRNA vectors contain puromycin resistance gene which was used for selection of infected cells. MCF7 cells were treated for 1 week with 1 μg/ml of puromycin (Gibco, #A11138-03) and HCT116 cell line for 1 week with 2 μg/ml. Puromycin was refreshed every second day. GIPZ™ Lentiviral shRNA vectors contain gene for turboGFP and degree of transduction was confirmed by fluorescent microscopy.

Overexpression

For overexpression of PCK2, a PCK2 Human ORFeome lentiviral particles (GeneCopoeia, # LP-OL06695-LX304-0200-S) were used. PCK2 Human ORFeome lentiviral were denominated L-PCK2.

Transduction was performed in the same manner as transduction of GIPZ™ Lentiviral particles. Only MCF7 cell line was transduced with PCK2 Human ORFeome lentiviral particles.

Lentiviral vector contains blasticidin resistance gene. Selection of transduced cells was completed by treating MCF7 cells with 2μg/ml of blasticidin (Sigma-Aldrich, #15205) for 1 week. ⓘ *PCK2 ORFeome lentiviral particles do not contain GFP gene.*

1.3 Neuronal primary cultures

Neurons were obtained from E15-E16 mice neocortex. Mouse (Swiss OF1, pregnant day 15-16) was sacrificed by cervical dislocation. The uterus was removed and pups were decapitated immediately and heads were placed in cold PBS containing 0.6% glucose and 0.3% BSA (filtered with 0.22 μm filter). Following protocol was used to dissect cortices:

- Remove the skin and skull using scissors and a pair of fine tweezers and place dissected brain into a Petri dish containing PBS with 0.6% glucose and 0.3% BSA in PBS (filtered with 0.22 μm filter) on ice.
- Remove midbrain, olfactory bulbs and hippocampus) and collect individual cortices in the solution of 0.6% glucose and 0.3% BSA in PBS (filtered with 0.22 μm filter) on ice. ⓘ *Do not perform dissection longer than one hour to avoid death of the neurons.*
- Place cortices gently into 6 cm culture plate containing warm trypsin-EDTA and DNase I (1:1000) and incubate 10 min at 37°C and 5% CO_2. ⓘ *To avoid degradation of DNase I, it should be added prior to use.*
- Disrupt the cortices mechanically by pipetting up and down first with 1000 μl tip and after with 200 μl tip.
- Centrifuge the suspension for 5 min at 400 g and resuspend the pellet in 2 ml of Neurobasal™ (Gibco, #21103049) media supplemented with 5% normal horse serum (NHS), 10 ml/l P/S, 0.5 mM Gln, 5.8 μl/ml $NaHCO_3$ and 2% B27® (Gibco).
- Pre-plated dissociated cells in a 10-cm culture dish for 30 min at 37°C in Neurobasal™ medium supplemented with 5% normal horse serum (NHS), 10 ml/l P/S, 0.5 mM Gln, 5.8 μl/ml $NaHCO_3$ and 2% B27® (Gibco). ⓘ *This helps to obtain enriched neuronal cultures as the glial cells get attached and floating neuronal cells can be recovered from the supernatant.*
- Recover neurons from floating supernatant and pass them through the 100 μm strainer. Wash the strainer with few ml of media to collect remaining cells.
- Centrifuge collected suspension with cells for 5 min at 200 g. Resuspended the pellet with neurons in Neurobasal™ medium with following supplementation: 1%

NHS, 10 ml/l P/S, 0.5 mM Gln, 22 µM glutamic acid, 2% B27® (Gibco) and 5.8 µl/ml $NaHCO_3$ and following concentrations of glucose and lactate: 25 mM glucose (glucose medium) or with 25 mM glucose and 4 mM lactic acid (glucose + lactate medium), or Neurobasal®-A Medium (Gibco, #05-0128DJ) with 4mM lactic acid only (glucose-free lactate medium). L-lactic acid was purchased from Sigma-Aldrich (#27714).

- After 24h change the medium and replace it with the same but serum-free medium without glutamate.

Cultures were incubated for 4 more days. In some experiments, lactate or glucose medium was replaced after 5 days *in vitro* (5div) with glucose or lactate medium for 1h (short incubation) or 2 days (long incubation).

All media were equilibrated in incubator for 1 h prior to use. Supplements used in media were purchased from Sigma-Aldrich unless mentioned otherwise. ⓘ *Plates for neuronal cultures require special treatment with Poly-D-lysine for 30 min at 37°C. It is recommended to treat the plates a day before primary cultures are processed. After poly-lysination, plates are washed 3 times with sterile mQ water and air-dried.*

2 Animals

2.1 Tumor xenograft model

For *in vivo* studies of tumor growth, 6 week old nude mice were used (Harlan). As xenografts, stable cell lines of MCF7 (sh1-PCK2 and shCtrl) and HCT116 (sh-PCK2 and shCtrl) were used. Mice were housed in pathogen free animal facility and all procedures were done in sterile conditions.

All animal housing and procedures were approved by the Institutional Animal Care and Use Committee of our institution in accordance with Spanish and EU regulations.

HCT116 xenografts

Cell suspension preparation: HCT116 cells grown in flasks were treated with trypsin and collected. Cells were washed and suspended in PBS at concentration $20x10^6$ cells/ml and stored on ice until injected.

Injection: Cells were injected subcutaneously into the left and right dorsal flank of nude male mice. Prior to injection, skin was sterilized with iodine and alcohol. Skin was lifted and 100 µl ($2x10^6$ cells) of cell suspension was injected with insulin syringe. ⓘ *Successful injection can be confirmed by checking the swelling of the skin.*

Tumor measurement: Growth of tumors was detected by palpation. The size of tumors was regularly measured by using calipers. The longest and shortest diameter was measured and the following formula was used to calculate tumor volume: $V=(length+width^2)/2$.

MCF7 xenografts

Estradiol pellets insertion: 24h prior to implantation of MCF7 cells, nude female mice were supplemented with 17β estradiol pellets (1.7 mg/pellet, 90-day release, Innovative research of America). Pellets were inserted subcutaneously to mice anesthetized with isoflurane. Skin on the back side of the neck was sterilized with iodine and alcohol and 0.5 mm incision was made in the skin. 1 cm beyond incision side a pocket was made using tweezers. Estradiol pellets were than inserted into these pockets. The wound was

closed using surgical staple, which were removed after wound healing.

Cell suspension preparation: MCF7 cells grown in flasks were treated with trypsin and collected. Cells were washed with DMEM media without FCS and suspended in the same media at concentration $100x10^6$ cells/ml. Cells were stored on ice until implanted.

Implantation: The orthotopic implantation was made surgically to fourth mammary fat pad. Nude female mice were anesthetized with isoflurane and their abdomen was sterilized with iodine and alcohol. Two lateral incisions were made in the skin between the fourth nipple and the midline. The mammary fat pad was exposed. ⓘ *Mammary fat pad has white color and is easy to be observed*.

Prior to injection, 100 µl of cell suspension ($10x10^6$ cells/ml) were mixed with matrigel matrix and injected into the fat pad using an insulin syringe. ⓘ *Successful injection can be confirmed by checking the swelling of the fat pad.* The wounds were closed using surgical staple. After surgery, analgesic Buprenorphine (0.05 mg/kg) was administrated by subcutaneous injection. After wound healing, surgical staples were removed.

Tumor measurement: Growth of tumors was detected by palpation. The size of tumors was regularly measured by using calipers. The longest and shortest diameter was measured and following formula was used to calculate tumor volume: $V=(length+width^2)/2$.

Samples preparation

At the end of the experiment, mice were sacrificed by CO_2 asphyxiation. Tumor tissue was dissected measured and weighted. The parts of the tumor intended for RNA and protein extraction were cut into small pieces and frozen in cryo-tubes immediately in LN_2. Tumor pieces for IF were embedded in OCT (Sakura) and frozen. Freezing of tissue was made in isopropanol placed in a metal beaker on dry ice. Cryo-molds with embedded tissue were placed in isopropanol and frozen ⓘ *OCT change color from transparent to white, when frozen.* Cryo-molds with frozen tissues were stored at -80°C until sectioned in cryostat. Tumors intended for IHC staining were first fixed O/N in 4% PFA for subsequent paraffin embedding and sectioning

2.2 Intraventricular brain injections in postnatal animals

For *in vivo* studies of neuronal progenitors, Swiss OF1 mice were used. All animal housing and procedures were approved by the Institutional Animal Care and Use Committee of our institution in accordance with Spanish and EU regulations.

Newborn mice (postnatal day 0, P0) were injected in the lateral ventricle of brain with 2 µL of lactic acid (5 mM, Sigma-Aldrich), MCT1/2 inhibitor AR-C155858 (100 nM, Adooq, # A11293), 3-mercaptopicolinic acid (100 µM, Toronto Research Chemicals), or vehicle (mQ H_2O). Injection was performed with glass micropipette adapted to a Hamilton syringe. This procedure is minimally invasive and there was no associated mortality.

Mice were sacrificed at postnatal day 3 (P3) by administration of anesthetic overdose followed by a transcardial perfusion with 4% paraformaldehyde (PFA) in 0.1 M phosphate buffer, pH 7.3. Brain tissue was dissected and meninges were removed. The following protocol was used to prepare gelatin blocks for IHC section preparation:

- Insert dissected brain into 50 ml tube containing 4% PFA (the volume should be 40 times or more of the tissue volume) and incubate 6h at RT or 12h at 4°C.
- Postfix brains for 8–12 h in cryopreservative solution (30% sucrose solution in PBS) at 4°C.
- Prepare embedding gelatin solution containing 8% gelatin and 15% sucrose in PBS. And keep it at 37°C. ⓘ *This solution has to be warmed in order to melt gelatin but should not be brought to a boil.*
- Add embedding gelatin solution to culture dish and place various pieces of brain tissue so it will be completely covered with the solution. Store culture dished with embedded tissues at 4°C.
- Once solidified, cut gelatin block of each piece of brain tissue and freeze by using LN_2. Store at -80°C until sectioned in cryostat.

Coronal sections of 40 µm thickness were collected in a cryoprotective solution and stored at −30°C.

3 Growth and cell death

3.1 MTT assay

Principle: MTT assay detects viability of cells through the activity of dehydrogenase enzymes. Yellow solution of MTT (3-(4, 5-dimethylthiazolyl-2)-2, 5-diphenyltetrazolium bromide) is reduced by metabolically active cells to purple formazan crystals, that can be solubilized in isopropanol.

Protocol: For MTT assay, cells were plated in 12 wells plates at a density of $0.05x10^6$ cells/well. Cells were than treated and analyzed at different time points. MTT 10x stock solution (5mg/ml, Sigma, #M2128) was prepared in DMEM media w/o phenol red. ⓘ *Stock solution can be stored at -20°C for up to 3 months.*

The following procedure was used:

- Aspirate media and add 500 µl of MTT 1x working solution (0.5mg/ml) diluted in DMEM media without phenol red supplemented with 25 mM glucose, 2mM Gln and 10% FCS.
- Incubate cells at 37°C with 5% CO_2 in the dark for 2-4 hours and observe formation of purple crystals.
- At the end of the assay aspirate media and add 500-1000 µl of isopropanol (depending on the confluence of the cells) to solubilize formazan.
- Acidic isopropanol (40 mM HCl in absolute Isopropanol) might be used when working with media containing phenol red to avoid interference of phenol red in absorbance reading. ⓘ *If floating cells containing crystals are present in the well, they should be centrifuged and used in the assay.*
- Transfer 200 µl of the liquid to 96 well plate in triplicates and read absorbance at 570nm with background subtraction at 650 nm.

Values of *a*ll time points were divided by corresponding value of 0h time point to normalize for the number of seeded cells.

3.2 Crystal violet assay

Principle: Crystal violet is a triarylmethane dye that binds in a non-specific manner to protein and DNA in cells. Captured dye can be solubilized by 2% SDS and measured spectrophotometrically.

Protocol: For CV assay, cells were plated in 12 wells plate at density $0.05x10^6$ cells/well. Cells were than treated and analyzed at different time points. Working solution of CV was prepared as solution of 0.2% CV (Sigma, #C-3886) in 2% ethanol. ⓘ *CV solution can be reutilized for several times, until it loose viscous appearance or until it contains debris.*

The following procedure was used:

- Aspirate media and add 400 µl of CV.
- Incubate cells at 37°C for 30 min.
- Recollect CV and wash plates 3x in tap water by immersion in a large beaker. Change the tap water between washes.
- Let the plates dry upside down. Add 1-2 ml of 2% SDS solution to each well (depending on the confluence of the cells) and agitate plates approximately 1h at RT until color is uniform. ⓘ *All plates can be analyzed at the end of the experiment. Although if plates are analyzed the same day as they were stained, crystal violet is easier to dissolve.*
- Transfer 200 µl of the liquid to 96 well plate in triplicates and read absorbance at 570nm.

Values of all time points were divided by the corresponding value of 0h time point to normalize for the number of seeded cells.

3.3 Soft agar colony formation assay

Principle: Cells are seeded in semi-solid agarose over a denser agar layer, which blocks cells to adhere to culture plate surface. Only cells able of anchorage-independent growth are able to grow in these conditions. Soft agar colony formation assay is commonly used to evaluate anchorage-independent growth ability of cells, which is one of the hallmarks of transformation (Borowicz *et al*, 2014; Horibata *et al*, 2015).

Protocol: 6-well plates were covered with 0.5% agar layer, prepared by dilution of agar in PBS. Agar solution was warmed up in a microwave until melted. 1 ml of agar solution was used to cover each well in six well plate. ⓘ *Add agar solution to plates while hot. To pipette hot solution use serological pipettes as they resist to high temperature.*

Seeding of the cell in the upper layer was done as described in the following protocol:

- Prepare 0.7% solution of agarose (Ecogen, #AG0120) in PBS by melting it in a microwave. Make aliquots of 500 µl in tubes and keep them in dry bath incubator at 37°C.
- Treat cells with trypsin and resuspend them in DMEM media (supplemented with 25 mM glucose, 20% FCS, 4 mM Gln and 20 ml/l P/S) at concentration $0.01x10^6$ cells/ml. Make 500 µl aliquots of cell suspension and keep them in dry bath incubator at 37°C.
- Mix 500 µl of agarose with 500 µl of cell suspension, pipette up and down and transfer to well of 6 well plate. ⓘ *Work quickly to avoid gelation before transferring to plate.*
- Let incubate 30 min and add 500 µl of complete media to each well.
- Let the cells grow for 2-3 weeks in incubator at 37°C and 5% CO_2 until colonies are formed. Change media every 3-4 days.

3.4 Annexin V/7AAD apoptosis assay

Principle: Annexin V belongs to group of calcium-dependent phospholipid-binding proteins. Annexin V binds preferentially to phosphatidylserine, which is exposed in outer plasma membrane, when cell undergo apoptosis. Annexin V is fluorescently labeled and therefore can be analyzed by measuring emitted light. Fluorescent viability dyes (e.g. 7-ADD, propidium iodide) are used in assay to help distinguish between early and late apoptosis. In the late stage of apoptosis, the cell membrane loses integrity and viability dye can enter the cell and bind to DNA.

Protocol: Annexin V Apoptosis Detection Kit APC (eBioscience, # 88-8007) in combination with 7-ADD were used to analyze apoptosis. Stained cells were analyzed by

flow cytometry. Analyzed cells were grown in 12 well plates and at the moment of analysis were at 60-75% of confluency. As a positive control we used cells treated O/N with 1 μM saturosporine. ⓘ *It is important to have good controls for flow cytometry settings adjustment. For general settings, apoptotic and live cells, both stained with combination of dyes (Annexin V only, Annexin V + 7-ADD, 7-ADD only and no stain), were used. Usage of GFP positive cell line requires also control of cells that do not express GFP.*

The following procedure was used:

- Collect media from wells to tubes to recollect dead floating cells.
- Wash wells with 1 ml PBS and add it to the corresponding tubes.
- Trypsinize cells with 250 μl of trypsin. After that, stop reaction with adding 500 μl of media and collect cells to corresponding tubes.
- Spin cells 5 min at 500 g and discard supernatant.
- Add 500 μl of binding buffer (BB, provided in the kit) to each sample and spin 5 min at 500 g. Discard the supernatant.
- Add 105 μl of Annexin V diluted in BB (100 μl of BB + 5 μl of Annexin V) to the samples and 100 μl of BB to the samples for controls without Annexin V staining. Incubate in dark for 15 min.
- Add 500 μl of BB to samples and spin 5 min at 500 g.
- Discard the supernatant and resuspend cells in 200 μl of BB.
- Add 105 μl of 7-ADD solution diluted in BB (100 μl of BB + 5 μl of 7-ADD) to corresponding samples and 100 μl of BB to the samples for control without 7-ADD staining.
- Excitation/emission (nm):7AAD = 546/647, APC = 650/660.

Samples were analyze by flow cytometry with FACSCanto™.

4 Protein and RNA analysis

4.1 Western blot

Protein extraction of cancer cells and tissues for western blot was done with RIPA buffer (Table M&M-1) containing the following protease inhibitors: PMSF (1 mM), Benzamidine (1 mM), Aprotinin (1 µg/ml), Leupeptin (1 µg/ml) and Pepstatin (1 µg/ml). Extracts were cleared from debris by centrifugation for 10 min at 15000 g at 4°C.

Protein extraction of neuronal cultures was done with modified RIPA buffer (Table M&M-2). Samples were incubated on orbital shaker for 20 min at 4°C and sonicated and in this case extracts were not centrifuged.

Protein concentration in samples was determined by commercial Pierce™ BCA protein assay kit (Thermo Scientific, #23225) using protocol specified by provider. Samples were diluted to required concentration, mixed with loading buffer () and boiled for 10 min at 95°C.

RIPA BUFFER	Final concentration	To prepare 200 ml
Tris/HCl pH 7.4	50 mM	10 ml (1 M)
NaCl	100 mM	6.67 ml (3 M)
Triton™ X-100	1%	2 ml
Na_3VO_4	1 mM	36.78 mg
NaF	50 mM	42 mg
EDTA	5 mM	2 ml (0.5 M)
Beta glycerophosphate	40 mM	1.73 g

Table M&M-1: Composition of RIPA buffer for protein extraction from cells and tissues.

Modified RIPA buffer	Final concentration	To prepare 10 ml
Tris/HCl pH 7.4	100 mM	1 ml (1 M)
NaCl	100 mM	334 µl (3 M)
NP-40 (add as the first)	1%	100 µl
NaF	50 mM	2.1 mg
Na_3VO_4	1 mM	1.84 mg
Triton™ X-100	1%	100 µl
SDS	0.1%	50 µl (20%)
Beta glycerophosphate	10 mM	0.43 g
cOmplete™ (Roche, #11836170001)	1x	1.43 ml (7x)
PMSF	1mM	17.42 g

Table M&M-2: Composition of modified RIPA buffer for protein extraction from neuronal cultures.

LOADING BUFFER (4x)	Final concentration (4x)	To prepare 10 ml
Glycerol	40%	4 ml (100%)
Tris/HCl pH 6.8	240 mM	2.4 ml (1 M)
SDS	8%	0.8 g
Bromophenol blue	0.04%	4 mg
Beta-mercaptoethanol	5%	0.5 ml

Table M&M-3: Loading buffer for western blot sample preparation.

Western blot was performed as mentioned elsewhere (Mahmood & Yang, 2012). Briefly, proteins were separated on SDS-polyacrylamide gel prepared at desired concentration (8-15%). Standardly, 25-30 µg of protein were loaded per lane. Electrophoresis was performed at constant voltage (120 V) in Towbin buffer (25 mM tris, 192 mM glycine, pH 8.3) with 0.1% SDS. Transfer to PVDF membrane (pore size 0.2 µm) was performed using two different methods. First, tank (wet) transfer, an older method that was long time used in our laboratory. This transfer method was made using Towbin buffer (25 mM tris, 192 mM glycine, pH 8.3) with 10% methanol at constant voltage (200 mA/gel) for 2h at 4°C.

Second, semi-dry transfer, which was established in our laboratory as a new and more efficient method to transfer proteins. The transfer time was reduced to 30 min by using discontinuous buffer system (Table M&M-4), where different buffers were used for cathode and anode side of transfer stack. Transfer was performed in Trans-Blot® Turbo™ semi-dry transfer cell with program Standard SD (30 min, 25 V, 1 A).

CATHODE BUFFER	Final concentration	To prepare 500 ml
6-aminocaproic acid	40 mM	2.6 g
Methanol	20 %	100 ml

ANODE BUFFER	Final concentration	To prepare 500 ml
Tris base	0.3 M	18.16 g
Methanol	20 %	100 ml

Table M&M-4: Discontinuous buffer system for semi-dry transfer by using Trans-Blot® Turbo™ semi-dry transfer system. Adjust volume to 500 ml with distilled water.

After blotting, membranes were blocked 1h at RT with 5% non-fat powdered milk resuspended in TBS-T 0.05%. Thereafter, incubation with primary antibodies (Table M&M-5) was performed O/N at 4˚C followed by washes and incubation with horseradish peroxidase conjugated secondary antibody for one hour at RT. Bands were visualized with EZ-ECL developing kit (Biological Industries, #20-500-500) and images were captured with CCD camera (Fujifilm LAS 3000). Relative expression of proteins was quantified by densitometry analysis using Fuji Film Multi Gauge software. γ-tubulin and β-actin were used as a loading control in western blots of cancer cells. Total actin and AKT were used as loading controls for neurons.

ANTIBODY against	Size (KDa)	Host	Dilution	Reference
SIR2	110	Rb	1:1000	Upstate, #07-31
Phospho-AKT (Ser473)	60	Rb	1:1000	Cell Signaling, #9271
ATF4 (C-20)	40/50	Rb	1:500	Santa Cruz, #sc-200
AKT	60	Gt	1:1000	Santa Cruz, #sc-1618
ACC	257 & 280	Rb	1:1000	Upstate, #07-439
PhosphoDetect PDH-E1α (Ser293)	44	Rb	1:1000	Calbiochem, # AP1062
Phospho-S6 (Ser235/236)	32	Rb	1:1000	Cell Signaling, #2211
HIF1a	110-120	Rb	1:1000	gift from the lab of Edurne Berra
SOX2	34	Rb	1:500	Abcam, #ab97959
TBR2	85	Rb	1:1000 (1:500)	Abcam, #ab23345
MCT2	40	Gt	1:500	Santa Cruz, #sc-14926
TUJ1	50-55	Ms	1:10 000 1:5000	Covance, #MMS-4359
Nestin	198-260	Ms	1:500 (1:200)	BD Pharmingen, #556309
Laminin	>200	Rb	1:500 1:250	Sigma, #L9393
SDH	70	Ms	1:1000	Invitrogen, #459200
GFAP	55	Rb	1:3000	Dako, #20334
PSD95	85	Rb	1:1000	Abcam, #18258
PAX6	47	Rb	1:500	Lsz Life Science, #CSB-PA017492DSR2HU
VDAC	32	Rb	1:1000	Cell Signaling, #4866
phospho-AMPK	62	Rb	1:1000	Cell Signaling, #25351
GPR81	40	Gt	1:500	Abcam, #ab106942
V5-tag	-	Ms	1:5000	Invitrogen, #46-0705
p53	53	Ms	1:1000	Abcam, #ab26
p21 (C-19)	21	Rb	1:1000	Santa Cruz, #sc-397

Table M&M-5: list of antibodies used in western blot, IHC and IF. Continue on the next page.

PEPCK-C	*71*	*Sp*	*1:1000*	*gift from the lab of Granner*
PEPCK-M	71	Rb	1:1000 (1:500)	Abcam, #ab70359
Phospho-ACC	280	Rb	1:1000	Cell Signaling, #3661
SOD2	25	Rb	1:2000	Abcam, #13534
γ-tubulin	48	Ms	1:10 000	Sigma, #T-6557
β-actin	46	Ms	1:1000	Santa Cruz, #sc-69879
caspase-3	17,34	Rb	1:500 (1:100)	Santa Cruz, #sc-98785
total actin	45	Gt	1:2 000	Santa Cruz, #sc-1616
anti-sheep	secondary	Rb	1:5000	Dako, #P0163
anti-mouse	secondary	Gt	1:20 000	Sigma, #A9917
anti-rabbit	secondary	Gt	1:10 000	Sigma, #A0545
anti-goat	secondary	Dk	1:5000	Santa Cruz, #sc-2056
anti-goat	secondary	Dk	1:5000	Santa Cruz, #sc-2056

Table M&M-5: List of antibodies used in western blot, IHC and IF. Primary antibodies for western blot were diluted in 5% BSA in TBS-T. Secondary antibodies for western blot were diluted in 5% non-fat milk TBS-T 0.05%. Dilution mentioned in parenthesis are for IF or IHC if it differed from that for western blot. Rb – rabbit, Gt – goat, Ms – mouse, Sp – sheep, Dk – donkey,

4.2 Immunohistochemistry

Immunohistochemistry (IHC) technique was used to analyze tissues obtained from *in vivo* xenograft experiments and combined cancer and normal tissue microarray panel BCN962 (US Biomax). Microarray panel BCN962 contains 17 types of common organs and 48 types of tumors with their matched or unmatched non-neoplastic tissue with single core per case.

The following protocol of IHC was used. Protocol is divided into 3 parts: deparaffinization and rehydratation, antigen retrieval and immunohistochemical staining by itself.

Deparaffinization and rehydration

- Place the slides in a rack and perform following washes:
- Xylene 4x10 min
- 100% ethanol 3x5 min

- 96% ethanol 3x5 min
- 70% ethanol 1x5 min
- Distilled water 1x5 min

Antigen retrieval

Antigen retrieval serves to reveal epitopes masked during sample processing.

- Fill press cooker with sodium citrate buffer (10 mM sodium citrate, pH 6).
- Insert slides in plastic rack and place them in press cooker. The slides has to be completely submerged. ⓘ *Avoid using the glass rack as it can be broken by high temperature reached in the press cooker.*
- Secure the pressure cooker and place it on hot plate.
- Wait 3 minutes after the pressure cooker reach full pressure and then remove cooker from hot plate and place it in a sink.
- De-pressure the cooker by running cold water on it and open it carefully. Let the samples to cool down in sodium citrate buffer (10mM sodium citrate, pH 6) for 20 min.
- Wash the slides 5 min in distilled water.

Immunohistochemical staining

- Deactivate endogenous peroxidases by submerging slides in 6% H_2O_2 for 15 min.
- Wash slides 5 min in distilled water.
- Wash slides 10 min in PBS-Triton™ X-100 0.1%.
- Incubate samples with blocking solution (20% goat serum in PBS) for 1h at RT in humid chamber.
- Incubate samples placed in humid chamber with primary Ab diluted in PBS O/N at 4°C. ⓘ *Use 70-100 µl of primary Ab solution/slide. Cover slides with parafilm to avoid drying.*
- Next day, temper samples at RT for 30 min.
- Wash slides 3x10 min in PBS-Triton™ X-100 0.1%.
- Incubate samples with secondary Ab (EnVision, Dako) diluted in PBS for 30 min

at RT and cover with parafilm.

- Wash slides 3x10 min in PBS-Triton™ X-100 0.1%.
- Develop the signal with Liquid DAB+ Substrate Chromogen System (Dako, #K3468) following the protocol supplied by manufacturer.
- Wash the slides 1x3 min with tap water.
- Counterstain samples with hematoxylin for 1-5 min and rinse in tap water.
- Dehydrate samples by passing them through solutions of alcohol and xylene. Incubate samples for 5 min in each solutions following this order: 3x70 % ethanol, 3x96 % ethanol, 3x100% ethanol and 2x xylene and finally 2x10 min in xylene.
- Mount samples with cover slip using DPX mountant. Let slides to dry in laminar flow hood.

Fluorescent preparations were visualized and images were captured with Nikon Eclipse 800 light microscope (Nikon, Tokyo, Japan).

4.3 Immunofluorescence

Free floating sections of brain (obtained as described on page 189), primary cultures of neurons and MCF7 cancer cell line were analyzed with immunofluorescence (IF). Cells analyzed by IF were seeded on coverslips (Ø15 mm) covered with poly-L-lysine at density $0.1x10^6$ cells/well. Poly-L-lysine coating is enhancing attachment of cells to glass surface of coverslip. In the case of neurons, coating was performed with poly-D-lysine as mentioned at the protocol of Neuronal primary cultures. The following protocol, divided in 3 parts was used for IF technique.

Staining of the free floating sections of brain tissue require only third part of the protocol (Immunofluorescent staining) and require a special treatment. In the case of free floating section staining, 0.025% triton™ X-100 was used instead of 0.1% triton™ X-100 in all solutions. Staining of samples was carried out in small open-ended plexiglass cylinders with nylon mesh bottoms that fit 12 well culture plate. Manipulation of sections was performed very carefully by using paint brush with natural bristles. Samples were maintained during all steps on shaker at slow speed.

Poly-L-lysine and coating

- Place coverslips (Ø15 mm) in 12 well plate and cover them with sterile solution of poly-L-lysine (Sigma). Incubate them for 1h at RT. ⓘ *Poly-L-lysine can be reused several times.*
- Rinse coverslips 3 times with sterile mQ H_2O and let them dry O/N in a laminar flow hood.
- Sterilize coverslips under UV light before seeding cells.

Fixation

- At the end of the experiment wash cells twice with warm PBS.
- Add 4% paraformaldehyde prepared in PBS and fix cells for 15 min at RT.
- Wash cells twice with cold PBS. ⓘ *At this point, cells can be stored for several weeks in PBS with 0.2% sodium azide at 4°C.*

Immunofluorescent staining

- Wash samples three times for 10 min with PBS.
- Wash samples twice for 10 min with blocking buffer (PBS, 1% NHS and 0.1% Triton™ X-100). ⓘ *Triton will permeabilize cells.*
- Block samples 2h at RT in blocking buffer.
- Incubate samples with primary antibody (Table M&M-5) diluted in blocking buffer (200-500 µl/well) O/N at 4°C in humid chamber. ⓘ *When working with cells, it is convenient to place out coverslips from 12 well plate on a parafilm placed in a humid chamber. In this case only 60 µl of primary Ab are used per coverslip. Thanks to the hydrophobic nature of parafilm there will not occur spill of primary antibody and drying out of sample.*
- Temper samples at RT for 30 min and wash them with blocking buffer three times for 10 min.
- Incubate samples with fluorescent secondary antibody and nuclear marker diluted in blocking buffer for 2h at RT in the dark. ⓘ *Secondary antibodies and nuclear markers with desired fluorescence were purchased from Thermo Fisher Scientific.*

- Wash samples three times for 10 min with blocking buffer in the dark.
- Wash samples twice for 10 min with PBS in the dark.
- Mount samples with mounting media: Mowiol® 4-88 (Sigma, #81381) or Fluoroshield™ (Sigma, #F6182). In case of free floating sections, mount samples with Mowiol on slides covered with gelatin.

Fluorescent preparations were visualized and images were captured with either a Leica TCS-SL Spectral confocal microscope (Leica Microsystems, Mannheim, Germany) or a Nikon Eclipse 800 light microscope (Nikon, Tokyo, Japan). Morphometric and quantitative analyses were performed using ImageJ software (National Institutes of Health, USA).

4.4 RNA extraction and RT-qPCR

Principle: RT-qPCR stands for reverse transcription and quantitative PCR. A combination of these techniques was used to analyze gene expression. The starting material analyzed is mRNA. mRNA is transcribed to cDNA by reverse transcription. The cDNA is used as template for qPCR and amplified. In each cycle exponentially increasing fluorescence is measured and threshold cycle (CT) is determined. CT is intersection between threshold line and amplification curve.

RNA extraction and reverse transcription

RNA of cell and tissue samples was extracted by using commercially available reagents Ultraspec 10500 (Biotecx, #BL-10050) and TRIsure™ (Bioline, #BIO-38032). In both cases, the protocol given by manufacturer was followed. Majority of RNA extractions was done by using TRIsure™. Use of Ultraspec reagent was discontinued because of quality problems.

After elution of extracted RNA in DEPC water (20 µl), concentration of RNA in samples was measured using Nanodrop spectrophotometer (Thermo Scientific). High-Capacity cDNA Reverse Transcription Kit (Applied Biosystems, #4368813) was used to reversely transcribe mRNA to cDNA. The protocol of manufacturer was followed. 100 ng/µl of RNA

were used in reaction of reverse transcription.

Real-time PCR (qPCR)

Routinely qPCR reaction was performed in MicroAmp® optical 384 well reaction plates (Applied Biosystems, #4309849) using SensiFAST™ Hi-ROX Kit (Bioline, #BIO-82005). Reaction was made at final volume 11 µl and following protocol was used:

- Mix 0.5 µl of cDNA with 4.5 µl of DEPC H_2O per well (multiply by number of wells you need and distribute using automatic pipette to wells). ⓘ *Count with 3-4 extra wells in calculation, because of dead volume of pipette.*
- Mix 0.5 µl probe (Applied Biosystems) and 5.5 µl of SensiFAST per well (multiply by number of wells you need and distribute using automatic pipette to wells). ⓘ *Count with 3-4 extra wells in calculation, because of dead volume of pipette. Do distribution of mixture in subdued lighting, as probes and SensiFAST are susceptible to light.*

Conditions of qPCR reaction were set up as described in protocol supplied by manufacturer. CT values were analyzed using SDS v2.2 software (Applied Biosystems). Threshold was set up automatically.

5 Fluorescent staining

5.1 Mitochondrial staining

MitoTracker® Red CMXRos (further mentioned as MitoTracker, Molecular probes, #M7512) was used as a probe for labeling of active mitochondria. MitoTracker stains mitochondria of live cells and is well retained during the fixation and permeabilization (Poot *et al*, 1996). Therefore it can be used together with subsequent IF staining (page 200) for colocalization of proteins and mitochondria.

Principle: MitoTracker is derivate of a red-fluorescent X-rosamine and passively diffuse across the plasma membrane and accumulate in active mitochondria. Its accumulation is dependent upon its membrane potential. MitoTracker contains a chloromethyl moiety, which reacts with thiols on proteins and peptides and an aldehyde-fixable conjugate is formed (Presley *et al*, 2003).

Protocol: MitoTracker stock solution was prepared at concentration 1 mM in DMSO and it was stored at -20°C protected from light. Cells were seeded on coverslips (Ø15 mm) covered with poly-L-lysine, or poly-D-lysine in case of neurons. When stained, cells were at confluency 50-60%. Cells were stained prior to fixation and the following protocol was used:

- Aspirate media and cover cells with working solution of MitoTracker (0.25 μM MitoTracker in media w/o FCS).
- Incubate cells for 30 min at 37°C protected from light.
- Wash cells three times with PBS and fix them with 4% PFA for 10 min at RT. ⓘ *If samples are not processed immediately, they can be stored O/N in PBS with 0.02% sodium azide.*
- At this step, cells can be permeabilized and processed by immunofluorescent staining as mentioned in the protocol on page 200.
- Mount the coverslips with mounting media: Mowiol® 4-88 (Sigma, #81381) or Fluoroshield™ (Sigma, #F6182) and let to dry.
- Excitation/emission (nm) = 579/599

Fluorescent preparations were visualized and images were captured with Leica TCS-SL Spectral confocal microscope (Leica Microsystems, Mannheim, Germany).

5.2 MitoSOX™ Red mitochondrial superoxide indicator

MitoSOX™ Red mitochondrial superoxide indicator (further mentioned as MitoSOX, Molecular probes, #M36008) was used to measure the production of superoxide in mitochondria. Stained cells were analyzed with flow cytometry.

Principle: MitoSOX is a derivate of dihydroethidium. It is live-cell permeant and is electrophoretically driven to actively respiring mitochondria due to the cationic triphenylphosphonium substituent (TPP). TPP cations target molecules to mitochondria. The movement of TPP is facilitated by lipophilic phenyl groups that surround the positive charge, which is accumulated into the mitochondrial matrix in response to the negative membrane potential (Ross *et al*, 2005). Oxidation of MitoSOX in mitochondria by superoxide leads to hydroxylation and 2-hydroxyethidium derivate is formed. This derivate exhibits a fluorescence excitation peak that is absent in the excitation spectrum of MitoSOX oxidized by other ROS (Zielonka *et al*, 2008). Oxidized MitoSOX becomes highly fluorescent after binding to nucleic acids.

Protocol: The stock solution of MitoSOX was prepared at concentration 5 mM in DMSO and stored at -20°C. Cells were seeded in 12 well plates. When stained, cells were at confluency 50-80%. As a positive control, cells were treated with 100 μM Antimycin A (inhibitor of electron transfer at complex III that induces ROS production, Sigma, #A8674) for 30 min prior to staining. As a negative control, cells were treated with 5 mM N-acetyl cysteine (NAC, Sigma, #A9165) for 30 min prior to staining. The following procedure is adapted from the protocol published by Li *et al.* (Li *et al*, 2011):

- Aspirate media and cover cells with working solution of MitoSOX. Working solution is prepared at concentration 5 μM in HBSS/Ca/Mg.
- Incubate cells for 15 min at 37°C protected from light.
- Wash cells three times with HBSS/Ca/Mg.
- Treat cells with 250 μl of trypsin for 3 min at 37°C.

- Add corresponding media (the same composition as they were grown in) w/o phenol red to cells, transfer them to tubes and centrifuge 5 min at 300 g.
- Resuspend cells in corresponding media w/o phenol red.
- Analyze samples immediately by flow cytometry. Excitation/emission (nm) = 510/580 ⓘ *At the end of the measurement of all the samples, it is good to repeat measurement of first two samples. It will tell us if the processing time affected fluorescence. We saw that 30 min does not affect the levels of MitoSOX fluorescence intensity.*

Samples were analyze by flow cytometry with Gallios™ flow cytometer. Alternatively, samples can be analyzed by microscopy. In this case, cells are seeded at on coverslips. After staining cells are fixed with 2% PFA for 10 min at RT, washed three times with PBS and mounted with Fluoroshield™ (Sigma, #F6182).

5.3 CellROX® Green

CellROX® green reagent (further mentioned as CellROX, Molecular probes, #C10444) was used to measure ROS in live cells. Stained cells were analyzed by microscopy.

Principle: The cell-permeable reagent CellROX is in its reduced state weakly fluorescent. ROS are able to oxidize CellROX which is in its oxidized state binding to DNA and exhibit bright green fluorescence. Therefore, signal is localized mainly in the nucleus and mitochondria.

Protocol: Concentration of the stock solution of CellROX is 2.5 mM and is stored at -20°C. Evaluation of ROS with CellROX was used for neuron cells. Cells were seeded on coverslips (Ø15 mm) covered with poly-D-lysine and grown in desired conditions.

The following procedure for ROS detection was used:

- Add CellROX to cells to obtain final concentration 5 µM.
- Incubate cells for 30 min at 37°C protected from light.
- Remove medium and wash cells three times with PBS.
- Fix cells with 4% paraformaldehyde 10 min at RT and wash three times with PBS.
- Mount coverslips with Fluoroshield™ (Sigma, #F6182) and let to dry.

- Image samples the same day as stained.
- Excitation/emission (nm) = 510/580

Fluorescent preparations were visualized and images were captured with Leica TCS-SL Spectral confocal microscope (Leica Microsystems, Mannheim, Germany). Morphometric and quantitative analyses were performed using ImageJ software (National Institutes of Health, USA).

5.4 Cell cycle analysis

Cell cycle analysis was made by using BD Pharmingen™ BrdU Flow Kit (BD biosciences, #552598). Analysis of the TCA cycle was made through analysis of 7AAD (7-aminoactinomycin D) staining as the BrdU staining was not working properly in our cell line.

Principle: 7AAD is fluorescent dye that stains DNA. During the cell cycle, DNA is duplicated and based on the changes in amount different phases of cycle can be identified. Cells in S phase will have proportionally more DNA and in G2 phase they will reach approximately double intensity of fluorescent staining.

Protocol: Cells were seeded in 6 cm culture dish at 15-20% in DMEM media with 25 mM glucose, 10% FCS and 2 mM Gln. Cells were recollected next day at exponential phase of the growth. The protocol of manufacturer was followed (BD biosciences, #552598). Samples were analyzed by flow cytometry using FACSCanto™. Excitation/emission (nm) of 7AAD = 546/647. Analysis of cell cycle was made by using ModFit LT V3.3.11 software.

6 Metabolite assays

For metabolite assays two different types of samples were used. Glucose and lactate concentrations were measured in media. Media samples were collected at different time points and stored at – 80°C until analyzed. Cell extracts to measure intracellular metabolites were prepared by perchloric acid, boiling water, methanol/water and methanol/chloroform extraction as mentioned in the chapter Metabolite extraction on page 216. Extracts were stored at -80°C until analyzed.

6.1 Glucose colorimetric determination assay

Principle: Colorimetric determination of glucose concentration is based upon two coupled enzymatic reactions and is utilizing o-dianisidine (ODD) as a colorimetric substrate. First, glucose oxidase catalyzes oxidation of glucose to gluconic acid and H_2O_2. Second reaction is catalyzed by peroxidase, which transfer 2 e^- from H_2O_2 to ODD, which in its oxidized state change color from colorless to brown. The intensity of brown color is proportional to glucose concentration.

Protocol: Peroxidase and glucose oxidase are commercially available as PGO enzymes (Sigma, #P7119) in capsules. Each capsule contains 500 units of glucose oxidase and 100 units of peroxidase. PGO solution was prepared by dissolving 1 capsule in 100ml of H_2O. ODD solution was prepared by dissolving 25 mg of ODD (Sigma) in 10 ml of H_2O. ⓘ *PGO enzyme solution can be stored up to 6 months at -20°C. ODD solution is stable at 2-8°C for 1 week. Both solutions are sensitive to light.*

The range of glucose standard (Sigma, #G6918) is 0 – 1 mg/ml, where reaction get saturated after 0.5 mg/ml point. Therefore, it is necessary to dilute samples depending on expected concentration.

The following procedure was used:

- In 96 well plate mix 15 µl of diluted media/standard with 200 µl of reaction mix. Reaction mix is obtained by adding 1.6 ml of ODD to 100ml of PGO enzyme solution.
- Incubate the plate at 37°C for 30 min.

- Read the absorbance at 450 nm.
- Calculate glucose concentration in samples using standard curve.

Absorbance was measured using a Tecan Sunrise™ Microplate Reader.
To calculate amount of consumed glucose we subtracted concentrations obtained at final time point from the value obtained by measuring original concentration in the medium. Protein concentration or CV were used to normalize the concentration of consumed glucose in samples.

6.2 Lactate assay

Principle: Concentration of lactate was determined using enzymatic reaction, which is catalyzed by lactate dehydrogenase (LDH). LDH converts NAD^+ and lactate to pyruvate and NADH. To keep the reaction in this direction, NAD^+ is added in excess. NADH exhibits strong light absorption around 340 nm. The amount of produced NADH is proportional to lactate concentration in the sample.
Protocol: Fluorescence or absorbance can be used to measure NADH. This depends on the concentration of lactate in the sample. Fluorescence is recommended to detect concentrations below 0.5 mM. Black 96 well plates with clear bottom were used if fluorescence is measured.
Reaction mix is composed of buffer (0.3 M hydrazin sulfate and 0.87 M glycine with pH 9.5) with added 2.5 M NAD (Sigma, #10127981001) and 0.19 M EDTA (pH 8.5).
Following procedure was used:

- In 96 well plate mix 10 µl of media/standard and 200 µl of reaction mix.
- Measure absorbance at 360 nm or fluorescence with excitation at 360 nm and emission at 460 – time T0 to detect the basal concentration of NADH.
- Add 25 µl of working solution of LDH (Roche, #10127876001). Working solution of LDH is prepared at final concentration 344 units/ml in 0.5x buffer.
- Incubate plate 20 min at RT.
- Measure the absorbance at 360 nm or fluorescence with excitation at 360 nm and emission at 460 – time T1.

- By subtraction of T0 from T1 calculate final absorbance of NADH produced in the reaction.
- Calculate lactate concentration in samples using standard curve.

To calculate the amount of produced lactate, we subtracted the original concentrations of lactate in medium from the value obtained by measuring lactate concentration in medium after culturing with cells.
Protein concentration or CV were used to normalize lactate concentration in samples.

6.3 Phosphoenolpyruvate assay

Principle: Phosphoenolpyruvate (PEP) assay is based on three coupling enzymatic reactions. In the first reaction of assay, PEP and ADP are converted to pyruvate and ATP. This reaction is catalyzed by pyruvate kinase enzyme (PK). Generated ATP is then used in the next reaction to form glucose-6-phosphate (glucose-6P) from glucose. This reaction is catalyzed by hexokinase (HK). Last reaction is catalyzed by glucose-6-phosphate dehydrogenase (G-6-PDH). In this reaction, glucose-6-P and NADP are converted to 6-phospho-gluconolacton (6-P-gluconolacton) and NADPH. NADPH exhibits strong light absorption around 340 nm. Amount of produced NADPH is proportional to amount of PEP in sample.
Protocol: Cells extracts for PEP assay were prepared by using perchloric acid as described on page 216. As the expected concentration of PEP in cell extracts is very low, we used at least $8x10^6$ cells per reaction. Fluorescence measurement is more sensitive and more suitable to detect small amounts of produced NADPH. Therefore we measured fluorescence and black 96 well plates with clear bottom were used.

Composition of reaction mix per one well is:

Compound (stock concentration)	volume (µl) sample	volume (µl) standard curve
Glycilglycine (0,4 M, pH 7,0)	25	25
KCl (2 M)	10	10
$MgCl_2$ (0,2 M)	5	5
Glucose (0,1 M)	4	4
MgADP (20 mM)	10	10
NADP (40 mM)	10	10
mQ H_20	6	96
Sample	100	-
PEP (std. curve)	-	10
G-6-PDH (18,2 U/ml), Boehringer Ingelheim #127043	10	10
HK (26,6 U/ml), Roche #1426362	10	10
PK (13,5 U/ml), Roche #10128155001	10	10

Table M&M-6: Reaction composition for PEP assay (per well). Final volume in one well is 200 µl.

The following procedure was used:

- Add samples/PEP standard to 96 well plate. Mix rest of the compounds of reaction mix except of enzymes and add it to wells.
- Mix HK and G-6-PDH enzymes together and add them to each well. Incubate plate 5 min at RT. Provide first measurement at 360 nm (T0), where is detected NADPH which is generated from intermediates presented in samples.
- After that, add PK and incubate plate for 15-20 min at RT. Measure fluorescence at 360 nm (T1).
- Final amount of produced NADPH is obtained by subtraction of T0 from T1.
- Calculate PEP concentration in samples based on standard curve, which range is 0 - 5 mM.

Protein concentration or CV were used to normalize PEP concentration in samples.

6.4 ATP bioluminescence assay

Principle: The amount of ATP in samples was detected by luciferin-luciferase-ATP depended reaction. In this reaction ATP is consumed and light is emitted when luciferase catalyzes the oxidation of luciferin. Emitted light is measured using a luminometer.

Protocol: Samples for ATP assay were prepared by boiling water extraction method described on page 217. Highly stable luciferin-luciferase reagent (rLucHS, Biovision, #K790-1000) was used. rLucHS is light sensitive and it is recommended to perform all steps of assay in subdued lighting. Additionally, rLucHS is very sensitive and is important to avoid contamination with exogenous sources of ATP (bacteria, fingerprints etc.).

The following procedure was used:

- Mix 80 µM of mQ H_2O with 10 µl of reconstituted rLucHS in an eppendorf tube. In case you measure very low levels of ATP, measure first background luminescence, before adding the sample.
- Add 10 µl of sample/standard to tube, mix and read total luminescence.
- Subtract background luminescence from total and calculate levels of ATP in samples based on the standard curve.

Luminescence was measured using TD 20/20 luminometer (Turner designs). Protein concentration was used to normalize ATP concentration in samples.

7 High-resolution respirometry.

Principle: Oxygen, as a gas dissolved in aqueous medium, can be measured by specific sensors. In the case of Oxygraph-2K, a polarographic oxygen sensor (Clark electrode) is used. Polarographic oxygen sensor is isolated from the chamber containing media by a membrane permeable to O2. Therefore, O2 can reach the cathode where it is reduced and this reduction allows a flow of current. The potential difference is recorded.

Protocol: The consumption was measured using a high-resolution Oxygraph respirometer (Oroboros, Innsbruck, Austria). MCF7 cells grown in high glucose DMEM medium were washed once with PBS and detached from the culture plate by using HyQTase (GE Healthcare, #SV30030.01). The respiration was assessed in the same solution. First, solution was equilibrated with air at 37°C and stirred at 750 rpm until a stable signal was obtained for calibration at air saturation. The cells were added to chambers that were closed. Temperature and stirring were maintained. Basal respiration levels were measured after reaching steady-state (routine respiration), which was completed within 10 min and values were acquired using computer-driven data acquisition system (Datlab; Oroboros). Values of basal respiration were normalized by cell number.

8 PEPCK activity

Principle: To asses PEPCK activity, the PEPCK reaction is coupled with malate dehydrogenase (MDH) reaction. MDH oxidizes malate to oxaloacetate and NADH is formed. After reaching the equilibrium of MDH reaction, PEPCK reaction is initiated by adding GTP to the reaction mix. PEPCK starts to consume oxaloacetate and therefore disturbs the established equilibrium of the MDH reaction. To counter this effect, MDH produces more oxaloacetate from malate by reducing NAD^+, resulting in the formation of NADH. NADH exhibits strong light absorption around 340 nm. Amount of produced NADH is proportional to PEPCK activity.

Protocol: To obtain sufficient amount of cell extract for PEPCK activity measurement, cells were grown in 150 cm^2 tissue culture dishes. The protocol is divided in two separate parts: the preparation of homogenate and the enzymatic reaction.

Homogenate preparation

- Wash the cells with generous amount of PBS (10-15 ml per culture dish) and trypsinize cells by adding 1.5 ml of trypsin.
- Add 20 ml of PBS to trypsin, collect cells in 50 ml tubes and centrifuge at 1200 rpm for 3 minutes at 4°C and discard the supernatant.
- Resuspend pellet in 200 µl of ice-cold homogenization buffer (100 mM HEPES-NaOH pH 7.2, 0.1% triton™ X-100, 2.5 mM DTT) by pipetting up and down. Transfer homogenate to eppendorf tubes and lyse cell suspension by performing 2 freeze (LN_2)/thaw (37°C) cycles. ⓘ *Avoid overheating the homogenates.*
- Clear homogenates by centrifugation at 100.000 g for 1h at 4°C. ⓘ *It is important to well balance eppendorf tubes and adaptors of ultracentrifuge.*
- Measure protein concentration of homogenates using Bradford assay (Bio-Rad protein assay dye reagent, #5000006) as recommended by manufacturer. Calculate how many µl of cell homogenate contain 400 µg of protein.

Enzymatic reaction

- Reactions are carried in cuvettes. For each reaction use 900 µl of reaction buffer

(Table M&M-7), the corresponding volume of sample to obtain 400 µg of protein and fill up to one ml with mQ water.

- Put the cuvette into the spectrophotometer and measure absorbance until it is stable (2-15 minutes).
- Add 10 µl of 20 mM GTP to cuvette to start PEPCK reaction. In the case of controls for the basal absorbance variation (to set the background activity) instead of GTP add 10 µl of water.
- Follow absorbance until it stabilizes. Record the rate of absorbance change (ΔA/min) taking into account only the lineal part of the activity assay. ⓘ *Alternatively you may record the absorbance values at different time points, including time 0.*
- For the calculation of NADH concentration (ΔC/min) use the Lambert-Beer law A=εlc, where A is absorbance at specific wavelength (in our case 340 nm), ε stands for absorption coefficient characteristic of the species at a given frequency (in our case 6200 $M.cm^{-1}$), l is thickness of the sample (in our case 1 cm) and c is the concentration that we need to calculate.

Absorbance was measured using a Beckman Culter DU® 800 spectrophotometer. Results were represented as nmol NADH per min^{-1} per mg $protein^{-1}$.

REACTION BUFFER	final concentration	to prepare 900 µl (for one reaction)
HEPES-NaOH (pH 7.2)	100 mM	100 µL (1 M)
Malate	2.5 mM	10 µl (300 mM)
NAD (Roche, #10127981011)	3 mM	10 µl (300 mM)
MgCl2	2 mM	10 µl (200 mM)
MnCl2	0.1 mM	20 µl (10 mM)
DTT	37 mM	37 µl (1 M)
MDH (Sigma, # M2634)	6 U /mL	≈ 0.5 µl
Water		*712.5 µl*

Table M&M-7: Composition of the reaction buffer for PEPCK activity assay.

9 Metabolite extraction protocols

The objective of metabolite extraction is to dissolve metabolites and to avoid their degradation. Therefore, fast quenching was performed before extraction. Quenching stop all cellular enzymatic activity and prevent the degradation of metabolites. This is essential since metabolite concentrations are very sensitive to any variation in the cell environment (Teng *et al*, 2009; Villas-Bôas *et al*, 2007).

9.1 Perchloric acid extraction

Perchloric acid extraction was used to obtain extracts for PEP assay.

Adherent cells were rinsed with cold PBS and immediately quenched by immersion in liquid nitrogen (LN_2). Cells were stored at -80°C until processed.

The following procedure was used to finish extraction:

- Add 200 – 300 µl of cold 1N $HClO_4$, scrap the cells and transfer them to tube. ⓘ *Keep samples on ice always when possible.*
- Vortex vigorously and spin at 10 000 g and 4˚C for 5 min. Save pellet from this step at -20°C for protein extraction.
- Transfer the supernatant into new tube and neutralize it with 3 M $KHCO_3$. Wait until the neutralization is completed before confirming pH. ⓘ *End of the reaction is indicated by disappearing of CO_2 bubbles, which is one of the neutralization products. Approximately 60 µl of 3 M KHCO3 are necessary to neutralize 300 µl of 1 N HClO4. This is the most critical step of protocol as the volumes are very small to allow pH measurement with pH meter. pH can be checked by dropping 1 µl of extract on pH strips, however this method is less accurate.*
- Spin the extracts at 10 000 g, 4˚C for 2 min to separate precipitate of KClO4.
- Transfer the supernatant into new tube and store at -80˚C.

Pellet obtained after first centrifugation was used for protein extraction and normalization. ⓘ *Proteins were extracted with 0.1 M NaOH and quantified by using Bradford assay (Bio-Rad protein assay dye reagent, #5000006) as recommended by manufacturer.*

9.2 Boiling water extraction

Extraction with boiling water was described as suitable for routine assay of cellular ATP (Yang *et al*, 2002; Hiller *et al*, 2007). Cells were quenched and lysed at the same time with boiling water. Cells were cultured in 12 wells plates before analysis.

The following procedure was used:

- Aspirate medium and wash cells twice with PBS. Suspend cells in boiling water (500 µl/well) by repeated pipetting. ⓘ *Pipettes with plastic tips lose accuracy, when hot water is used. Therefore, glass Pasteur pipettes with mark of 500 µl were used to add boiling water.*
- Transfer the extracts to tubes, vortex them vigorously and spin at 12 000 g and 4°C for 5 min.
- Transfer supernatants to new tubes and store at -80°C until used.

Pellets were used for protein normalization. ⓘ *Proteins were extracted with RIPA buffer and quantified with BCA protein assay kit (Thermo Scientific, #23223).*

9.3 Methanol/water extraction

Methanol (MeOH) based solutions are recommended for the extraction of polar metabolites (Dettmer *et al*, 2011). Aqueous solution of MeOH (MeOH (80%)/H_2O (20%)) is suitable for combined harvesting and extraction in eukaryotic cells (Bennett *et al*, 2008; Fan *et al*, 2013). This method was used to extract OA and AA for enrichment studies and concentration determination by mass spectrometry. Adherent cells growing in 6 well plates were rinsed three times with cold PBS. 200 µl of mQ H_2O was added and cells were immediately quenched by immersion in LN_2. When concentration of metabolites was analyzed, internal standards for AA and OA were added to cells before freezing them in LN_2. Cells were stored at -80°C until processed.

The following procedure was used to finish the extraction:

- Add 800 µl of 100% MeOH to each well, scrap the cell and transfer them to eppendorf tubes. ⓘ *Two wells of 6 well plate were joined for enrichment studies.*
- Vortex cell extracts vigorously for 3 minutes and spin them at 14 000 g and 4°C

for 10 min.

- Divide supernatant into two glass vial tubes for AA analysis (40%) and for OA analysis (60%).
- Dry supernatants under air flow at RT and store them at -80°C until further utilization.

Pellets obtained after centrifugation were used for protein extraction and normalization.

ⓘ *Proteins were extracted with SDS sample buffer (Tris-HCl (50 mM, pH 6.8), SDS (2%), glycerol (10%), β-mercaptoethanol (1%), EDTA (12.5 mM)) and quantified with BCA protein assay kit (Thermo Scientific, #23223).*

9.4 Methanol/chloroform extraction

MeOH (25%)/chloroform (75%) extraction was used for extraction of non-polar metabolites, such as fatty acids (FA). Cells growing in 10 cm culture dish were rinsed three times with cold PBS and cells were immediately quenched by immersion in LN_2 and following extraction protocol was performed:

- Add 1 ml of 100% MeOH to plate and scrape the cells with cell scraper. Transfer the extract to a glass vial. Wash the plate with 1 ml of 100% MeOH and add it to the cell extract.
- Add 6 ml of pure chloroform and keep vortexing for 30 minutes.
- Add 1.2 ml of saline solution (0.9% NaCl in water) and separate phases by centrifugation at 4°C and 1000 rpm for 10 min.
- Transfer chloroform phase containing FA into a 5 ml volumetric flask. Let it stand still for 4h to confirm there is no aqueous phase. If there is any rest of aqueous phase it has to be removed.
- Fill up the samples to 5 ml with pure chloroform and take 200 µl and 400 µl for quantification of FA levels and evaporate the rest of the sample.
- Prior to NMR analysis, samples were reconstituted in pure chloroform with internal standard of pyrazine (4% D_5-pyrazine/ 96% pyrazine, 2 mg/ml).

10 Metabolomics

10.1 Gas and liquid chromatography mass spectrometry (GC/MS; LC/MS)

This technique features gas and liquid chromatography coupled to mass spectrometry. This powerful combination allows separation of sample components, identification of their mass spectra and quantification.

Principle: In all chromatography, separation occurs when the sample mixture is injected into a mobile phase. In GC, the mobile phase is formed by an inert gas and in LC is formed by liquid solvent. In both cases, samples are transported through the column by the flow of mobile phase. The columns contain a stationary phase, which interacts with analyzed samples. This interaction and other factors (e.g. column length, temperature (for GC) and properties of mobile phase) cause that different components exit the column at different time (retention time). After that, sample components enter the mass spectrometer and in case of LC/MS are vaporized. Sample is then ionized in ionization chamber and positive ions are accelerated by ion-accelerating electric field. The beam of ions pass through a magnetic field, which deflect the ions according to their mass (m) and charge (z). Ions are then detected by ion multiplier and abundance and mass spectrum is calculated (mass to charge ratio = m/z). Each compound has near unique mass spectrum and can be therefore identified.

GC/MS

GC/MS was used to analyze the enrichment of amino acids and enrichment and concentration of organic acids. For the enrichment studies, cells were treated with 2 mM [U-^{13}C] glutamine for 4h under different conditions.

Sample preparation and analysis: Cells were extracted as mentioned on page 217 in the protocol of Methanol/water extraction. Metabolites were derivatized prior to analysis to ensure better volatility. GC/MS spectrometry and analysis of the spectra using GC/MS Agilent 5975C were performed by Dr. Xiarong FU in the laboratory of Dr. Shawn Burgess

at University of Texas.

Mass isotopomer distribution was calculated and corrected for natural isotope abundance. The quantification of organic acid was determined by using internal standard that contains U-^{13}C, U-^{2}H labeled citrate, sodium pyruvate, sodium lactate, alpha-ketoglutarate and succinate.

Following protocols of derivatization were used:

OA derivatization (samples for analysis of enrichment and concentration by GC/MS)

- Add 350 µl of 0.8% sulfosalicylic acid, 50 µl of 5 M hydroxylamine hydrochloride (fresh) and 80 µl of 2M KOH to each sample.
- Sonicate for 15min and incubate 1h at 65°C.
- Add 80 µl of 2 M HCl and 220 mg NaCl and mix.
- Add 2 ml of ethyl acetate to each sample and vortex for 1min. Take the upper phase and transfer it to conical vials. Add 2 ml of ethyl acetate to down phase and reextract.
- Let the samples to dry under air flow at RT.
- Add 80 µl of ACN/MTBSTFA (1:1) and incubate 1h at 60°C.
- Transfer samples to eppendorf tubes and fast spin to get rid of salts and precipitates.
- Transfer clear supernatant to vials for mass spec analysis.

AA derivatization (samples for analysis of enrichment by GC/MS)

- Add 100 µl of ACN/MTBSTFA (1:1) to each sample and incubate 40 min at 90°C.
- Transfer samples to eppendorf tubes and fast spin to get rid of salts and precipitates.
- Transfer clear supernatant to vials for mass spec analysis

LC/MS

LC/MS was used to determine the concentration of amino acids. For the calibration, amino acid standard from Sigma was used (#AAS18).

Sample preparation and analysis: Cells were extracted as mentioned on page 217 in the protocol of Methanol/water extraction. Metabolites from media were directly derivatized and we used 50 µl of media/sample. Samples were analyzed by using mass spectrometer API 3200 triple quadrupole LC-MS/MS (Applied Biosystems/Sciex Instruments) by Dr. Xiarong Fu in the laboratory of Dr. Shawn Burgess at University of Texas.

Mass isotopomer distribution was calculated and corrected for natural isotope abundance. The quantification of amino acids was determined by using internal standard from Cambridge Isotope laboratories.

Following protocol of derivatization was used:

AA derivatization (used for analysis of concentration by LC/MS)

- Add 500 µl of 3 M BuOH.HCl to each sample and vortex for 1min.
- Let samples incubate for 15-20 min at 65°C
- Dry sample under air flow (40-50°C) and dissolve it in 50/50 ACN/H_2O + 0.025% formic acid
- Transfer 80 µl to vials for mass spec analysis

10.2 Nuclear magnetic resonance (NMR) spectroscopy

NMR spectroscopy is a technique that allows the determination of the structure of molecules.

Principle: This technique is based on the fact that atomic nuclei with spinning charge generate magnetic field. This allows atoms to behave as a magnet. When external magnetic field is applied, atomic nuclei with magnetic properties are preferentially orientating themselves with the magnetic field. This alignment with the field is called alpha spin state and it is a low energy state. NMR machine emits radio frequency radiation that provides energy to nuclei to move to a beta state (the higher energy position). The NMR machine detects how much energy is given off to flip back from beta

spin state to alpha spin state. This difference of energy (ΔE) is usually given as a frequency and is converted into the peaks. In general ΔE is very small and therefore strong magnetic field needs to be applied. The energy difference between alpha and beta spin state of the same atoms can differ and this is affected by local magnetic field generated by electrons. The peaks from NMR contain various information that is used to identify analyzed compounds.

In our case, we measured fatty acid synthesis. Cells were treated with deuterated water (D_2O) that is incorporated into newly synthetized fatty acids. Using NMR, deuterium enrichment value and deuterium enrichment position can be assessed.

Sample preparation: Cells were seeded in 10 cm culture dish at density $1.5x10^6$ cells per dish. Next day, medium was changed and cells were treated 16h with high glucose media containing 30% D_2O. Samples were extracted with MeOH/chloroform as mentioned on page 218.The samples were later processed and analyzed by Dr. Joao Duarte in the laboratory of Dr. Shawn Burgess by NMR spectroscopy. Spectra were obtained with a Varian Inova 14.1 T spectrometer equipped with a standard 3 mm broadband probe as described in study by Duarte *et al.* (Duarte *et al*, 2014).

11 Statistical analysis

Graphic visualization of the data and statistical analysis was performed using GraphPad Prism 6.0. If not stated otherwise, two-tailed t-test were conducted for data analysis. P value ranking is specified in each figure.

Generally, experiments were repeated at least three times and plotted values are presented as mean ± SEM, unless otherwise mentioned in the figure legend. Metabolomics experiments were performed in triplicate wells per condition (LC-MS and GC-MS) or 6 wells per condition (NMR).

Acknowledgments

During the years of completing this thesis I was lucky to meet in our department lot of great people that made these years unforgettable, full of laugh, discoveries and great conversations. I will not list all names, but my THANKS is dedicated to all of you who I met or I'm still meeting every day at the Department of Physiological Sciences. Thanks to each one of you I learned a lot of important things not only about science, but also life and relations. I think I get a bit spoiled here, because anytime I needed help, advice or antibody:), I knew I could ask anyone and that person wouldn't say no. I think this is quite unique and I'm very thankful I could experience this scientific family ambient.

However, there are several names that need to be mentioned, all 4162 crew and all people that helped me finish this thesis.

First of all, I want to thank to my supervisor Jose Carlos that was always there for me whether it was about science or not. You were a great teacher and science guru to me. Thank you very much for all your help, support and also for all tips for good restaurants!

Many thanks to Jana, you actually made all this experience possible and started Slovakian colonization of the lab. *Ďakujem za spríjemnenie mojich zahraničných začiatkov, za tvoje rady a nadhľad. Tiež vďaka za všetko čo som sa od teba naučila.*

Next, I want to thank to Andy, the biggest PEPCK-M fan I know. You showed me how devoted someone can be to his project, and you taught me a lot about PEPCK-M and science.

Many thanks to Elena. It was great to work with you on the project. I really enjoyed the time we spent together. By the way, do you remember PEPCKale?

Juan, thank you for helping me out whenever I needed it. Wish you good luck with your thesis!

Anna, thank you for all your help with enzymatic activities and glutathione and in general for everything. You were great company and one of the most empathetic persons I get to know.

And few words for the newest lab members, Pablo and Pau. Pablo, thank you for stopping by from time to time in the "biblio" and asking "how are you". Also many thanks for all our daily conversations and for being so supportive.

Pau, you liar, famous culture man with unbelievable memory for scientific papers, thanks for trying to teach me art of respirometry, for making me laugh at least once a day and for your friendship.
Jordi, thank you for all your help.
Also, thanks to all labmates who shared the bench with me: Sandra, Nuria, Rex, Amal, Xevi, Sonia, Guillem and Andrea. It was nice to spent time with you.

Many thanks to people I met in Dallas!
First of all, Shawn Burgess. Thank you for the opportunity to spent time in your laboratory and for opening the world of metabolomics to me. It was amazing experience!
Thank you, Xiarong, for helping me out with all mass spec analyses and for teaching me all the protocols!
Joao, thank you for NMR analyses and thank you for being such a great company in the lab. Also thank you for taking care of my social life during my stay in Dallas :). It was great to meet you and Raquel, which I'm also very thankful!
And also many thanks to Austin and Santosh for all your help and nice moments.

I'm also very grateful to Soledad Alcántara and Zaida. Sole, thank you for the opportunity to work on the project with neuronal progenitors and for all your advices and for your help whenever I needed it.
Zaida, you taught me so many new techniques and it was lovely to work with you. Thank you!

Next, the three musketeers from "serveis" at the third floor. Thank you Esther, Benja and Bea for all your help with flow cytometry, microscopy and real time.

Many thanks to Francesc Viñals and all his group for helping me with *in vivo* studies and IHC. Mainly, I would like to thank to Agnes and Mar.

….

I cannot forget to thank to my scientific soulmates comedoras GORDAS! Beuki, Bettushi and Cristikuki, I think sharing my PhD experience with you was one of the reasons, why I enjoyed it so much. Thanks for being my BCN family (also Edu and Aleix), for great times we had and many more to come! With you science was more fun :). Os quiero! ❤

Also, I would like to thank to cerveza team, Sonia, Taiane, Carol, Helga, José and Ana. It was a great and quite cheap kind of therapy. I had so much fun with you! And Ene! No worries I didn't forget about you. Thanks for your lovely company in the "biblio" and Spetses times!

And as last, I want to thank to my husband Michal, family and friends.
Miško aka Bubik, s tebou je to všetko akosi ľahšie. Ďakujem ti za tvoju podporu a lásku a možnosť byť sama sebou.
A taktiež veľká vďaka mojej veľkej rodine a priateľom, za podporu a lásku.
Najviac vám Mami a Reni! Vďaka, že ste ma sprevádzali na tejto dobrodružnej ceste aj na diaľku, že ste ma vždy podporovali a verili, že to dokážem.

Bibliography

Abbas T & Dutta A (2009) P21 in Cancer: Intricate Networks and Multiple Activities. *Nat. Rev. Cancer* **9:** 400–414

Adeva-Andany M, López-Ojén M, Funcasta-Calderón R, Ameneiros-Rodríguez E, Donapetry-García C, Vila-Altesor M & Rodríguez-Seijas J (2014) Comprehensive review on lactate metabolism in human health. *Mitochondrion* **17:** 76–100

Agathocleous M, Love NK, Randlett O, Harris JJ, Liu J, Murray AJ & Harris WA (2012) Metabolic differentiation in the embryonic retina. *Nat. Cell Biol.* **14:** 859–64

Agostini, Rome, Inoue, Niklison-Chirou, Elia, Dinsdale, Morone, Knight, Mak & Melino (2016) Metabolic reprogramming during neuronal differentiation. *Cell Death Differ.* **23:** 1–13

Ahmed K, Tunaru S, Tang C, Müller M, Gille A, Sassmann A, Hanson J & Offermanns S (2010) An Autocrine Lactate Loop Mediates Insulin-Dependent Inhibition of Lipolysis through GPR81. *Cell Metab.* **11:** 311–319

Aich S & Delbaere LTJ (2007) Phylogenetic study of the evolution of PEP-carboxykinase. *Evol. Bioinform. Online* **3:** 333–40

Akram M (2014) Citric Acid Cycle and Role of its Intermediates in Metabolism. *Cell Biochem. Biophys.* **68:** 475–478

El Alami M, Vina-Almunia J, Gambini J, Mas-Bargues C, Siow RCM, Penarrocha M, Mann GE, Borras C & Vina J (2014) Activation of p38, p21, and NRF-2 mediates decreased proliferation of human dental pulp stem cells cultured under 21% O2. *Stem Cell Reports* **3:** 566–573

Alberts B, Johnson A, Lewis J, Raff M, Roberts K & Walter P (2002) Cancer as a microevolutionary process. In *Molecular Biology of the Cell* pp 1205–1256. Garland Science

Álvarez Z, Hyroššová P, Perales JC & Alcántara S (2014) Neuronal Progenitor Maintenance Requires Lactate Metabolism and PEPCK-M-Directed Cataplerosis. *Cereb. Cortex***:** 1–13

Alvarez Z, Mateos-Timoneda MA, Hyroššová P, Castaño O, Planell JA, Perales JC, Engel E & Alcántara S (2013) The effect of the composition of PLA films and lactate release on glial and neuronal maturation and the maintenance of the neuronal progenitor niche. *Biomaterials* **34:** 2221–2233

Alves R, Chaleil RAG & Sternberg MJE (2002) Evolution of enzymes in metabolism: A network perspective. *J. Mol. Biol.* **320:** 751–770

Amelio I, Cutruzzolá F, Antonov A, Agostini M & Melino G (2014) Serine and glycine metabolism in cancer. *Trends Biochem. Sci.* **39:** 191–198

Andersson A, Ritz C, Lindgren D, Edén P, Lassen C, Heldrup J, Olofsson T, Råde J, Fontes M, Porwit-Macdonald A, Behrendtz M, Höglund M, Johansson B & Fioretos T (2007) Microarray-based classification of a consecutive series of 121 childhood acute leukemias: prediction of leukemic and genetic subtype as well as of minimal residual disease status. *Leukemia* **21:** 1198–203

Arai Y, Pulvers JN, Haffner C, Schilling B, Nüsslein I, Calegari F & Huttner WB (2011) Neural stem and progenitor cells shorten S-phase on commitment to neuron production. *Nat. Commun.* **2:** 154

Azuma H, Inamoto T, Sakamoto T, Kiyama S, Ubai T, Shinohara Y, Maemura K, Tsuji M, Segawa N, Masuda H, Takahara K & Katsuoka Y (2003) γ -Aminobutyric Acid as a Promoting Factor of Cancer Metastasis□ ; Induction of Matrix Metalloproteinase Production Is Potentially Its Underlying Mechanism □ -Aminobutyric Acid as a Promoting Factor of Cancer Metastasis□ ; Induction of Matrix Metalloprotein. *Cancer Res.* **63:** 8090–8096

Balan MD, McLeod MJ, Lotosky WR, Ghaly M & Holyoak T (2015) Inhibition and Allosteric Regulation of Monomeric Phosphoenolpyruvate Carboxykinase by 3-Mercaptopicolinic Acid. *Biochemistry* **54:** 5878–5887

Baldini N, Sonveaux P, De Milito A, Supuran CT, Otto AM, Stock CM, Pedersen SF, Favicchio R & Avnet S (2016) Metabolism and microenvironment in cancer plasticity. *Cancer Metab.* **4:** 1–7

Balkwill FR, Capasso M & Hagemann T (2012) The tumor microenvironment at a glance. *J. Cell Sci.* **125:** 5591–5596

Ballard FJ (1970) Kinetic studies with cytosol and mitochondrial phosphoenolpyruvate carboxykinases. *Biochem. J.* **120:** 809–814

Ballard FJ & Hanson RW (1969) Purification of phosphoenolpyruvate carboxykinase from the cytosol fraction of rat liver and the immunochemical demonstration of differences between this enzyme and the mitochondrial phosphoenolpyruvate carboxykinase. *J. Biol. Chem.* **244:** 5625–5630

Ballard FJ, Hanson RW & Leveille GA (1967) Phosphoenolpyruvate Carboxykinase and the

Synthesis from Pyruvate in Adipose Tissue *. *J. Biol. Chem.* **242:** 2746–2750

Barberi T, Willis LM, Socci ND & Studer L (2005) Derivation of multipotent mesenchymal precursors from human embryonic stem cells. *PLoS Med.* **2:** 0554–0560

Barretina J, Taylor BS, Banerji S, Ramos AH, Lagos-Quintana M, Decarolis PL, Shah K, Socci ND, Weir BA, Ho A, Chiang DY, Reva B, Mermel CH, Getz G, Antipin Y, Beroukhim R, Major JE, Hatton C, Nicoletti R, Hanna M, et al (2010) Subtype-specific genomic alterations define new targets for soft-tissue sarcoma therapy. *Nat. Genet.* **42:** 715–721

Bartelds B, Knoester H, Beaufort-Krol GCM, Smid GB, Takens J, Zijlstra WG, Heymans HSA & Kuipers JRG (1999) Myocardial lactate metabolism in fetal and newborn lambs. *Circulation* **99:** 1892–1897

Barthel A, Okino ST, Liao J, Nakatani K, Li J, Whitlock JP & Roth RA (1999) Regulation of GLUT1 gene transcription by the serine/threonine kinase Akt1. *J. Biol. Chem.* **274:** 20281–20286

Battaglia FC & Meschia G (1978) Principal Substrates of Fetal Metabolism. *Physiol. Rev.* **58:** 499–527

Battello N, Zimmer AD, Goebel C, Dong X, Behrmann I, Haan C, Hiller K & Wegner A (2016) The role of HIF-1 in oncostatin M-dependent metabolic reprogramming of hepatic cells. *Cancer Metab.* **4:** 3

Beard RW & Nathanielsz PW (1984) Fetal Physiology and Medicine: The Basis of Perinatology. In *Fetal Physiology and Medicine: The Basis of Perinatology* BMJ Group

Becerra A, Rivas M, Garcia-Ferris C, Lazcano A & Pereto J (2014) A phylogenetic approach to the early evolution of autotrophy: The case of the reverse TCA and the reductive acetyl-CoA pathways. *Int. Microbiol.* **17:** 91–97

Bennett BD, Yuan J, Kimball EH & Rabinowitz JD (2008) Absolute quantitation of intracellular metabolite concentrations by an isotope ratio-based approach. *Nat. Protoc.* **3:** 1299–311

Bergersen LH & Gjedde A (2012) Is lactate a volume transmitter of metabolic states of the brain? *Front. Neuroenergetics* **4:** 5

Beroukhim R, Brunet JP, Di Napoli A, Mertz KD, Seeley A, Pires MM, Linhart D, Worrell RA, Moch H, Rubin MA, Sellers WR, Meyerson M, Linehan WM, Kaelin WG & Signoretti S (2009) Patterns of gene expression and copy-number alterations in von-Hippel Lindau

disease-associated and sporadic clear cell carcinoma of the kidney. *Cancer Res.* **69:** 4674–4681

Biewenga P, Buist MR, Moerland PD, van Themaat EVL, van Kampen AHC, ten Kate FJW & Baas F (2008) Gene expression in early stage cervical cancer. *Gynecol. Oncol.* **108:** 520–526

Bissonnete JM, Hohimer R & Chao CR (1991) Unidirectional transport of glucose and lactate into brain of fetal sheep and guinea-pig. *Exp. Physiol.* **76:** 515–523

Bittar PG, Charnay Y, Pellerin L, Bouras C & Magistretti PJ (1996) Selective distribution of lactate dehydrogenase isoenzymes in neurons and astrocytes of human brain. *J. Cereb. Blood Flow Metab.* **16:** 1079–1089

Bliss TM & Sapolsky RM (2001) Interactions among glucose, lactate and adenosine regulate energy substrate utilization in hippocampal cultures. *Brain Res.* **899:** 134–141

Bobrovnikova-Marjon E, Hatzivassiliou G, Grigoriadou C, Romero M, Cavener DR, Thompson CB & Diehl JA (2008) PERK-dependent regulation of lipogenesis during mouse mammary gland development and adipocyte differentiation. *Proc. Natl. Acad. Sci. U. S. A.* **105:** 16314–16319

Bode BP, Fuchs BC, Hurley BP, Conroy JL, Suetterlin JE, Tanabe KK, Rhoads DB, Abcouwer SF & Souba WW (2002) Molecular and functional analysis of glutamine uptake in human hepatoma and liver-derived cells. *Am. J. Physiol. Gastrointest. Liver Physiol.* **283:** G1062-73

Bolaños JP & Medina JM (1993) Lipogenesis from lactate in fetal rat brain during late gestation. *Pediatr. Res.* **33:** 66–71

Borowicz S, Van Scoyk M, Avasarala S, Karuppusamy Rathinam MK, Tauler J, Bikkavilli RK & Winn RA (2014) The soft agar colony formation assay. *J. Vis. Exp.* **92:** e51998

Bouzier-Sore A-K, Voisin P, Canioni P, Magistretti PJ & Pellerin L (2003) Lactate is a preferential oxidative energy substrate over glucose for neurons in culture. *J. Cereb. blood flow Metab.* **23:** 1298–306

Brand K a & Hermfisse U (1997) Aerobic glycolysis by proliferating cells: A protective strategy against reactive oxygen species. *FASEB J.* **11:** 388–395

Brooks GA, Brown MA, Butz CE, Sicurello JP & Dubouchaud H (1999a) Cardiac and skeletal muscle mitochondria have a monocarboxylate transporter MCT1. *J. Appl. Physiol.* **87:**

1713–8

Brooks GA, Dubouchaud H, Brown M, Sicurello JP & Butz CE (1999b) Role of mitochondrial lactate dehydrogenase and lactate oxidation in the intracellular lactate shuttle. *Proc. Natl. Acad. Sci. U. S. A.* **96:** 1129–1134

Brune V, Tiacci E, Pfeil I, Döring C, Eckerle S, Noesel CJM van, Klapper W, Falini B, Heydebreck A von, Metzler D, Bräuninger A, Hansmann M-L & Küppers R (2008) Origin and pathogenesis of nodular lymphocyte – predominant Hodgkin lymphoma as revealed by global gene expression analysis. *J. Exp. Med.* **205:** 2251–2268

Burgess SC, Hausler N, Merritt M, Jeffrey FMH, Storey C, Milde A, Koshy S, Lindner J, Magnuson MA, Malloy CR & Sherry AD (2004) Impaired tricarboxylic acid cycle activity in mouse livers lacking cytosolic phosphoenolpyruvate carboxykinase. *J. Biol. Chem.* **279:** 48941–48949

Burgess SC, He T, Yan Z, Lindner J, Sherry AD, Malloy CR, Browning JD & Magnuson MA (2007) Cytosolic Phosphoenolpyruvate Carboxykinase Does Not Solely Control the Rate of Hepatic Gluconeogenesis in the Intact Mouse Liver. *Cell Metab.* **5:** 313–320

Caetano-Anollés G, Yafremava LS, Gee H, Caetano-Anollés D, Kim HS & Mittenthal JE (2009) The origin and evolution of modern metabolism. *Int. J. Biochem. Cell Biol.* **41:** 285–97

Cai TQ, Ren N, Jin L, Cheng K, Kash S, Chen R, Wright SD, Taggart AKP & Waters MG (2008) Role of GPR81 in lactate-mediated reduction of adipose lipolysis. *Biochem. Biophys. Res. Commun.* **377:** 987–991

Candelario KM, Shuttleworth CW & Cunningham LA (2013) Neural stem/progenitor cells display a low requirement for oxidative metabolism independent of hypoxia inducible factor-1alpha expression. *J. Neurochem.* **125:** 420–9

Casás-Selves M & Degregori J (2011) How cancer shapes evolution, and how evolution shapes cancer. *Evolution (N. Y).* **4:** 624–634

Castillo X, Rosafio K, Wyss MT, Drandarov K, Buck A, Pellerin L, Weber B & Hirt L (2015) A probable dual mode of action for both L- and D-lactate neuroprotection in cerebral ischemia. *J. Cereb. Blood Flow Metab.* **30:** 1–9

Castresana J & Saraste M (1995) Evolution of energetic metabolism: the respiration-early hypothesis. *Trends Biochem. Sci.* **20:** 443–448

Cetinbas NM, Sudderth J, Harris RC, Cebeci A, Negri GL, Yılmaz ÖH, DeBerardinis RJ &

Sorensen PH (2016) Glucose-dependent anaplerosis in cancer cells is required for cellular redox balance in the absence of glutamine. *Sci. Rep.* **6:** 32606

Chandramouli V, Ekberg K, Schumann WC, Kalhan SC, Wahren J & Landau BR (1997) Quantifying gluconeogenesis during fasting. *Am. J. Physiol.* **273:** E1209–E1215

Chaneton B, Hillmann P, Zheng L, Martin ACL, Maddocks ODK, Chokkathukalam A, Coyle JE, Jankevics A, Holding FP, Vousden KH, Frezza C, O'Reilly M & Gottlieb E (2012) Serine is a natural ligand and allosteric activator of pyruvate kinase M2. *Nature* **491:** 458–62

Chang CH, Qiu J, O'Sullivan D, Buck MD, Noguchi T, Curtis JD, Chen Q, Gindin M, Gubin MM, Van Der Windt GJW, Tonc E, Schreiber RD, Pearce EJ & Pearce EL (2015) Metabolic Competition in the Tumor Microenvironment Is a Driver of Cancer Progression. *Cell* **162:** 1229–1241

Char VC & Creasy RK (1976) Lactate and Pyruvate as Fetal Metabolic Substrates. *Pediatr. Res.* **10:** 231–234

Chen X, Leung SY, Yuen ST, Chu K-M, Ji J, Li R, Chan ASY, Law S, Troyanskaya OG, Wong J, So S, Botstein D & Brown PO (2003) Variation in gene expression patterns in human gastric cancers. *Mol. Biol. Cell* **14:** 3208–3215

Chen Y-J, Mahieu NG, Huang X, Singh M, Crawford PA, Johnson SL, Gross RW, Schaefer J & Patti GJ (2016) Lactate metabolism is associated with mammalian mitochondria. *Nat. Chem. Biol.* **12:** 937–943

Cheng T, Sudderth J, Yang C, Mullen AR, Jin ES, Matés JM & DeBerardinis RJ (2011) Pyruvate carboxylase is required for glutamine-independent growth of tumor cells. *Proc. Natl. Acad. Sci. U. S. A.* **108:** 8674–9

Chiaradonna F, Sacco E, Manzoni R, Giorgio M, Vanoni M & Alberghina L (2006) Ras-dependent carbon metabolism and transformation in mouse fibroblasts. *Oncogene* **25:** 5391–5404

Chih CP & Roberts Jr EL (2003) Energy substrates for neurons during neural activity: a critical review of the astrocyte-neuron lactate shuttle hypothesis. *J Cereb Blood Flow Metab* **23:** 1263–1281

Cho JY, Lim JY, Cheong JH, Park YY, Yoon SL, Kim SM, Kim SB, Kim H, Hong SW, Park YN, Noh SH, Park ES, Chu IS, Hong WK, Ajani JA & Lee JS (2011) Gene expression signature-based prognostic risk score in gastric cancer. *Clin. Cancer Res.* **17:** 1850–1857

Chouchani ET, Pell VR, Gaude E, Aksentijević D, Sundier SY, Robb EL, Logan A, Nadtochiy SM, Ord ENJ, Smith AC, Eyassu F, Shirley R, Hu C-H, Dare AJ, James AM, Rogatti S, Hartley RC, Eaton S, Costa ASH, Brookes PS, et al (2014) Ischaemic accumulation of succinate controls reperfusion injury through mitochondrial ROS. *Nature* **515:** 431–435

Christofk HR, Vander Heiden MG, Harris MH, Ramanathan A, Gerszten RE, Wei R, Fleming MD, Schreiber SL & Cantley LC (2008) The M2 splice isoform of pyruvate kinase is important for cancer metabolism and tumour growth. *Nature* **452:** 230–233

Cooper GM (2000a) The Origin and Evolution of Cells. In *The Cell: A Molecular Approach* Sinauer Associates

Cooper GM (2000b) Cell Proliferation in Development and Differentiation. In *The Cell: A Molecular Approach* p 848. Sinauer Associates

Cremer JE, Braun LD & Oldendorf WH (1976) Changes during development in transport processes of the blood-brain barrier. *Biochim. Biophys. Acta - Biomembr.* **448:** 633–637

Croniger CM, Chakravarty K, Olswang Y, Cassuto H, Reshef L & Hanson RW (2002a) Phosphoenolpyruvate carboxykinase revisited: II. Control of PEPCK-C gene expression. *Biochem. Mol. Biol. Educ.* **30:** 353–362

Croniger CM, Olswang Y, Reshef L, Kalhan SC, Tilghman SM & Hanson RW (2002b) Phosphoenolpyruvate Carboxykinase Revisited: Insight into its metabolic role. *Biochem. Mol. Biol. Educ.* **30:** 14–20

Cuezva JM, Moreno FJ, Medina JM & Mayor F (1980) Prematurity in the rat. I. Fuels and gluconeogenic enzymes. *BIOL. NEONATE* **37:** 88–95

Currie E, Schulze A, Zechner R, Walther TC & Farese R V (2013) Cellular fatty acid metabolism and cancer. *Cell Metab.* **18:** 153–161

Curtis C, Shah SP, Chin S-F, Turashvili G, Rueda OM, Dunning MJ, Speed D, Lynch AG, Samarajiwa S, Yuan Y, Gräf S, Ha G, Haffari G, Bashashati A, Russell R, McKinney S, Langerød A, Green A, Provenzano E, Wishart G, et al (2012) The genomic and transcriptomic architecture of 2,000 breast tumours reveals novel subgroups. *Nature* **486:** 346–52

Dashko S, Zhou N, Compagno C & Piškur J (2014) Why, when, and how did yeast evolve alcoholic fermentation? *FEMS Yeast Res.* **14:** 826–832

Deberardinis R & Cheng T (2010) Q's next: the diverse functions of glutamine in metabolism,

cell biology and cancer. *Oncogene* **29:** 313–324

DeBerardinis RJ & Chandel NS (2016) Fundamentals of cancer metabolism. *Sci. Adv.* **2:** e1600200

DeBerardinis RJ, Lum JJ, Hatzivassiliou G & Thompson CB (2008) The biology of cancer: metabolic reprogramming fuels cell growth and proliferation. *Cell Metab.* **7:** 11–20

DeBerardinis RJ, Lum JJ & Thompson CB (2006) Phosphatidylinositol 3-kinase-dependent modulation of carnitine palmitoyltransferase 1A expression regulates lipid metabolism during hematopoietic cell growth. *J. Biol. Chem.* **281:** 37372–37380

DeBerardinis RJ, Mancuso A, Daikhin E, Nissim I, Yudkoff M, Wehrli S & Thompson CB (2007) Beyond aerobic glycolysis: transformed cells can engage in glutamine metabolism that exceeds the requirement for protein and nucleotide synthesis. *Proc. Natl. Acad. Sci. U. S. A.* **104:** 19345–50

Debernardi R, Pierre K, Lengacher S, Magistretti PJ & Pellerin L (2003) Cell-specific expression pattern of monocarboxylate transporters in astrocytes and neurons observed in different mouse brain cortical cell cultures. *J. Neurosci. Res.* **73:** 141–155

Delbaere LTJ, Sudom AM, Prasad L, Leduc Y & Goldie H (2004) Structure/function studies of phosphoryl transfer by phosphoenolpyruvate carboxykinase. *Biochim. Biophys. Acta* **1697:** 271–278

DeNicola GM, Chen P-H, Mullarky E, Sudderth JA, Hu Z, Wu D, Tang H, Xie Y, Asara JM, Huffman KE, Wistuba II, Minna JD, DeBerardinis RJ & Cantley LC (2015) NRF2 regulates serine biosynthesis in non–small cell lung cancer. *Nat. Genet.* **47:** 1475–1484

Denne SC & Kalhan SC (1986) Glucose carbon recycling and oxidation in human newborns. *Am. J. Physiol.* **251:** E71-7

Dettmer K, Nürnberger N, Kaspar H, Gruber MA, Almstetter MF & Oefner PJ (2011) Metabolite extraction from adherently growing mammalian cells for metabolomics studies: Optimization of harvesting and extraction protocols. *Anal. Bioanal. Chem.* **399:** 1127–1139

DeVivo DC, Leckie MP & Agrawal HC (1975) D-Beta-Hydroxybutyrate: A Major Precursor of Amino Acids in Developing Rat Brain. *J. Neurochem.* **25:** 161–170

Dienel GA (2012) Brain lactate metabolism: the discoveries and the controversies. *J. Cereb. blood flow Metab.* **32:** 1107–38

Ding B, Parmigiani A, Divakaruni AS, Archer K, Murphy AN & Budanov A V (2016) Sestrin2 is induced by glucose starvation via the unfolded protein response and protects cells from non-canonical necroptotic cell death. *Sci. Rep.* **6:** 22538

Drahota Z, Rauchová H, Miková M, Kaul P & Bass a (1983) Phosphoenolpyruvate shuttle--transport of energy from mitochondria to cytosol. *FEBS Lett.* **157:** 347–9

Dringen R, Gebhardt R & Hamprecht B (1993) Glycogen in astrocytes: possible function as lactate supply for neighboring cells. *Brain Res.* **623:** 208–214

Duarte JAG, Carvalho F, Pearson M, Horton JD, Browning JD, Jones JG & Burgess SC (2014) A high-fat diet suppresses de novo lipogenesis and desaturation but not elongation and triglyceride synthesis in mice. *J. Lipid Res.* **55:** 2541–2553

Dunn MF, Ramírez-Trujillo JA & Hernández-Lucas I (2009) Major roles of isocitrate lyase and malate synthase in bacterial and fungal pathogenesis. *Microbiology* **155:** 3166–3175

Dwong527 (2013) Diagram showing glycolytic and gluconeogenic pathways (CC BY-SA 3.0). Available at: https://en.wikipedia.org/wiki/File:Glycolytic_and_gluconeogenic_pathways.jpg [Accessed December 13, 2016]

Dyrskjøt L, Kruhøffer M, Thykjaer T, Marcussen N, Jensen JL, Møller K & Ørntoft TF (2004) Gene Expression in the Urinary Bladder : A Common Carcinoma in Situ Gene Expression Signature Exists Disregarding Histopathological Classification. *Cancer Res.* **64:** 4040–4048

Edgar R, Domrachev M & Lash AE (2002) Gene Expression Omnibus: NCBI gene expression and hybridization array data repository. *Nucleic Acids Res* **30:** 207–210

Elstrom RL, Bauer DE, Buzzai M, Karnauskas R, Harris MH, Plas DR, Zhuang H, Cinalli RM, Alavi A, Rudin CM & Thompson CB (2004) Akt stimultes aerobic glycolysis in cancer cells. *Cancer Res.* **64:** 3892–3899

Englund C, Fink A, Lau C, Pham D, Daza RAM, Bulfone A, Kowalczyk T & Hevner RF (2005) Pax6, Tbr2, and Tbr1 are expressed sequentially by radial glia, intermediate progenitor cells, and postmitotic neurons in developing neocortex. *J. Neurosci.* **25:** 247–51

Estrella V, Chen T, Lloyd M, Wojtkowiak J, Cornnell HH, Ibrahim-Hashim A, Bailey K, Balagurunathan Y, Rothberg JM, Sloane BF, Johnson J, Gatenby RA & Gillies RJ (2013) Acidity generated by the tumor microenvironment drives local invasion. *Cancer Res.* **73:**

1524–1535

Ewaschuk JB, Naylor JM & Zello GA (2005) D-lactate in human and ruminant metabolism. *J. Nutr.* **135:** 1619–25

Exton JH & Park CR (1967) Control of Gluconeogenesis in Liver. *J. Biol. Chem.* **242:** 2622–2636

Fan J, Kamphorst JJ, Rabinowitz JD & Shlomi T (2013) Fatty acid labeling from glutamine in hypoxia can be explained by isotope exchange without net reductive isocitrate dehydrogenase (IDH) flux. *J. Biol. Chem.* **288:** 31363–31369

Fani R & Fondi M (2009) Origin and evolution of metabolic pathways. *Phys. Life Rev.* **6:** 23–52

Fell DA (2010) Evolution of Central Carbon Metabolism. *Mol. Cell* **39:** 663–664

Fendt S-M, Bell EL, Keibler MA, Olenchock BA, Mayers JR, Wasylenko TM, Vokes NI, Guarente L, Vander Heiden MG & Stephanopoulos G (2013) Reductive glutamine metabolism is a function of the α-ketoglutarate to citrate ratio in cells. *Nat. Commun.* **4:** 2236

Finak G, Bertos N, Pepin F, Sadekova S, Souleimanova M, Zhao H, Chen H, Omeroglu G, Meterissian S, Omeroglu A, Hallett M & Park M (2008) Stromal gene expression predicts clinical outcome in breast cancer. *Nat. Med.* **14:** 518–27

Finley LWS & Thompson CB (2014) The Metabolism of Cell Growth and Proliferation. In *The molecular basis of cancer* pp 191–208.

Folmes CDL, Dzeja PP, Nelson TJ & Terzic A (2012) Metabolic plasticity in stem cell homeostasis and differentiation. *Cell Stem Cell* **11:** 596–606

Folmes CDL, Nelson TJ, Martinez-Fernandez A, Arrell DK, Lindor JZ, Dzeja PP, Ikeda Y, Perez-Terzic C & Terzic A (2011) Somatic oxidative bioenergetics transitions into pluripotency-dependent glycolysis to facilitate nuclear reprogramming. *Cell Metab.* **14:** 264–271

Franco SJ & Müller U (2013) Shaping Our Minds: Stem and Progenitor Cell Diversity in the Mammalian Neocortex. *Neuron* **77:** 19–34

Fritz V & Fajas L (2010) Metabolism and proliferation share common regulatory pathways in cancer cells. *Oncogene* **29:** 4369–4377

Fukuda W, Fukui T, Atomi H & Imanaka T (2004) First characterization of an archaeal GTP-dependent phosphoenolpyruvate carboxykinase from the hyperthermophilic archaeon

Thermococcus kodakaraensis KOD1. *J. Bacteriol.* **186:** 4620–4627

Gaedcke J, Grade M, Jung K, Camps J, Jo P, Emons G, Gehoff A, Sax U, Schirmer M, Becker H, Beissbarth T, Ried T & Ghadimi BM (2010) Mutated KRAS results in overexpression of DUSP4, a MAP-kinase phosphatase, and SMYD3, a histone methyltransferase, in rectal carcinomas. *Genes Chromosom. Cancer* **49:** 1024–1034

Gaglio D, Metallo CM, Gameiro PA, Hiller K, Danna LS, Balestrieri C, Alberghina L, Stephanopoulos G & Chiaradonna F (2011) Oncogenic K-Ras decouples glucose and glutamine metabolism to support cancer cell growth. *Mol. Syst. Biol.* **7:** 523

Gallagher CN, Carpenter KLH, Grice P, Howe DJ, Mason A, Timofeev I, Menon DK, Kirkpatrick PJ, Pickard JD, Sutherland GR & Hutchinson PJ (2009a) The human brain utilizes lactate via the tricarboxylic acid cycle: a 13C-labelled microdialysis and high-resolution nuclear magnetic resonance study. *Brain* **132:** 2839–49

Gallagher CN, Carpenter KLH, Grice P, Howe DJ, Mason A, Timofeev I, Menon DK, Kirkpatrick PJ, Pickard JD, Sutherland GR & Hutchinson PJ (2009b) The human brain utilizes lactate via the tricarboxylic acid cycle: a 13C-labelled microdialysis and high-resolution nuclear magnetic resonance study. *Brain* **132:** 2839–49

Gansler TS, Hardman W, Hunt DA, Schaffel S & Hennigar RA (1997) Increased expression of fatty acid synthase (OA-519) in ovarian neoplasms predicts shorter survival. *Hum. Pathol.* **28:** 686–692

Gao P, Tchernyshyov I, Chang T-C, Lee Y-S, Kita K, Ochi T, Zeller KI, De Marzo AM, Van Eyk JE, Mendell JT & Dang C V. (2009) c-Myc suppression of miR-23a/b enhances mitochondrial glutaminase expression and glutamine metabolism. *Nature* **458:** 762–765

Gatenby RA & Gillies RJ (2008) A microenvironmental model of carcinogenesis. *Nat. Rev. Cancer* **8:** 56–61

Gertz EW, Wisneski JA, Stanley WC & Neese RA (1988) Myocardial substrate utilization during exercise in humans. Dual carbon-labeled carbohydrate isotope experiments. *J. Clin. Invest.* **82:** 2017–2025

Gladden LB (2004) Lactate metabolism: a new paradigm for the third millennium. *J. Physiol.* **558:** 5–30

Glenn TC, Martin NA, Horning MA, McArthur DL, Hovda DA, Vespa P & Brooks GA (2015) Lactate: brain fuel in human traumatic brain injury: a comparison with normal healthy

control subjects. *J. Neurotrauma* **32:** 820–32

Goldman AD, Baross JA & Samudrala R (2012) The enzymatic and metabolic capabilities of early life. *PLoS One* **7:** e39912

Greenspan HP (1972) Models for the Growth of a Solid Tumor by Diffusion. *Stud. Appl. Math.* **51:** 317–340

Gumz ML, Zou H, Kreinest PA, Childs AC, Belmonte LS, LeGrand SN, Wu KJ, Luxon BA, Sinha M, Parker AS, Sun LZ, Ahlquist DA, Wood CG & Copland JA (2007) Secreted frizzled-related protein 1 loss contributes to tumor phenotype of clear cell renal cell carcinoma. *Clin. Cancer Res.* **13:** 4740–4749

Győrffy B, Lanczky A, Eklund AC, Denkert C, Budczies J, Li Q & Szallasi Z (2010) An online survival analysis tool to rapidly assess the effect of 22,277 genes on breast cancer prognosis using microarray data of 1,809 patients. *Breast Cancer Res. Treat.* **123:** 725–731

Hakimi P, Johnson MT, Yang J, Lepage DF, Conlon R a, Kalhan SC, Reshef L, Tilghman SM & Hanson RW (2005) Phosphoenolpyruvate carboxykinase and the critical role of cataplerosis in the control of hepatic metabolism. *Nutr. Metab. (Lond).* **2:** 1–12

Halestrap AP & Wilson MC (2012) The monocarboxylate transporter family-Role and regulation. *IUBMB Life* **64:** 109–119

Hanson RW, Ballard FJ & Reshef L (2006) Glyceroneogenesis, the pathway that almost wasn't. *Biochem. Mol. Biol. Educ.* **34:** 317–323

Hanson RW & Garber AJ (1972) Phosphoenolpyruvate carboxykinase. I. Its role in gluconeogenesis. *Am. J. Clin. Nutr.* **25:** 1010–1021

Hanson RW & Hakimi P (2008) Born to run; the story of the PEPCK-Cmus mouse. *Biochimie* **90:** 838–842

Hanson RW & Patel YM (1994) Phosphoenolpyruvate Carboxykinase (GTP): the Gene and the Enzyme. *Adv. Enzymol. Relat. Subj.* **69:** 203–81

Hanson RW & Reshef L (1997) Regulation of Phosphoenolpyruvate Carboxykinase (GTP) Gene Expression. *Annu. Rev. Biochem.* **66:** 581–611

Hashimoto T, Hussien R, Cho HS, Kaufer D & Brooks GA (2008) Evidence for the mitochondrial lactate oxidation complex in rat neurons: Demonstration of an essential component of brain lactate shuttles. *PLoS One* **3:** e2915

Hedeskov CJ (1968) Early Effects of Phytohaemagglutinin on Glucose Metabolism of Normal Human Lymphocytes. *Biochem. J.* **110:** 373–80

Vander Heiden MG, Cantley LC & Thompson CB (2009) Understanding the Warburg effect: the metabolic requirements of cell proliferation. *Science* **324:** 1029–33

Vander Heiden MG, Lunt SY, Dayton TL, Fiske BP, Israelsen WJ, Mattaini KR, Vokes NI, Stephanopoulos G, Cantley LC, Metallo CM & Locasale JW (2011) Metabolic pathway alterations that support: Cell Proliferation. *Cold Spring Harb. Symp. Quant. Biol.* **76:** 325–334

Hermann A, Gastl R, Liebau S, Popa MO, Fiedler J, Boehm BO, Maisel M, Lerche H, Schwarz J, Brenner R & Storch A (2004) Efficient generation of neural stem cell-like cells from adult human bone marrow stromal cells. *J. Cell Sci.* **117:** 4411–4422

Hiller J, Franco-Lara E & Weuster-Botz D (2007) Metabolic profiling of Escherichia coli cultivations: Evaluation of extraction and metabolite analysis procedures. *Biotechnol. Lett.* **29:** 1169–1178

Ho PC, Bihuniak JD, MacIntyre AN, Staron M, Liu X, Amezquita R, Tsui YC, Cui G, Micevic G, Perales JC, Kleinstein SH, Abel ED, Insogna KL, Feske S, Locasale JW, Bosenberg MW, Rathmell JC & Kaech SM (2015) Phosphoenolpyruvate Is a Metabolic Checkpoint of Anti-tumor T Cell Responses. *Cell* **162:** 1217–1228

Holmberg J, He X, Peredo I, Orrego A, Hesselager G, Ericsson C, Hovatta O, Oba-Shinjo SM, Marie SKN, Nistér M & Muhr J (2011) Activation of neural and pluripotent stem cell signatures correlates with increased malignancy in human glioma. *PLoS One* **6:** e18454

Hopgood MF & Ballard FJ (1973) Synthesis and degradation of phosphoenolpyruvate carboxylase in rat liver and adipose tissue. Changes during a starvation-re-feeding cycle. *Biochem J* **134:** 445–453

Horibata S, Vo T V, Subramanian V, Thompson PR & Coonrod SA (2015) Utilization of the Soft Agar Colony Formation Assay to Identify Inhibitors of Tumorigenicity in Breast Cancer Cells Video Link. *J. Vis. Exp* **99:** e52727

Hsieh CW, Millward CA, DeSantis D, Pisano S, Machova J, Perales JC & Croniger CM (2009) Reduced milk triglycerides in mice lacking phosphoenolpyruvate carboxykinase in mammary gland adipocytes and white adipose tissue contribute to the development of insulin resistance in pups. *J Nutr* **139:** 2257–2265

Hsu PP & Sabatini DM (2008) Cancer cell metabolism: Warburg and beyond. *Cell* **134:** 703–707

Hu S, Balakrishnan A, Bok RA, Anderton B, Larson PEZ, Nelson SJ, Kurhanewicz J, Vigneron DB & Goga A (2011) 13C-pyruvate imaging reveals alterations in glycolysis that precede c-Myc-induced tumor formation and regression. *Cell Metab.* **14:** 131–142

Huttner WB & Kosodo Y (2005) Symmetric versus asymmetric cell division during neurogenesis in the developing vertebrate central nervous system. *Curr. Opin. Cell Biol.* **17:** 648–657

Huynen MA, Dandekar T & Bork P (1999) Variation and evolution of the citric-acid cycle: A genomic perspective. *Trends Microbiol.* **7:** 281–291

Itoh Y, Esaki T, Shimoji K, Cook M, Law MJ, Kaufman E & Sokoloff L (2003) Dichloroacetate effects on glucose and lactate oxidation by neurons and astroglia in vitro and on glucose utilization by brain in vivo. *Proc. Natl. Acad. Sci. U. S. A.* **100:** 4879–84

Jaakkola P, Mole DR, Tian Y-M, Wilson MI, Gielbert J, Gaskell SJ, Kriegsheim A von, Hebestreit HF, Mukherji M, Schofield CJ, Maxwell PH, Pugh CW & Ratcliffe PJ (2001) Targeting of HIF-a to the von Hippel–Lindau Ubiquitylation Complex by O2-Regulated Prolyl Hydroxylation. *Science* **292:** 468–472

Jády AG, Nagy ÁM, Kőhidi T, Ferenczi S, Tretter L & Madarász E (2016) Differentiation-Dependent Energy Production and Metabolite Utilization: A Comparative Study on Neural Stem Cells, Neurons, and Astrocytes. *Stem Cells Dev.* **25:** scd.2015.0388

Jiang P, Du W & Wu M (2014) Regulation of the pentose phosphate pathway in cancer. *Protein Cell* **5:** 592–602

Jiang W, Wang S, Xiao M, Lin Y, Zhou L, Lei Q, Xiong Y, Guan KL & Zhao S (2011) Acetylation Regulates Gluconeogenesis by Promoting PEPCK1 Degradation via Recruiting the UBR5 Ubiquitin Ligase. *Mol. Cell* **43:** 33–44

Jiménez J, Page-Peñuelas A, Ros M, García-Ruíz JP & Moreno FJ (1987) Glycerogenic pathway in the rat mammary gland. *Int. J. Biochem.* **19:** 201–204

Jin L, Alesi GN & Kang S (2016) Glutaminolysis as a target for cancer therapy. *Oncogene* **35:** 3619–3625

Jones CT (1976) Fetal metabolism and fetal growth. *J. Reprod. Fertil.* **47:** 189–201

Jones J, Otu H, Spentzos D, Kolia S, Inan M, Beecken WD, Fellbaum C, Gu X, Joseph M,

Pantuck AJ, Jonas D & Libermann TA (2005) Gene signatures of progression and metastasis in renal cell cancer. *Clin. Cancer Res.* **11:** 5730–5739

Jones RG & Thompson CB (2009) Tumor suppressors and cell metabolism: a recipe for cancer growth. *Genes Dev.* **23:** 537–548

Jose C, Bellance N & Rossignol R (2011) Choosing between glycolysis and oxidative phosphorylation: A tumor's dilemma? *Biochim. Biophys. Acta - Bioenerg.* **1807:** 552–561

Jurtshuk P (1996) Bacterial Metabolism. In *Medical Microbiology*, Baron S (ed) pp 129–198. Galveston: University of Texas Medical Branch at Galveston

Kaiser S, Park Y-K, Franklin JL, Halberg RB, Yu M, Jessen WJ, Freudenberg J, Chen X, Haigis K, Jegga AG, Kong S, Sakthivel B, Xu H, Reichling T, Azhar M, Boivin GP, Roberts RB, Bissahoyo AC, Gonzales F, Bloom GC, et al (2007) Transcriptional recapitulation and subversion of embryonic colon development by mouse colon tumor models and human colon cancer. *Genome Biol.* **8:** R131

Kalhan SC, Bier DM, Savin SM & Adam PAJ (1980) Estimation of glucose turnover and 13C recycling in the human newborn by simultaneous [1-13C]glucose and [6, 6-2H2]glucose tracers. *J. Clin. Endocrinol. Metab.* **50:** 456–460

Kalhan SC, Mahajan S, Burkett E, Reshef L & Hanson RW (2001) Glyceroneogenesis and the Source of Glycerol for Hepatic Triacylglycerol Synthesis in Humans. *J. Biol. Chem.* **276:** 12928–12931

Kardos GR, Wastyk HC & Robertson GP (2015) Disruption of Proline Synthesis in Melanoma Inhibits Protein Production Mediated by the GCN2 Pathway. *Mol. Cancer Res.* **13:** 1408–1420

Kasinskas RW, Venkatasubramanian R & Forbes NS (2014) Rapid uptake of glucose and lactate, and not hypoxia, induces apoptosis in three-dimensional tumor tissue culture. *Integr. Biol. (Camb).* **6:** 399–410

Kazanis I, Lathia JD, Vadakkan TJ, Raborn E, Wan R, Mughal MR, Eckley DM, Sasaki T, Patton B, Mattson MP, Hirschi KK, Dickinson ME & Ffrench-Constant C (2010) Quiescence and activation of stem and precursor cell populations in the subependymal zone of the mammalian brain are associated with distinct cellular and extracellular matrix signals. *J. Neurosci.* **30:** 9771–81

Ke N, Albers A, Claassen G, Yu DH, Chatterton JE, Hu X, Meyhack B, Wong-Staal F & Li QX

(2004) One-week 96-well soft agar growth assay for cancer target validation. *Biotechniques* **36:** 826–833

Keibler MA, Wasylenko TM, Kelleher JK, Iliopoulos O, Vander Heiden MG & Stephanopoulos G (2016) Metabolic requirements for cancer cell proliferation. *Cancer Metab.* **4:** 16

Kelly B & O'Neill LA (2015) Metabolic reprogramming in macrophages and dendritic cells in innate immunity. *Cell Res.* **25:** 771–84

Khan M, Biswas D, Ghosh M, Mandloi S, Chakrabarti S & Chakrabarti P (2015) mTORC2 controls cancer cell survival by modulating gluconeogenesis. *Cell Death Discov.* **1:** 15016

Kibbey RG, Pongratz RL, Romanelli AJ, Wollheim CB, Cline GW & Shulman GI (2007) Mitochondrial GTP Regulates Glucose-Stimulated Insulin Secretion. *Cell Metab.* **5:** 253–264

Kilburn DG, Lilly MD & Webb FC (1969) The Energetics of Mammalian Cell Growth. *J. Cell Sci.* **4:** 645–654

Knobloch M, Braun SMG, Zurkirchen L, Schoultz C von, NicolaZamboni, Arau MJ, ´zo-Bravo, J.Kovacs W, OzlemKaralay, Suter U, C.Machado RA, MartaRoccio, Lutolf MP, F.Semenkovich C & Jessberger S (2013) Metabolic control of adult neural stem cell activity by Fasn-dependent lipogenesis. *Nature* **493:** 226–230

Korangath P, Teo WW, Sadik H, Han L, Mori N, Huijts CM, Wildes F, Bharti S, Zhang Z, Santa-Maria CA, Tsai H, Dang C V., Stearns V, Bhujwalla ZM & Sukumar S (2015) Targeting glutamine metabolism in breast cancer with aminooxyacetate. *Clin. Cancer Res.* **21:** 3263–3273

Kuhajda FP, Jennert K, Wood FD, Hennigart RA, Jacobs LB, Dick JD & Pasternack GR (1994) Fatty acid synthesis: A potential selective target for antineoplastic therapy since inhibition of FAS inhibits growth of human carcinoma cell lines commensurate with their FAS levels. Since FAS activity in the tissues of humans eating a diet containing. *Med. Sci.* **91:** 6379–6383

Kumar Verma A, Arjun J & Chillawar R (2013) Homology Modeling and characterization of Phosphoenolpyruvate Carboxykinase (PEPCK) from Schistosoma japonicum. *IOSR J. Pharm. Biol. Sci.* **8:** 82–93

Labuschagne CF, van den Broek NJF, Mackay GM, Vousden KH & Maddocks ODK (2014) Serine, but not glycine, supports one-carbon metabolism and proliferation of cancer

cells. *Cell Rep.* **7:** 1248–1258

LaMonte G, Tang X, Chen JL-Y, Wu J, Ding C-K, Keenan MM, Sangokoya C, Kung H-N, Ilkayeva O, Boros LG, Newgard CB & Chi J-T (2013) Acidosis induces reprogramming of cellular metabolism to mitigate oxidative stress. *Cancer Metab.* **1:** 23

Lampe KJ, Namba RM, Silverman TR, Bjugstad KB & Mahoney MJ (2009) Impact of lactic acid on cell proliferation and free radical-induced cell death in monolayer cultures of neural precursor cells. *Biotechnol. Bioeng.* **103:** 1214–1223

Lathia JD, Patton B, Eckley DM, Magnus T, Mughal MR, Sasaki T, Caldwell MA, Mattson MP & Ffrench-Constant C (2007) Patterns of Laminins and Integrins in the Embryonic Ventricular Zone of the CNS. *J Comp Neurol* **505:** 630–643

Latorre P, Burgos C, Hidalgo J, Varona L, Carrodeguas JA & López-Buesa P (2016) c.A2456C-substitution in Pck1 changes the enzyme kinetic and functional properties modifying fat distribution in pigs. *Sci. Rep.* **6:** 19617

Lauritzen KH, Morland C, Puchades M, Holm-Hansen S, Hagelin EM, Lauritzen F, Attramadal H, Storm-Mathisen J, Gjedde A & Bergersen LH (2014) Lactate receptor sites link neurotransmission, neurovascular coupling, and brain energy metabolism. *Cereb. Cortex* **24:** 2784–2795

Lavrentovich MO, Koschwanez JH & Nelson DR (2013) Nutrient shielding in clusters of cells. *Phys. Rev. E - Stat. Nonlinear, Soft Matter Phys.* **87:** 62703

Le A, Lane AN, Hamaker M, Bose S, Gouw A, Barbi J, Tsukamoto T, Rojas CJ, Slusher BS, Zhang H, Zimmerman LJ, Liebler DC, Slebos RJC, Lorkiewicz PK, Higashi RM, Fan TWM & Dang C V (2012a) Glucose-independent glutamine metabolism via TCA cycling for proliferation and survival in B cells. *Cell Metab.* **15:** 110–21

Le A, Rajeshkumar N V., Maitra A & Dang C V. (2012b) Conceptual framework for cutting the pancreatic cancer fuel supply. *Clin. Cancer Res.* **18:** 4285–4290

Le A, Stine ZE, Nguyen C, Afzal J, Sun P, Hamaker M, Siegel NM, Gouw AM, Kang B-H, Yu S-H, Cochran RL, Sailor KA, Song H & Dang C V (2014) Tumorigenicity of hypoxic respiring cancer cells revealed by a hypoxia-cell cycle dual reporter. *Proc. Natl. Acad. Sci. U. S. A.* **111:** 1–6

Lee MH, Hebda CA & Nowak T (1981) The role of cations in avian liver phosphoenolpyruvate carboxykinase catalysis. Activation and regulation. *J. Biol. Chem.* **256:** 12793–12801

Leithner K, Hrzenjak A, Trötzmüller M, Moustafa T, Köfeler HC, Wohlkoenig C, Stacher E, Lindenmann J, Harris AL, Olschewski A & Olschewski H (2015) PCK2 activation mediates an adaptive response to glucose depletion in lung cancer. *Oncogene* **34:** 1044–1050

Lenburg ME, Liou LS, Gerry NP, Frampton GM, Cohen HT & Christman MF (2003) Previously unidentified changes in renal cell carcinoma gene expression identified by parametric analysis of microarray data. *BMC Cancer* **3:** 31

Lepski G, Jannes CE, Nikkhah G & Bischofberger J (2013) cAMP promotes the differentiation of neural progenitor cells in vitro via modulation of voltage-gated calcium channels. *Front. Cell. Neurosci.* **7:** 155

Li R, Jen N, Yu F & Hsiai TK (2011) Assessing mitochondrial redox status by flow cytometric methods: Vascular response to fluid shear stress. *Curr. Protoc. Cytom.***:** chapter unit 9.37

Li Y, Luo S, Ma R, Liu J, Xu P, Zhang H, Tang K, Ma J, Zhang Y, Liang X, Sun Y, Ji T, Wang N & Huang B (2015) Upregulation of cytosolic phosphoenolpyruvate carboxykinase is a critical metabolic event in melanoma cells that repopulate tumors. *Cancer Res.* **75:** 1191–1196

Liberti M V. & Locasale JW (2016) The Warburg Effect: How Does it Benefit Cancer Cells? *Trends Biochem. Sci.* **41:** 211–218

Lim J-H, Luo C, Vazquez F & Puigserver P (2014) Targeting Mitochondrial Oxidative Metabolism in Melanoma Causes Metabolic Compensation through Glucose and Glutamine Utilization. *Ther. Targets, Chem. Biol.* **74:** 3535–3545

Lin Y yi, Lu J ying, Zhang J, Walter W, Dang W, Wan J, Tao SC, Qian J, Zhao Y, Boeke JD, Berger SL & Zhu H (2009) Protein Acetylation Microarray Reveals that NuA4 Controls Key Metabolic Target Regulating Gluconeogenesis. *Cell* **136:** 1073–1084

Ling B, Peng F, Alcorn J, Lohmann K, Bandy B & Zello GA (2012) D-Lactate altered mitochondrial energy production in rat brain and heart but not liver. *Nutr. Metab. (Lond).* **9:** 6

Liu C, Wu J, Zhu J, Kuei C, Yu J, Shelton J, Sutton SW, Li X, Su JY, Mirzadegan T, Mazur C, Kamme F & Lovenberg TW (2009) Lactate inhibits lipolysis in fat cells through activation of an orphan G-protein-coupled receptor, GPR81. *J. Biol. Chem.* **284:** 2811–2822

Liu H, Radisky DC, Yang D, Xu R, Radisky ES, Bissell MJ & Bishop JM (2012a) MYC suppresses cancer metastasis by direct transcriptional silencing of αv and β3 integrin subunits. *Nat. Cell Biol.* **14:** 567–74

Liu W, Hancock CN, Fischer JW, Harman M & Phang JM (2015) Proline biosynthesis augments tumor cell growth and aerobic glycolysis: involvement of pyridine nucleotides. *Sci. Rep.* **5:** 1–13

Liu W, Le A, Hancock C, Lane AN, Dang C V, Fan TW-M & Phang JM (2012b) Reprogramming of proline and glutamine metabolism contributes to the proliferative and metabolic responses regulated by oncogenic transcription factor c-MYC. *Proc. Natl. Acad. Sci.* **109:** 8983–8988

Lobo C, Ruiz-Bellido MA, Aledo JC, Márquez J, Núñez De Castro I & Alonso FJ (2000) Inhibition of glutaminase expression by antisense mRNA decreases growth and tumourigenicity of tumour cells. *Biochem. J.* **348:** 257–261

Locasale JW & Cantley LC (2011) Metabolic flux and the regulation of mammalian cell growth. *Cell Metab.* **14:** 443–451

Locasale JW, Grassian AR, Melman T, Lyssiotis CA, Mattaini KR, Bass AJ, Heffron G, Metallo CM, Muranen T, Sharfi H, Sasaki AT, Anastasiou D, Mullarky E, Vokes NI, Sasaki M, Beroukhim R, Stephanopoulos G, Ligon AH, Meyerson M, Richardson AL, et al (2011) Phosphoglycerate dehydrogenase diverts glycolytic flux and contributes to oncogenesis. *Nat. Genet.* **43:** 869–74

Lodish H, Berk A, Zipursky SL, Matsudaira P, Baltimore D & Darnell J (2000) Molecular Cell Biology 4th ed. New York

Lorenz MC & Fink GR (2001) The glyoxylate cycle is required for fungal virulence. *Nature* **412:** 83–86

Löscher W & Hörstermann D (1994) Differential effects of vigabatrin, γ-acetylenic GABA, aminooxyacetic acid, and valproate on levels of various amino acids in rat brain regions and plasma. *Naunyn. Schmiedebergs. Arch. Pharmacol.* **349:** 270–278

Lu P, Weaver VM & Werb Z (2012) The extracellular matrix: A dynamic niche in cancer progression. *J. Cell Biol.* **196:** 395–406

Lü WD, Zhang L, Wu CL, Liu ZG, Lei GY, Liu J, Gao W & Hu YR (2014) Development of an acellular tumor extracellular matrix as a three-dimensional scaffold for tumor

engineering. *PLoS One* **9:** e103672

Lunt SY & Vander Heiden MG (2011) Aerobic Glycolysis: Meeting the Metabolic Requirements of Cell Proliferation. *Annu. Rev. Cell Dev. Biol.* **27:** 441–464

Lussey-Lepoutre C, Hollinshead KER, Ludwig C, Menara M, Morin A, Castro-Vega L-J, Parker SJ, Janin M, Martinelli C, Ottolenghi C, Metallo C, Gimenez-Roqueplo A-P, Favier J & Tennant DA (2015) Loss of succinate dehydrogenase activity results in dependency on pyruvate carboxylation for cellular anabolism. *Nat. Commun.* **6:** 8784

Lust WD, Pundik S, Zechel J, Zhou Y, Buczek M & Selman WR (2003) Changing metabolic and energy profiles in fetal, neonatal, and adult rat brain. *Metab. Brain Dis.* **18:** 195–206

Ma C, Yao M, Zhai Q-W, Jiao J, Yuan X & Poo M-M (2014) SIRT1 suppresses self-renewal of adult hippocampal neural stem cells. *Development* **141:** 4697–4709

Ma L, Tao Y, Duran A, Llado V, Galvez A, Barger JF, Castilla EA, Chen J, Yajima T, Porollo A, Medvedovic M, Brill LM, Plas DR, Riedl SJ, Leitges M, Diaz-Meco MT, Richardson AD & Moscat J (2013a) Control of nutrient stress-induced metabolic reprogramming by PKCz in tumorigenesis. *Cell* **152:** 599–611

Ma R, Zhang W, Tang K, Zhang H, Zhang Y, Li D, Li Y, Xu P, Luo S, Cai W, Ji T, Katirai F, Ye D & Huang B (2013b) Switch of glycolysis to gluconeogenesis by dexamethasone for treatment of hepatocarcinoma. *Nat. Commun.* **4:** 2508

Ma W, Tavakoli T, Derby E, Serebryakova Y, Rao MS & Mattson MP (2008) Cell-extracellular matrix interactions regulate neural differentiation of human embryonic stem cells. *BMC Dev. Biol.* **8:** 90

Ma X-J, Dahiya S, Richardson E, Erlander M & Sgroi DC (2009) Gene expression profiling of the tumor microenvironment during breast cancer progression. *Breast Cancer Res.* **11:** R7

Maddocks ODK, Berkers CR, Mason SM, Zheng L, Blyth K, Gottlieb E & Vousden KH (2013) Serine starvation induces stress and p53-dependent metabolic remodelling in cancer cells. *Nature* **493:** 542–6

Maden BEH (1995) No soup for starters? Autotrophy and the origins of metabolism. *Trends Biochem. Sci.* **20:** 337–341

Maessen DE, Scheijen JL, Gaens KH, Greevenbroek MM van, Kallen CJ van der, Stehouwer C DA & Schalkwijk CG (2014) Higher Plasma Concentrations of the Methylglyoxal

Metabolite D-lactate are Independently Associated with Insulin Resistance: The CODAM Study. *J. Diabetes Metab.* **5:** 1000457

Mahmood T & Yang PC (2012) Western blot: Technique, theory, and trouble shooting. *N. Am. J. Med. Sci.* **4:** 429–434

Malatesta P, Appolloni I & Calzolari F (2008) Radial glia and neural stem cells. *Cell Tissue Res.* **331:** 165–78

Marbet Y (2009) Glycolysis pathway overview (CC BY-SA 3.0). Available at: https://commons.wikimedia.org/wiki/File:Glycolysis.svg [Accessed December 15, 2016]

Markert EK & Vazquez A (2015) Mathematical models of cancer metabolism. *Cancer Metab.* **3:** 14

Mattaini KR, Brignole EJ, Kini M, Davidson SM, Fiske BP, Drennan CL & Vander Heiden MG (2015) An epitope tag alters phosphoglycerate dehydrogenase structure and impairs ability to support cell proliferation. *Cancer Metab.* **3:** 5

Mattaini KR, Sullivan MR & Vander Heiden MG (2016) The importance of serine metabolism in cancer. *J. Cell Biol.* **214:** jcb.201604085

Mazurkiewicz M, Opolski A, Wietrzyk J, Radzikowski C & Kleinrok Z (1999) GABA level and GAD activity in human and mouse normal and neoplastic mammary gland. *J Exp Clin Cancer Res* **18:** 247–253

McKee EE, Bentley AT, Smith Jr. RM, Kraas JR & Ciaccio CE (2000) Guanine nucleotide transport by atractyloside-sensitive and -insensitive carriers in isolated heart mitochondria. *Am J Physiol Cell Physiol* **279:** C1870-9

Medes G, Weinhouse S & Thomas A (1953) Metabolism of Neoplastia Tissue. IV. A Study of Lipid Synthesis in Neoplastia Tissue Slices in Vitro. *Cancer Res.* **13:** 27–29

Medina JM, Tabernero A, Tovar JA & Martín-Barrientos J (1996) Metabolic fuel utilization and pyruvate oxidation during the postnatal period. *J. Inherit. Metab. Dis.* **19:** 432–42

Meiser J, Delcambre S, Wegner A, Jäger C, Ghelfi J, D'Herouel AF, Dong X, Weindl D, Stautner C, Nonnenmacher Y, Michelucci A, Popp O, Giesert F, Schildknecht S, Krämer L, Schneider JG, Woitalla D, Wurst W, Skupin A, Weisenhorn DMV, et al (2016a) Loss of DJ-impairs antioxidant response by altered glutamine and serine metabolism. *Neurobiol. Dis.* **89:** 112–125

Meiser J, Krämer L, Sapcariu SC, Battello N, Ghelfi J, D'Herouel AF, Skupin A & Hiller K

(2016b) Pro-inflammatory macrophages sustain pyruvate oxidation through pyruvate dehydrogenase for the synthesis of itaconate and to enable cytokine expression. *J. Biol. Chem.* **291:** 3932–3946

Méndez-Lucas A, Duarte JAG, Sunny NE, Satapati S, He T, Fu X, Bermúdez J, Burgess SC & Perales JC (2013) PEPCK-M expression in mouse liver potentiates, not replaces, PEPCK-C mediated gluconeogenesis. *J. Hepatol.* **59:** 105–13

Méndez-Lucas A, Hyroššová P, Novellasdemunt L, Viñals F & Perales JC (2014) Mitochondrial phosphoenolpyruvate carboxykinase (PEPCK-M) is a pro-survival, endoplasmic reticulum (ER) stress response gene involved in tumor cell adaptation to nutrient availability. *J. Biol. Chem.* **289:** 22090–22102

Mergenthaler P, Lindauer U, Dienel GA & Meisel A (2013) Sugar for the brain: The role of glucose in physiological and pathological brain function. *Trends Neurosci.* **36:** 587–597

Merz K, Herold S & Lie DC (2011) CREB in adult neurogenesis - master and partner in the development of adult-born neurons? *Eur. J. Neurosci.* **33:** 1078–1086

Metallo CM, Gameiro PA, Bell EL, Mattaini KR, Yang J, Hiller K, Jewell CM, Johnson ZR, Irvine DJ, Guarente L, Kelleher JK, Heiden MG Vander, Iliopoulos O & Stephanopoulos G (2012) Reductive glutamine metabolism by IDH1 mediates lipogenesis under hypoxia. *Nature* **481:** 380–384

Metsalu T & Vilo J (2015) ClustVis: A web tool for visualizing clustering of multivariate data using Principal Component Analysis and heatmap. *Nucleic Acids Res.* **43:** W566–W570

Mills EL, Kelly B, Logan A, Costa ASH, Varma M, Bryant CE, Tourlomousis P, D??britz JHM, Gottlieb E, Latorre I, Corr SC, McManus G, Ryan D, Jacobs HT, Szibor M, Xavier RJ, Braun T, Frezza C, Murphy MP & O'Neill LA (2016) Succinate Dehydrogenase Supports Metabolic Repurposing of Mitochondria to Drive Inflammatory Macrophages. *Cell* **167:** 457–470.e13

Mithieux G, Bady I, Gautier A, Croset M, Rajas F & Zitoun C (2004) Induction of control genes in intestinal gluconeogenesis is sequential during fasting and maximal in diabetes. *Am. J. Physiol. Endocrinol. Metab.* **286:** E370–E375

Mithieux G, Misery P, Magnan C, Pillot B, Gautier-Stein A, Bernard C, Rajas F & Zitoun C (2005) Portal sensing of intestinal gluconeogenesis is a mechanistic link in the diminution of food intake induced by diet protein. *Cell Metab.* **2:** 321–329

Modaressi S, Brechtel K, Christ B & Jungermann K (1998) Human mitochondrial phosphoenolpyruvate carboxykinase 2 gene. Structure, chromosomal localization and tissue-specific expression. *Biochem. J.* **333:** 359–66

Montal ED, Dewi R, Bhalla K, Ou L, Hwang BJ, Ropell AE, Gordon C, Liu WJ, DeBerardinis RJ, Sudderth J, Twaddel W, Boros LG, Shroyer KR, Duraisamy S, Drapkin R, Powers RS, Rohde JM, Boxer MB, Wong KK & Girnun GD (2015) PEPCK Coordinates the Regulation of Central Carbon Metabolism to Promote Cancer Cell Growth. *Mol. Cell* **60:** 571–583

Mori S, Chang JT, Andrechek ER, Matsumura N, Baba T, Yao G, Kim JW, Gatza M, Murphy S & Nevins JR (2009) Anchorage-independent cell growth signature identifies tumors with metastatic potential. *Oncogene* **28:** 2796–2805

Mullarky E, Mattaini KR, Vander Heiden MG, Cantley LC & Locasale JW (2011) PHGDH amplification and altered glucose metabolism in human melanoma. *Pigment Cell Melanoma Res.* **24:** 1112–1115

Müller M, Mentel M, van Hellemond JJ, Henze K, Woehle C, Gould SB, Yu R-Y, van der Giezen M, Tielens AGM & Martin WF (2012) Biochemistry and evolution of anaerobic energy metabolism in eukaryotes. *Microbiol. Mol. Biol. Rev.* **76:** 444–95

Mustafi R, Cerda S, Chumsangsri A, Fichera A & Bissonnette M (2006) Protein Kinase-zeta inhibits collagen I-dependent and anchorage-independent growth and enhances apoptosis of human Caco-2 cells. *Mol. Cancer Res.* **4:** 683–694

Narayanese, WikiUserPedia Y & TotoBaggins (2008) Tricarboxylic acid cycle (CC BY-SA 3.0). Available at: https://commons.wikimedia.org/wiki/File:Citric_acid_cycle_with_aconitate_2.svg [Accessed December 12, 2016]

Nazarenko I, Jenny M, Keil J, Gieseler C, Weisshaupt K, Sehouli J, Legewie S, Herbst L, Weichert W, Darb-Esfahani S, Dietel M, Schäfer R, Ueberall F & Sers C (2010) Atypical protein kinase C zeta exhibits a proapoptotic function in ovarian cancer. *Mol. Cancer Res.* **8:** 919–934

Neermann J & Wagner R (1996) Comparative analysis of glucose and glutamine metabolism in transformed mammalian cell lines, insect and primary liver cells. *J. Cell. Physiol.* **166:** 152–169

Neglia D, De Caterina A, Marraccini P, Natali A, Ciardetti M, Vecoli C, Gastaldelli A, Ciociaro

D, Pellegrini P, Testa R, Menichetti L, L'Abbate A, Stanley WC & Recchia FA (2007) Impaired myocardial metabolic reserve and substrate selection flexibility during stress in patients with idiopathic dilated cardiomyopathy. *Am. J. Physiol. Heart Circ. Physiol.* **293:** 3270–3278

Nehlig A & Pereira de Vasconcelos A (1993) Glucose and ketone body utilization by the brain of neonatal rats. *Prog. Neurobiol.* **40:** 163–220

Nelson DL & Cox MM (2000) LEHNINGER PRINCIPLES OF BIOCHEMISTRY 5th ed. New York: W.H. Freeman

Nielsen J (2003) It Is All about Metabolic Fluxes. *J. Bacteriol.* **185:** 7031–7035

Nieman KM, Kenny HA, Penicka C V, Ladanyi A, Buell-Gutbrod R, Zillhardt MR, Romero IL, Carey MS, Mills GB, Hotamisligil GS, Yamada SD, Peter ME, Gwin K & Lengyel E (2011) Adipocytes promote ovarian cancer metastasis and provide energy for rapid tumor growth. *Nat. Med.* **17:** 1498–503

Nishi K, Suzuki K, Sawamoto J, Tokizawa Y, Iwase Y, Yumita N & Ikeda T (2016) Inhibition of fatty acid synthesis induces apoptosis of human pancreatic cancer cells. *Anticancer Res.* **36:** 4655–4660

Noctor SC, Martinez-Cerdeno V, Ivic L, Kriegstein AR, Martínez-Cerdeño V, Ivic L, Kriegstein AR, Martinez-Cerdeno V, Ivic L & Kriegstein AR (2004) Cortical neurons arise in symmetric and asymmetric division zones and migrate through specific phases. *Nat Neurosci* **7:** 136–144

Nogueira V, Park Y, Chen CC, Xu PZ, Chen ML, Tonic I, Unterman T & Hay N (2008) Akt Determines Replicative Senescence and Oxidative or Oncogenic Premature Senescence and Sensitizes Cells to Oxidative Apoptosis. *Cancer Cell* **14:** 458–470

Nordlie RC & Lardy HA (1963) Mammalian Liver Phosphoenolpyruvate Carboxykinase Activities*. *J. Biol. Chem.* **238:** 2259–2263

Nowotny M & Yang W (2009) Structural and functional modules in RNA interference. *Curr. Opin. Struct. Biol.* **19:** 286–93

Nye CK, Hanson RW & Kalhan SC (2008) Glyceroneogenesis is the dominant pathway for triglyceride glycerol synthesis in vivo in the rat. *J. Biol. Chem.* **283:** 27565–27574

Oncomine® Platform (2015) Available at: https://www.oncomine.org/ [Accessed December 18, 2016]

Orive G, Anitua E, Pedraz JL & Emerich DF (2009) Biomaterials for promoting brain protection, repair and regeneration. *Nat. Rev. Neurosci.* **10:** 682–692

Osthus RC, Shim H, Kim S, Li Q, Reddy R, Mukherjee M, Xu Y, Wonsey D, Lee LA & Dang C V (2000) Deregulation of glucose transporter 1 and glycolytic gene expression by c-Myc. *J. Biol. Chem.* **275:** 21797–21800

Owen OE, Kalhan SC & Hanson RW (2002) The key role of anaplerosis and cataplerosis for citric acid cycle function. *J. Biol. Chem.* **277:** 30409–30412

Pacold ME, Brimacombe KR, Chan SH, Rohde JM, Lewis CA, Swier LJYM, Possemato R, Chen WW, Sullivan LB, Fiske BP, Cho S, Freinkman E, Birsoy K, Abu-Remaileh M, Shaul YD, Liu CM, Zhou M, Koh MJ, Chung H, Davidson SM, et al (2016) A PHGDH inhibitor reveals coordination of serine synthesis and one-carbon unit fate. *Nat. Chem. Biol.* **12:** 452–458

Pardal R, Molofsky S & Morrison SJ (2005) Stem Cell Self-Renewal and Cancer Cell Proliferation Are Regulated by Common Networks That Balance the Activation of Proto-oncogenes and Tumor Suppressors. *Cold Spring Harb. Perspect. Biol.* **70:** 177–185

Park J-W, Kim SC, Kim WK, Hong JP, Kim K-H, Yeo HY, Lee JY, Kim MS, Kim JH, Yang SY, Kim DY, Oh JH, Cho JY & Yoo BC (2014) Expression of phosphoenolpyruvate carboxykinase linked to chemoradiation susceptibility of human colon cancer cells. *BMC Cancer* **14:** 1–24

Paton JB, Levitsky LL & Fisher DE (1989) Placental transfer and fetal efects of maternal sodium ß-hydroxybutyrate infusion in the baboon. *Ped. Res.* **25:** 435–439

Patra KC & Hay N (2014) The pentose phosphate pathway and cancer. *Trends Biochem. Sci.* **39:** 347–54

Pavlides S, Whitaker-Menezes D, Castello-Cros R, Flomenberg N, Witkiewicz AK, Frank PG, Casimiro MC, Wang C, Fortina P, Addya S, Pestell RG, Martinez-Outschoorn UE, Sotgia F & Lisanti MP (2009) The reverse Warburg effect: Aerobic glycolysis in cancer associated fibroblasts and the tumor stroma. *Cell Cycle* **8:** 3984–4001

Pavlova NN & Thompson CB (2016) The Emerging Hallmarks of Cancer Metabolism. *Cell Metab.* **23:** 27–47

Pellerin L & Magistretti PJ (1994) Glutamate uptake into astrocytes stimulates aerobic glycolysis: a mechanism coupling neuronal activity to glucose utilization. *Proc. Natl. Acad. Sci. U. S. A.* **91:** 10625–9

Pellerin L, Pellegri G, Bittar PG, Charnay Y, Bouras C, Martin J, Stella N & Magistretti PJ (1998) Evidence Supporting the Existence of an Activity-Dependent Astrocyte-Neuron Lactate Shuttle. *Dev. Neurosci.* **20:** 291–299

Pérez-Escuredo J, Van Hée VF, Sboarina M, Falces J, Payen VL, Pellerin L & Sonveaux P (2016) Monocarboxylate transporters in the brain and in cancer. *Biochim. Biophys. Acta - Mol. Cell Res.* **1863:** 2481–2497

Petersen KF, Price TB & Bergeron R (2004) Regulation of net hepatic glycogenolysis and gluconeogenesis during exercise: Impact of type 1 diabetes. *J. Clin. Endocrinol. Metab.* **89:** 4656–4664

Pfeiffer T, Schuster S & Bonhoeffer S (2001) Cooperation and competition in the evolution of ATP-producing pathways. *Science* **292:** 504–507

Phang JM, Liu W, Hancock C & Christian KJ (2012) The proline regulatory axis and cancer. *Front. Oncol.* **2:** 60

Phang JM, Liu W, Hancock CN & Fischer JW (2015) Proline metabolism and cancer: emerging links to glutamine and collagen. *Curr. Opin. Clin. Nutr. Metab. Care* **18:** 71–77

Phannasil P, Thuwajit C, Warnnissorn M, Wallace JC, MacDonald MJ & Jitrapakdee S (2015) Pyruvate carboxylase is up-regulated in breast cancer and essential to support growth and invasion of MDA-MB-231 cells. *PLoS One* **10:** e0129848

Piccaluga PP, Agostinelli C, Califano A, Rossi M, Basso K, Zupo S, Went P, Klein U, Zinzani PL, Baccarani M, Dalla Favera R & Pileri SA (2007) Gene expression analysis of peripheral T cell lymphoma, unspecified, reveals distinct profiles and new potential therapeutic targets. *J. Clin. Invest.* **117:** 823–34

Pierre K & Pellerin L (2005) Monocarboxylate transporters in the central nervous system: distribution, regulation and function. *J. Neurochem.* **94:** 1–14

Platt MW & Deshpande S (2005) Metabolic adaptation at birth. *Semin. Fetal Neonatal Med.* **10:** 341–350

Poitry-Yamate CL, Poitry S & Tsacopoulos M (1995) Lactate released by Müller glial cells is metabolized by photoreceptors from mammalian retina. *J. Neurosci.* **15:** 5179–5191

Poon E, Yan B, Zhang S, Rushing S, Keung W, Ren L, Lieu DK, Geng L, Kong CW, Wang J, Wong HS, Boheler KR & Li RA (2013) Transcriptome-Guided Functional Analyses Reveal Novel Biological Properties and Regulatory Hierarchy of Human Embryonic Stem Cell-

Derived Ventricular Cardiomyocytes Crucial for Maturation. *PLoS One* **8:** 7–10

Poot M, Zhang YZ, Kramer JA, Wells KS, Jones L, Hanzel DK, Lugade, AG, Singer VL & Haughland RP (1996) Analysis of mitochondrial morphology and function with novel fixable fluorescent stains. *J. Histochem. Cytochem.* **44:** 1363–1372

Possemato R, Marks KM, Shaul YD, Pacold ME, Kim D, Birsoy K, Sethumadhavan S, Woo H-K, Jang HG, Jha AK, Chen WW, Barrett FG, Stransky N, Tsun Z-Y, Cowley GS, Barretina J, Kalaany NY, Hsu PP, Ottina K, Chan AM, et al (2011) Functional genomics reveal that the serine synthesis pathway is essential in breast cancer. *Nature* **476:** 346–50

Presley AD, Fuller KM & Arriaga EA (2003) MitoTracker Green labeling of mitochondrial proteins and their subsequent analysis by capillary electrophoresis with laser-induced fluorescence detection. *J. Chromatogr. B* **793:** 141–150

Previs SF, Brunengraber DZ & Brunengraber H (2009) Is there glucose production outside of the liver and kidney? *Annu Rev Nutr* **29:** 43–57

Prozorovski T, Schulze-Topphoff U, Glumm R, Baumgart J, Schröter F, Ninnemann O, Siegert E, Bendix I, Brüstle O, Nitsch R, Zipp F & Aktas O (2008) Sirt1 contributes critically to the redox-dependent fate of neural progenitors. *Nat. Cell Biol.* **10:** 385–94

Pyeon D, Newton MA, Lambert PF, Den Boon JA, Sengupta S, Marsit CJ, Woodworth CD, Connor JP, Haugen TH, Smith EM, Kelsey KT, Turek LP & Ahlquist P (2007) Fundamental differences in cell cycle deregulation in human papillomavirus-positive and human papillomavirus-negative head/neck and cervical cancers. *Cancer Res.* **67:** 4605–4619

Qing G, Li B, Vu A, Skuli N, Walton ZE, Liu X, Mayes PA, Wise DR, Thompson CB, Maris JM, Hogarty MD & Simon MC (2012) ATF4 Regulates MYC-Mediated Neuroblastoma Cell Death upon Glutamine Deprivation. *Cancer Cell* **22:** 631–644

Qiu X, Forman HJ, Schönthal AH & Cadenas E (1996) Induction of p21 mediated by reactive oxygen species formed during the metabolism of aziridinylbenzoquinones by HCT116 cells. *J. Biol. Chem.* **271:** 31915–31921

Qu H, Håberg A, Haraldseth O, Unsgård G & Sonnewald U (2000) (13)C MR spectroscopy study of lactate as substrate for rat brain. *Dev. Neurosci.* **22:** 429–36

Ramanujan VK (2015) Metabolic Plasticity in Cancer Cells: Reconnecting Mitochondrial Function to Cancer Control. *J. Cell Sci. Ther.* **6:**

Rathmell JC, Fox CJ, Plas DR, Hammerman PS, Cinalli RM & Thompson CB (2003) Akt-directed glucose metabolism can prevent Bax conformation change and promote growth factor-independent survival. *Mol. Cell. Biol.* **23:** 7315–28

Reid MA, Wang WI, Rosales KR, Welliver MX, Pan M & Kong M (2013) The B55α Subunit of PP2A Drives a p53-Dependent Metabolic Adaptation to Glutamine Deprivation. *Mol. Cell* **50:** 200–211

Reitzer J & Wice M (1979) Evidence That Glutamine, Not Sugar, Is the Major Energy Source for Cultured HeLa Cells. *J. Biol. Chem.* **254:** 2669–2676

Reshef L, Hanson RW & Ballard FJ (1969) Glyceride- Glycerol Synthesis from Pyruvate. *J. Biol. Chem.* **244:** 1994–2001

Reshef L, Olswang Y, Cassuto H, Blum B, Croniger CM, Kalhan SC, Tilghman SM & Hanson RW (2003) Glyceroneogenesis and the triglyceride/fatty acid cycle. *J. Biol. Chem.* **278:** 30413–30416

Reya T, Morrison SJ, Clarke MF & Weissman IL (2001) Stem cells, cancer, and cancer stem cells. *Nature* **414:** 105–111

Rhodes DR, Yu J, Shanker K, Deshpande N, Varambally R, Ghosh D, Barrette T, Pandey A & Chinnaiyan AM (2004) ONCOMINE: a cancer microarray database and integrated data-mining platform. *Neoplasia* **6:** 1–6

Riedel C, Rittmann D, Dangel P, Möckel B, Petersen S, Sahm H & Eikmanns BJ (2001) Characterization of the phosphoenolpyruvate carboxykinase gene from Corynebacterium glutamicum and significance of the enzyme for growth and amino acid production. *J. Mol. Microbiol. Biotechnol.* **3:** 573–583

Rinholm JE, Hamilton NB, Kessaris N, Richardson WD, Bergersen LH & Attwell D (2011) Regulation of oligodendrocyte development and myelination by glucose and lactate. *J. Neurosci.* **31:** 538–48

Roberts Jr EL (2009) The support of energy metabolism in the central nervous system with substrates other than glucose. In *Handbook of Neurochemistry and Molecular Neurobiology*, Lajtha A (ed) pp 137–179. Springer

Roessler S, Jia HL, Budhu A, Forgues M, Ye QH, Lee JS, Thorgeirsson SS, Sun Z, Tang ZY, Qin LX & Wang XW (2010) A unique metastasis gene signature enables prediction of tumor relapse in early-stage hepatocellular carcinoma patients. *Cancer Res.* **70:** 10202–

10212

Ross MF, Kelso GF, Blaikie FH, James AM, Cochem?? HM, Filipovska A, Da Ros T, Hurd TR, Smith RAJ & Murphy MP (2005) Lipophilic triphenylphosphonium cations as tools in mitochondrial bioenergetics and free radical biology. *Biochem.* **70:** 222–230

Rozpędowska E, Hellborg L, Ishchuk OP, Orhan F, Galafassi S, Merico A, Woolfit M, Compagno C & Piskur J (2011) Parallel evolution of the make-accumulate-consume strategy in Saccharomyces and Dekkera yeasts. *Nat. Commun.* **2:** 302

Ruan GX & Kazlauskas A (2013) Lactate engages receptor tyrosine kinases Axl, Tie2, and vascular endothelial growth factor receptor 2 to activate phosphoinositide 3-kinase/AKT and promote angiogenesis. *J. Biol. Chem.* **288:** 21161–21172

Rui L (2014) Energy metabolism in the liver. *Compr. Physiol.* **4:** 177–197

Rustin P, Bourgeron T, Parfait B, Chretien D, Munnich A & Rötig A (1997) Inborn errors of the Krebs cycle: A group of unusual mitochondrial diseases in human. *Biochim. Biophys. Acta - Mol. Basis Dis.* **1361:** 185–197

Salomoni P & Calegari F (2010) Cell cycle control of mammalian neural stem cells: putting a speed limit on G1. *Trends Cell Biol.* **20:** 233–243

Sanchez-Alvarez R, Martinez-Outschoorn UE, Lamb R, Hulit J, Howell A, Gandara R, Sartini M, Rubin E, Lisanti MP & Sotgia F (2013) Mitochondrial dysfunction in breast cancer cells prevents tumor growth: Understanding chemoprevention with metformin. *Cell Cycle* **12:** 172–182

Sanchez-Carbayo M, Socci ND, Lozano J, Saint F & Cordon-Cardo C (2006) Defining molecular profiles of poor outcome in patients with invasive bladder cancer using oligonucleotide microarrays. *J. Clin. Oncol.* **24:** 778–789

Satapati S, Kucejova B, Duarte JAG, Fletcher JA, Reynolds L, Sunny NE, He T, Nair LA, Livingston K, Fu X, Merritt ME, Sherry AD, Malloy CR, Shelton JM, Lambert J, Parks EJ, Corbin I, Magnuson MA, Browning JD & Burgess SC (2015) Mitochondrial metabolism mediates oxidative stress and inflammation in fatty liver. *J.Clin.Invest* **125:** 1–16

Sato K, Morris HP & Weinhouse S (1972) Phosphorylase: A New Isozyme in Rat Hepatic Tumors and Fetal Liver. *Science (80-.).* **178:** 879–81

Scholzen T & Gerdes J (2000) The Ki-67 protein: From the known and the unknown. *J. Cell. Physiol.* **182:** 311–322

Schug ZT, Peck B, Jones DT, Zhang Q, Grosskurth S, Alam IS, Goodwin LM, Smethurst E, Mason S, Blyth K, McGarry L, James D, Shanks E, Kalna G, Saunders RE, Jiang M, Howell M, Lassailly F, Thin MZ, Spencer-Dene B, et al (2015) Acetyl-CoA synthetase 2 promotes acetate utilization and maintains cancer cell growth under metabolic stress. *Cancer Cell* **27:** 57–71

Seaberg RM & Van Der Kooy D (2003) Stem and progenitor cells: The premature desertion of rigorous definitions. *Trends Neurosci.* **26:** 125–131

Sebastiani V, Visca P, Botti C, Santeusanio G, Galati GM, Piccini V, Capezzone de Joannon B, Di Tondo U & Alo PL (2004) Fatty acid synthase is a marker of increased risk of recurrence in endometrial carcinoma. *Gynecol Oncol* **92:** 101–105

Selak MA, Armour SM, MacKenzie ED, Boulahbel H, Watson DG, Mansfield KD, Pan Y, Simon MC, Thompson CB & Gottlieb E (2005) Succinate links TCA cycle dysfunction to oncogenesis by inhibiting HIF-a prolyl hydroxylase. *Cancer Cell* **7:** 77–85

Sellers K, Fox MP, Bousamra M, Slone SP, Higashi RM, Miller DM, Wang Y, Yan J, Yuneva MO, Deshpande R, Lane AN, Fan TW-MM, Ii MB, Slone SP, Higashi RM, Miller DM, Wang Y, Yan J, Yuneva MO, Deshpande R, et al (2015) Pyruvate carboxylase is critical for non-small-cell lung cancer proliferation. *J. Clin. Invest.* **125:** 687–698

Semakova J, Hyroššová P, Méndez-Lucas A, Cutz E, Bermudez J, Burgess S, Alcántara S & Perales JC (2017) PEPCK-C reexpression in the liver counters neonatal hypoglycemia in Pck1 del/del mice, unmasking role in non-gluconeogenic tissues. *J. Physiol. Biochem.* **73:** 89–98

Serganova I, Rizwan A, Ni X, Thakur SB, Vider J, Russell J, Blasberg R & Koutcher JA (2011) Metabolic imaging: A link between lactate dehydrogenase A, lactate, and tumor phenotype. *Clin. Cancer Res.* **17:** 6250–6261

Servier Medical Art (2016) Powerpoint image bank (CC BY 3.0). Available at: http://www.servier.com/Powerpoint-image-bank [Accessed January 25, 2017]

Sessa A, Mao C an, Hadjantonakis AK, Klein WH & Broccoli V (2008) Tbr2 Directs Conversion of Radial Glia into Basal Precursors and Guides Neuronal Amplification by Indirect Neurogenesis in the Developing Neocortex. *Neuron* **60:** 56–69

Shim H, Dolde C, Lewis BC, Wu CS, Dang G, Jungmann RA, Dalla-Favera R & Dang C V (1997) c-Myc transactivation of LDH-A: implications for tumor metabolism and growth.

Proc. Natl. Acad. Sci. U. S. A. **94:** 6658–63

Shirwany NA & Zou MH (2014) AMPK: a cellular metabolic and redox sensor. A minireview. *Front Biosci* **19:** 447–474

Shu J, Qiu G & Mohammad I (2013) A semi-automatic image analysis tool for biomarker detection in immunohistochemistry analysis. In *Proceedings - 2013 7th International Conference on Image and Graphics, ICIG 2013* pp 937–942.

Shyh-Chang N & Daley GQ (2015) Metabolic switches linked to pluripotency and embryonic stem cell differentiation. *Cell Metab.* **21:** 349–350

Shyh-Chang N, Daley GQ & Cantley LC (2013) Stem cell metabolism in tissue development and aging. *Development* **140:** 2535–2547

Simoes R V, Serganova IS, Kruchevsky N, Leftin A, Shestov AA, Thaler HT, Sukenick G, Locasale JW, Blasberg RG, Koutcher JA & Ackerstaff E (2015) Metabolic Plasticity of Metastatic Breast Cancer Cells: Adaptation to Changes in the Microenvironment. *Neoplasia* **17:** 671–684

Simpson IA, Carruthers A & Vannucci SJ (2007) Supply and demand in cerebral energy metabolism: the role of nutrient transporters. *J Cereb Blood Flow Metab* **27:** 1766–1791

Simsek T, Kocabas F, Zheng J, Deberardinis RJ, Mahmoud AI, Olson EN, Schneider JW, Zhang CC & Sadek HA (2010) The distinct metabolic profile of hematopoietic stem cells reflects their location in a hypoxic niche. *Cell Stem Cell* **7:** 380–390

Skrzypczak M, Goryca K, Rubel T, Paziewska A, Mikula M, Jarosz D, Pachlewski J, Oledzki J & Ostrowsk J (2010) Modeling oncogenic signaling in colon tumors by multidirectional analyses of microarray data directed for maximization of analytical reliability. *PLoS One* **5:** e13091

Söling HD, Kleineke J, Janson G, Kuhn A & Willms B (1973) Relationship between Intracellular Distribution of Phosphoenolpyruvate Carboxykinase, Regulation of Gluconeogenesis, and Energy Cost of Glucose Formation. *Eur. J. Biochem.* **37:** 233–243

Sounni NE & Noel A (2013) Targeting the Tumor Microenvironment for Cancer Therapy. *Clin. Chem.* **59:** 85–93

Stark R, Guebre-Egziabher F, Zhao X, Feriod C, Dong J, Alves TC, Ioja S, Pongratz RL, Bhanot S, Roden M, Cline GW, Shulman GI & Kibbey RG (2014) A role for mitochondrial phosphoenolpyruvate carboxykinase (PEPCK-M) in the regulation of hepatic

gluconeogenesis. *J. Biol. Chem.* **289:** 7257–7263

Stark R & Kibbey RG (2014) The mitochondrial isoform of phosphoenolpyruvate carboxykinase (PEPCK-M) and glucose homeostasis: Has it been overlooked? *Biochim. Biophys. Acta - Gen. Subj.* **1840:** 1313–1330

Stark R, Pasquel F, Turcu A, Pongratz RL, Roden M, Cline GW, Shulman GI & Kibbey RG (2009) Phosphoenolpyruvate cycling via mitochondrial phosphoenolpyruvate carboxykinase links anaplerosis and mitochondrial GTP with insulin secretion. *J. Biol. Chem.* **284:** 26578–26590

Sudarsan S, Dethlefsen S, Blank LM, Siemann-Herzberg M & Schmid A (2014) The Functional Structure of Central Carbon Metabolism in Pseudomonas putida KT2440. *Appl. Environ. Microbiol.* **80:** 5292–5303

Sullivan LB, Gui DY, Hosios AM, Bush LN, Freinkman E & Vander Heiden MG (2015) Supporting Aspartate Biosynthesis Is an Essential Function of Respiration in Proliferating Cells. *Cell* **162:** 552–563

Sun L, Song L, Wan Q, Wu G, Li X, Wang Y, Wang J, Liu Z, Zhong X, He X, Shen S, Pan X, Li A, Wang Y, Gao P, Tang H & Zhang H (2015) cMyc-mediated activation of serine biosynthesis pathway is critical for cancer progression under nutrient deprivation conditions. *Cell Res.* **25:** 429–44

Szász AM, Lánczky A, Nagy Á, Förster S, Hark K, Green JE, Boussioutas A, Busuttil R, Szabó A, Győrffy B, Szász AM, Lánczky A, Nagy Á, Förster S, Hark K, Green JE, Boussioutas A, Busuttil R, Szabó A & Győrffy B (2016) Cross-validation of survival associated biomarkers in gastric cancer using transcriptomic data of 1,065 patients. *Oncotarget* **7:** 49322–49333

Tabernero A, Vicario C & Medina JM (1996) Lactate spares glucose as a metabolic fuel in neurons and astrocytes from primary culture. *Neurosci. Res.* **26:** 369–376

Tang F, Lane S, Korsak A, Paton JFR, Gourine A V, Kasparov S & Teschemacher AG (2014) Lactate-mediated glia-neuronal signalling in the mammalian brain. *Nat. Commun.* **5:** 3284

Teng Q, Huang W, Collette TW, Ekman DR & Tan C (2009) A direct cell quenching method for cell-culture based metabolomics. *Metabolomics* **5:** 199–208

Tilghman SM, Hanson RW, Reshef L, Hopgood MF & Ballard FJ (1974) Rapid loss of

translatable messenger RNA of phosphoenolpyruvate carboxykinase during glucose repression in liver. *Proc. Natl. Acad. Sci.* **71:** 1304–1308

Tomitsuka E, Kita K & Esumi H (2009) Regulation of succinate-ubiquinone reductase and fumarate reductase activities in human complex II by phosphorylation of its flavoprotein subunit. *Proc. Jpn. Acad. Ser. B. Phys. Biol. Sci.* **85:** 258–265

Tomiyasu M, Aida N, Shibasaki J, Tachibana Y, Endo M, Nozawa K, Shimizu E, Tsuji H & Obata T (2016) Normal lactate concentration range in the neonatal brain. *Magn. Reson. Imaging* **34:** 1269–1273

Tonchev AB, Yamashima T, Zhao L, Okano HJ & Okano H (2003) Proliferation of neural and neuronal progenitors after global brain ischemia in young adult macaque monkeys. *Mol. Cell. Neurosci.* **23:** 292–301

Tong X, Zhao F & Thompson CB (2009) The molecular determinants of de novo nucleotide biosynthesis in cancer cells. *Curr. Opin. Genet. Dev.* **19:** 32–7

Trosko JE & Kang KS (2012) Evolution of energy metabolism, stem cells and cancer stem cells: How the warburg and barker hypotheses might be linked. *Int. J. Stem Cells* **5:** 39–56

Troy S, Soty M, Ribeiro L, Laval L, Migrenne S, Fioramonti X, Pillot B, Fauveau V, Aubert R, Viollet B, Foretz M, Leclerc J, Duchampt A, Zitoun C, Thorens B, Magnan C, Mithieux G & Andreelli F (2008) Intestinal Gluconeogenesis Is a Key Factor for Early Metabolic Changes after Gastric Bypass but Not after Gastric Lap-Band in Mice. *Cell Metab.* **8:** 201–211

Tsatmali M, Walcott EC, Makarenkova H & Crossin KL (2006) Reactive oxygen species modulate the differentiation of neurons in clonal cortical cultures. *Mol. Cell. Neurosci.* **33:** 345–357

Utter M & Kurahashi K (1954a) Mechanism of action of oxalacetic carboxylase. *J. Biol. Chem.* **207:** 821–841

Utter M & Kurahashi K (1954b) Purification of Oxalacetic Carboxylase from chicken liver. *J. Biol. Chem.* **207:** 787–802

Valle A, Cabrera G, Cantero D & Bolivar J (2017) Heterologous expression of the human Phosphoenol Pyruvate Carboxykinase (hPEPCK-M) improves hydrogen and ethanol synthesis in the Escherichia coli dcuD mutant when grown in a glycerol-based medium.

N. Biotechnol. **35:** 1–12

Varum S, Rodrigues AS, Moura MB, Momcilovic O, Easley IV CA, Ramalho-Santos J, van Houten B & Schatten G (2011) Energy metabolism in human pluripotent stem cells and their differentiated counterparts. *PLoS One* **6:** e20914

Végran F, Boidot R, Michiels C, Sonveaux P & Feron O (2011) Lactate influx through the endothelial cell monocarboxylate transporter MCT1 supports an NF-kB/IL-8 pathway that drives tumor angiogenesis. *Cancer Res.* **71:** 2550–2560

Vicario C & Medina JM (1992) Metabolism of Lactate in the Rat Brain During the Early Neonatal Period. *J. Neurochem.* **59:** 32–40

Villas-Bôas SG, Roessner U, Hansen MAE, Smedsgaard J & Nielsen J (2007) Sampling and sample preparation. In *Metabolome Analysis* pp 39–83. Hoboken, NJ, USA: John Wiley & Sons, Inc.

Villee CA (1953) The Metabolism of Human Placenta in Vitro. *J. Biol. Chem.* **205:** 113–123

Vincent EE, Sergushichev A, Griss T, Gingras MC, Samborska B, Ntimbane T, Coelho PP, Blagih J, Raissi TC, Choinière L, Bridon G, Loginicheva E, Flynn BR, Thomas EC, Tavaré JM, Avizonis D, Pause A, Elder DJE, Artyomov MN & Jones RG (2015) Mitochondrial Phosphoenolpyruvate Carboxykinase Regulates Metabolic Adaptation and Enables Glucose-Independent Tumor Growth. *Mol. Cell* **60:** 195–207

Visca P, Sebastiani V, Botti C, Diodoro MG, Lasagni RP, Romagnoli F, Brenna A, De Joannon BC, Donnorso RP, Lombardi G & Alo PL (2004) Fatty Acid Synthase (FAS) is a marker of increased risk of recurrence in lung carcinoma. *Anticancer Res.* **24:** 4169–4173

De Vitto H, Pérez-Valencia J & Radosevich JA (2016) Glutamine at focus: versatile roles in cancer. *Tumor Biol.* **37:** 1541–1558

Volker M and L-M (2001) Bacterial fermentation. *Encycl. Life Sci.***:** 1–7

Wang B, Hsu SH, Frankel W, Ghoshal K & Jacob ST (2012) Stat3-mediated activation of microRNA-23a suppresses gluconeogenesis in hepatocellular carcinoma by down-regulating Glucose-6-phosphatase and peroxisome proliferator-activated receptor gamma, coactivator 1 alpha. *Hepatology* **56:** 186–197

Wang J Bin, Erickson JW, Fuji R, Ramachandran S, Gao P, Dinavahi R, Wilson KF, Ambrosio ALB, Dias SMG, Dang C V & Cerione RA (2010) Targeting mitochondrial glutaminase activity inhibits oncogenic transformation. *Cancer Cell* **18:** 207–219

Warburg O (1956) On the Origin of Cancer Cells. *Science (80-.).* **123:** 309–314

Watford M & Alicia A (1989) Metabolism and Hormonal Regulation Phosphoenolpyruvate Carboxykinase of Rat Small Intestine : Distribution and Regulation of Activity and mRNA Levels1 T. *Distribution* **119:** 268–272

White D (2006) Central Metabolic Pathways Oxford University Press

Wilmanski T, Buhman K, Donkin SS, Burgess JR & Teegarden D (2016) 1α,25-dihydroxyvitamin D inhibits de novo fatty acid synthesis and lipid accumulation in metastatic breast cancer cells through down-regulation of pyruvate carboxylase. *J. Nutr. Biochem.* **40:** 194–200

Wise DR, DeBerardinis RJ, Mancuso A, Sayed N, Zhang X-Y, Pfeiffer HK, Nissim I, Daikhin E, Yudkoff M, McMahon SB & Thompson CB (2008) Myc regulates a transcriptional program that stimulates mitochondrial glutaminolysis and leads to glutamine addiction. *Proc. Natl. Acad. Sci.* **105:** 18782–18787

Wise DR, Ward PS, Shay JES, Cross JR, Gruber JJ, Sachdeva UM, Platt JM, DeMatteo RG, Simon MC & Thompson CB (2011) Hypoxia promotes isocitrate dehydrogenase-dependent carboxylation of α-ketoglutarate to citrate to support cell growth and viability. *Proc. Natl. Acad. Sci. U. S. A.* **108:** 19611–6

Witkiewicz AK, Whitaker-Menezes D, Dasgupta A, Philp NJ, Lin Z, Gandara R, Sneddon S, Martinez-Outschoorn UE, Sotgia F & Lisanti MP (2012) Using the 'reverse Warburg effect' to identify high-risk breast cancer patients: Stromal MCT4 predicts poor clinical outcome in triple-negative breast cancers. *Cell Cycle* **11:** 1108–1117

Wohnsland S, Bürgers HF, Kuschinsky W & Maurer MH (2010) Neurons and neuronal stem cells survive in glucose-free lactate and in high glucose cell culture medium during normoxia and anoxia. *Neurochem. Res.* **35:** 1635–42

Wu S-X, Goebbels S, Nakamura K, Nakamura K, Kometani K, Minato N, Kaneko T, Nave K-A & Tamamaki N (2005) Pyramidal neurons of upper cortical layers generated by NEX-positive progenitor cells in the subventricular zone. *Proc. Natl. Acad. Sci. U. S. A.* **102:** 17172–7

Xiong G, Deng L, Zhu J, Rychahou PG & Xu R (2014) Prolyl-4-hydroxylase α subunit 2 promotes breast cancer progression and metastasis by regulating collagen deposition. *BMC Cancer* **14:** 1

Yamada Y, Haga H & Yamada Y (2014) Concise review: dedifferentiation meets cancer development: proof of concept for epigenetic cancer. *Stem Cells Transl. Med.* **3:** 1182–1187

Yang C, Ko B, Hensley CT, Jiang L, Wasti AT, Kim J, Sudderth J, Calvaruso MA, Lumata L, Mitsche M, Rutter J, Merritt ME & DeBerardinis RJ (2014a) Glutamine oxidation maintains the TCA cycle and cell survival during impaired mitochondrial pyruvate transport. *Mol. Cell* **56:** 414–424

Yang C, Sudderth J, Dang T, Yang C, Sudderth J, Dang T, Bachoo RM, Mcdonald JG & Deberardinis RJ (2009a) Glioblastoma Cells Require Glutamate Dehydrogenase to Survive Impairments of Glucose Metabolism or Akt Signaling Glioblastoma Cells Require Glutamate Dehydrogenase to Survive Impairments of Glucose Metabolism or Akt Signaling. *Cancer Res.* **69:** 7986–7993

Yang J, Kalhan SC & Hanson RW (2009b) What is the metabolic role of phosphoenolpyruvate carboxykinase? *J. Biol. Chem.* **284:** 27025–27029

Yang J, Reshef L, Cassuto H, Aleman G & Hanson RW (2009c) Aspects of the Control of Phosphoenolpyruvate Carboxykinase Gene Transcription. *J. Biol. Chem.* **284:** 27031–27035

Yang L, Moss T, Mangala LS, Marini J, Zhao H, Wahlig S, Armaiz-Pena G, Jiang D, Achreja A, Win J, Roopaimoole R, Rodriguez-Aguayo C, Mercado-Uribe I, Lopez-Berestein G, Liu J, Tsukamoto T, Sood AK, Ram PT & Nagrath D (2014b) Metabolic shifts toward glutamine regulate tumor growth, invasion and bioenergetics in ovarian cancer. *Mol. Syst. Biol.* **10:** 728

Yang M & Vousden KH (2016) Serine and one-carbon metabolism in cancer. *Nat. Rev. Cancer* **16:** 650–662

Yang N-C, Ho W-M, Chen Y-H & Hu M-L (2002) A Convenient One-Step Extraction of Cellular ATP Using Boiling Water for the Luciferin–Luciferase Assay of ATP. *Anal. Biochem.* **306:** 323–327

Yang Z & Xiong H-R (2012) Culture Conditions and Types of Growth Media for Mammalian Cells. In *Biomedical Tissue Culture* pp 3–18.

Ye J, Kumanova M, Hart LS, Sloane K, Zhang H, De Panis DN, Bobrovnikova-Marjon E, Diehl JA, Ron D & Koumenis C (2010) The GCN2-ATF4 pathway is critical for tumour cell

survival and proliferation in response to nutrient deprivation. *EMBO J.* **29:** 2082–2096

Ye J, Mancuso A, Tong X, Ward PS, Fan J, Rabinowitz JD & Thompson CB (2012) Pyruvate kinase M2 promotes de novo serine synthesis to sustain mTORC1 activity and cell proliferation. *Proc. Natl. Acad. Sci.* **109:** 6904–6909

Yoshihara K, Tajima A, Komata D, Yamamoto T, Kodama S, Fujiwara H, Suzuki M, Onishi Y, Hatae M, Sueyoshi K, Fujiwara H, Kudo Y, Inoue I & Tanaka K (2009) Gene expression profiling of advanced-stage serous ovarian cancers distinguishes novel subclasses and implicates ZEB2 in tumor progression and prognosis. *Cancer Sci.* **100:** 1421–1428

Yuneva M, Zamboni N, Oefner P, Sachidanandam R & Lazebnik Y (2007) Deficiency in glutamine but not glucose induces MYC-dependent apoptosis in human cells. *J. Cell Biol.* **178:** 93–105

Yuneva MO, Fan TWM, Allen TD, Higashi RM, Ferraris D V, Tsukamoto T, Matés JM, Alonso FJ, Wang C, Seo Y, Chen X & Bishop JM (2012) The metabolic profile of tumors depends on both the responsible genetic lesion and tissue type. *Cell Metab.* **15:** 157–170

Yusoff AAM, Ahmad F, Idris Z, Jaafar H & Abdullah JM (2015) Understanding Mitochondrial DNA in Brain Tumorigenesis. In *Molecular Considerations and Evolving Surgical Management Issues in the Treatment of Patients with a Brain Tumor* pp 3–28. InTech

Zhan F, Barlogie B, Mulligan G, Shaughnessy JD & Bryant B (2008) High-risk myeloma: A gene expression-based risk-stratification model for newly diagnosed multiple myeloma treated with high-dose therapy is predictive of outcome in relapsed disease treated with single-agent bortezomib or high-dose dexamethasone [7]. *Blood* **111:** 968–969

Zhang J, Ahn WS, Gameiro PA, Keibler MA, Zhang Z & Stephanopoulos G (2014) 13C isotope-assisted methods for quantifying glutamine metabolism in cancer cells. *Methods Enzymol.* **542:** 369–389

Zhang J, Nuebel E, Daley GQ, Koehler CM & Teitell MA (2012) Metabolic regulation in pluripotent stem cells during reprogramming and self-renewal. *Cell Stem Cell* **11:** 589–595

Zhang Q, Wang S-Y, Fleuriel C, Leprince D, Rocheleau J V, Piston DW & Goodman RH (2007) Metabolic regulation of SIRT1 transcription via a HIC1:CtBP corepressor complex. *Proc. Natl. Acad. Sci. U. S. A.* **104:** 829–33

Zhao S, Xu W, Jiang W, Yu W, Lin Y, Zhang T, Yao J, Zhou L, Zeng Y, Li H, Li Y, Shi J, An W,

Hancock SM, He F, Qin L, Chin J, Yang P & Guan K-L (2010) Regulation of Cellular Metabolism by Protein Lysine Acetylation. *Science (80-.).* **237:** 1000–1004

Zhao X, Wang F & Hou M (2016) Expression of stem cell markers nanog and PSCA in gastric cancer and its significance. *Oncol. Lett.* **11:** 442–448

Zheng J (2012) Energy metabolism of cancer: Glycolysis versus oxidative phosphorylation (review). *Oncol. Lett.* **4:** 1151–1157

Zheng X, Boyer L, Jin M, Mertens J, Kim Y, Ma L, Ma L, Hamm M, Gage FH & Hunter T (2016) Metabolic reprogramming during neuronal differentiation from aerobic glycolysis to neuronal oxidative phosphorylation. *Elife* **5:** 859–864

Zhou B, Weigel JA, Saxena A & Weigel PH (2002) Molecular cloning and functional expression of the rat 175-kDa hyaluronan receptor for endocytosis. *Mol Biol Cell* **13:** 2853–2868

Zhu Q, Wong AK, Krishnan A, Aure MR, Tadych A, Zhang R, Corney DC, Greene CS, Bongo LA, Kristensen VN, Charikar M, Li K & Troyanskaya OG (2015) Targeted exploration and analysis of large cross-platform human transcriptomic compendia. *Nat Methods* **12:** 211–214

Zielonka J, Vasquez-Vivar J & Kalyanaraman B (2008) Detection of 2-hydroxyethidium in cellular systems: a unique marker product of superoxide and hydroethidine. *Nat. Protoc.* **3:** 8–21

Zimmer DB & Magnuson MA (1990) Immunohistochemical localization of phosphoenolpyruvate carboxykinase in adult and developing mouse tissues. *J. Histochem. Cytochem.* **38:** 171–178

Zong W-X, Rabinowitz JD & White E (2016) Mitochondria and Cancer. *Mol. Cell* **61:** 667–676

Zu XL & Guppy M (2004) Cancer metabolism: Facts, fantasy, and fiction. *Biochem. Biophys. Res. Commun.* **313:** 459–465